



**University of
Nottingham**

UK | CHINA | MALAYSIA

Manufacturing Metrology Team

Faculty of Engineering

**Real-time target alignment system for high-power
laser operations using a hybrid mechanism**

By

Shah Karim

February 2020

Thesis submitted to the University of Nottingham for the degree of

Doctor of Philosophy

Supervisors: Prof. Richard Leach, Dr Samanta Piano

Dedicated to

My wife Saaiqa Hassan

And

Our daughters – my “Jaan Pakhis” – Alveena Karim and Omairah Karim

I love you all.

Declaration

I hereby declare that except where specific reference is made to work of others, the contents of this thesis are original and have not been submitted in whole or in part for consideration for any other degree or qualification in this, or any other university. This dissertation is my own work and contains nothing which is the outcome of work done in collaboration with others, except as specified in the text and Acknowledgements. This dissertation contains fewer than 100,000 words including appendices, bibliography, footnotes, tables and equations and has fewer than 150 figures.

This work has been carried out with the support of the Engineering and Physical Sciences Research Council and the Science and Technology Facilities Council (grants EP/M008993/1 and EP/L016567/1).

Shah Karim

February 2020

Acknowledgements

All praise is due to Almighty God who has given me the strength to carry out this significant task, and peace and blessings upon Prophet Muhammad (SAW) who taught us patience and perseverance in their best forms.

First and foremost, I would like to express my gratitude to my supervisors, Prof Richard Leach and Dr Samanta Piano. I am indebted to them for their help and support in every step of my PhD. I have learnt so much in my PhD journey, and Richard's encouragement has been priceless. I cannot remember a time when I needed help, and Samanta was not there. My sincere appreciation goes to Dr David Branson for his advice and guidance to my research works, especially in the control system.

I would also like to express my gratitude to my industrial supervisor Dr Martin Tolley (Central Laser Facility, STFC, Oxfordshire) for his unreserved support throughout my PhD. Discussions with him about the high-repetition rate laser operation and HAMS (sorry, you have to look inside for this) have been extremely valuable. I am also grateful to Martin and Chris Spindloe for kindly letting us lend the HAMS system to carry out the experiments at Nottingham. Both Martin and Chris made it easy for me to access to the facilities of the Central Laser Facility. My special thanks go to Sam Astbury of the Central Laser Facility who helped me in so many ways by facilitating my research work at the Central Laser Facility. I want to take the opportunity to thank all the people of the target fabrication group of the central laser facility for their support.

I would also like to thank my colleagues and friends, Teguh Santoso and Wahyudin Syam, for helping me in so many ways and making my PhD enjoyable. It has been a privilege for me to work in an excellent environment with the wonderful people of MMT - I want to thank them all. This includes, but is not limited to Waiel Elmadih,

Taufiq Widjanarko, Amrozia Shaheen, Patrick Bointon, Danny Sims-Waterstone, Luke Todhunter, Lewis Newton, Adam Thomson, Rong Su, Carlos Gomez and Hamid Hadian.

I do not know how to thank my wife Saaqa Hassan. She has showered me with her love and support all my life- not to mention this four year. The sweet love of my daughters for their daddy has inspired me all the way – thank you, my precious ones. I am also gratefully remembering my parents and my in-laws for their love and encouragement even from abroad. I also wish to thank all my family members who are not with me but have been always there for me.

Abstract

To utilise the full potential of high-power lasers, such as for fusion energy applications, large-scale facilities need to operate at high-repetition rates. The challenge of positioning and aligning a target at the laser beam focus with an accuracy of few micrometres (typically $\pm 4 \mu\text{m}$) is significant, but it is a fundamental requirement for a high-power laser interaction to ensure that targets are reproducibly accessible to the highest intensities available. This requirement represents a serious problem for a high-repetition rate laser system in which a fresh target has to be positioned and aligned at the laser beam focus at a rate of at least 0.1 Hz (with plans for 10 Hz or higher in future). Research presented in this thesis is the only known comprehensive study to focus on the demonstration of a real-time target alignment system to fulfil the requirements for the application of high-power high-repetition rate laser operation.

High-accuracy target alignment for high-repetition rate operation means that a real-time position compensation method is required to maintain the target's reference position and plane throughout the operation. Achieving this requirement with a real-time target alignment (position and orientation) system comes with challenges, which can be broadly categorised in two areas: 1. capability development of the elements which are used for the real-time target alignment control system, and 2. design of the real-time target alignment control system. In this research, the performance improvement issues of the target's position control system, in terms of its capability of delivering high-accuracy target positioning and orientation, were addressed before focusing on the development of the real-time position and orientation control system.

The position control system used in this research for the target alignment is a five degree-of-freedom hybrid kinematic mechanism, comprising both serial and parallel kinematic mechanisms. Although parallel and hybrid mechanisms have recently

received much attention, and research is underway to extend their use in industrial applications, comprehensive studies of their design, kinematics, dynamics and error sources are lacking. For accuracy improvement of a hybrid or parallel mechanism, a high level of complexity, as compared to a serial mechanism, arises mainly due to the very high number of error parameters required to describe the mechanism kinematically. For solving the problem, this research presents a method for developing a simplified error model for a complex spatial mechanism with closed loops. The model was used to demonstrate a practical calibration procedure to significantly improve the positional accuracy of a hybrid or parallel mechanism. The procedure outlines effective strategies for carrying out simple measurements to determine the error parameters and compensating for the positional deviations of target with simple steps using software-based compensation technique.

For the real-time target alignment system, the design of the control system is based on an Abbe-compliant, in-process position measurement system of targets, employing a plane mirror interferometer and the hybrid mechanism. An error model was developed for the kinematic error analysis of the mechanism (dynamic influences, e.g. vibration, were not considered) associated with the high-repetition rate process to determine the position feedback information of the target during a high-repetition rate process. The model was also used to identify the effects of the non-collocation of the target and the measurement point of the interferometer on the control system's performance - a challenge for the real-time position control of targets. The behaviour of the control system was investigated with the error model and experimental data. It was found that the controller's position compensation scheme can be ineffective due to erroneous position feedback for the non-linear position information representing the non-collocated measurement point and the actual target. To solve the problem, an angular

compensation technique was proposed for high-accuracy, real-time position and orientation control of targets.

The findings of this research are valid for wider applications. For example, 1. The method of simplifying the error model and the strategies developed for the calibration and compensation procedure can be used for other types of parallel or hybrid mechanisms, 2. The design principle of the real-time control system, the error model and the position and orientation compensation strategies can be applicable to the design of positioning systems requiring highly accurate position control of the end-effector.

Table of Contents

List of figures

List of tables

Chapter 1 - Introduction.....	1
1.1 Background.....	1
1.2 Research questions.....	5
1.3 Thesis structure.....	5
1.4 Contribution to knowledge.....	7
Chapter 2 - Literature review.....	12
2.1 High-power lasers.....	12
2.2 Microtargets for the lasers.....	14
2.2.1 Microtarget manufacturing.....	15
2.2.2 Microtarget characterisation.....	16
2.3 Microtarget delivery for high repetition rate laser system.....	16
2.3.1 Target positioning system.....	16
2.3.2 Main features of HAMS system.....	21
2.4 Accuracy of a mechanism.....	24
2.4.1 Errors and accuracy.....	25
2.4.2 Sources of error.....	26
2.4.3 Description of kinematic errors.....	26
2.5 Measurement errors.....	28
2.6 Methods of error elimination.....	30
2.7 Conclusion.....	32
Chapter 3 - Performance improvement of hybrid mechanism.....	35
3.1 Kinematic structure.....	35
3.1.1 Serial kinematic structure.....	35
3.1.2 Parallel kinematic structures.....	37
3.1.3 Hybrid kinematic structures.....	40
3.1.4 Current research on parallel and hybrid kinematic mechanisms.....	42

3.2	Calibration of hybrid mechanism.....	43
3.3	Method of kinematic calibration.....	44
3.3.1	Model for kinematic calibration.....	45
3.3.2	Pose measurements	51
3.3.3	Parameter identifications.....	53
3.3.4	Implementation of calibration.....	55
3.4	Key issues in calibrating parallel and hybrid kinematic mechanism	56
3.4.1	Issues related to kinematic model for position analysis.....	56
3.4.2	Issues related to error model	58
3.4.3	Issues related to measurements	62
3.4.4	Issues related to parameter identification.....	63
3.4.5	Issues related to implementation of the calibration: compensation	64
3.5	Real-time position control of target	64
3.5.1	Requirements for real-time position control	66
3.5.2	In-process position sensor for high-repetition rate laser operations.....	78
3.6	Conclusion	82
Chapter 4 -	Research methodologies.....	85
4.1	Introduction.....	85
4.2	Selection of research methods.....	85
4.2.1	Research methods for the performance improvement of HAMS.....	86
4.2.2	Research methods used for error estimation and real-time position compensation for target.....	88
4.2.3	Key parameters to determine in the research	92
4.3	Research methods used	94
4.3.1	Analytical approach	94
4.3.2	Empirical approach	96
4.3.3	Experimental method	99
Chapter 5 -	Error modelling of the hybrid mechanism	105
5.1	Introduction.....	105
5.2	Motions of HAMS	107

5.3	Error mapping of the parallel mechanism of HAMS	108
5.3.1	Analysing the error sources of tripod.....	108
5.3.2	Strategy to develop error model for the parallel mechanism	117
5.4	Kinematic analysis of HAMS	120
5.4.1	Kinematic representation of HAMS for model development	120
5.4.2	Method of kinematic model	121
5.5	Modelling the parallel mechanism with no error	124
5.6	Modelling for the mechanism with error	129
5.6.1	Error definitions	129
5.6.2	Model analysis: tip error only	133
5.6.3	Model analysis: tilt error only	135
5.7	Analytical equations to describe the error parameters	136
5.7.1	Tip error parameters.....	137
5.7.2	Tilt error parameters.....	138
5.8	Conclusion	139
Chapter 6 -	Calibration and compensation.....	143
6.1	Introduction.....	143
6.2	Strategy for the calibration.....	144
6.3	Kinematic modelling for calibration	148
6.4	Measurements	150
6.4.1	Types of measurements.....	150
6.4.2	Methods of the measurements.....	152
6.5	Error parameter identification	154
6.5.1	Identifying the error parameters of the tripod (RPS mechanism)	154
6.5.2	Identifying the error parameters affecting the target position T	157
6.6	Implementation of the calibration results: compensation	161
6.7	Results and discussions.....	163
6.7.1	Performance improvement of HAMS	163
6.7.2	Evaluation of the compensation technique applied.....	165

6.7.3	Improvement of the compensation technique	167
6.7.4	Calibration uncertainty.....	170
6.7.5	Positional deviations of the target T for tilt (v) motion	173
6.8	Conclusion	175
Chapter 7 -	Development of a real-time target alignment system.....	177
7.1	Introduction.....	177
7.2	The need for closed loop control for precision target alignment	178
7.3	Design of the control system for high-repetition rate laser operations	179
7.3.1	Target position measurement for the high-repetition rate operation: applying the Abbe principle	180
7.3.2	In-process measurement system for real-time target alignment.....	182
7.4	Positional deviation of target during wheel rotation: model	183
7.5	Design of the closed loop control system	191
7.6	Experimental validation of the closed loop design for the high-repetition rate laser operation	194
7.6.1	Experimental procedure	194
7.6.2	Measurement uncertainties.....	196
7.7	Results and discussion	197
7.7.1	Characterisation of the high-repetition rate process in the open-loop control system	197
7.7.2	Performance evaluation of the closed loop design.....	199
7.7.3	Investigating the closed loop design issues using the model	201
7.8	Improvement of the closed loop control design	212
7.9	Conclusion	215
Chapter 8 -	Conclusions and future work	218
8.1	Overview	218
8.2	Conclusions.....	219
8.2.1	Requirements for the target alignment for high-repetition rate laser operation	219
8.2.2	Error model for HAMS	221

8.2.3	Performance improvement of HAMS	223
8.2.4	Real-time target alignment.....	225
8.3	Future work.....	226
8.3.1	High-repetition rate laser operation.....	227
8.3.2	Error model and the calibration process for parallel and hybrid mechanisms .	228
8.3.3	Real-time alignment control for target.....	229

References

Appendix A	An example of uncertainty budget for distance measurement by a laser interferometer
Appendix B	Properties of the actuators used in the motion stages of HAMS
Appendix C	Inverse kinematics of HAMS extracted from the HAMS control software
Appendix D	Example of a motion programme for generating compensation for the positional deviation of target in the z direction for a given tip rotation of HAMS
Appendix E	The elements of the matrix in equation (7.12) of section 7.4
Appendix F	The elements of the matrix in equation (7.25) of section 7.4
Appendix G	Procedure to avoid the plane mirror's misalignment during the experimental set-up

List of figures

Figure 2.1 Conceptual view of a laser fusion power plant with fusion chamber and turbine generator [8].	12
Figure 2.2 MEMS fabricated micro-parts (a) plastic disc targets (on Si wafer): 7.5 μm diameter and 1 μm thick; (b) thin film targets of silicon nitride: 32 μm diameter and 50 nm thick [12]......	15
Figure 2.3 Centre positioning of the silicon wafer [16]......	17
Figure 2.4 Representation of Gaussian beam in which target needs to be positioned within depth of focus [16]......	18
Figure 2.5 HAMS for the high-power high repetition rate laser operations: (a) laser beam-target interaction; (b) HAMS with the target interface wheel; (c) features of HAMS; (d) target interface wheel with two target sections; (e) targets patterned around the circumference of a target section.	22
Figure 2.6 Eight silicon wafer target sectors attached to the interface wheel (scale in millimetre). Microtargets are patterned around the circumference of the sectors [16].	22
Figure 2.7 Accuracy, precision and trueness; trueness dominated accuracy (left) and precision dominated accuracy (right)......	24
Figure 2.8 Kinematic errors of a one-axis mechanism [33]......	28
Figure 2.9 A 2D depiction of a calibre when measuring a circular object: a perfect measurement with no error (top); measurement with Abbe error (bottom)......	29
Figure 2.10 A one-dimensional depiction of cosine error [37]......	30
Figure 2.11 Pre-calibrated error compensation.	31
Figure 2.12 Real-time error compensation.	31
Figure 3.1 Serial kinematic machines abstracted to kinematic chain (t: tool, b: bed, w: work piece) [31]......	36

Figure 3.2 A schematic of 6-DOF Puma robot (serial kinematic structure).	36
Figure 3.3 Five-bar-link parallel kinematic structure.	37
Figure 3.4 Some parallel kinematic structures (R, P, S and U denote revolute, prismatic, spherical and universal joints respectively): (a) two degree of freedom 5R structure, (b) three degree of freedom planar 3-RRR structure, (c) three degree of freedom 3-RPS structure, (d) four degree of freedom structure with four RPUR chains, (e) five degree of freedom structure with three PRRRR chains, (f) six degree of freedom general Stewart platform.....	38
Figure 3.5 Schematic representation of two types of hybrid mechanism: Tricept (left) and Exechon (right).....	41
Figure 3.6 D-H parameters representation for a revolute joint.	46
Figure 3.7 A simple closed loop mechanism with a 2D constraint.....	47
Figure 3.8 Constraint equation calculation (a) mechanism with a prismatic joint (b) mechanism with a revolute joint.	59
Figure 3.9 Block diagram of a feedforward-controlled position system.	68
Figure 3.10 Block diagram of a feedback-controlled position system.	69
Figure 3.11 An Ishikawa diagram showing the factors that affect the performance of an in-process measurement instrument [100]......	73
Figure 3.12 A design of a machine tool with the linear encoders configured to achieve an in-line path of the functional point and the effective point of the scale [89].	76
Figure 3.13 Main components of a laser interferometer for the position measurement of a moving stage.	80
Figure 3.14 Plane mirror interferometer [119].....	81
Figure 4.1 Laser interaction chamber.	90

Figure 4.2 Steps of the microtarget alignment method during the laser operation of CLF.	97
Figure 4.3 Angular motion measurement using interferometer with retro-reflector.	100
Figure 5.1 Hybrid mechanism of HAMS.....	105
Figure 5.2 Spatial 3-DOF RPS mechanism: (a) one of the three closed loops; (b) RPS mechanism showing relevant structural parameters and a closed loop.	109
Figure 5.3 Spherical contact in the spherical joints [44].....	115
Figure 5.4 Kinematic representation of HAMS for model development.....	121
Figure 5.5 Five constraints applied to a cube result in a rotational degree of freedom at its centre [125].	124
Figure 5.6 Error motions associated with: (a) tip (u) and (b) tilt (v).....	130
Figure 6.1 The calibration process flow-diagram for HAMS.....	148
Figure 6.2 Schematic representation of the interferometer setup. The setup shown in the figure is to measure (a) the tip angular error $uerr$ close to the centroid of the moving platform E (b) tip displacement error $\delta xerr$ in the x direction close to E , and (c) positional deviation $Dxttilt error + arch.$ close to the target in the x direction due to tip motion.....	153
Figure 6.3 HAMS showing Abbe offsets and generalised error parameters for tip motion.	154
Figure 6.4 Translational error motions $\delta zerr$ and $\delta xerr$ of the tripod in the z and x directions.....	155
Figure 6.5 Rotational error motion $uerr$ of the tripod (RPS mechanism) of HAMS.	155
Figure 6.6 Error parameters of the RPS mechanism (tripod) and the controller's compensation in the z direction.....	156

Figure 6.7 Comparison of the target’s positional deviations determined by the forward and inverse kinematics experiments and predicted by the error model.	158
Figure 6.8 Theoretically calculated (equations (6.1) to (6.3)) positional deviations at varying tip angular motions (no tilt motion ν or errors considered).	159
Figure 6.9 Comparison of the target’s positional deviations determined by the forward kinematics experiments (same results for the inverse kinematics experiments) and predicted by the error model.	160
Figure 6.10 Target position accuracy improvement in the z direction through the calibration and compensation process.	164
Figure 6.11 Target position accuracy improvement in the x direction through the calibration and compensation process.	164
Figure 6.12 Comparison of the two compensation techniques to improve the target positional accuracy in the z direction.	168
Figure 6.13 Comparison of the two compensation techniques to improve the target positional accuracy in the x direction.	169
Figure 6.14 Comparison of the accuracy of the motions of z stage when measured at the stage and at the tool point (z stage travel range is ± 40 mm).	172
Figure 6.15 Comparison of the calculated and measured positional deviations of target (tool point) due to tilt rotational errors (in z and x directions).	174
Figure 7.1 Concept of the closed loop control for z position compensation.	181
Figure 7.2 Plane mirror position (a) ideal mirror setting (b) actual mirror setting.	182
Figure 7.3 Coordinate systems for the error model (a) with the effective and functional points shown in (b) and (c).	184
Figure 7.4 Hardware set-up for the closed loop control of the target.	192
Figure 7.5 Control diagram of the closed loop control for HAMS motion stages.	192

Figure 7.6 Simplified flow-diagram of the motion program for the high-repetition rate operations.....	193
Figure 7.7 Profiles of the position feedback (z positional deviations) for eight locations of the target wheel.....	198
Figure 7.8 Closed loop control system in which mirror position setting represents the target position (i.e. complaint case where position feedback from EP and FP are same).	199
Figure 7.9 Closed loop control system in which mirror position setting does not represent the target position (non-complaint case where position feedback from EP and FP are not same).....	200
Figure 7.10 Experimental data (in open-loop) and model fitting for both mirror (EP) and target position (FP) settings.	202
Figure 7.11 Tip motion error (θx) of the wheel calculated from the model fitting... ..	203
Figure 7.12 Tilt motion error (θy) of the wheel calculated from the model fitting... ..	203
Figure 7.13 Examination of the wheel rotation path for 1.5° when no or minimum positional deviation read by EP.	205
Figure 7.14 Examination of the wheel rotation path for 1.5° when maximum positional	206
Figure 7.15 Resultant angular error α for some selective locations of the wheel as calculated from the θx and θy associated with EP (a) and FP (b).	208
Figure 7.16 Comparison of the resultant angular errors α of the wheel between two settings as calculated from the information in Figure 7.11 and 7.12.....	211
Figure 7.17 Performance of the improved scheme of the closed loop control using angular compensation.	212

Figure 7.18 Performance of the improved closed loop control using different approach to angular compensation. 214

Figure 8.1 Conceptual flow-diagram of the target alignment process and other processes for the high-repetition rate laser operations. 220

List of tables

Table 2.1 Motions required by the target position system [15,16].	20
Table 2.2 Possible sources of error in HAMS [7,13,14,16].	23
Table 3.1 Key characteristics of a sensor for an application.....	72
Table 4.1 Key parameters for the development of real-time position and orientation control for target.	93
Table 4.2 Sensitivity of the measured length L_{Meas} with respect to environment (atmospheric) condition [121].....	102
Table 7.1 Different categories of behaviour of the open-loop high-repetition rate system (i.e. wheel rotation).	204
Table 7.2 Slopes of the θ_x , θ_y and α profiles as shown in Figure 7.11, 7.12 and 7.15.	208

List of publications

Journal papers

Karim S, Piano S, Leach RK, Tolley M. Error modelling and validation of a high-precision five degree of freedom hybrid mechanism for high-power high-repetition rate laser system. *Prec. Eng.*, 2018;54:182-197.

Karim S, Piano S, Branson D, Santoso T, Leach RK, Tolley M. Real-time target alignment system for high-power high-repetition rate laser operations using a five degree-of-freedom hybrid mechanism. *Intl. J. of Control*, 2020 (under review).

Conference papers

Karim S, Piano S, Leach R, Tolley M. Error analysis for a high-precision five degree of freedom hybrid mechanism for high-power high-repetition rate laser system. *Proc. 32nd Annal. Meet. ASPE, Charlotte, North Carolina, 29 Oct-3 Nov 2017.*

Karim S, Piano S, Leach RK, Branson D, Tolley M. Calibration and adjustment of high-precision five degree of-freedom hybrid mechanism. *Proc. 33rd Annal. Meet. ASPE, Las Vegas, 4-9 Nov 2018.*

Non-paper conference presentations

Karim S, Piano S, Leach R, Tolley M. Error modelling of a hybrid five degree of freedom mechanism for manipulation of high repetition rate laser microtargets. *6th Target Fabrication Workshop 2017, Greenwich, London, 8-11 May 2017.*

Karim S, Piano S, Leach R, Tolley M. Performance improvement of a hybrid five degree-of-freedom mechanism for manipulation of high-repetition rate laser microtargets. *7th Target Fabrication Workshop 2017, Darmstadt, Germany, 17-20 September 2018.*

Book chapter

Karim S, Weber U. Kinematic design. In: Leach RK, Smith ST, (ed.). *Basics of precision engineering*. CRC Press: 2018.

Chapter 1 - Introduction

1.1 Background

Pulsed lasers with high-power (petawatt class lasers) have seen significant development in the last few decades. High-power lasers are used for advanced research activities in physics, chemistry and biology, for example, to accelerate subatomic particles to high energies, to study biochemical and biophysical processes, and for cutting-edge applications, such as fusion energy, radiation therapy and secondary source generation (X-rays, electrons, protons, neutron and ions) [1-3]. To utilise the full potential of high-power lasers, large-scale facilities need to operate at high-repetition rates, which presents many engineering challenges [3,4]. One such challenge is the positioning and aligning of a micro-scale target relative to the focus of the laser beam(s) with an accuracy of few micrometres - a fundamental requirement for a high-power laser-target interaction to ensure that targets are reproducibly accessible to the highest intensities available, that is in the region of the laser beam focus as determined by the Rayleigh range [5,6]. Fulfilling this requirement for a high-repetition rate laser system means that fresh targets have to be positioned and orientated at the laser beam focus at a rate of at least 0.1 Hz (with plans for 10 Hz or higher in future) [4-6]. For example, clinically relevant experiments require several thousands of laser shots, which demand for an automated target positioning system. However, no work, as the literature review suggests, has been carried out to develop a solution that can fulfil the requirements for the target alignment (positioning and orientation) for high-repetition rate laser operation. One method of automated positioning of nano-scale targets was reported by Gao et al. [7]. With the use of a six-axis hexapod, a specially designed target wheel, a microscope and a confocal chromatic displacement sensor, they achieved a target positioning accuracy of around 5 μm in all spatial dimensions at 0.5 Hz repetition rate. However,

this method represents a pre-calibrated compensation for target's positional deviations and is inadequate to fulfil the requirements for the target alignment for high-repetition rate laser operation as clearly outlined in this thesis for the first time in the research of high-power high-repetition rate laser. Another method of automated target alignment can be found in the form of an integrated target solution developed by the Central Laser Facility (CLF) [8-10]. The target solution of the CLF, known as the "High Accuracy Microtarget Supply" (HAMS) system, uses a number of identical targets manufactured with MEMS technology and delivers the targets to the laser focus within specifications at high speed (hertz level). Demonstration of an automated target alignment system using HAMS is the focus of this research.

The target alignment at high-repetition rate depends on the ability of the motion stages of HAMS to generate the translational and rotational motions to locate the target with the required accuracy and repeatability. In fact, the position accuracy of a target (tool or end-effector, but hereafter just called target) is one of the most important requirements for many precision applications, such as ultra-precision machine tools, coordinate measuring machines and surgical robots. Positional accuracy is generally achieved by carrying out one or more of these processes: design - following precision engineering principles; calibration, requiring steps, such as kinematic modelling, error identification and error compensation; and compensation for the target's path (or trajectory), requiring in-process measurement of the position of the target while the operation is taking place (i.e. real-time compensation) [1-10]. Real-time compensation has been playing an increasingly important role in recent years in the process chain for manufacturing of precision workpieces with complex shapes and/or tight tolerances [6,7]. However, developing a real-time compensation technique for a precision application comes with many challenges. For example, finding a suitable metrology

solution for in-process position measurements of targets can be difficult for a number of reasons, e.g. appropriate mounting of the sensor in the manufacturing machine, high measurement speeds to follow the manufacturing operation and avoidance of environmental disturbances [5-7]. For high-power laser applications, finding a suitable system for the real-time target alignment for high-repetition rate operation has its own challenges, which can be broadly categorised in two areas: first, capability development of the elements which are used in the real-time target alignment control system, and second, design of the real-time target alignment control system. As such, in this research, the performance improvement issues of HAMS, in terms of its capability of delivering high-accuracy target positioning and orientation, were addressed before focusing on the development of the real-time position and orientation control system for target for high-repetition rate operation.

HAMS has a hybrid kinematic structure, comprising parallel and serial mechanisms. Although it has been shown that kinematic calibration can be a practical and economical way for enhancing the accuracy of mechanisms, the calibration process is more complex for a parallel or hybrid mechanism than for a serial mechanism. This complexity is due to the significant difficulty in describing the kinematic mechanism using a minimum set of error parameters, representing the need for a computationally demanding error model for the calibration process [20-23]. Further difficulties may arise from the need for a costly measurement scheme [23,24], a complex method for identifying many error parameters [20,25,26] and specialised technical knowledge and information for implementing the calibration results into the mechanism's controller [20,22,23,27-31]. On the other hand, finding a real-time compensation method to maintain the target's reference position and plane throughout the high-repetition rate operation comes with a separate set of challenges [32,33]. For example, the change of

target's reference plane during the high-repetition rate operation may give rise to the Abbe errors while measuring target's positions by the sensors, indicating that the position feedback to the controller may be incorrect. In such cases, position and orientation compensations for target become ineffective for the real-time target alignment control for high-repetition rate operation. By addressing such challenges in two stated areas, this research demonstrates a model for the real-time target alignment for high-repetition rate laser operations.

To summarise, there is a significant gap in research and knowledge concerning the capability development of the target alignment (position and orientation) process for high-power high-repetition rate laser operations. Capability development covers a wide range of areas of target alignment in terms of requirements (e.g. accuracy/repeatability/speed of the target alignment process), tasks (e.g. set reference position and orientation, maintain reference position and orientation during high-repetition rate operation), methods (e.g. initial alignment, real-time alignment during high-repetition rate operation) and enabling technologies (e.g. position control system, sensor for closed-loop feedback, closed-loop control system for target alignment). Furthermore, the hybrid mechanism, used in this research for the real-time target alignment system for high-repetition rate laser operations, actually represents a new generation of kinematic mechanisms as opposed to serial and parallel mechanisms. Hybrid mechanisms have recently received much attention and research is underway on how to use them in industrial applications. As such, comprehensive studies of these new types of mechanism in terms of their designs, kinematics, dynamics and performance improvements are lacking. In addition, the development of an effective design strategy for a real-time target alignment system for an industrial application represents an in-process metrology system - a highly active research area of today's manufacturing.

1.2 Research questions

The aim of the research is to demonstrate a system of controlling the position and orientation of targets in real-time so that they can be located in space in the x , y and z directions of a reference coordinate system within specifications as determined by the requirements for high-repetition rate laser operations.

To meet the aim, three research questions need to be answered:

1. Does the motion control system (i.e. HAMS) used in the real-time target alignment have the capabilities to fulfil the requirements of the positional and orientation accuracies of targets?
2. What method can be applied to determine the positional and orientation deviations of targets caused by the errors arising from high-repetition process?
3. What method can be applied to effectively compensate for the positional and orientation deviations of targets during the high-repetition rate operation?

To answer the first question, two sub-questions need to be answered:

- A. How can the errors of the mechanism be analysed to understand their effects on the positional and orientation deviations of targets?
- B. What procedure can be applied to improve the performance of the mechanism?

1.3 Thesis structure

To answer the research questions, the thesis is structured in the following way:

1. Chapter 2 gives an overview of high-power laser, the high-repetition rate laser operations, the requirements for a high-repetition rate laser operation and the description of HAMS. Chapter 2 also outlines the important features concerning the accuracy of a mechanism and methods of accuracy improvement.
2. Chapter 3 begins by introducing the different types of kinematic mechanism (serial, parallel and hybrid mechanisms) with their characteristics. The kinematic

calibration as a method to improve the performance of parallel and hybrid mechanisms is then discussed with a comparison to the calibration method usually carried out for a serial mechanism, thus highlighting the challenges of developing a calibration method for a parallel mechanism. Chapter 3 also gives an overview of the elements (e.g. sensors, control system) required for the real-time position and orientation compensation for target in a precision application. The development issues of the real-time position and orientation compensation for target are also detailed.

3. Chapter 4 describes different methods used to answer the research questions.
4. Chapter 5 aims to answer the first research question by answering the first sub-question. The process of error analysis and the development of an error model for HAMS are detailed in this chapter.
5. Chapter 6 answers the second sub-question of the first research question and gives details to the kinematic calibration and compensation procedure for HAMS.
6. Chapter 7 gives answer to the second research question by describing an analytical model to characterise the high-repetition rate process. The chapter answers the third research question by laying out the following features: the design principle of an in-process position measurement system for target, the design of the closed loop control system, the analysis of the behaviours of the real-time control system with the help of the model and experimental data, and solutions to overcome the limitations of the control system.
7. Chapter 8 concludes the thesis by explaining how the outcomes of the research represent a model to fulfil the requirements for the real-time target alignment for high-repetition rate laser operation. The chapter also shows the research findings

that have generic characteristics to be valid for wider applications. Some avenues of future research opportunity are also outlined based on the outcomes of the research.

1.4 Contribution to knowledge

The significance of the research work in terms of contributing to the relevant research field can be listed as follows:

- A. There has been a notable increase in the number of high-power laser facilities across the world and therefore an increase in the number of laser shots available. This recent laser development indicates the prospect of switching of the laser facilities from experimental-based facilities to application-based facilities with high-repetition rate laser operations, e.g. laser fusion energy application [33]. As the research and development in high-repetition rate laser operation have begun only recently, the multi-faceted engineering challenges have started emerging – solutions to many of these are still unknown. Target alignment at the laser focus at a speed comparable with the laser shot rate (at least 0.1 Hz) represents one such challenge; this includes problems that must be addressed when trying to align targets within short timescale (few seconds). Although an automated target alignment method can be found in the literature (section 1.1), the research presented in this thesis is the only known comprehensive study for the development of a real-time target alignment system for the application of high-power high-repetition rate laser operation. This research demonstrates a model of the real-time target alignment system by outlining the requirements, tasks, methods and technologies for the high-repetition rate laser operations (discussed in Chapter 4 to 8).

B. The principles, methods and findings related to the development of the real-time target alignment have some generic features that can be applicable to wider precision applications requiring high positional accuracy. For example,

a) In many applications, e.g. high-speed motion control stages, getting accurate and reliable feedback of the target position (i.e. in-process measurement) during an operation, e.g. machining, poses a significant challenge for the control system of a mechanism. One of the main reasons for this is due to the inclusion of Abbe errors to the target position measurement, since the functional point (target) and the effective point (where the target position is actually measured) are often not same. The inclusion of Abbe errors to the position measurement of target represents uncertainty, limiting the positional accuracy of the target of the motion control system. For most of the applications using motion control systems, optical sensors are used to measure the displacements of the stages to determine the position of the target, and Abbe errors are unavoidable. Recently, few designs have emerged as Abbe-complaint motion control systems for high-accuracy applications (an example of the application is given in section 7.3.1). However, these designs are for the motion control of stages, and are not necessarily for the real-time position and orientation control of target.

The research in this thesis presents a closed loop control system based on an in-process target position measurement system designed to avoid Abbe errors (Chapter 7). The design has been demonstrated for the real-time alignment control for a high-accuracy application (i.e. target alignment for high-power laser operation).

b) The research findings suggest that an Abbe-complaint design on its own may not be enough to control the target alignment with high-accuracy due to the

uncertainty in determining a target's position. An error model is developed to predict this position uncertainty with the consideration that a high-repetition process with a periodic motion is subject to kinematic errors arising from the high-repetition process (Chapter 7). Using this model and the experimental data, it has been proposed that two conditions, involving the error and structural parameters, are important in determining the uncertainty of the target position measurement due to non-collocation of the effective and functional points.

The periodic motion of the high-repetition process, its associated motion parameters and the structural parameters of the system used in the model and in the proposed conditions are believed to be non-application-specific and can be found in wider applications. For example, the error model and the conditions can be used at the design stage of a high-accuracy positioning system to predict the uncertainty in the measurement of the target position in the presence of periodic error/s (i.e. straightness error) that may arise from the drive system of the motion stage/s.

- c) Chapter 7 also presents strategies to overcome the position uncertainty for the alignment (both position and orientation) control of target, whereas most of the precision application research focuses only on the position control of target.
- C. Parallel mechanisms represent newer varieties of kinematic mechanism as compared to serial mechanisms. Hybrid mechanisms have emerged in recent years to overcome the inherent limitations of serial and parallel mechanisms, such as low accuracy and limited workspace, respectively, while exploiting the advantageous characteristics of both types, namely large workspace and high accuracy [9,10]. Although hybrid mechanisms have recently received much attention, and research is underway on how to use them in industrial applications, comprehensive studies of their design,

kinematics, dynamics and error sources are lacking. Since HAMS has a hybrid mechanism and the focus of research question one is about capability development of HAMS, the knowledge and understanding achieved from the current research will contribute to the areas of parallel and hybrid mechanisms in the following ways:

- a) A detailed literature review highlights the issues of developing an effective kinematic calibration method for the performance improvement of the parallel mechanisms (Chapter 3).
- b) An analytical approach is presented to simplify the error mapping of the complex kinematic structure of a hybrid mechanism (Chapter 4).
- c) An error model is developed and demonstrated for the hybrid mechanism based on only few error parameters as opposed to many parameters generally used to describe a parallel or hybrid mechanism kinematically (Chapter 5 and 6).
- d) A cost- and time-effective calibration procedure is proposed and demonstrated for the positional and orientational accuracy improvement of the hybrid mechanism. A modular approach, in which mechanisms are treated individually, is adopted for the calibration process, and strategies are outlined for practical implementation of the calibration results following simple steps (Chapter 6).

Chapter 2 - Literature review

2.1 High-power lasers

The use of high-power laser radiation has provided ever-increasing opportunities to investigate the interaction of ultra-strong laser fields with matter, contributing to the exploration of new avenues of research in different branches of science [34]. Advanced lasers enable the investigation of the science of extreme conditions that cannot be produced elsewhere on earth (temperatures of millions of degrees of Celsius, pressures of billions of atmospheres, and extremely strong electric and magnetic fields) [34,35].

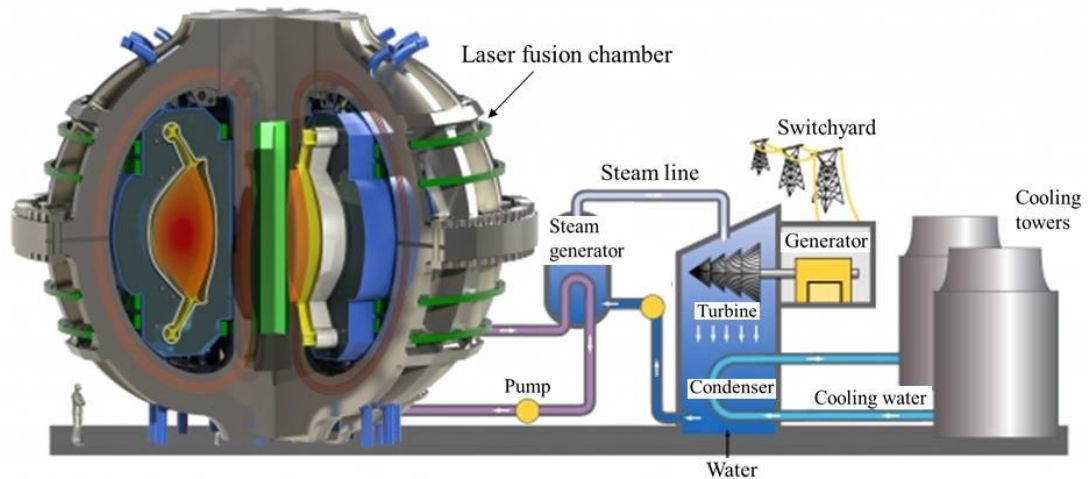


Figure 2.1 Conceptual view of a laser fusion power plant with fusion chamber and turbine generator [39].

Pulsed lasers with high-power have seen significant development in the last few decades. Up until now, over fifty petawatt class lasers worldwide are currently operational, under construction or in the planning phase [2]. These advancements in laser systems have opened up the opportunities of pursuing extraordinary research experiments for physics, chemistry and biology in the laboratory conditions, for example particle acceleration, inertial confinement fusion, radiation therapy and secondary source generation (X-rays, electrons, protons, neutron and ions) [2]. Of particular

interest, lasers also have the potential to provide a significant proportion of the global energy supply in the process of inertial fusion energy (IFE) [36,37]. IFE is the creation of a fusion reaction in a mixture of deuterium and tritium, contained within a microtarget (see Figure 2.1) [36]. Extremely powerful lasers fire a very short but intense pulses to compress this mixture to a density of hundreds of grams per centimetre cubed and a temperature of 10^8 °C. At this point, a fusion reaction can begin, releasing highly energetic neutrons, whose energy can be captured and converted into electricity [38].

To achieve the full potentials, high-power lasers (HPLs) need to be operated at high- repetition rate. However, many challenges in terms of scientific, engineering and technological aspects are yet to overcome. Two major challenges are: 1. the production of high-volume of laser targets (popularly known as microtargets) and 2. delivery of the laser targets to the target chambers at a rate compatible with the high-repetition laser systems [5,33,39]. For example, the GEMINI upgrade of the Astra laser at the Rutherford-Appleton Laboratory (RAL) represents an experimental repetition rate of one shot per 20 s with HPL (approximately 0.5 PW from two laser beams). The stated GEMINI upgrade entails almost two orders of magnitude increase in the number of targets required for Astra laser experiments. This prospect of operating HPL in high-repetition rate represents two problems with regard to current laser facilities [5,33]:

1. Current production facilities of the microtarget can only supply nine weeks' worth of the annual demand for microtargets for high-repetition rate operation.
2. With current target delivery systems, several minutes, as opposed to a few seconds for high-repetition rate operation, are required to position and orientate the target (i.e. target alignment) to the laser focus inside the target chamber.

It is forecasted by the high-power laser user community that the demand for the high-repetition rate laser operation will be even higher in the future (high-power laser

systems such as Extreme Light Infrastructure (ELI) and The High-Power laser Energy Research facility (HiPER) will run at rates of hertz and kilohertz) [2]. Therefore, research and development are required to enhance the capabilities of current laser facilities to meet the requirements for the high-repetition rate operation. Delivery of microtargets for high-repetition rate laser systems must fulfil the following requirements [5,33]:

- A. Appropriate fabrication technologies capable of producing targets at the required rate with the required accuracy and precision;
- B. Appropriate characterisation techniques in line with the production techniques to maintain quality control;
- C. Appropriate technologies to position and orientate the targets at the laser focus with high accuracy at a speed compatible with the high-repetition rate operation;
- D. Appropriate supporting systems to interface the processes, such as design, production, quality control, delivery, end-of-life disposal and so on.

The scope of this research project is limited to the development of the appropriate technologies for the position and orientation of the targets at a speed appropriate for high-repetition rate laser operation.

2.2 Microtargets for the lasers

Microtargets used in laser experiments and applications have a very wide range of design and material combinations, but typically they have a size of less than a few millimetres with a dimensional accuracy of better than 2 μm [5]. The surface texture of the components is another important factor that can be of the order of 50 nm (*Ra*). Foil-type microtargets, made with a variety of materials such as carbon, plastic or gold, are one of the most commonly used in experiments and their thickness can range from a few nanometres to tens of micrometres [5].

2.2.1 Microtarget manufacturing

Traditional target production techniques, such as precision micromachining, thin film coating, micro-assembly, are at their limit to deliver to high repetition laser systems and new technologies are in demand to fulfil the requirements [3,5,40]. Micro-electro-mechanical systems (MEMS) are potentially a promising candidate for mass-producing target components with high accuracies and at a high number. MEMS techniques use silicon wafer-based techniques to mass produce geometries, and it has been possible to fabricate a series of 2D and 3D targets at RAL (Figure 2.2). Although initial investment can be very high for these techniques, it can potentially be very economical if large numbers are required [33,41].

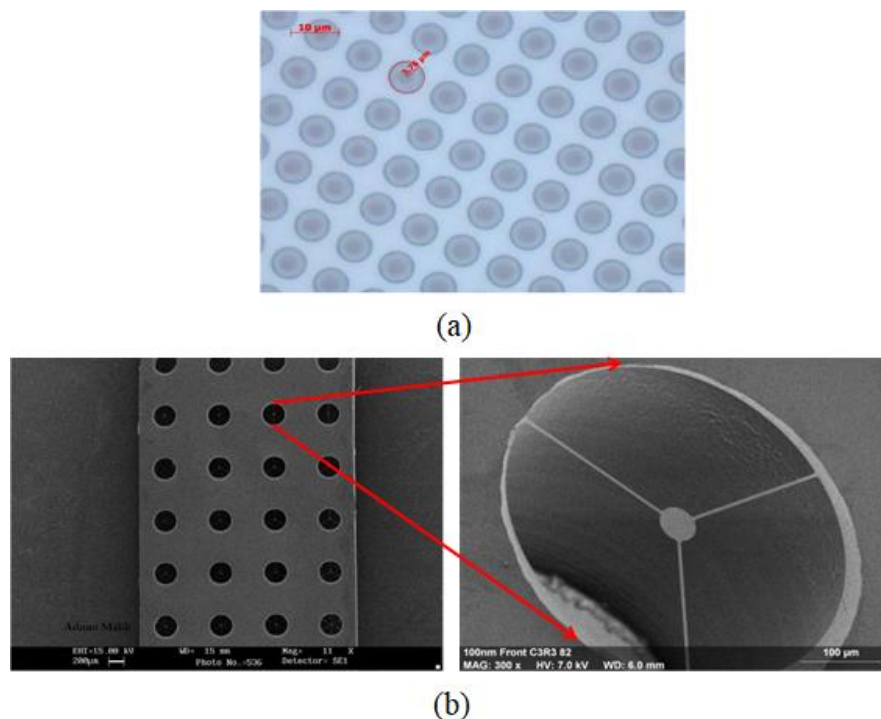


Figure 2.2 MEMS fabricated micro-parts (a) plastic disc targets (on Si wafer): 7.5 µm diameter and 1 µm thick; (b) thin film targets of silicon nitride: 32 µm diameter and 50 nm thick [41].

Not only the 2D membrane targets produced by MEMS are promising for high-repetition rate laser operations, but the produced targets are usually very flat. For

example, the Parylene membrane of Figure 2.2a has a roughness of 180 nm (Ra) and waviness of 32 nm (Wa) [33]. As will be discussed in section 2.3.1, the target flatness is an important parameter in determining whether the targets can be placed reproducibly at the laser focus within specified tolerance.

2.2.2 Microtarget characterisation

It is essential that any target fabricated is characterised to ensure that the parameters which are important for the laser experiments are measured and verified before the target is issued to the user [5]. Some of the most commonly used instruments in a target fabrication laboratory are: optical microscopy, scanning electron microscopy, coherence scanning interferometry and confocal microscopy. However, none of the stated instruments is considered suitable for the characterisation of the mass targets produced for high-repetition rate operations due to their low characterisation speed [41].

2.3 Microtarget delivery for high repetition rate laser system

One of the requirements for high-repetition rate operations, as mentioned previously, is the ability to deliver a large number of microtargets inside the laser chamber and place the microtargets to the laser focus with correct alignment. This requirement cannot be met without firstly, an appropriate target positioning and alignment technique and secondly, an appropriate metrology technique to make sure the targets are reproducibly placed at the target focus within specifications.

2.3.1 Target positioning system

Designing a system for the target positioning of high repetition-rate laser operations poses many technical challenges. Not only the positioning system be capable of delivering the target into the chamber with high accuracy and repeatability at the speed of laser shot rates, the positioning system also needs to maintain positional stability and

resistance to the electromagnetic pulses and debris that are produced in the ultra-intense interaction environment [4]. In fact, although there are several factors that define the specifications of the target positioning system, the main driver is the f -number of the focusing optics [6,42]. According to [32], some important aspects of target positioning and alignment determine the specifications for the accurate target positioning in the x , y and z directions. The target positioning system should have the capabilities to fulfil the specifications. The position specifications for targets and the motion requirements for target alignment are discussed in the following sub-sections.

2.3.1.1 x and y -target centre positioning

The focal spot of the laser beam is $2\ \mu\text{m}$ diameter. The minimum target diameter is $300\ \mu\text{m}$ with the hole normal to the front plane of the target (Figure 2.3). The front plane of the target plate needs to be positioned at a maximum angle of 50° , minimising the free aperture. [32].

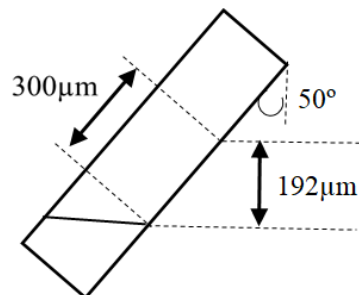


Figure 2.3 Centre positioning of the silicon wafer [32].

It is preferable to hit the target at the centre, within $\pm 10\ \mu\text{m}$ to ensure that the laser-target interaction is symmetric. However, for most applications it is acceptable for the laser to interact with the target at any point where the target mount will not interfere with the reaction.

2.3.1.2 z- laser focus

As explained in [32,43,44], the focus of the laser is critical as the intensity of the laser is inversely related to the cross-sectional area of the focal spot of the laser beam. The beam is modelled as a Gaussian beam (see Figure 2.4), so the Rayleigh length, Z_R , is considered as the region of focus for the beam. The Rayleigh range is the distance over which the target is in the intense focus and is defined as: $Z_R = \frac{\pi w_0^2}{\lambda}$, where w_0 is the beam waist and λ is the wavelength used.

For a Gaussian beam, w_0 is related to the focal spot size. For the F/2 parabola where a focal spot of $2.5 \mu\text{m}$ is achieved, the Rayleigh range is $10.4 \mu\text{m}$.

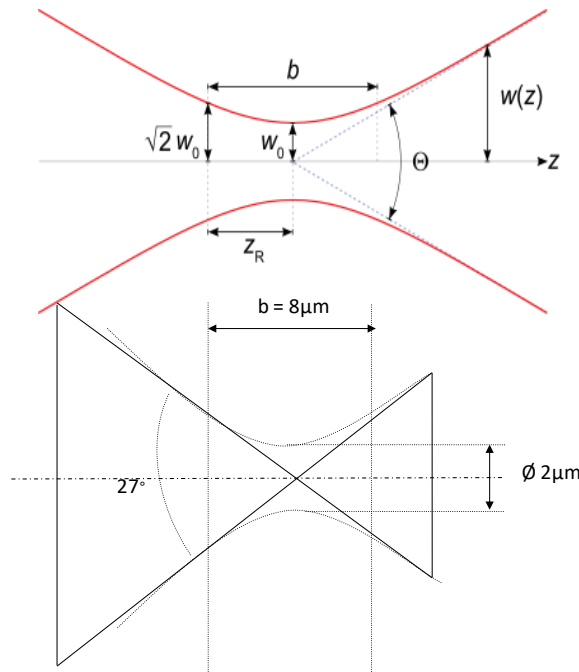


Figure 2.4 Representation of Gaussian beam in which target needs to be positioned within depth of focus [32].

The beam characteristics described highlight the importance of accurate target positioning since if the target is out of focus by just a few micrometres, the intensity can be halved. The positioning and orientation of the target in space is therefore of vital importance because of the short Rayleigh range of the F/2 parabola. Ideally, this loss in

intensity is minimised by keeping the target within $\pm 1 \mu\text{m}$ of the beam waist (Figure 2.4). However, for practicality, achieving target positioning within $\pm 4 \mu\text{m}$ (i.e. the depth of focus b of the beam) is considered satisfactory with respect to the capability of current target positioning system of CLF's Gemini high-power laser (Figure 2.4). As such, in this research, $\pm 4 \mu\text{m}$ has been used as the required target position accuracy in the z direction.

The current method of positioning of target is to image the rear surface of the target to ensure that it is in the same plane as the focal spot of the laser. For this purpose, a Mitutoyo microscope objective with a long working distance (13 mm) is used [43,45].

2.3.1.3 u and v -laser plane

The tip (u) and tilt (v) rotations are required to ensure that the front plane of the wafer is perpendicular to the axis of the laser. This is required to ensure that the x , y and z target positions are kept within the x , y and z position specifications during the rotation of the target wheel [32]. It is important to understand that misorientation of target will cause translation in z , resulting in de-focus of the laser [45].

2.3.1.4 Rotation of target – w

To supply large number of identical targets for a high-repetition rate operation, a target wheel system is used. Targets are patterned on the wafer target sector using a MEMS technique. The target sectors are placed around the circumference of the wheel (see Figure 2.5 and 2.6), so that the wheel rotation w delivers targets into the focal spot of the laser. It is required that the x , y and z positions of each target are within the position specification during the complete wheel rotation.

2.3.1.5 Motions for target alignment

For the accurate position and orientation of the target in space, translational and rotational motions, as shown in Table 2.1, are required by the target positioning system (i.e. motion control system).

Table 2.1 Motions required by the target positioning system [6,32].

Name	Description	Reference axis required during rotation	Motion required
x	Linear – horizontal – perpendicular to axis of laser beam – parallel to chamber floor	None	To get the spot in the centre of the target
y	Linear – vertical – perpendicular to axis of laser beam – perpendicular to chamber floor	None	To get the spot in the centre of the target
z	Linear - along axis of laser beam	None	To get the target in focus
u	Rotation around x axis	Target	To make wafer plane parallel to laser plane
v	Rotation around y axis	Target	To make wafer plane parallel to laser plane
w	Rotation around z axis	Central axis of wheel mount	To move between targets on a radial pattern

As shown in Table 2.1, target wafer needs five degrees of freedom (x, y, z, u, v) with low range and high resolution for positioning of the target relative to the laser focal spot and the focal plane. In addition, a secondary rotation stage (v_b) is needed to turn the wafer at an angle to the laser beam to ensure that any debris or unexpected reflections do not occur which may damage valuable tools/equipment. This functionality can be achieved

by the v motion as shown in Table 2.1. A high-speed rotational motion (w) is required to rotate the target wheel to deliver targets to the laser focal spot with high repetition. All linear axis planes and the rotation axis need to be referred to the focal spot and focal planes, except for the w rotation, to avoid the target positional deviations.

To fulfil the position specifications and the motion requirements, a five degree-of-freedom (DOF) motion control system, known as high accuracy microtargetry system (HAMS), has been designed and developed for accurate position and orientation of the targets for the high-power Gemini laser to run at high-repetition rate [4]. An additional motor added to the HAMS system provides the wheel's rotational motion (w). In that sense, HAMS can be said to have six DOFs.

2.3.2 Main features of HAMS system

2.3.2.1 Stages

Figure 2.5 shows the motion stages and other features of the HAMS. An x, z linear translation stage with a tripod attached to the top allows the stages to achieve the required positions. A target interface wheel sits on the rotating platform of the tripod. A rotatory motor actuates the rotating platform mounted on the moving platform of the tripod. The positioning of a target needs to be within an accuracy of $\pm 4 \mu\text{m}$ in the direction of the laser (z) to ensure it is within the laser focus. Furthermore, positional accuracy in the x and y needs to be of $\pm 10 \mu\text{m}$ [4,6,32].

2.3.2.2 Interface wheel

To ensure that the targets can be attached to the stages, an interface wheel is needed (Figure 2.5*d*). The wheel is essentially the target mount. The interface wheel needs to be flat ($1.4 \mu\text{m}$) since any movement in the z direction would take the target out of the focal

plane. A machined ceramic wheel with good thermal stability is used for the target mount.

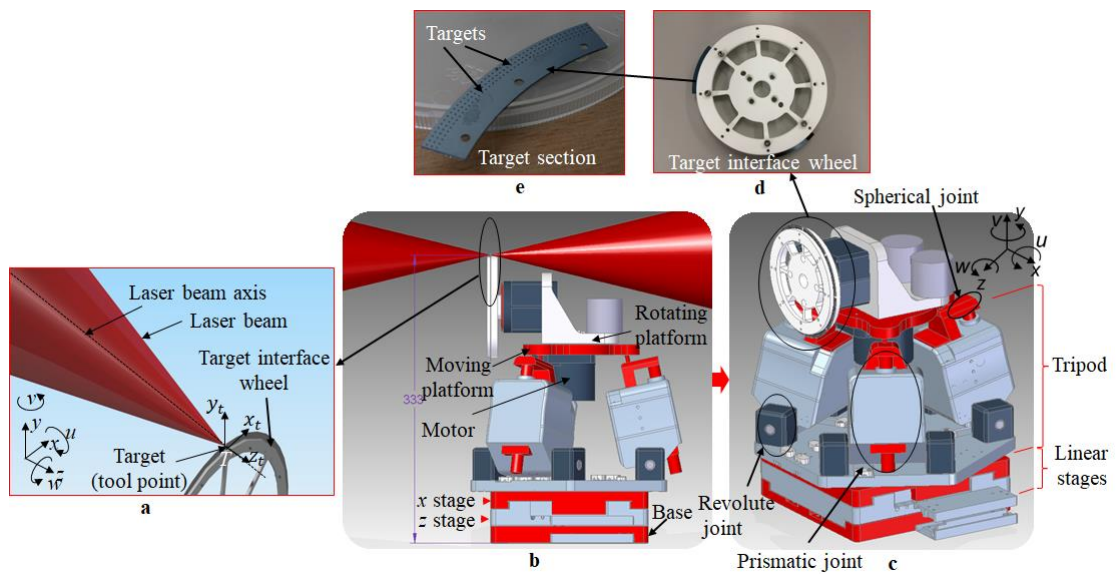


Figure 2.5 HAMS for the high-power high repetition rate laser operations: (a) laser beam-target interaction; (b) HAMS with the target interface wheel; (c) features of HAMS; (d) target interface wheel with two target sections; (e) targets patterned around the circumference of a target section.

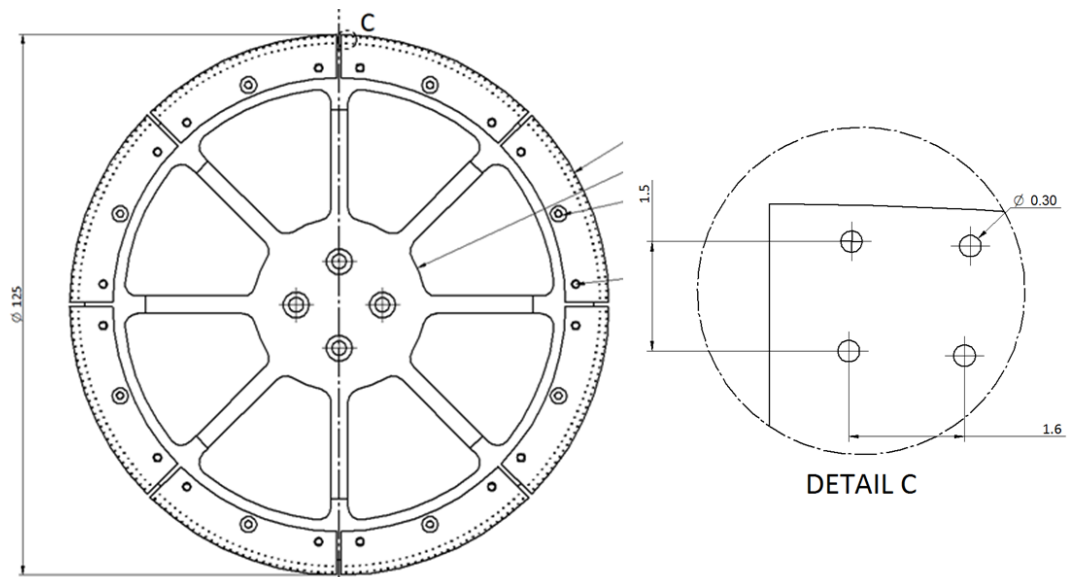


Figure 2.6 Eight silicon wafer target sectors attached to the interface wheel (scale in millimetre). Microtargets are patterned around the circumference of the sectors [32].

2.3.2.3 Target sectors

For HAMS system, MEMS based silicon wafer target sections are mounted on the interface wheel as shown in Figure 2.5e and 2.6. Each target section can be designed for a number of different target sizes but essentially the targets are patterned around the circumference of the section. MEMS based silicon target sections are usually very flat (less than 0.5 μm) [32,42].

2.3.1 Performance of HAMS

HAMS provides the necessary motions, as shown in Table 2.1, for the target alignment. However, target alignment for high-power laser operations depends on a number of factors. For example, Table 2.2 shows typical sources of error in a target alignment process, how they affect the position and orientation of the target and what motions of HAMS are required to correct the resulting position and orientation error of the target.

Table 2.2 Possible sources of error in HAMS [4,32,33,42].

Source of error	Impact	Related motion of HAMS
Flatness of wafer target	Target falls out of focus	z
Mechanical mounting of wafer to mount	Target falls out of focus	z
Wobble of rotating stage	Target falls out of focus	z
Eccentricity of rotating stage	Laser misses target	x, y
Wobble of the target interface wheel	Target falls out of focus as planes not maintained.	u
Laser Pointing jitter	Laser misses target or falls out of focus	x, y, z

The ability of HAMS to position and orientate the targets within the specifications (see section 2.3.11 to 2.3.14) depends on HAMS' performance in terms of its positional and orientation accuracy, which can be affected by different errors, especially kinematic

errors. Kinematically, HAMS has a hybrid mechanism – a combination of serial and parallel mechanisms (see section 3.1.3 and Chapter 5). While the performance improvement of a hybrid mechanism is discussed in Chapter 3, some important aspects of the performance improvement of a mechanism are reviewed in the following sections.

2.4 Accuracy of a mechanism

According to Miller [46], accuracy is “qualitatively, the ability to achieve with precision the true measurement quantity of a product characteristic or related process parameter”. Precision is “the ability to obtain the same measured quantity value over multiple attempts”, while the trueness is “the closeness of the average of repeated measurements to the measurand value that is consistent with its definition”. The three concepts are often explained with the example of an archer’s attempts to hit the bull’s eye of a target. A well-grouped (i.e. repeatable) set of attempts may be said to have precision. When the average position over a sufficient number of attempts is compared with the true value, it represents trueness. Accuracy depends on both trueness and precision, as shown in the Figure 2.7.

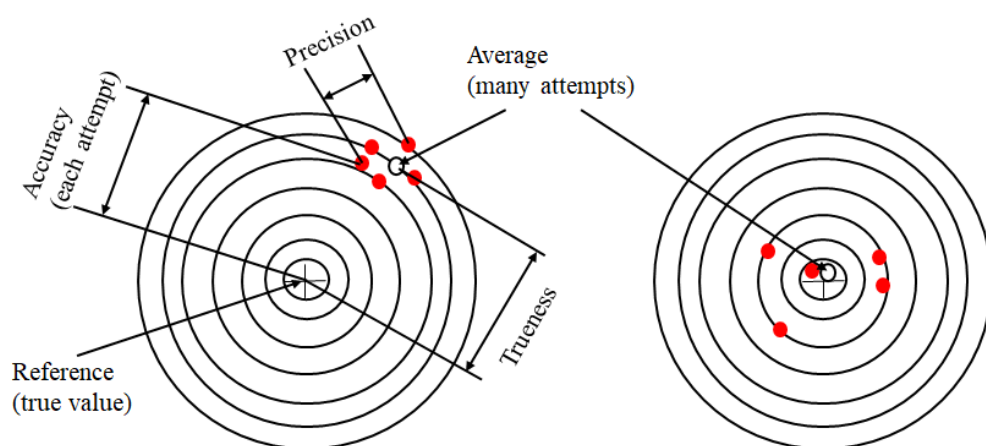


Figure 2.7 Accuracy, precision and trueness; trueness dominated accuracy (left) and precision dominated accuracy (right).

2.4.1 Errors and accuracy

Mechanical devices and structures used in precision operations, such as a computer numerical control (CNC) machine or a coordinate-measuring machine (CMM), are basically closed structural loops which maintain a relative position between two components in a loop. For example, a machine tool can form the following loop: the spindle shaft, the bearings, the housing, the guideways, the drives and the tools [47]. The critical ‘open’ connection in the loop is between the work surface and the tool [48]. Any positional error between tool and work surface will result in a dimensional error on the part surface (tolerance, form, surface, sub-surface damage and so on). Thus, anything that contributes to a positional error must be determined as per the ‘deterministic’ design philosophy of Donaldson and Bryan [48-50].

If ‘error’ can be defined as any deviation in the position of the tool point or ‘end effector’ from the theoretically required value to produce a workpiece of the specified tolerance, the ‘accuracy’, on the other hand, can be alternatively defined as the degree of agreement or conformance of a finished part with the required dimensional and geometrical accuracy [48]. As such, the extent of error in machine gives a measure of its accuracy, which is actually the maximum translational error between any two points in the work volume of the machine [14].

Given that in instruments, mechanisms and machines (called only “mechanism” hence forth) many parts interact to achieve a final accuracy and each part contributes to the total error of the mechanism, keeping track of these errors becomes a complicated work for designers and engineers. The best way to keep track of the errors is to formulate an ‘error budget’ [48,51-53]. An error budget allocates resources among the different components of a mechanism. It is considered as a system analysis tool used for the prediction and control of the total error of a mechanism [52]. An error budget can also

be a useful tool to keep track of the errors that occur between the measurement point and the feedback point, which are not the same for a mechanism [14,54].

2.4.2 Sources of error

Although the accuracy of a precision mechanism can be affected by many error sources, the following are considered as the major sources affecting the accuracy of the relative end-effector position and orientation [14,47,55]:

- 1 geometric and kinematic errors;
- 2 thermo-mechanical errors;
- 3 loads;
- 4 dynamic forces;
- 5 motion control and control software.

The first three types of the error belong to quasi-static errors, whereas the fourth and fifth types belong to dynamic errors. Quasi-static errors slowly vary with time and related to the structural loop of the machine. The dynamic errors are more dependent on the particular operating condition.

Quasi-static errors are considered as 70% of the total error of a machine tool [14]. Other error sources may cause a change in the geometry of the machine's components present in the machine's structural loop, resulting in error in the final position and orientation of the tool point or end effector. The magnitude of this positioning and orientation error depends on the sensitivity of the machine's structural loop to various error sources [47].

2.4.3 Description of kinematic errors

Geometric errors are due to the imperfect geometrical features of a mechanism's structural components, for example, machine tool guideways, machine bed, bearings,

carriages, lead-screws, rams, and their misalignment in the machine structural configuration [56,57]. Geometric errors can be ‘systematic’, ‘hysteresis’ or ‘random’ in behaviour [52,56]. Kinematic errors are due to the relative motion errors of several moving components in a mechanism and arise from geometric errors. Kinematic errors occur during the execution of linear, circular or other types of interpolation algorithm and are more pronounced during actual machine operations [45,56].

To take a closer look at the nature of kinematic errors, consider the motion of a simple one-axis mechanism, as shown in Figure 2.8 [48]. With respect to a typical mechanism and its behaviour, six DOF relative to the three axes (x , y and z) of motion can be identified - three translational motions along the x , y and z and three rotational motions about the x , y and z axes. Three rotational DOFs associated with any of the three axes are traditionally referred as “roll” (rotation about x , affecting y and z axes), “pitch” (rotation about y , affecting the x and z axes) and “yaw” (rotation about z axis, affecting the x and y axes). Thus, all rigid bodies have three translational and three rotational error components associated with their motions. However, altogether there are 21 kinematic errors, arising from the geometric sources, on a three-axis mechanism, e.g. a machine tool [48]:

1. Linear displacement errors from three axes (3×1)
2. Vertical straightness errors from three axes (3×1)
3. Horizontal straightness errors from three axes (3×1)
4. Roll angular errors from three axes (3×1)
5. Pitch angular errors from three axes (3×1)
6. Yaw angular errors from three axes (3×1)
7. Squareness or orthogonality errors from three planes (3)

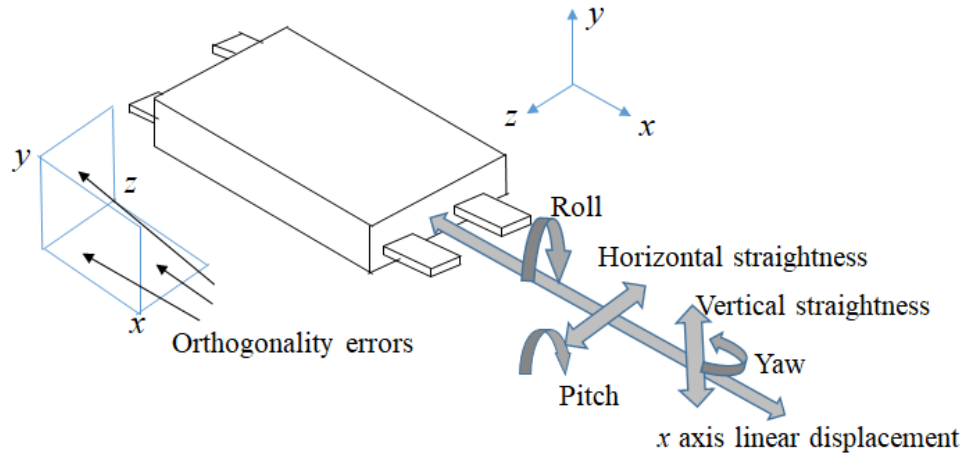


Figure 2.8 Kinematic errors of a one-axis mechanism [58].

2.5 Measurement errors

Design considerations for a precision mechanism are directly affected by some key measurement principles. Non-adherence to these principles gives rise to measurement errors, leading to incorrect information about the position of the tool/target/end-effector of a mechanism. While improving the performance of a mechanism, the quantification of the measurement errors and their effects on the positional deviation of the target/tool/end-effector of the mechanism are needed.

An important principle is called the Abbe principle, which Bryan (1979) considers to be ‘the first principle of machine tool design and dimensional metrology’ [59]. The Abbe principle, first formulated by Ernst Abbe in 1890, states that a measurement system shall be collinear with the axis along with the displacement is to be measured [60-62]. This principle is often explained with a two-dimensional calliper measuring a circular object as shown in Figure 2.9. Two lines are important in this measurement operation – the horizontal line of motion at the functional point (FP) where measurement needs to be taken and the measurement line at the effective point (EP) where the measurement is actually taken. Displacement measurement at the actual plane BB, instead of the ideal measurement plane AA, causes non-coincidence of EP and FP,

resulting in Abbe error ϵ_{Abbe} . Due to this error, the L distance in the calliper will be read as L_{error} , where $L_{error} = L + \epsilon_{Abbe}$.

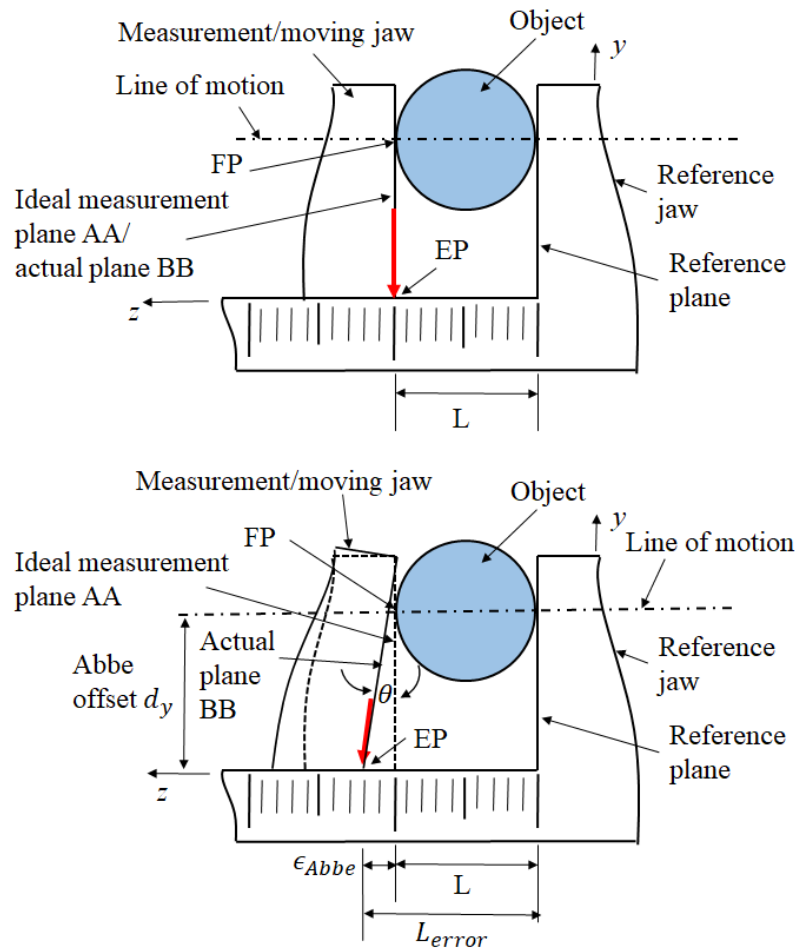


Figure 2.9 A 2D depiction of a calibre when measuring a circular object: a perfect measurement with no error (top); measurement with Abbe error (bottom).

In addition to Abbe error, a cosine error can also affect the measurement results. The cosine error occurs when the measurement axis is not parallel to the motion axis, which means the measurement axis is not properly aligned to the motion axis [62]. As shown in Figure 2.10, the cosine error can be calculated as,

$$\epsilon_{cost} = L_{error} - L = L_{error} - L_{error} \cos \alpha_x = L_{error}(1 - \cos \alpha_x) \quad (2.8)$$

Another error, called the sine error, can also be present in a measurement system. This error is commonly seen in the cases when a measurement system requires a

mechanical contact, such as a micrometre or a tactile probe, to perform a measurement [62]. Also, the sine error occurs when a cosine error is present.

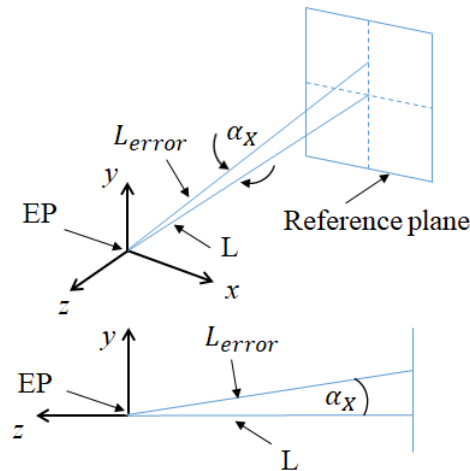


Figure 2.10 A one-dimensional depiction of cosine error [62].

2.6 Methods of error elimination

One of the main performance criteria of a modern production facility is its ability to manufacture accurate workpieces. In fact, the increasing demand for complex workpieces with shorter product life cycles and the small-scale production have made the importance of the accuracy improvement of the machines/mechanism more than ever [47]. There are fundamentally two types of strategy for the accuracy improvement of a mechanism: error avoidance and error compensation [14,16]. The first approach aims to build a more accurate mechanism through design and manufacturing so that the sources of error are minimised. However, it is a costly strategy, and very often results in over-designing. On the other hand, the aim of the error compensation is to build a relatively lower grade machine with higher accuracy at lower cost. Error compensation is now considered as the primary method of error reduction in industry [14].

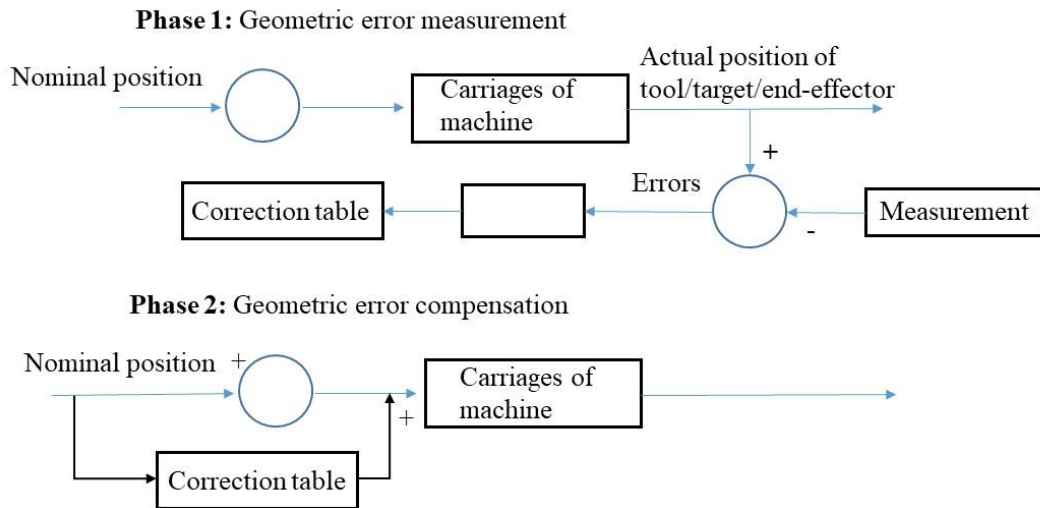


Figure 2.11 Pre-calibrated error compensation.

There are two approaches for error compensation: pre-calibrated error compensation and real-time error compensation. In the first type, the error is measured either before or after the calibration operation and then corrections are applied to the measurement system by software compensation (Figure 2.11). As such, calibration and compensation can take place at significantly different times. The other approach for error compensation is a closed loop technique with the need for built-in metrology, which means the errors are monitored during a process, for example machining, and the compensation is carried out continuously as and when the machine/mechanism is in operation to constantly correct the inaccuracies (Figure 2.12) [14,16].

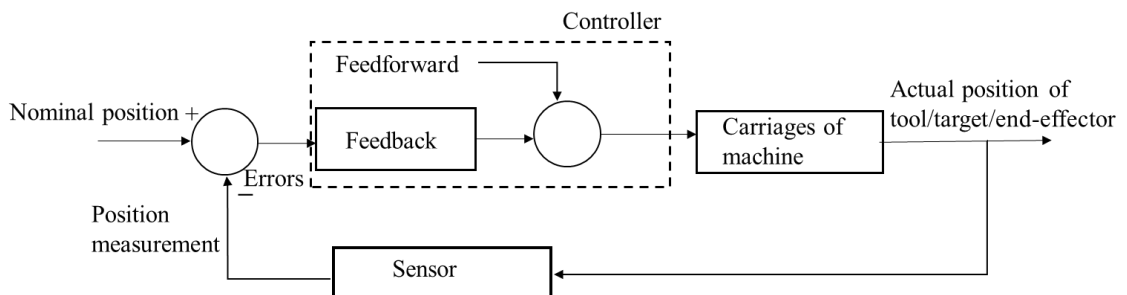


Figure 2.12 Real-time error compensation.

As mentioned in section 2.5.1, since the accuracy of a machine is affected by the interactions of the error sources, dealing with these errors individually should be

replaced with a continuous basis. In other words, the error compensation techniques can be broadly categorised as static error compensation and dynamic error compensation. As such, the pre-calibrated error compensation dealing with the systematic errors of the machine/mechanism is static compensation techniques. The real-time compensation, on the other hand, is a dynamic compensation. This technique is desirable in industry since it involves a combination of high accuracy, low cost and high production rate [14,47,49,52]. It is to note that error compensation techniques are not concentrated with reduction of the absolute value of the errors, but simply to reduce the effect of the errors on the accuracy of the machine or mechanism's operation.

2.7 Conclusion

High-power lasers have seen significant development in the last few decades. To utilise the full potential of high-power lasers, large-scale facilities need to operate at high-repetition rates, which presents many engineering challenges. One such challenge is the positioning and aligning of a micro-scale target relative to the focus of the laser beam(s) with an accuracy of few micrometres to ensure that targets are reproducibly accessible to the highest intensities available, that is in the region of the laser beam focus as determined by the Rayleigh range. Fulfilling this requirement for a high-repetition rate laser system means that new targets have to be positioned and aligned at the laser beam focus at a high speed (at least 0.1 Hz).

To develop an automated solution for target alignment for high-repetition rate laser operations, it is important, as has been shown in this chapter, to understand the accuracy requirements (i.e. specifications) for the target positioning and alignment, the desired motions to meet the specifications and the characteristics of the motion control system used. Since the ability of the motion control system to position and orientate the target to the specifications depend on a number of factors, including the kinematic errors

arising from the geometric errors of a mechanism, the main sources of error of a mechanism and the common methods of error elimination are discussed in this chapter.

The background literature presented in this chapter is important to understand the various issues in relation to the two types of performance improvement strategy - pre-calibrated error compensation (calibration in short) and real-time error compensation – of a parallel or hybrid mechanism. As will be seen in the next chapter, the performance improvement of a parallel or hybrid mechanism through error compensation can be a complicated process due to the complexities of the kinematic characteristics of a parallel or hybrid mechanism. Hybrid and parallel mechanisms are new breed of mechanisms as compared to the traditional serial mechanisms, and comprehensive studies of these new mechanisms in terms of their designs, kinematics, dynamics and performance improvements are lacking. In the next chapter, research gaps are identified while reviewing the literature involving the performance improvement techniques used parallel and hybrid mechanisms. In addition, a brief introduction of the parallel and hybrid mechanisms in terms of the characteristics of their kinematic structures is given at first.

Chapter 3 - Performance improvement of hybrid mechanism

3.1 Kinematic structure

All machines or mechanisms have structures made up of different parts. One of the first considerations in the design of a structure is choosing how the parts of the structure move in order to perform the functions for which the structure is designed [63,64]. Essentially, a kinematic structure represents the kinematic chain or loop without considering the detailed geometric, kinematic and functional aspects of the mechanisms used. A kinematic chain can be described as a set of rigid bodies attached to each other. For a metal cutting machine, a kinematic chain shows the flow of the motion in a kinematic structure using all axes, the work piece, the tool and the bed of the machine [15,65].

Kinematic structures can be arranged in serial, parallel and hybrid (combination of serial and parallel) kinematic relationships, with different numbers of links and connections to satisfy the functional requirements. The mobility of the kinematic structures will depend on the number of joints and links, and the joints' DOF, as can be determined by Equation (3.1) [66]

$$M = 6(n - 1 - j) + \sum_j f_j, \quad (3.1)$$

where n is the number of links in the mechanism, j is the number of joints and $\sum_j f_j$ is the total number of DOF of the joints.

3.1.1 Serial kinematic structure

3.1.1.1 Characteristic features

Traditional precision machines and most industrial robots are based on serial kinematic structures (only having one open kinematic chain), in which multiple parts (considering the parts as rigid bodies, ignoring elasticity and any deformation caused by

large load conditions) are connected in series (Figure 3.1 and Figure 3.2). The two most commonly used engineering joints used in serial structure are (1) prismatic joints (allows two links to produce relative displacement along the common axis), and (2) revolute joints, pivot joints or pin joints (allows two links to produce relative rotation about the joint axis). Combining these two types of joints, many useful mechanisms are made for precision machines and robots. [67,68].

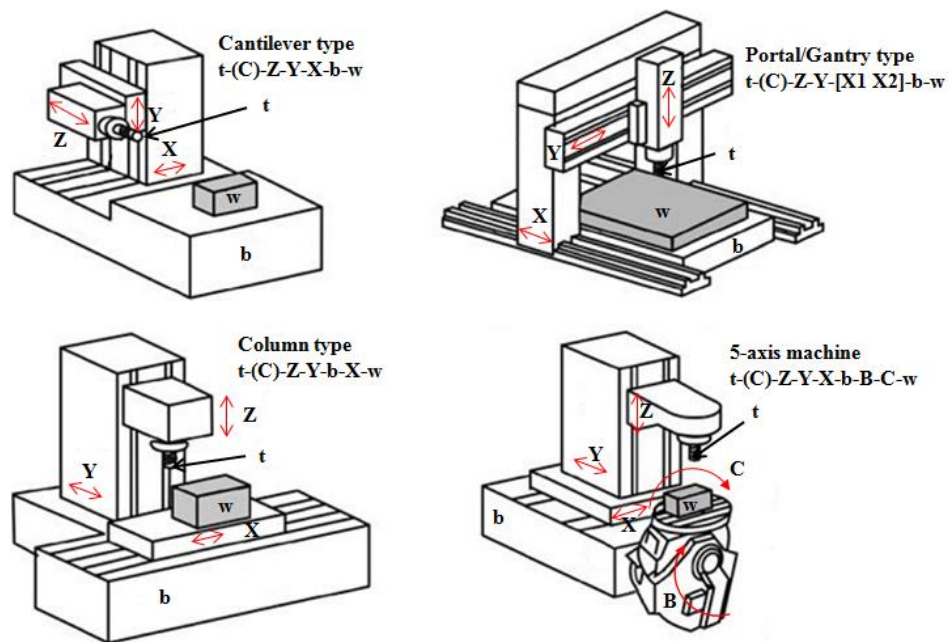


Figure 3.1 Serial kinematic machines abstracted to kinematic chain (t: tool, b: bed, w: work piece) [56].

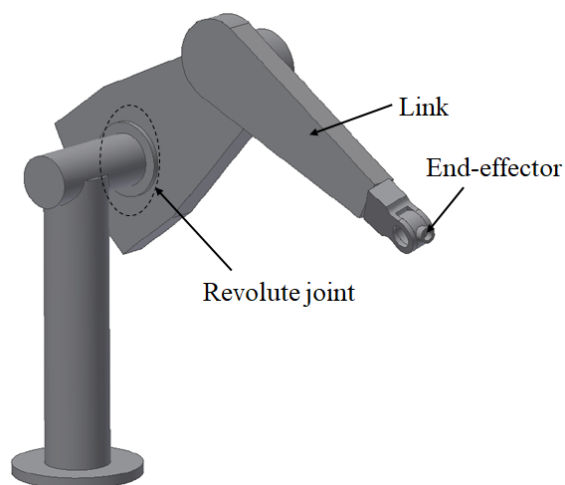


Figure 3.2 A schematic of 6-DOF Puma robot (serial kinematic structure).

3.1.1.2 Benefits and limitations of serial kinematic structures

Serial kinematic machines usually have the advantages of a well-defined structure and configuration and have comparatively large working volumes of simple shape. In serial structures, the direct correlation between positioning actuators and machine axes means the machine and workpiece coordinate systems can be the same, resulting in straightforward control of the structure [69]. On the other hand, serial machines suffer from large bending moments and second moments of mass, especially at the extremes of axis travel if large masses are to be moved. Furthermore, these machine structures are highly dependent on the precision of each positioning element in the kinematic chain and are prone to compound error [69,70].

3.1.2 Parallel kinematic structures

3.1.2.1 Characteristic features

Parallel kinematic structures, which include parallel mechanisms and parallel machines, have closed kinematic chain or loop architectures in which the end effector is connected to the base by at least two independent kinematic chains [71]. In parallel structures, the positioning actuators are arranged in parallel rather than being stacked one on top of the other, requiring all the actuators to move simultaneously to effect any change in end effector position or orientation [69].

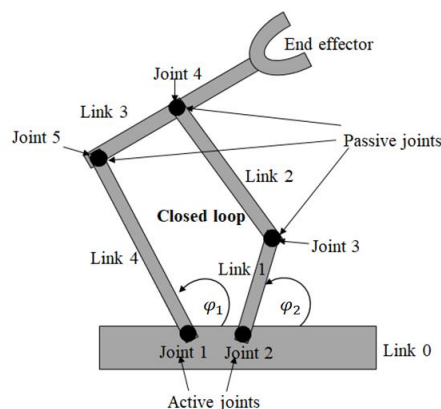


Figure 3.3 Five-bar-link parallel kinematic structure.

To illustrate the principles of parallel kinematic structures, consider the following example [67,72]: Figure 3.3 illustrates a five-bar linkage kinematic structure in which five links (including the base link) are connected by five joints, therefore, having a mobility of two. Essentially, two serial linkages are connected at a particular joint, point A, thus forming a closed kinematic chain and indicating that serial linkages must conform to a geometric constraint. Here, if two of the five joint angles are known (φ_1 and φ_2 in Figure 3.3), the position of the end effector can be determined. By controlling joints 1 and 2 with two actuators, the end effector can be positioned within the vertical plane of the structure. Thus, only two joints are active joints, driven by independent actuators, while the other two joints are passive joints, which are free to rotate [72].

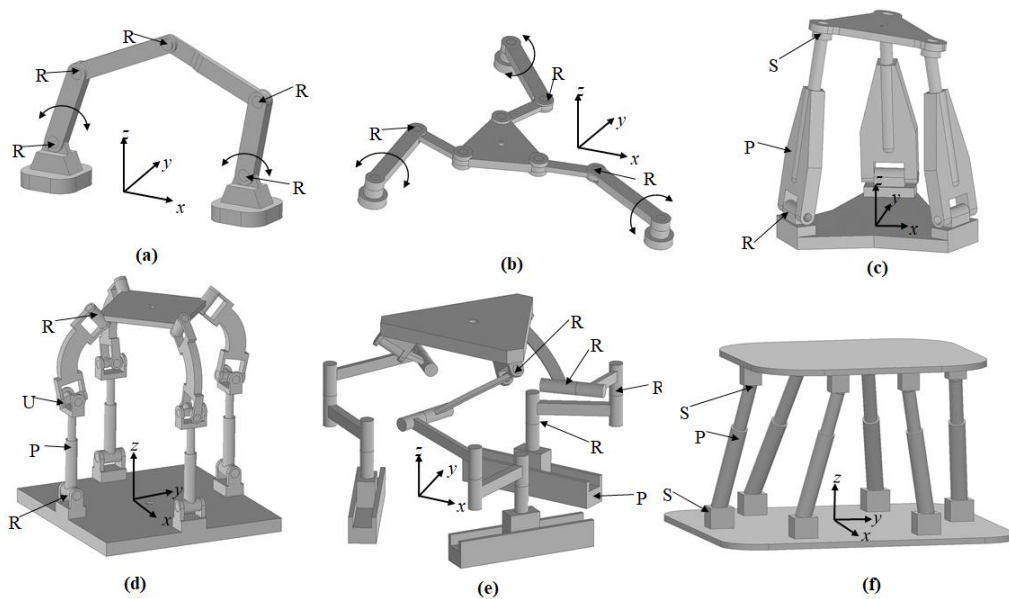


Figure 3.4 Some parallel kinematic structures (R, P, S and U denote revolute, prismatic, spherical and universal joints respectively): (a) two degree of freedom 5R structure, (b) three degree of freedom planar 3-RRR structure, (c) three degree of freedom 3-RPS structure, (d) four degree of freedom structure with four RPUR chains, (e) five degree of freedom structure with three PRRRR chains, (f) six degree of freedom general Stewart platform.

In Figure 3.4, some examples of different classes of parallel structure are shown [71,73]. Note that a parallel kinematic structure's characteristics can be described symbolically by showing the types of joint present in the kinematic chain or leg, and by stating the number of kinematic chains/legs available in the mechanism, for example, a 3RPS mechanism has three legs and three types of joint, namely revolute (R), prismatic (P) and spherical (S).

3.1.2 Benefits and limitations of parallel kinematic structures

Parallel kinematic structures offer higher stiffness, lower moving mass, higher acceleration, reduced installation requirements and mechanical simplicity as compared to existing conventional machines with serial kinematic structures [67]. The parallel structures have the potential to be highly modular, highly reconfigurable and high-precision machines [65,69,71].

Parallel kinematic structures have received considerable attention in industry. They have found their applications mainly in machine tools, medical applications for ophthalmic surgeries, manipulators (Delta robot for very fast pick-and-place tasks of light load, micromanipulator), flight/automobile/tank/earthquake simulators, and precision positioning for very large telescopes, receiving antennas and as satellite platforms for manoeuvring in space [71,74,75].

However, parallel kinematic structures have some limitations that pose challenges to their widespread adoption [76,77]:

A. The main disadvantage of parallel structures is the limited workspace and the difficulty of their motion control due to singularity problems. Singularity is a point in the workspace where a kinematic machine/mechanism cannot move its end effector due to certain geometric configuration(s) of the structure, for example, collinear alignment of two or more axes of a robotic structure.

- B. Parallel structures have more complex working envelopes than traditional serial machines. These working envelopes often take the form of an onion or mushroom and depend on the exact layout of the machine structure.
- C. Many parallel structures have limited ranges of motion, particularly rotational motion.
- D. The positioning and orientation inaccuracies of parallel kinematic structures can stem from a number of sources: manufacturing errors of parallel structure elements, assembly errors, error resulting from distortion by force and heat, control system errors and actuator errors, errors due to overhanging structures, calibration and even the accuracy of the mathematical models used.
- E. The design-specific cost of parallel kinematic structures in comparison with conventional machines can be high.

3.1.3 Hybrid kinematic structures

In recent years, many new types of parallel structures have been developed to enhance the capabilities and performance of parallel kinematic machines, such as maximising workspace, and increasing rotational capability [78]. However, considering that some limitations are inherent to parallel kinematic structures, a new shift in addressing the issues with parallel structures has occurred, motivating researchers to look at hybrid structures, which consist of parallel and serial kinematic structures. This shift, in fact, has created new research and development needs and promises interesting innovations in design [79].

A mechanism with a hybrid structure is a combination of serial and parallel kinematic structures to exploit the advantageous characteristics of both. This is generally implemented by either connecting two parallel structures in series (one of the parallel structures is the upper stage and the other is the lower stage, where the moving platform

of the lower stage is the base platform of the upper stage) or connecting the series and the parallel structures in series [67]. Mechanisms with hybrid structures, as compared to the mechanisms with parallel structures, can improve the ratio of workspace to architecture size and accuracy.

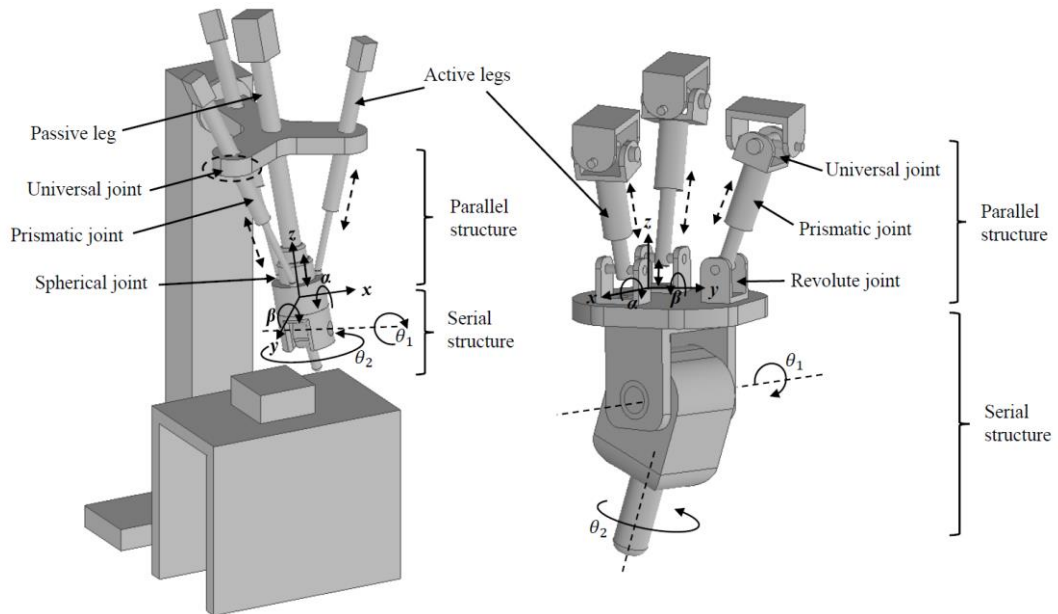


Figure 3.5 Schematic representation of two types of hybrid mechanism: Tricept (left) and Exechon (right).

To understand how a hybrid structure can be designed for a mechanism to achieve five degrees of freedom of motion, consider the following design options [73]:

A. A structure can be arranged such that the upper stage provides the motions of three degrees of freedom (rotations about the x and y axes and a translation along the z axis), while the lower stage provides the motions of two degrees of freedom (translations along the x and y axes). The hybrid motions (five degrees of freedom) of the structure can be realised in two ways:

1. 3SPR (spherical-prismatic-revolute) as upper stage and ‘liner guiding system’ as the lower stage.
2. 3SPR as upper stage and 3RRR (three revolute joints), which is a planar

parallel structure, as the lower stage.

B. The hybrid structure can also be arranged such that the upper stage provides the motions of three degrees of freedom (translations along x , y and z axes), while the lower stage provides the motions of two degrees of freedom (rotations about the x and y axes). The motions of the structures can be achieved by a combination of a 3SRR parallel structure as the upper stage and a two-degrees-of-freedom spherical parallel structure as the lower stage. However, spherical parallel structures are complex to manufacture and have low stiffness, low precision and small workspace, hence, they are not currently popular in practice.

Among the early hybrid kinematic designs, the Tricept was considered as the first commercially successful hybrid machine tool [80]. The Tricept has a three-degrees-of-freedom parallel kinematic structure and a standard two-degrees-of-freedom wrist end effector (Figure 3.5, left). Another hybrid machine, the Exechon, was introduced later as an improvement over the Tricept design (Figure 3.5, right). The Exechon has an over-constrained structure with eight links and a total of nine joints.

3.1.4 Current research on parallel and hybrid kinematic mechanisms

Parallel mechanisms using parallel kinematic structures offer some unique benefits to some applications, and, as such, the design of parallel mechanisms and their adaptations to various applications are under active research. Researchers are also seeking solutions to overcome the limitations of the parallel mechanism, especially in the areas of singularity problem, working envelop optimisation and positioning and orientation inaccuracies [76-78]. The performance improvement of the parallel mechanism in terms of positional and orientation accuracy represents a significant challenge. In all parallel mechanisms, various types of geometric error can be related to some physical errors, particularly machining and assembly errors of the mechanism,

such as platform frame errors, revolute joint errors and spherical joint assembly errors. Theoretical analysis to understand the effects of all these physical errors can be a complex and time-consuming process. Although some studies have been pursued to understand the effects of the significant geometric errors of some parallel mechanisms [80-81], in most cases, the actual effects of the errors on the final position of the target remain unclear, since it is assumed that some error averaging effects take place for the parallel mechanisms as opposed to the cumulative addition of errors for the serial mechanisms.

As for the hybrid mechanisms, although hybrid structures have recently received much attention, and research is underway on how to use them in industrial applications, e.g. machine with high-accuracy motion over a relatively larger workspace, comprehensive studies of the mechanism's design, kinematics, dynamics and error sources are lacking [82,83].

Since a major focus of this research is to improve the performance of the hybrid mechanism in terms of position and orientation accuracy, the following sections present the findings of an in-depth literature survey of the state-of-the-arts of two performance improvement approaches – kinematic calibration and real-time position control.

3.2 Calibration of hybrid mechanism

Although precision mechanisms consist of accurate mechanical components and their assemblies, the precision of their motion is affected by many error sources [21]. The final positional accuracy of a mechanism is predominantly influenced by the kinematic errors of the mechanism arise from the geometric errors, such as manufacturing and assembly errors of the joints, by load deformation due to external forces, and by thermal deformation [21,84]. Kinematic errors are considered as the main sources of error for a mechanism.

The above statements regarding kinematic error and accuracy are true for the serial mechanism as well as for the parallel and hybrid mechanism [21]. However, some researchers report that compared to serial mechanisms, parallel and hybrid mechanisms' performance in terms of accuracy can be limited by their large number of links and joints [85]. Irrespective of the mechanism, as indicated in section 2.7, the errors need to be eliminated with an appropriate error compensation method rather than changing the structure or design of the mechanism, which is often expensive. One method to compensate for geometric errors is to carry out kinematic calibration and adjustment (hereafter, just called calibration). In the following sections of the literature survey, various aspects of the kinematic calibration of serial and parallel mechanisms are discussed to identify the research gaps.

Kinematic calibration of a mechanism (serial or parallel) can be defined as a procedure to estimate the numerical values of the errors, which represent the differences between the actual and nominal values of the kinematic parameters to better describe the kinematics of the mechanism, and these values are used to improve the mechanism's accuracy by acting on the mechanism's controller [21]. Generally, the calibration process has four steps: development of a model to relate the 3D Cartesian position of the end-effector (or target) to the kinematic parameters of the mechanism; acquisition of the actual end-effector positions and orientations using a measuring instrument; identification of the kinematic error parameters based on the model and measurement; and error compensation by adjusting the parameters of the controller [86].

3.3 Method of kinematic calibration

Although the methodology for the calibration of serial, parallel and hybrid mechanisms fundamentally follows the same procedure, a number of issues make the development of a calibration process for a parallel or hybrid mechanism more difficult

than for a serial mechanism. For the sake of the convenience of the discussion, the four-step calibration method is described at first, and then the challenges of developing a kinematic model for a parallel mechanism is discussed with appropriate references to the research works in the field of calibration of the parallel mechanisms.

3.3.1 Model for kinematic calibration

Works related to the model development for the calibration actually involves two steps: kinematic model and error model [87].

3.3.1.1 Kinematic model

For a mechanism to perform a task, the location of the end effector relative to a global reference coordinate system (often it is the base of the mechanism) needs to be established. This is called position analysis problem [72]. Kinematic model is required to solve this problem. There are two types of kinematic model for solving position analysis problems: forward or direct kinematic model and backward or inverse kinematic model. For direct model, the joint variables are given, and the model computes the location of the end-effector. On the other hand, inverse model determines the joint variable that are necessary to bring the end effector to the desired location [24,72]. Both types of model generally come into play during the kinematic calibration of the mechanisms. In most cases, especially for the serial mechanism, direct kinematic model is used in the first phase of the calibration (i.e. model development). The inverse kinematic model is required during the implementation phase of the calibration (i.e. last phase or compensation phase).

A number of different kinematic models are available for the kinematic analysis of the kinematic mechanisms. For example, vector algebra method by Chase (1963) and Lee and Liang (1988); the geometric method by Duffy and Rooney (1975); Denavit and

Hartenberg (4×4 matrix method), the screw algebra method and so on [72,89,91]. However, the Denavit and Hatenberg method (or D-H method in short) based on homogeneous transformation matrix (HTM) is the most popular one for the kinematic analysis of the mechanisms due to its explicit physical interpretation of mechanisms and the relatively simple implementation in the programming of the mechanism [88]. In this method, coordinate systems are assigned to each joint and then each coordinate system is related to the next one through a specific set of coefficients in the HTMs:

$$\mathbf{T} = \mathbf{A}_1 \cdot \mathbf{A}_2 \cdot \mathbf{A}_3 \dots \mathbf{A}_n \quad (3.2)$$

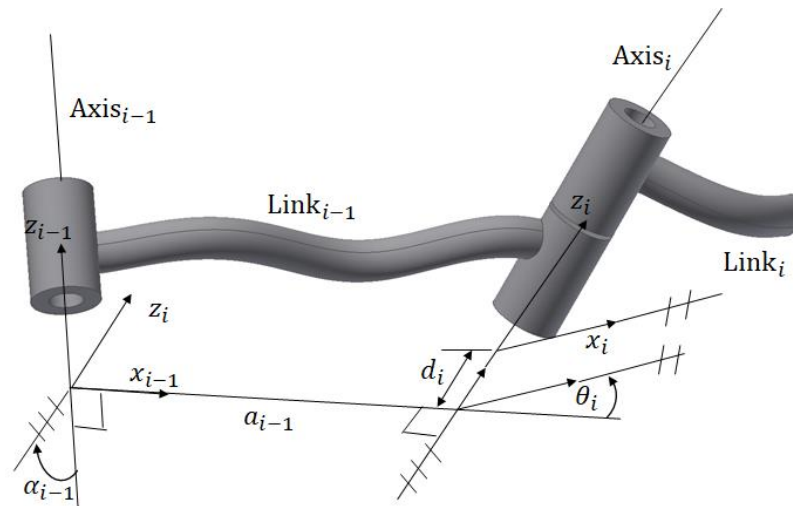


Figure 3.6 D-H parameters representation for a revolute joint.

Figure 3.6 shows the spatial relationship between two consecutive links and their associated coordinate systems according to the D-H method. The spatial relationship between two consecutive links is a function of the joint type connecting them together. A number of rotations and translations are required for the transformation, as summarised below

$$\mathbf{A}_i^{i-1} = \mathbf{T}(z, d)\mathbf{T}(z, \theta)\mathbf{T}(x, a)\mathbf{T}(x, \alpha), \quad (3.3)$$

where a_i represents the offset between two adjacent joint axes,

d_i is the translational distance between two incident normal of a joint axis,

α_i is the twist angle between two adjacent joint axes, and

θ_i represents the joint angle between two incident normal of a joint axis.

For D-H representation, equation (3.3) becomes

$$A_i^{i-1} = \begin{bmatrix} \cos \theta_i & -\cos \alpha_i \sin \theta_i & \sin \alpha_i \sin \theta_i & a_i \cos \theta_i \\ \sin \theta_i & \cos \alpha_i \cos \theta_i & -\sin \alpha_i \cos \theta_i & a_i \sin \theta_i \\ 0 & \sin \alpha_i & \cos \alpha_i & d_i \\ 0 & 0 & 0 & 1 \end{bmatrix}. \quad (3.4)$$

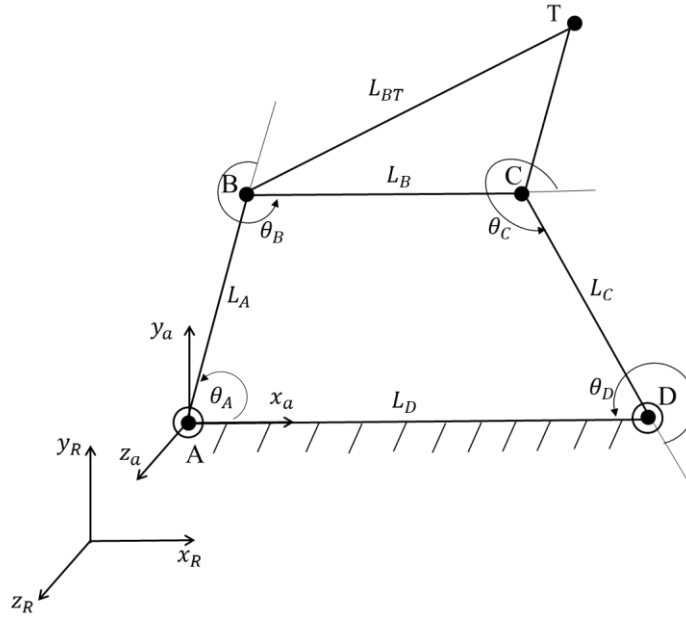


Figure 3.7 A simple closed loop mechanism with a 2D constraint.

Unlike open-loop mechanisms, all the coordinate systems in a closed loop mechanism are defined by the geometry of the linkages, such that the coordinates of the last linkage coincide with the base (zeroth) coordinate system, see example in Figure 3.7. In fact, while an open-loop mechanism can be described by one type equation, such as equation (3.4), two types of equations are needed for the modelling of a parallel mechanism with closed loops [72,90]:

1. An equation, such as equation (3.5), that shows the open-loop transformation to relate the end effector to the world coordinate or reference frame,
2. A closed loop constrain equation, such as equation (3.6), that shows closed loop transformation.

Figure 3.7 shows a simple closed loop mechanism with four links (L_A, L_B, L_C and L_D) with two joints A and D with motors to locate the target point T . The following two equations are required to describe the mechanism

$$\mathbf{T}_{target} = \mathbf{A}_{RA}\mathbf{A}_{AB}\mathbf{A}_{BT}, \quad (3.5)$$

$$\mathbf{T}_C = \mathbf{A}_{AB}\mathbf{A}_{BC}\mathbf{A}_{CD}\mathbf{A}_{DA} = \mathbf{I}, \quad (3.6)$$

where \mathbf{A}_{RA} is the HTM from the reference frame $x_R y_R z_R$ to joint A ; \mathbf{A}_{BT} is the HTM from the joint B to target T and so on; \mathbf{I} is the identity vector because of the return to the original system.

Although the D-H method is popular for modelling the mechanisms, it has several limitations, as following:

- A. In the D-H method, the link coordinate frames are located at the intersection of the joint axis and the common normal. This means that the link coordinate frames are function of the mechanism's geometry and a small variation in the geometry will cause the link coordinate frame to shift. This is a significant problem when developing modelling for the mechanism's calibration. In some modified D-H methods, the dependence of the common normal is eliminated so that the small deviations of the axis orientation can produce proportional changes to the parameters [90].
- B. Many serial mechanisms have revolute joints with nearly parallel axes, indicating no unique common normal as per the D-H method. However, if it is found in the calibration process that two axes are actually slightly inclined, and a unique common normal exists, then the link coordinate frame will change significantly. This may propagate through widely varying location of the coordinate frames and cause the kinematic parameters to change to a wider extent [63,72,90].

C. For parallel mechanisms, the D-H method is very complicated due to existence of multiple closed loops in 3D mechanisms. For closed loop mechanism, geometric method can offer more convenient way of kinematic analysis since the vector loop equation can be written for each limb and the passive joint variables are eliminated in these equations [72].

3.3.1.2 Error model

Correct identification of the kinematic error in the model is vital to increase the effectiveness of the calibration process and thereby to improve the mechanism's positioning accuracy. The characteristics of an effective error model for a mechanism's calibration can be best described by defining a term, "Minimum complete and parametrically continuous" (or MCPC), as below [20]:

- A. A model must describe all the possible sources of error (i.e. it should be complete).
- B. In the model, small geometrical errors must be described by small changes in the values of the corresponding parameters, for example link length, joint offset (i.e. it is parametrically continuous or proportional) to avoid singularity.
- C. Each source of error can be described by one parameter (absence of redundant parameters); in another word, the model is minimum.

MCPC model makes the error identification process easier at the later stage of the calibration process, and it is possible to obtain unique numerical solution during the implementation stage of the calibration process when inverse kinematics becomes important [20].

Various strategies to develop error models for individual parallel mechanisms are found in the literature based on the geometric method or the vector-loop equation method [92], homogenous transformation matrix method [93], D-H method [92] and

Jacobian method [27,94]. Considering the characteristics of a MCPC model, there are fundamentally two approaches to develop an error model:

1. Objective function model and
2. Differential error model.

In the objective function model, errors are described by the variations of a specific set of parameters used to define the mechanism's structure, such as link lengths, joint axes inclination and joint coordinates offsets. In terms of forward kinematics, the model can be represented as [21]

$$\mathbf{S} = \mathbf{f}(\mathbf{Q}, \mathbf{s}_n + \Delta), \quad (3.7)$$

where $\mathbf{S} = [x, y, z, \alpha, \beta, \gamma]^T$ represents the end-effector's pose, $\mathbf{Q} = [\mathbf{q}_1, \dots, \mathbf{q}_n]^T$ is the vector of the joint coordinates, $\mathbf{s} = [\mathbf{s}_1, \dots, \mathbf{s}_n]^T$ is the vector of the nominal structure parameters, and Δ is the vector of their errors. In many cases, these parameters are defined by adopting the D-H approach (see section 3.3.1.1). However, for calibration purposes, an MCPC model has to be ensured, meaning that minimum structure parameters should be used.

In the differential error model, errors are represented by a separate set of parameters describing the differences between the nominal and actual geometry of the mechanism. The forward kinematics of the model can be represented as [21]

$$\mathbf{S} = \mathbf{f}(\mathbf{Q}, \mathbf{s}_n, \Delta), \quad (3.8)$$

where $\Delta = [e_1, e_2, e_3, \dots]$, which consists of geometrical error parameters. For calibration purposes, using a differential error model does not require to select minimum number of structure parameters. However, the error parameters Δ must be defined by the minimum numbers as per the definition of MCPC. The differential error model is commonly used for the kinematic calibration of the parallel mechanisms.

3.3.2 Pose measurements

Suitable measurement schemes need to be selected to obtain accurately the pose (position and orientation) data or the subset of the pose data of the moving platform of the parallel mechanism [22,28]. In principle, a pose data set is obtained by moving the mechanism to some location of the workspace, record the joint displacement (lengths of the legs) and then use a measurement equipment to determine the full or some part of the pose. The measurement procedure is repeated many times for enough number of locations of the workspace [90]. In terms of using the measuring equipment, existing calibration method for the parallel mechanisms can be usually categorised as: external calibration and self-calibration [22,23,92]:

1. for external calibration, the mechanism's end-effector's actual poses are measured by an external measurement system (such as, laser tracker, camera, interferometer),
2. for internal or self-calibration, redundant measurement information is collected either from some sensors placed on the passive joints of the mechanism or directly from the sensors of the active joints of the mechanism.

External calibration can be carried out by either full pose measurements or partial pose measurements [21,22]. For full-pose measurements, the full end-effector's pose in terms of the complete information about the possible degree of freedom of the mechanism is collected. The calibration problem in this measurement type is treated as finding the kinematic parameters that minimise the residual, which is the difference between the recorded joint displacements and the ones calculated from the inverse kinematic model [22,23,92]. Full-pose measurement can be attractive for the kinematic calibration of the parallel mechanism since each loop can be considered independently for the calibration purpose, like the case of a serial mechanism. However, full-pose

measurement is time-consuming, laborious and generally expensive, especially when high-accuracy of the mechanism is required, advanced or special measurement equipment are necessary [24,92]. On the other hand, in partial pose measurements, incomplete motion information of the end-effector is used, and all the structural error parameters cannot be identified through the calibration process [90,92]. In partial-pose measurement, calibration problem is treated as finding the kinematic parameters that minimise the errors between the measured pose and the ones determined by the direct kinematic model [22]. Partial pose measurements may offer limited accuracy improvement for the parallel mechanism. Furthermore, partial pose measurements use direct kinematic model, and it is very difficult to find the analytical solutions to the direct kinematic model for the parallel mechanism [90,92]. This will be discussed in section 3.4 when finding the issues of the calibration for the parallel mechanism.

Self-calibration is a newly emerged measurement and calibration technique for the parallel mechanism [23,29,92]. It is a potentially attractive, economical solution mainly for two reasons: elimination of the pose measurements and facilitation of the on-line accuracy compensation [23,24]. So far, two approaches can be identified in the literature for the self-calibration. In one method, extra sensors are added to the several passive joints of the parallel mechanism to obtain redundant measuring information. Calibration problem then becomes adjusting the kinematic parameters to minimise the difference between the measured joint displacements and calculated joint displacements using inverse kinematic model. However, adding extra sensors of suitable type to an existing parallel mechanism to receive joint displacements is practically very difficult [23,29,92].

Another method of self-calibration is to impose constraints on some motions of the parallel mechanism and measure the active joints. This is an attractive solution to the problem mentioned above. However, appropriate mechanical fixtures are required to

impose the constraints. Furthermore, using fixture can have two effects: 1. it can reduce the workspace of the calibration, reducing the sensitivity of the kinematic parameters in the calibration process; 2. deformation of the fixture can affect the calibration results [23].

3.3.3 Parameter identifications

Once the error model and the measurement data are available, the next phase of the calibration is to determine the parameters of the model (for differential error model, error parameters) which enables predicted model data match closely with the measured data. [21,90]. The identification process can be explained mathematically in the following way [90].

Let A_i^{i-1} be a HTM that represents the position and orientation of a mechanism's frame i relative to frame $i-1$. Using the D-H notation, it can be written that

$$A_i^{i-1} = A_i^{i-1}(s_i), \quad (3.9)$$

where s_i is the mechanism's parameter vector for joint i and $s_i = [\theta_i \ r_i \ l_i \ \alpha_i]^T$.

A kinematic equation can be written by taking the HTMs from the last frame to the base frame of the mechanism

$$T_n^0 = T_n^0(k) = A_1^0 A_2^1 \dots A_n^{n-1} = \prod_{i=1}^n (A_i^{i-1}), \quad (3.10)$$

where k is the parameter vector for the mechanism and $k = [s_1 \ s_2 \ s_3 \ \dots \ s_n]^T$.

Let $\delta_{s_i} = [\delta_{\theta_i} \ \delta_{r_i} \ \delta_{l_i} \ \delta_{\alpha_i}]^T$ where δ_{s_i} is the link parameter error vector. The actual link transformation B_i^{i-1} is defined as

$$B_i^{i-1} = A_i^{i-1}(s_i) + d A_i, \text{ where } d A_i = d A_i(\delta_{s_i}). \quad (3.11)$$

The actual mechanism transformation $T_{B,n}^0$ can be written as

$$T_{B,n}^0 = \prod_{i=1}^n (B_i^{i-1}). \quad (3.12)$$

The error transformation for the mechanism can be defined as:

$$d\mathbf{T} = \mathbf{T}_{B,n}^0 - \mathbf{T}_n^0. \quad (3.13)$$

Let \mathbf{q} be vector of joint variables (θ_i or r_i) and $\delta\mathbf{k} = [\delta s_1 \delta s_2 \delta s_3 \dots \delta s_n]^T$ be the mechanism parameter error vector. Also, let $d\mathbf{T} = \mathbf{T}_n^0 \Delta\mathbf{T}$, in which $\Delta\mathbf{T}$ is the transformation representing the change in \mathbf{T}_n^0 expressed in the coordinate frame n . The mechanism's transformation error $\Delta\mathbf{T}$ is a non-linear function of the mechanism's parameter error $\delta\mathbf{k}$. Thus, $\Delta\mathbf{T} = \Delta\mathbf{T}(\mathbf{q}, \delta\mathbf{k})$.

The parameter identification problem of the mechanism's calibration aims to determine the $\delta\mathbf{k}$ from the measurements that have the information about $\Delta\mathbf{T}$. By expanding the equation (3.12) and ignoring the second order products, an identification Jacobian relating the change in manipulator transformation to the parameter error vector can be found as:

$$\delta\mathbf{T}_m = \mathbf{J}_m \delta\mathbf{k}, \text{ where } m=1,2,\dots,j; \quad (3.14)$$

$\delta\mathbf{T}$ is a differential translation and rotational vector which can take the following form

$$\delta\mathbf{T} = \begin{bmatrix} 0 & -\delta z_n & \delta y_n & dx_n \\ \delta z_n & 0 & -\delta x_n & dy_n \\ -\delta y_n & \delta x_n & 0 & dz_n \\ 0 & 0 & 0 & 1 \end{bmatrix}, \quad (3.15)$$

where dx_n, dy_n and dz_n are the small displacements from \mathbf{T}_n^0 and $\delta x_n, \delta y_n$ and δz_n are the small rotations about x_n, y_n and z_n axes respectively; and j is the number of observations during the measurements. Equation (3.14) represents a linear system which can be solved using the least-square approach as:

$$\delta\mathbf{k} = [(\mathbf{J}^T \mathbf{J})^{-1} \mathbf{J}^T] \delta\mathbf{T}, \quad (3.16)$$

where $\mathbf{J} = [\mathbf{J}_1 \mathbf{J}_1 \mathbf{J}_1 \dots \dots \mathbf{J}_j]^T$ and $\delta\mathbf{T} = [\delta\mathbf{T}_1 \delta\mathbf{T}_2 \delta\mathbf{T}_3 \dots \dots \delta\mathbf{T}_j]^T$. If equation (3.16) is applied iteratively, it may converge if the kinematic error parameters of the mechanism are small enough. The procedure of identification of the error parameters described is

called as the linear least-square method and is most commonly used for the calibration of the parallel mechanisms.

There is another method of parameter identification in which the problem is seen as one of fitting a nonlinear regression model. For this method, the non-linear model for the actual mechanism's transformation of equation (3.12) can be written as

$$\mathbf{y}_m = \mathbf{f}(\mathbf{q}_m, \mathbf{k}), \text{ where } m=1,2,\dots,j; \quad (3.17)$$

\mathbf{y} is the actual mechanism's end-effector pose which refers to \mathbf{B}_n^0 of equation (3.11); and j is the number of observations during the experiments.

The residuals for the model are:

$$\mathbf{e}_m(\delta\mathbf{k}) = \mathbf{x}_m - \mathbf{f}(\mathbf{q}_m, \mathbf{k}), \text{ where } m=1,2,\dots,j; \text{ and} \quad (3.18)$$

\mathbf{x}_m is the vector that represents the measured pose of the mechanism at location m . The aim of the parameter identification is to find the least square estimate of \mathbf{k} that minimises the function

$$L = \sum_{m=1}^j \mathbf{e}_m^T \mathbf{e}_m. \quad (3.19)$$

The procedure of the parameter identification described is known as non-linear least-squares method.

3.3.4 Implementation of calibration

The previous three phases of calibration provide a more accurate kinematic model with known parameters that should represent the accurate relationship between the pose and the joint displacements. For a mechanism, when it accepts a command for a certain pose, it converts it to some joint variables through an inverse kinematics model of the control software. Therefore, to improve the mechanism's performance, the calibration data should be included in the inverse kinematics of the control software of the mechanism [90]. However, the detail architecture of a mechanism is usually not available to the user and making necessary changes to the inverse model may not be

possible. Implementation of the calibration using inverse kinematics is often carried out by the mechanism's supplier.

An alternative option of implementing calibration data is through off-line pre-processor [47,57,90] software. In this method, the desired 3D Cartesian positions are used in the correct inverse model of the pre-processor to calculate the joint displacements. These values are then used in nominal forward kinematics model of the control software of the mechanism to calculate new 3D compensated positions for the end-effector. When loaded these values in the control software, its nominal inverse kinematic model calculates the necessary joint displacements so that the real desired position of the end-effector is achieved. Therefore, in reality, the mechanism is commanded to move to a position offset to the desired one, and due to the error of the mechanism, the mechanism's end-effector reach to the desired position.

3.4 Key issues in calibrating parallel and hybrid kinematic mechanism

Developing an economical kinematic model for a complex structure is always a great challenge. While the accuracy improvement through kinematic calibration has been well studied and reported for the serial mechanism, the accuracy improvement of spatial parallel mechanisms through kinematic calibration is, still, a field of active research, and the researchers have proposed various approaches to overcome different issues related to the four steps of the kinematic calibration. Kinematic calibration for parallel mechanism, as compared to a serial mechanism, is challenging for various reasons. The key issues are briefly discussed below.

3.4.1 Issues related to kinematic model for position analysis

For calibration purposes, the position analysis of a target (or tool or end-effector) using a kinematic model – direct or inverse kinematic model - determines the method to

use for the error model, the selection of the measurement method and the method of error identification [90,22,23,27-29]. As has been discussed before, 1. both methods of the error model - the objective function and the differential methods - depend on direct and inverse kinematic model; 2. full pose or partial pose measurement is carried out depending on whether inverse or direct kinematic model is used in the error model; and 3. the use of linear or non-linear least squares method for parameter indemnification depends on whether inverse or direct kinematic model is used in the error model. Carrying out position analysis using direct kinematic model is generally not difficult for the serial mechanisms for several reasons, such as 1. an open-loop structure, 2. presence of actuated and sensed joints (primarily, prismatic and revolute joints) in the structure, 3. availability of established method of kinematic model (e.g. the D-H method) [21,24,84-87,90] However, inverse kinematic models can be complex for the serial mechanism if the kinematic structures are not simple enough.

As opposed to serial mechanism, the presence of closed loops in the parallel mechanism makes it difficult to develop a kinematic model for position analysis. As has been shown in section 3.3.1.1 and Figure 3.7, two loop equations, including constraint equation, are required to determine the relationship between the base coordinate frame of the mechanism and the pose of the end-effector. The constraint equations in the kinematic model introduce some dependent parameters, in addition to independent parameters, in the model [21,90]. The problem of the position analysis in the presence of the dependent parameters of parallel mechanism can be explained by referring to the closed loop example in section 3.3.1.1 and Figure 3.7. It can be noted that with the joint encoder readings, equation (3.6) is used to calculate the dependent variables, which are used to calculate T_{target} to locate the target position with respect to the reference coordinate. For example, θ_B is required to calculate T_{target} of equation (3.5). Also, note

the presence of HTM A_{AB} in both equations. As such, observation of equations (3.5) and (3.6) highlights the major difference of the kinematic analysis for the open-loop (serial mechanism) and closed loop (parallel) mechanisms. Some joint variables are dependent parameters for the closed loop analysis. Since the dependent parameters can be determined from the constraint equations, closed loop kinematic analysis usually has fewer independent parameters than an open-loop kinematic analysis, which can make the direct kinematic analysis of a closed loop (i.e. parallel) mechanism very difficult [90].

Furthermore, unlike serial mechanism, many parallel mechanisms have passive joints with no actuator or feedback system (no measured angles) – see section 3.1.2. These passive joints, such as spherical joints, do not have unique axis of motion, unlike the prismatic and revolute joints of the serial mechanism. This issue makes the kinematic analysis of parallel mechanism more complicated.

For the above reasons, position analysis using forward kinematic model is generally not adopted for the kinematic calibration of parallel mechanisms; instead, inverse kinematics models are commonly used. In some cases, calibration works based on direct and inverse kinematic models have been used to take the advantages of using an inverse model along with the partial-pose measurements and linear least-square method for parameter identification; however, the problem of the determination of a high number of error parameters of the parallel mechanism still remains [23].

3.4.2 Issues related to error model

As mentioned before while describing the characters of a MCPC model, each source of error should be represented by only one parameter. In other words, an error model for calibration should have enough coefficients to express the deviation of the mechanism's structure from the nominal design [21,90]. For this purpose, the model should contain

required number of independent kinematic parameters. The number of independent parameters is equal to the number of constraint equations required to specify completely the pose of the tool and the joint coordinate frame (note that all the relevant coordinate frames, such as world/reference frame, tool frame and joint coordinate frame, are defined in the kinematic analysis) [90]. For example, a prismatic mechanism needs eight constraint equations and a revolute joint requires ten equations to completely specify the pose of a tool (or end-effector) and the joint coordinate frame (see Figure 3.8). As such the total number of independent parameters for a serial mechanism with multiple joints (prismatic and revolute) can be determined by the following equation in order the kinematic model to become complete:

$$N = 4R + 2P + 6, \quad (3.20)$$

where N is the required number of independent parameters, R is the number of revolute joints and P is the number of prismatic joints.

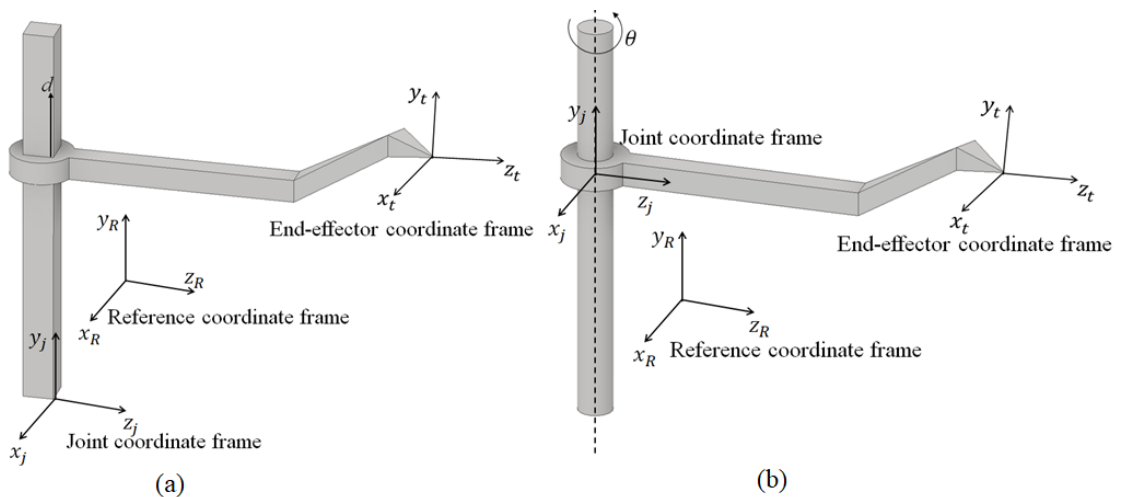


Figure 3.8 Constraint equation calculation (a) mechanism with a prismatic joint (b) mechanism with a revolute joint.

According to equation (3.20), a PUMA 560 manipulator (a 6-DOF robot arm in the form of a shoulder, an elbow and a wrist and six revolute joints) needs thirty independent kinematic parameters to define a complete kinematic model [90]. Among

these thirty parameters, six are joint variables and 24 are constant parameters to represent links, offsets, arbitrary zero position and arbitrary location of the tool frame. When these 30 independent parameters are used in a suitable method of generating a direct model, a unique relationship between the joints and the pose are established for the PUMA 560 manipulator, and this model can be easily implemented with active controlled joints (i.e. motorised joints). Thus, the number of error parameters determined by equation (3.20) gives an indication of number of independent parameters required to define an error model with MCPC characteristics.

The example above actually explains why developing an error model based on MCPC characteristics for the serial mechanism is relatively easy. Vast majority of the serial mechanisms uses mainly two types of joints- prismatic and revolute joints, and the error sources of these joints are well-known (for example, ten independent parameters required for a revolute joint as mentioned above). When the D-H method is used for the model development (d_i , α_i , a_i and θ_i) and joint type and numbers are known, equation (3.20) gives an idea of how many error parameters should be included in the error model to completely define the mechanism.

Developing an error model based on MCPC model characteristics for the parallel mechanism is, however, challenging for various reasons. The main reasons are following:

- A. Besides parallel and revolute joints, it is common to find other types of joints in the parallel mechanism, such as universal joint, spherical joint, where the use of spherical joint is quite common (see section 3.1.2). The error sources of these joints are not well-studied [20]. Like the equation (3.20) for a serial mechanism, there is no commonly accepted method of determining the minimum number of independent parameters required to define a mechanism that contains a combination

of various types of joint, e.g. prismatic, revolute, spherical joints. For this reason, researchers in the field of calibration have identified the error sources of mechanism based on individual methods and types of parallel mechanism [22-24,27,28,85-87,92-94]. For example, Wang and Masory [55] modelled the leg of the Stewart platform as serial chains, and they considered the errors of platform, actuators and errors in the link-joint connections, Wang and Fan [31] introduced 18 error sources in the error model of 3-RPS mechanism, but the posture errors of the prismatic and revolute joints are ignored. As reported by Huang et al. [23], the total error sources of 3-RPS should be 33, including all possible errors caused by manufacturing and assembling. It has also been found in the literature that up to 138 error parameters for a 6-DOF Stewart-Gough platform and a minimum of 38 parameters for a 5-DOF parallel mechanism are required to describe the error model for the stated parallel mechanisms [20,24].

- B. The non-standard joints and the large number of different types of errors that may come from different sources, e.g. joints, platform, legs, indicate that commonly used D-H method cannot be used directly to develop an error model, and further parameters other than usual (i.e. d_i , α_i , a_i and θ_i) are needed to describe the errors [20]. Such modification of D-H method for a complex kinematic structure with multiple loops is very complicated [72]. For this reason, for parallel mechanism's kinematic model, geometric method is preferred, in which a vector loop equation is written for each limb or leg. In such cases, full-pose measurements need to be adopted for measuring the pose of the end-effector. This is because, for multi-loop mechanism, some parameters become dependent. Unless the end-effector's poses are not measured for all possible degree of freedom (six for a spatial mechanism) and for sufficiently high number of mechanism's configuration, it is not possible to

determine all possible error parameters of the mechanism [23,24]. As mentioned before, full-pose measurements for kinematic calibration can be expensive, time-consuming and laborious for a complex kinematic structure.

C. As discussed before, position analysis for parallel mechanism using direct kinematic model is generally not preferred due to the presence of dependent parameters for multiple closed loops in the mechanism. This indicates that the objective function method for error model development is difficult to adopt for the calibration of the parallel mechanisms. Objective function method actually offers some benefits in the calibration [22,87] process, such as:

- a) Objective model is built on the direct kinematic model, the use of which can facilitate the use of partial pose measurements. In many applications, partial pose measurements, instead of full-pose measurements, are more desirable.
- b) When D-H method is used for the objective function model, the offset errors in the joint coordinates are explicitly present, which can be advantageous during the implementation of calibration as the offset errors can be compensated in the controller.

D. For the parallel mechanism's calibration, the popular use of differential method, which uses inverse kinematic model and the full-pose measurements, means that linear least squared method is easier to apply for the error parameter identification. However, for multi-loop mechanisms with many error parameters, a large number of measurement data and an identification Jacobian (equation 3.14) with large dimensions are required for the parameter identification.

3.4.3 Issues related to measurements

The issues related to different types of measurement – full pose or partial pose or self-calibration - used for the kinematic calibration are already discussed in section 3.3.2.

The most important point to remember when selecting a measurement scheme is that the accuracy of the error parameter determination depends on the quality of the measurement data. A number of factors may affect the measurement data quality, for example, the measurement accuracy, encoder resolution and accuracy, the number of poses measured, the selection of the measurement configurations and the range of motions of the mechanism's joints during the observation [90]. A particular issue during the calibration of a parallel mechanism arises because of the ill-conditioning problem when solving the identification equations at the third phase or identification phase [23,24,72,90]. Ill-conditioning problem indicates that errors in each leg of the parallel mechanism cannot be decoupled due to dependent parameters mentioned before [23]. In such condition, some of the linear algebraic equations in the set of measurement equations (the relation between the end-effector's pose and the corresponding joints) are linearly dependent on other equations, and these redundant equations need to be removed for the parameter identification [90].

3.4.4 Issues related to parameter identification

Although fundamentally two types of approach – linear and non-linear least square algorithm- are most commonly used for the parameter identification, various approaches have been used by the researchers based on inverse kinematic model to avoid the ill-conditioning problem induced by the dependent parameters of the parallel mechanism. For example, Levenburg-Marquardt algorithm for a 2-DOF parallel mechanism, genetic algorithm for 3-RPS mechanism, Kalman filtering approach and Regularisation method for a 3-P(4R)S-XY hybrid machine and a 5-DOF parallel machine [20,24]. However, all these methods are sophisticated and time-consuming. These methods may be suitable for high-accuracy calibration provided by the mechanism's supplier, but generally not suitable for high-efficient, economical calibration solution to be carried out by the users

of the parallel mechanism to evaluate the mechanism's performance and apply software-based position compensation [24,90].

Furthermore, some researchers have focused on developing algorithms to optimise the measurement pose to solve ill-conditioning problems [25,26]. However, pose optimisation method is not suitable for all types of parallel mechanism, for example a 3-P(4R)S mechanism that has chains with shape approximately same in the whole workspace, meaning that the identification vectors are nearly similar and approximately linearly dependent. For this, it will be difficult to reduce the coupled parameters of the chains, and, therefore, the ill-condition problem using measurement pose optimisation [23].

3.4.5 Issues related to implementation of the calibration: compensation

As mentioned before, implementation of the kinematic results in the real parallel mechanism can be a major obstacle for the users if they do not have access to the information required to make changes to the parameters used in the kinematic models of the control software. Calibration implementation issues are real-world problems, and greatly vary with many factors such as the types of mechanism, user's level of knowledge and expertise in the mechanism and its control software, level of accuracy required for the mechanism for a particular application and so on. Unfortunately, very little information can be found in the literature about the details of calibration implementation [22-26,30,31,84-87,92-94].

3.5 Real-time position control of target

As indicated in section 2.7, in manufacturing and precision applications, real-time compensation to eliminate the errors of the mechanism or the motion stages is desirable for many reasons, for example, low cost and high production rate. A high

repetition-rate laser operation requires such type of real-time compensation so that the positioning and orientating of the fresh targets to the laser beam focus are possible with an accuracy of few micrometres at a rate of at least a few Hertz, as indicated in section 2.4.1. For example, clinically relevant experiments require several thousands of laser shots, which demands an automated target positioning system [7].

An extensive literature survey suggests that no research work on real-time target position control for high-repetition rate operation has been suggested so far. Only one method of automated positioning of nano-targets was reported by Gao et al [7]. For developing an automated positioning of the 1683 targets held in a target wheel, which functions as a high-repetition rate system, Gao et al followed the pre-alignment procedure, involving the steps such as pre-characterisation of the wheel by assigning the coordinate to each target, performing real time measurement for each target with a microscope and a distance sensor, and recording the data in the controller. A hexapod is then used to correct for the measured deviations during the alignment process [32]. In this automated positioning system, the positioning error of the target is reduced by a pre-calibration error compensation. However, as indicated in section 2.7, error compensation by pre-calibration can be very time-consuming for a wheel with many targets, and random errors from dynamic disturbances may still be there to affect the positional accuracy of targets.

In fact, most real-time position control based on in-process measurement solutions are application-specific, and research covering different aspects of in-process metrology, such as instrumentation, acquisition, calibration, is just increasing [95]. In the following sections, the relevant characteristics of the real-time compensation are studied - at first from general perspective and then more specifically from the requirements for a high-repetition rate laser operation.

3.5.1 Requirements for real-time position control

The position accuracy of a target (tool or end-effector, but hereafter just called target) is one of the most important requirements for many precision systems, such as ultra-precision machine tools, coordinate-measuring machines and surgical robots. Positional accuracy is generally achieved by carrying out one or more of these processes: design following precision engineering principles (e.g. the avoidance of Abbe errors, the separation of the metrology loop from the force loop); calibration requiring steps, such as kinematic modelling, error identification and error compensation; and compensation for the target's path (or trajectory) requiring in-process measurement of the position of the target while the operation is taking place (i.e. real-time compensation) [8-13].

The role of metrology in design and calibration, in terms of position measurement of the target is discussed in sections 2.3 and 3.3.1 to 3.3.3, and also discussed elsewhere [14,56,57]. Real-time compensation is a vital task for in-process metrology which has been playing an increasingly important role in recent years in the process chain of manufacturing to fabricate precision workpieces with complex shapes and/or tight tolerances [12,13]. For the manufacturing of workpieces with such characteristics, the role of in-process metrology goes beyond the post-manufacturing inspection of a manufactured workpieces for quality control purpose to make sure the measured parameters of the workpiece, such as dimension, surface topography, meet the design requirements [95]. As stated by McKeown, the maximum efficiency of the quality control is possible when the measurement takes places at the closest possible point to the manufacturing process, which can be availed by employing some kind of in-process metrology [96]. Beyond the task of quality control for workpieces, in-process metrology has been proven effective for manufacturing process control by allowing optimisation the process and the machine tool settings [95,97]. This is because, the measured

parameters of the workpieces are actually representative of the process characteristics and errors incorporated in the workpiece are the footprints of the machine tool imperfections.

In-process metrology is defined as the measurement of the parameter, e.g. length, surface topography, position, of the workpiece on a manufacturing machine (on-machine), where the workpiece is manufactured while the manufacturing is taking place [95]. Depending upon the parameters to be measured, various types of in-process measurement systems are available [95]. However, since this research is about position and orientation control of target, the position and angular measurement will be focused in the discussion. Fundamentally, as discussed in section 2.5, the position errors and angular errors, arising from the geometric and non-geometric sources, affect the positional accuracy of target.

As shown in Figure 2.12, there are three fundamental components for a real-time position:

1. A control loop for the positioning system,
2. A sensor for the feedback, and
3. Positioning mechanism's actuator.

Among these three, the positioning mechanism uses its actuators to produce position compensation/s for the target. Different types of mechanism are already discussed in section 3.1, noting that the mechanism associated with this research is a hybrid mechanism.

3.5.1.1 Control loop

As shown in the Figure 2.12, the control loop of a positioning system consists of a feedforward and feedback path. Although control system can, in principle, consist of

either feedforward or feedback path, applying combination is advantageous since both have their own advantages and disadvantages [98].

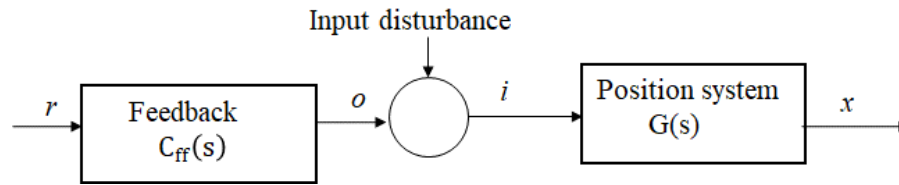


Figure 3.9 Block diagram of a feedforward-controlled position system.

Figure 3.9 shows a basic configuration of a feedforward control, which is also known as open-loop control. In this configuration, when the reference or guidance signal r is applied to the controller, which has a frequency dependent transfer function $C_{ff}(s)$, the output o becomes input i to the position system (mechanism), which has a frequency dependent transfer function $G(s)$, to become output x , which is target position. Therefore, theoretically, if a perfect control (no difference between the reference position and the actual position) to be achieved, the combined transfer G_{comb} function of the overall system has to be one, which means [63,98]:

$$G_{comb_{ff}} = \frac{x}{r} = C_{ff}(s)G(s) = 1. \quad (3.21)$$

In this situation, the feedforward controller becomes exact inverse of the mechanism,

$$C_{ff}(s) = \frac{1}{G(s)}. \quad (3.22)$$

If no dynamics are involved, the feedforward controller represents a gain, which scales the reference signal. For systems that are open-loop stable (no or negligible dynamics), the feedforward controller can improve the system's performance when following a predefined trajectory like a reference signal or a repeating scanning motion [99]. In the presence of dynamics associated with the mechanism, such as amplifiers and actuators, the feedforward can function as a filter, which is placed in series with the mechanism to compensate its dynamics. In such cases, the system's dynamic behaviour

may not need to be modelled [98]. The external dynamics, such as vibrations from the operating environment, can partly be solved by adding a feedback system to the feedforward controller. Such control system is called the adaptive feedforward control [99].

Overall feedforward controller has the following advantages [99-100]:

- A. Sensor is not required, which can reduce the cost of the control system. Also, measurement noise from the sensor is not introduced to the controller. This advantage may be important for the precision positioning system to avoid positioning noise.
- B. Feedforward is particularly suited for the applications with predictable motions.
- C. Unlike feedback system, feedforward control is stable in behaviour since the poles of the controlled system are not changed.

The feedforward system has the following disadvantages [98-100]:

- A. It is not suitable for applications that requires a controller with a very high gain at very high frequencies.
- B. Unstable system cannot be controlled using pure feedforward control.
- C. This control can only compensate for known disturbances. Even with the additional measurements, these disturbances can be compensated partially since for perfection, the controller has to react infinitely fast (i.e. immediately when the disturbances occur), which is practically not possible.

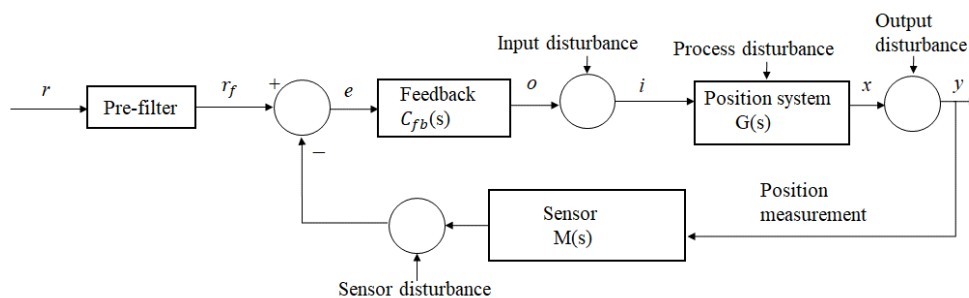


Figure 3.10 Block diagram of a feedback-controlled position system.

In feedback control system, the actual status of the position system is monitored by a sensor and the controller generates the control action to compensate the position based on the difference between the desired position (reference signal) and the actual position of the system (sensor signal) [63]. In this way, the feedback controller makes a closed loop control for the position system. Figure 3.10 shows a configuration of a closed loop control system where position output y is measured and compared with r_f , which is the reference r after filtering [98]. The transfer function of the feedback loop is derived from the following equation:

$$e = r_f - M(s)y \quad (3.23)$$

$$y = G(s)C_{fb}(s)e \quad (3.24)$$

$$G_{comb_{fb}} = \frac{y}{r_f} = \frac{G(s)C_{fb}(s)}{1+M(s)G(s)C_{fb}(s)} \quad (3.25)$$

where e is the position error, $C_{fb}(s)$ is the frequency dependent transfer function of the feedback controller, $M(s)$ is the frequency dependent transfer function of the sensor, $G(s)$ is the frequency dependent transfer function of the position system, and $G_{comb_{fb}}$ is the combined transfer function of the overall control system.

When input filter is added, equation (3.25) becomes,

$$G_{comb_{fb}} = \frac{y}{r} = \frac{G(s)C_{fb}(s)}{1+M(s)G(s)C_{fb}(s)}F(s) \quad (3.26)$$

where $F(s)$ is the frequency dependent transfer function of the input filter. In a control system design, $F(s)$ and $C_{fb}(s)$ are selected such that the $G_{comb_{fb}}$ meets the position specification of the positioning system.

Closed loop control can offer the following benefits [101,102]:

- A. While some motion systems can be inherently stable, some motions systems can be marginally stable, and some can be even unstable like an inverted pendulum system.

With feedback control system, such unstable system can be stabilised.

- B. Disturbances of the motion systems are observed in the sensor signal and appropriate compensations can be made.
- C. PID (proportional-integral-derivative) feedback control is the most versatile control system used in motion control systems. PID can offer a robust control system since the stability and performance requirements for the motion control system can be ensured even for the parameter variations of the controlled position systems.

Feedback control suffers from some limitations, such as [98,101,102]:

- A. Sensors are required for the feedback loop. For precision positioning systems, sensors with high accuracy with high resolution and bandwidth are required, which can be very expensive.
- B. Obviously, feedback control cannot function unless the error is occurred in the system to correct it.
- C. In the closed loop system, the positioning noise of the position system and the sensor noise are also part of the feedback. This needs to be taken into consideration while designing the feedback system.

It is worth noting that for a precision positioning of a target/tool/end-effector, one may suggest the use of a feed-forward control system as an alternative to a closed loop control system. In fact, feed-forward control systems are effectively used in some applications, for example, in the track following control of the hard disk drive (HDD), in which the read/write (R/W) head follows the track centre precisely in the presence of several disturbances [103]. The repeatable runout (RRO) error (the difference between the servo-written track centre and the ideal circular track centre), which is periodic and synchronised with the disc rotation, can be compensated by the controller by making the R/W head to follow the servo-written track centre. This feed-forward system might not be very effective when the RRO disturbance is not coherent at different tracks. This

problem can be solved by another type of control scheme, called adaptive feed-forward, in which an appropriate compensation signal is subtracted from the raw measurement signal to make the R/W head to follow the ideal circular track centre more closely. For this, an accurate estimation of the compensation signal for all the tracks is required, which can be stored in the controller as a runout table. However, the estimation of compensation signals for all the tracks could be time consuming and may even require modelling of the disturbances affecting the positions of target/tool/end-effector, especially for those applications where the high accuracy of the positions of the target/tool/end-effector with respect to rotating disk or wheels are required [98,103].

3.5.1.2 Sensor

According to Soloman [104], some key characteristics of a sensor, as shown in the Table 3.1, should be taken into consideration while selecting a position and motion sensor for an industrial application.

Table 3.1 Key characteristics of a sensor for an application.

Key point	Consideration
Range	How far is the object to be detected by the sensor?
Performance	What level of accuracy, resolution and bandwidth (frequency response) is required?
Environment	What is the operating condition, such as dirt, debris, darkness?
Accessibility	What accessibility is there to both sides of the object to be detected?
Wiring	Is wiring possible to one or both sides of the object?
Size	What size is the object?
Consistency	Is object consistent in size, shape and reflectivity?
Requirements	What are the mechanical and electrical requirements?
Output signal	What kind of output is needed?
Logic functions	Are logic functions needed at the sensing point?
Integration	Is the sensor required to be integrated to other system, e.g. a positioning system?
Cost	What will be the capital investment cost and life-cycle cost for the sensor?

The characteristics of the sensor, as shown in Table 3.1, indicate that many factors, such as range, performance, environment, integration, need to take into considerations during the design and implementation of an in-process position measurement system for the real-time position control system. In a manufacturing environment, in-process measurement activities in a production machine introduce additional issues compared to off-line measurements or ex-situ measurements carried out in a controlled laboratory. For example, Figure 3.11 shows a list of factors that influence the performance of in-process optical measuring instruments in a production line [105]. Some key design considerations, identified from the literature, for in-process position measurement instruments are discussed below.

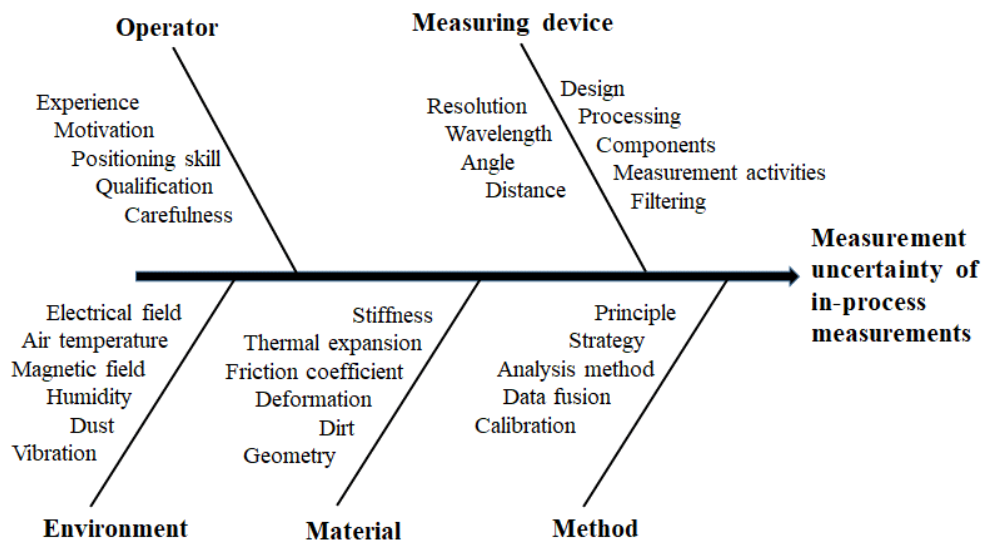


Figure 3.11 An Ishikawa diagram showing the factors that affect the performance of an in-process measurement instrument [105].

3.5.1.2.1 Tactile vs non-tactile instrument

Although both tactile (contact) and non-tactile (non-contact) instruments can be used for all in-line and off-line measurements of the workpiece's position in manufacturing, non-tactile instruments are best suited for the in-process position measurement because 1. the instrument can be flexibly positioned in the machine, 2. the measurement speed

can be faster than the cycle of the operation of a process, 3. the instrument offers damage-free measurement [95]. The discussion in the next sections will be limited to optical instruments.

3.5.1.2.2 Sensor position

Many in-process position measurement equipment uses motion control systems which are used, for example, to move the optical system to scan a surface or to measure a part from different angles or positions. The motion system used for a measurement equipment can span from a small-range linear axis motion system to five axes (or more) rotational robotic arm. The overall dimension of an in-process measurement equipment depends on employed measuring techniques and the production machine in which the instrument is integrated [95]. For example, in a milling machine, a measurement equipment can be attached to a production machine without much difficulty, say, by mounting the instrument onto a tool holder. However, in forming machines usually used for mass product manufacturing, measurements can usually be performed once a formed workpiece is detached from the mould and die, since the production cycle time is very fast [106].

However, a small and compact measurement instrument is preferable, making it possible for the equipment to be easily and flexibly integrated to various production machines. Also, another important factor is that the housing of an in-line optical sensor should be designed to protect the optics and electronics from the harsh environments, such as moisture, oil and dirt [106].

3.5.1.2.3 Environment

Disturbances, such as vibrations, temperature variations, dirt/dust/oil and humidity variations negatively affect instruments' performance and, thereby, the accuracy of the measurement results. For example, the variation of pressure, humidity and temperature

of an environment can change the wavelength of the laser of an interferometer system, and dirt, dust, oil and moisture can adhere onto the surfaces of the lens of an optical system and a part [106,107].

Heat generating from the surrounding equipment and production machines can increase the temperature of a measured part and may cause the expansions of various components or mechanical structures inside the measurement instrument, affecting the performance of an in-process measurement instrument [108]. For example, a measurement instrument featuring with a linear axis to perform measurement is susceptible to the thermal effects on the drivetrain system and the axis scale, resulting in positioning errors [108]. These positioning errors, in certain conditions, can be compensated by the machine controllers, say by incorporating an error model of the system and a close-loop feedback [48].

Vibration during the measurement process degrades the measurement results, for instance, vibration can increase the measurement noise of an in-process measuring instrument [109]. Vibration can arise from a number of sources, such as machine vibration, vibration induced by the motion system of the instrument and vibration from the operating environment. Generally, vibration effects are reduced by minimising the vibration sources, isolating the vibration sources and/or isolating the instrument [137,138].

3.5.1.2.4 Design of instrument

Besides vibration and thermal effects, some other important issues, as reported in various literature, need to be considered while selecting an in-process measurement instrument for a position control system. The concept of force and metrological loops is important in instrument design in many ways, for example to find the optimum structural design and optimum locations for the sensors and actuators [84]. The force loop is a

closed path of the force that flows and propagates around the structure of the machine, and the metrology loop is a closed path containing all the elements between the sensor and the workpiece that affect the measurement [110,111]. Figure 3.12 shows an example of a precision machine, demonstrating how the measuring scale attached to a metrology frame and the tool can be separated.

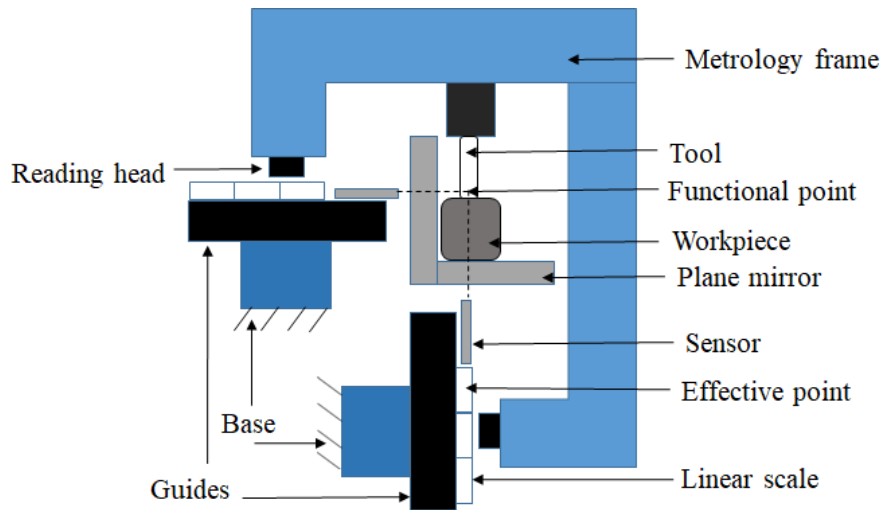


Figure 3.12 A design of a machine tool with the linear encoders configured to achieve an in-line path of the functional point and the effective point of the scale [11].

3.5.1.2.5 Integration

Several important sources of measurement error should be taken into consideration when integrating a sensor into a machine, e.g. a positioning system, for in-process position measurement. Measurement errors such as Abbe errors, sine and cosine errors are discussed in section 2.6. It is important to understand how these errors affect the measurement results and what compensation methods can be applied to eliminate the effects of the error [95]. Compensation method applied should also cater for the measurements influenced by the machine errors caused by external disturbances, such as thermal error and vibration [56,57].

3.5.1.2.6 Software and interface system

To combine and control all the functional elements of optical in-process measuring instruments, namely motion systems, acquisition systems, machine interfaces and data processing, appropriate software and interface systems are essential [95]. One important aspect is the establishment of communications among the production machine's controller, the controller of the in-line instrument and the user interface software for the measurement instrument. As such, acquiring feedback data for the position compensation of target/tool/end-effector is not always straightforward, since most of the production machines come with their own commercial controllers and not open for the users to access [112,113].

3.5.1.2.7 Traceability

Traceability is very important in measurement to ensure measurement results are consistent, comparable, accurate and can be traced to the fundamental unit of measurements through a documented unbroken chain of calibrations [114,115]. For many high-accuracy applications, length and surface measurement by the sensors need to be traceable to metre, which is defined "by taking the fixed numerical value of the speed of light in vacuum, c , to be 299 792 458 when expressed in the unit m s^{-1} , where the second is defined in terms of the caesium frequency $\Delta\nu$ " (the wording of the definition of metre was updated in 2019) [116,117]. For this reason, interferometer is widely used as a sensor for high-accuracy applications for its natural superiority of traceability and for long measuring range, high sensitivity, high speed measurement and high-resolution [17].

Based on the above discussion, the in-process measurement system for a laser operation should fulfil the following requirements:

1. Measurement speed,

2. Compact size sensor,
3. Location of the sensor in the machine/mechanism,
4. Environmental condition,
5. Precision alignment,
6. Output signal,
7. Software,
8. Integration with the controller, and
9. Traceability.

3.5.2 In-process position sensor for high-repetition rate laser operations

A few optical instruments can potentially be the candidates to fulfil the requirements for the in-process position measurement sensor for the high-repetition rate laser operations. For example, laser triangulation sensor, confocal sensor, laser interferometry.

3.5.2.1 Triangulation sensor

Triangulation sensors have become frequently used in-process metrology, especially for the measurement of car bodies in the automotive industry. The main components of the triangulation sensor are a collimated light source (usually laser diode) and a detector unit, which consists of an imaging lens and a position-sensitive detector (CCD or position-sensitive diode PSD) [118]. In this arrangement, when the laser points at the workpiece, the reflected beam spreads through the imaging lens and focuses on the detector. The optical axes of the light source and the imaging lens form a fixed angle, and the position of the image on the detector is a function of the distance between the sensor and the workpiece. The triangulation sensor can be used for the measurement range between 2 mm to 200 mm [98,118]. The main errors can come from 1. the slope of the workpiece (may cause direct reflection to the detector), 2. optical character of the

workpiece surface, for example very smooth surface, 3. inhomogeneous surface texture [118]. Triangulation sensor is considered not a good choice as an in-process sensor for the real-time target position control for the laser applications for two reasons: 1. the measurement range is small (will not exceed $\pm 20 \mu\text{m}$), 2. the slope of the target is expected to change during the high-repetition operation, 3. the position of the sensor system in the vicinity of high-power laser is not suitable since the debris and electromagnetic pulse (EMP) will affect the sensor performance.

3.5.2.2 Confocal sensor

In confocal sensor, the collimated light from laser diode is focused on the target and the reflected light is directed to a focus detector. Depending upon the position of the surface of the target relative to the focal plane, when the light intensity becomes maximum, the position of the sensor relative to the target is determined [119]. Confocal sensor can offer a range of advantages in displacement measurement, such as compact design, high accuracy, measurement in tilt surface, small focal spot and flexible integration into the machine [119,120]. However, confocal sensor needs to be placed within a short distance (maximum 30 mm) of the target to take the measurements. As mentioned before, the sensor cannot be placed in the vicinity of the target during high-repetition laser operation.

3.5.2.3 Displacement interferometer

To measure displacement with high accuracy, optical interferometer is often used. Typical applications of the optical interferometer are the calibration of the precision axes of the machine tools and CMMs and position measurement of high-precision motion control stages [17,118].

The principle of length interferometry is based on Michelson type interferometer invented in 1881. Since then, various types of interferometry methods have been

developed for displacement, distance, profile and surface measurements. Optical interferometry can be categorised based on types of interference used by the instrument, e.g. Michelson, Fizeau, Mirau, Twyman-Green, Mach-Zehnder and Faby-Perot [121,122]. Optical interferometry can also be classified based on light source or the number of wavelengths used in the instruments depending on the measuring range, for example, single wavelength interferometer, multi-wavelength interferometer and white light interferometer [118]. For displacement measurements, a homodyne interferometer is considered as the simplest interferometer in which monochromatic coherent light of a laser is used. However, most of the commercial interferometers use heterodyne or dual frequency interferometry, for example a He-Ne laser ($\lambda=632.8$ nm). Heterodyne interferometers are free from the DC drift of the single-frequency laser interferometer and has the advantages of low noise measurement [17].

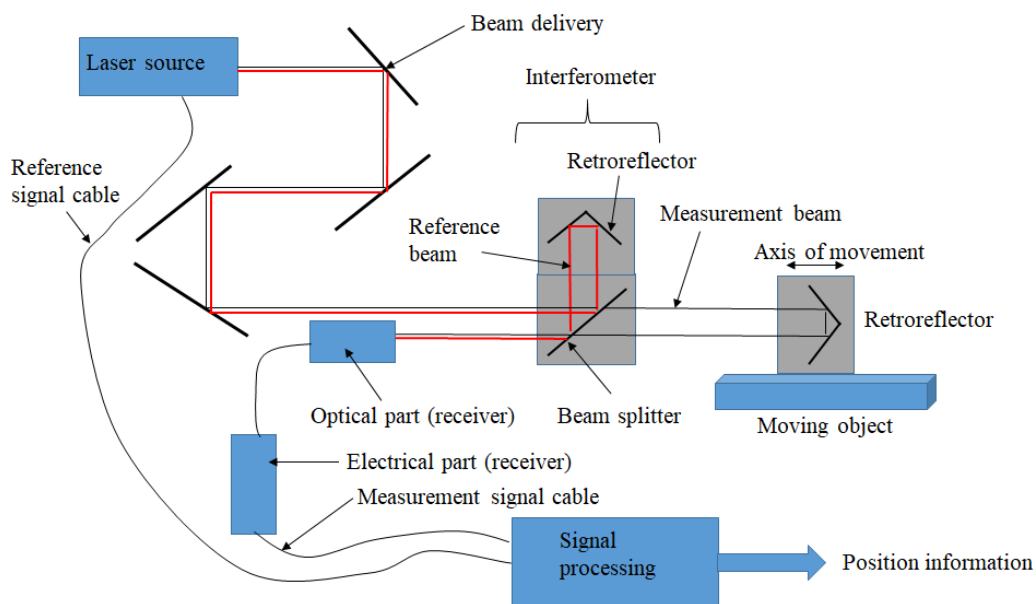


Figure 3.13 Main components of a laser interferometer for the position measurement of a moving stage.

Figure 3.13 shows a schematic arrangement of a laser interferometer system to measure the displacement of a moving object. As can be seen from the figure, the laser

from the source enters the beam splitter and split in two beams with a known phase and frequency relationship. While one beam travels to a reference reflector (or retroreflector), the other to a reflector (or a retroreflector) placed on the moving object whose displacement must be measured. After returning to the interferometer, both beams are mixed and interfere. The resultant interference pattern is an irradiance-modulated light signal as the function of the phase difference between two beams due to change of displacement [98].

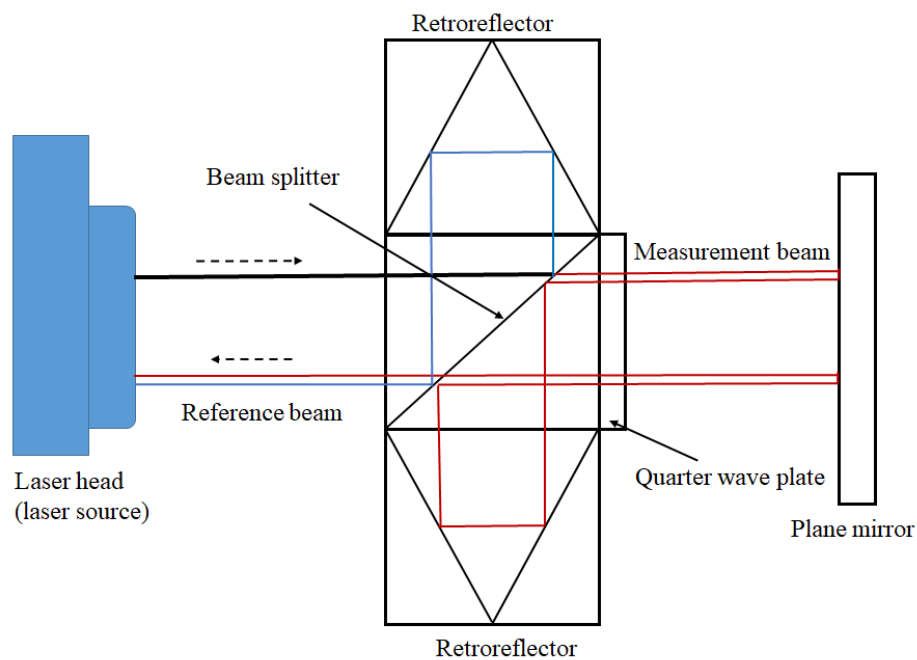


Figure 3.14 Plane mirror interferometer [123].

For dual-axis motion measurement, e.g. in a xz linear stage, a plane mirror interferometer is preferred than a usual interferometer using retroreflector (Figure 3.14). In plane-mirror interferometer, a plane mirror, instead of a retro reflector, is placed on the moving object whose displacement has to be measured. A plane mirror has the advantage of having a lower mass than the standard retro reflector. Plane mirror interferometer, as opposed to usual interferometer with a retroreflector, uses an additional component, called a quarter wave plate (QWP) as shown in Figure 3.14. QWP

converts linear polarization to circular and then back to an orthogonal linear polarization after reflection from the plane mirror (that is, object mirror), which is now free to move orthogonal to the line of sight without disturbing the beam paths. The double pass to the object mirror with a retro-reflection compensates for a tilt of the mirror [122]. An additional benefit of the double pass is a finer measurement resolution.

3.6 Conclusion

Kinematically, HAMS has a hybrid mechanism – a combination of serial and parallel kinematic structures. As compared to serial structures, parallel structures can offer certain distinct kinematic advantages, for example, structural rigidity and high-reconfiguration, but many areas of parallel structure are still under active research, for example accuracy improvement due to the presence of a large number of sources of error in the kinematic structure. Furthermore, although hybrid structures have recently received much attention, and research is underway on how to use them in industrial applications, comprehensive studies of their design, kinematic design and analysis, dynamics and error sources are lacking.

Although it has been shown that kinematic calibration can be a practical and economical way for enhancing the accuracy of parallel or hybrid mechanism, the calibration process is more complex than for a serial mechanism. This complexity is due to the significant difficulty in identifying the kinematic parameters using a minimum set of error data, which can be easily determined in a time- and cost-effective manner, without compromising the accuracy of the calibration results. Although some general strategies for calibration based on minimum set of error data exist for serial mechanisms, for parallel mechanisms only calibration methods for individual mechanisms have been reported. Finding general strategies for the cost-effective calibration is an important area of the research in parallel mechanisms.

Another effective approach for error compensation, i.e. real-time compensation, is a closed loop technique with the need for an in-process metrology, which means the errors are monitored during a process, for example machining, and the compensation is carried out continuously as and when the machine/mechanism is in operation to constantly correct the inaccuracies. Real-time compensation is a vital task for in-process metrology and has been playing an increasingly important role in recent years in the process chain for manufacturing of precision workpieces with complex shapes and/or tight tolerances. This compensation technique is desirable in industry since it involves a combination of high accuracy, low cost and high production rate. However, developing an instrument for in-process measurements for a real-time compensation techniques comes with many challenges, e.g. appropriate selection of a sensor, mounting of the sensor in the manufacturing machine to avoid measurement errors, high measurement speeds to follow the manufacturing operation, avoidance of environmental disturbances and traceability issues. For these challenges, most in-process measurement solutions are application-specific, and research covering different aspects of in-process metrology, such as instrumentation, acquisition and calibration, is increasing. Although real-time error compensation can be an attractive solution for the high-power laser operation that requires high-accuracy target positioning and alignment in high speed, no technique has been reported so far as to how real-time compensation can be implemented in practice for high-repetition rate laser operations.

Chapter 4 - Research methodologies

4.1 Introduction

In this PhD research, a combination of approaches - analytical modelling, experimental methods and empirical approaches [124,125] - are used to answer the research questions outlined in Chapter 1. While the details of the analytical modelling and experimental methods are given in the relevant chapters (i.e. 5, 6 and 7), this chapter gives an overview of how three different approaches were used in the research and the working principles associated with the three approaches.

4.2 Selection of research methods

It has been indicated in the literature review (section 2.3.1 to 2.3.3) that HAMS plays two role in the target alignment (position and orientation) process:

1. To provide translational and rotational motions for the targets to locate them in space (with respect to a global reference coordinate system) within specifications (e.g. $\pm 4 \mu\text{m}$ in the z direction), and
2. To provide compensatory motions for the positional and orientation errors of the target in the alignment process.

It has also been indicated (section 3.5) that fundamentally, three elements are required for an effective, real-time position control for target during the high-repetition rate laser operations:

1. An in-process sensor,
2. A control system, and
3. A mechanism with its actuators.

It should be noted that, irrespective of the type of sensor or control system used, the target cannot be positioned and orientated within specifications if the mechanism

(i.e. HAMS) does not have the abilities to generate the required motions to locate the target in space with sufficient accuracies to meet the specifications. Therefore, in this research, the issues of the performance improvement of the mechanism (HAMS) were dealt at first.

4.2.1 Research methods for the performance improvement of HAMS

The performance improvement of HAMS (as indicated in two sub-questions of the first research question in Chapter 1) is related to:

1. Error mapping of the mechanism, and
2. Performance improvement procedure of the mechanism.

The error mapping for the mechanism was carried out following the procedure below:

- A. A complete understanding of the kinematic structure of the hybrid mechanism of HAMS based on literature review and the documents, e.g. user's manual, whitepapers published by the suppliers, e.g. ALIO industries, PI, Aerotech, of HAMS and the mechanisms of similar kind (parallel and hybrid mechanisms),
- B. Identification of a suitable method for kinematic analysis of the mechanism by carrying our extensive literature review,
- C. Identification of the key kinematic error sources of the mechanism based on the above information,
- D. Developing an error model with analytical equations to find the relation between the error parameters identified and the target's positional deviations.

After mapping the error of the mechanism, a four-step kinematic calibration and compensation ("calibration" in short) procedure, as discussed in section 3.3, was applied for the performance improvement of the mechanism. The research methods used in the calibration procedure are following:

- A. To develop a cost-effective and practical calibration procedure, the capabilities of the mechanism's control software were investigated at first. For this, a detailed understanding of the software-specific parameters, e.g. kinematic and motor parameters, motion programme and compensation techniques were required to decide the most effective way of implementing the calibration results into the control software and to determine what parameters must be known from the rest of the three steps of the calibration process.
- B. The error model from the error mapping process was developed to begin with the calibration process.
- C. To measure the positional deviation of the target, displacement measurement experiments were performed using interferometer with the retroreflectors.
- D. The errors of the mechanism were identified by carrying out displacement and angular displacement measurement experiments using interferometer with the retroreflectors.
- E. To implement the calibration results, error compensation was carried out with the modifications of the kinematic models of the control software and the development of a motion programme to generate compensatory motions.
- F. After mapping the error of the mechanism, a four-step kinematic calibration and compensation ("calibration" in short) procedure, as discussed in section 3.3, was applied for the performance improvement of the mechanism. The research methods used in the calibration procedure are following:
- G. To develop a cost-effective and practical calibration procedure, the capabilities of the mechanism's control software were investigated at first. For this, a detailed understanding of the software-specific parameters, e.g. kinematic and motor parameters, motion programme and compensation techniques were required to

decide the most effective way of implementing the calibration results into the control software and to determine what parameters must be known from the rest of the three steps of the calibration process.

- H. The error model from the error mapping process was developed to begin with the calibration process.
- I. To measure the positional deviation of the target, displacement measurement experiments were performed using interferometer with the retroreflectors.
- J. The errors of the mechanism were identified by carrying out displacement and angular displacement measurement experiments using interferometer with the retroreflectors.
- K. To implement the calibration results, error compensation was carried out with the modifications of the kinematic models of the control software and the development of a motion programme to generate compensatory motions.

It should be noted that only the geometric and kinematic error sources of the mechanism were considered in this research for the performance improvement of HAMS due to the fact that geometric and kinematic errors form the major part of the total errors of a mechanism (see section 2.4.2). As such, the effects of various individual sources of mechanical error, for example errors due to joints' friction and backlash behaviours, were not considered in the error analysis of HAMS presented in Chapters 5 and 7.

4.2.2 Research methods used for error estimation and real-time position compensation for target

Research methods in this section are used to answer the second and third research questions as indicated in Chapter 1. To estimate the positional deviation of the target that may arise during the high-repetition rate process, an analytical model was developed, followed by the characterisation of the high-repetition rate by displacement

measurements using plane mirror interferometer. Then, a closed loop control system using a sensor for in-process measurement of the target position was designed, tested and implemented. The overall development of a real-time position and orientation control of target was carried out following the procedure below:

A. The design of the in-process measurement for the target position is a crucial part of the development of a real-time position control for target. During the design phase of the in-process position measurement system for target, the following key points were considered:

- a) Range – The wheel characterisation study of the high-repetition rate process showed that the displacement range to be measured would not exceed $100\ \mu\text{m}$.
- b) Performance – The position sensor should have nanometre level position accuracy and resolution and should operate at least at kHz level for faster data reading during 1 Hz repetition-ratio operations.
- c) Position – The positioning of the sensor was, perhaps, the most challenging design consideration due to the following difficulties:
 - The real target is very small ($300\ \mu\text{m}$) and 2D solid with a film-like character, e.g. transparent. The sector in which targets are patterned are narrow, semi-hemispherical shape silicon wafer with non-reflective surface (see Figure 2.5 and 2.6).
 - The electro-magnetic pulse (EMP) from the high-power laser is a big issue for placing an electronic and/or precision equipment near the laser-target interaction. Also, very high-speed debris is produced during the laser-target interaction, which can easily damage any sensitive measurement equipment.

- The space inside the compact-sized laser chamber is very limited (Figure 4.1). Any sensor equipment should ideally be placed outside the chamber to perform the measurements through the chamber window.
 - Besides the EMP and debris, the sensor may be subject to high-frequency vibration from the operating environment, although the vibration effect was not studied in this research.
- d) Integration - To integrate with the robot's controller, the sensor is required to produce quadrature output signal.

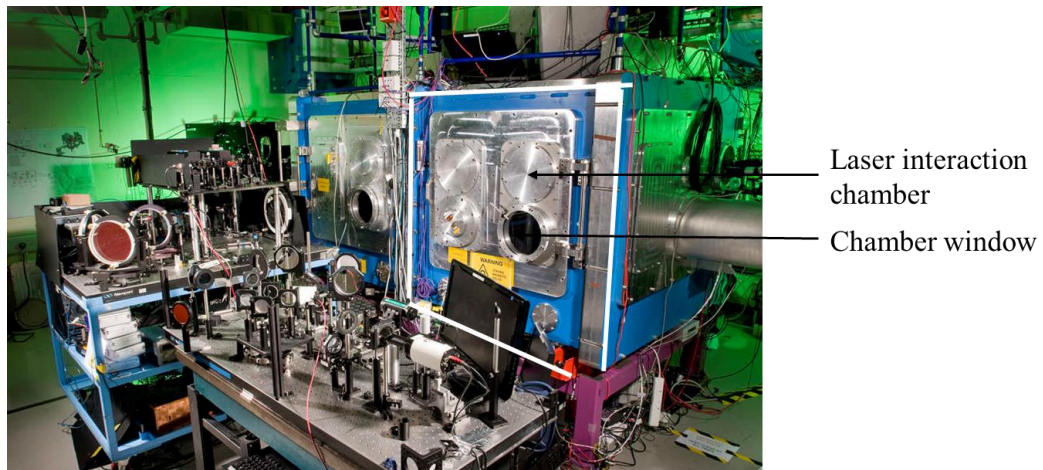


Figure 4.1 Laser interaction chamber.

- B. To design a high-accuracy measurement system, it is important to understand the effects of the measurement error. For this, precision engineering principles for designing a high-accuracy position measurement system were reviewed from the literature and from the whitepapers published by various leading manufacturers, e.g. Renishaw, Zygo and Aerotech, of precision machines and measurement systems.
- C. After selecting the measurement system (i.e. plane mirror interferometer – discussed in section 4.3), a series of experiments were carried out (1) to find a suitable position for the sensor (reflector of the interferometer in this case) and (2) to find a suitable

technique to align all the plane mirrors attached to the wheel with respect to the measurement laser beam of the interferometer (see Figure 3.14).

- D. The next step was integrating the sensor system with the robot's controller, requiring set-ups for both hardware and control software. Some typical activities in this step were: 1. establishing encoder connections between the sensor and the robot's controller, 2. setting up quadrature signal from the interferometer for the controller, 3. setting up encoder conversion table of the control software (digital quadrature signal from interferometer is converted to position data with a format usable by the servo motors) and so on.
- E. Once the sensor was functioning properly in open-loop condition, the next step was to carry out experiments in closed loop conditions where control software receives target position feedback and uses motion programme to actuate the motor to generate compensations for the target's positional deviation. A series of closed loop control experiments were carried out to find different techniques of compensating the position deviation of target. The aim was to find the best technique/s of the position compensation that will maintain the reference position and orientation of the target within specifications throughout the high-repetition rate operation. The details are discussed in Chapter 7.

It is, however, to note that the real-time position control system for targets based on a closed loop control represents a quasi-static system in this research (see section 2.4.2). This is because the closed loop control system was used to address the positional deviations of the target arising from the kinematic errors associated with the motions of the HAMS during the high-repetition operation. The dynamics of the system in the presence of external disturbances (e.g. vibration) were not considered in the research assuming their negligible effects in laboratory condition (also see section 8.3.1), and, as

such, the tuning of the control system's P, I and D parameters was not the main focus of the research.

4.2.3 Key parameters to determine in the research

Considering the above discussion, Table 4.1 shows the key parameters associated with the different phases of the development of a real-time position and orientation control system for target – the aim of the research.

Table 4.1 Key parameters for the development of real-time position and orientation control for target.

Research area	Key parameters	Nature of the parameters	Method of determination
Kinematic analysis and error modelling (Sub-question 1 of the first research question)	- x , y and z linear motions - u (tip) and v (tilt) angular motions of tripod - Linear error Motions - Angular error motions	-Displacement -Rotational angle -Displacement -Rotational angle	Analytical technique and experimental
Target position measurements for calibration (Sub-question 2 of the first research question)	Positional deviation of target	Displacement	Experimental (using interferometer)
Error parameters identification (Sub-question 2 of the first research question)	-Angular error motions of the tripod -Linear error motions of tripod	-Rotational angle -Displacement	Experimental (using interferometer)
Error compensation for calibration (Sub-question 2 of the first research question)	Positional deviation of target	Displacement	Experimental (with robot's motion controller, robot's encoders and interferometer)
High-repetition rate process characterisation (Second research question)	Positional deviation of target	Displacement	Experimental (using plane mirror interferometer)
Development of in-process sensor (Third research question)	Positional deviation of target	Displacement	Experimental (using plane mirror interferometer and the motion controller in open-loop control)
Real-time position control of target using in-process sensor in closed-loop control (Third research question)	Positional deviation of target	Displacement	Experimental (using plane mirror interferometer and the motion controller in closed-loop control)

4.3 Research methods used

4.3.1 Analytical approach

Error models were used in this research for the error analysis of HAMS, for carrying out kinematic calibration and for characterising the high-repetition rate process to develop real-time position control for targets. While the details of the development of the relevant error models are described in Chapter 5 and 7, the principles of the analytical techniques used are briefly outlined below.

The type of a mechanism's kinematic structure and the number and type of axes (linear or rotary) determine the errors presented in a kinematic model of a mechanism [14,47]. In a machine tool, for example, if the position of tool point and the corresponding position on the workpiece can be determined in space with respect to a reference coordinate system, then the difference between the two positions will represent the positional error as a result of the effects of all errors of the system [52]. For this, understanding of homogeneous transformation matrix (HTM) is required [48,52]. The coordinate transformation between two neighbouring rigid body frames can be described by an HTM. HTM is used in the following ways for the coordinate transformation [52]:

1. A 4x4 matrix is needed to represent the relative position and orientation of a rigid body in three-dimensional space with respect to a given coordinate system (reference), for example

$$\mathbf{T}_n^R = \begin{bmatrix} O_{ix} & O_{iy} & O_{iz} & P_x \\ O_{jx} & O_{jy} & O_{jz} & P_y \\ O_{kx} & O_{ky} & O_{kz} & P_z \\ 0 & 0 & 0 & P_s \end{bmatrix} \quad (4.1)$$

\mathbf{T}_n^R is a HTM that represents the coordinate transformation to the reference coordinate system ($x_R y_R z_R$) from that of the rigid body frame ($x_n y_n z_n$). The first three columns are direction cosines (unit vectors i, j, k) representing the

orientation of the rigid body's x_n, y_n and z_n axes with respect to the reference coordinate frame and there scale factors are zero. The last column represents the position of the rigid body's coordinate system's origin with respect to the reference coordinate frame.

2. Based on the definition of equation (4.1), if, for example, the $x_1 y_1 z_1$ coordinate system is translated by an amount x along the x axis, the HTM that transforms the coordinate of a point in the $x_1 y_1 z_1$ coordinate frame into the xyz frame will be

$$T_{x_1 y_1 z_1}^{xyz} = \begin{bmatrix} 1 & 0 & 0 & x \\ 0 & 1 & 0 & 0 \\ 0 & 0 & 1 & 0 \\ 0 & 0 & 0 & 1 \end{bmatrix} \quad (4.2)$$

3. If the $x_1 y_1 z_1$ coordinate system is rotated by an amount θ_x about the x axis, the HTM that transforms the coordinate of a point in the $x_1 y_1 z_1$ coordinate frame into the xyz frame will be

$$T_{x_1 y_1 z_1}^{xyz} = \begin{bmatrix} 1 & 0 & 0 & 0 \\ 0 & \cos \theta_x & -\sin \theta_x & 0 \\ 0 & \sin \theta_x & \cos \theta_x & 0 \\ 0 & 0 & 0 & 1 \end{bmatrix} \quad (4.3)$$

Similar HTMs can be constructed considering translations along and rotations about y and z axes.

4. For axes with simultaneous combinations of these motions, these HTMs can be multiplied in series to obtain a single HTM for the axis, as given below

$$T_n^R = \prod_{m=1}^N T_m^{m-1} = T_1^0 T_2^1 T_3^2 \dots \dots \dots \quad (4.4)$$

5. It is important to note that during kinematic analysis using HTM, a rigid body assumption is required, which says that a body or link is completely rigid neglecting any deviations in its shape caused under stress.

4.3.2 Empirical approach

Some empirical approaches were used in this research where data and information were embedded into various sources, such as, process, machine, procedure, documents and people (e.g. technical experts, scientists), target alignment method of CLF, knowledge and experience of laser experiment scientists/engineers, technical documents of HAMS. In such cases, carrying out direct experiments was not a viable option to collect relevant data and information effectively. Some examples of empirical approach used are: (1) observation of the laser operation at the central laser facility and discussion with the scientists of the central laser facility (2) experience gathered from solving problems related to HAMS, mechanism's controller and in-process sensor; (3) collection of information from the technical experts on HAMS, mechanism's controller and in-process sensors and (4) analyses of documents, e.g. technical manuals and design specifications, of HAMS, mechanism's controller and in-process sensor.

In association with the literature survey, empirical approaches, such as first-hand observations, provided very useful insight into the laser operation of the CLF and the procedure to follow to position and orientate the target at the focus of the laser beam. Two important outcomes of this empirical research were: (1) development of a conceptual method to use HAMS for the real-time position and orientation control of targets during the high-repetition rate process and (2) an understanding of the tasks and requirements for the metrology for the high-repetition rate laser operations. The stated outcomes are described briefly in the following subsections.

4.3.2.1 Conceptual target alignment method for high-repetition rate operation

The target interface wheel, mounted on the rotating platform of the tripod can accommodate at least 464 targets (8 target sectors, each contains at least 58 targets with

an angular separation of 1.5° between each target, are placed around the circumference of the wheel's edge) as shown in Figure 2.6. The laser needs to hit the target at target point T (Figure 2.5) within x , y and z specifications, ensuring that front plane of the target sector is perpendicular to the axis of the laser. This is achieved by the x and z motions of the linear stages of the hybrid system, and the tip (u) and tilt (v) rotational motions of the tripod. For example, a typical target positioning and alignment set-up can take the following 1 to 4 steps (Figure 4.2):

1. position target in the x , y and z with respect to HAMS coordinate system and align the target wheel to laser - Tip(u), Tilt(v), x , y , z ;
2. turn target wheel to offset angle - v ;
3. reposition target to focal spot - x , z ;
4. turn target wheel in 1° steps - w .

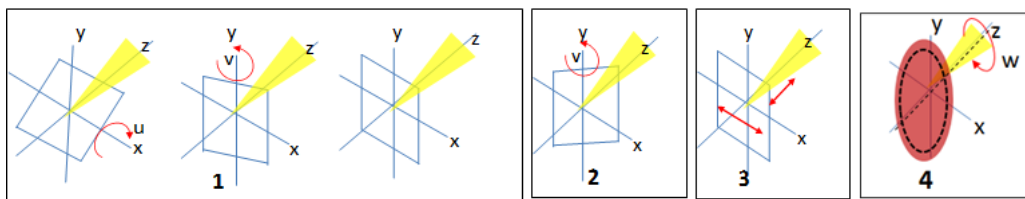


Figure 4.2 Steps of the microtarget alignment method during the laser operation of CLF.

The procedure described is the initial alignment of target, which is essentially considered as the set-up phase for a laser operation, and is usually carried out by the laser operator, requiring the manipulations of the motion stages and other supporting equipment, for example, diagnostic and alignment equipment (e.g. Mitutoyo microscope and camera imaging system). This set-up is called static alignment and is based on the understanding of the alignment method observed at CLF and [4,6,32,42].

Once the target is positioned at the optimum laser focus and laser plane, this location (position and orientation) of the target can be used as the reference or set point for any further alignments required later when targets need to be positioned

automatically at the laser focus during the high-speed wheel rotation. Any positional deviation of the target from the reference point can be compensated by the motion stages of the hybrid system provided that a position measurement system with sufficient accuracy sends the target position feedback to the controller of the system. The procedure described is the dynamic alignment of target for achieving target positional accuracy within specifications in high repetition-rate laser operations. Dynamic alignment requires a real-time position control system for the target. Currently there is no provision for the dynamic alignment during the laser operation.

While the relevant literature of the real-time position control is covered in section 3.5, the development of a real-time position control of target for the high-repetition operation is described in Chapter 7.

4.3.2.2 Tasks and requirements for metrology for high-repetition rate laser operations

The target alignment procedure described clearly indicates two tasks for metrology for high-repetition rate laser operations:

1. initial positioning and alignment of target, and
2. compensation for target position during high-repetition rate operation.

To fulfil the stated tasks, the metrology system requires that the positioning stages of HAMS will have sufficient positioning accuracy (e.g. less than $\pm 4 \mu\text{m}$ in the z direction). If the motions of HAMS do not have sufficient accuracy, the high-repetition operation will be affected in the following ways:

- A. significant time and effort by the operator, with the help of alignment equipment, will be required to find the reference target position at the initial set-up stage, causing downtime to the laser operation;

B. HAMS motions will not be able to generate required compensations to the position deviations that may arise from various sources described below. As such, reposition of the target within the z specification of the reference position, and, therefore, automated target position control (i.e. dynamic alignment) will not be possible during high-repetition rate operation.

The successful target alignment during high-repetition rate operation depends on the performance improvement of the mechanism of HAMS in terms of improving its ability to deliver accurate target position and orientation. As will be seen in Chapter 5 and 6, performance improvement of a mechanism is only possible when the errors can be identified and quantified. By doing so, a relationship between the errors and the positional deviation of the target (or tool or end-effector) can be established by taking into account other relevant factors, for example the structural parameters of the mechanism, leading to finding an appropriate methods for performance improvement.

4.3.3 Experimental method

As can be seen from the Table 4.1, the key parameters that need to be measured are of two types: displacement measurement and rotational angle measurement. To measure the displacements and rotation angles experimentally, two types of interferometer were used in this research:

1. Interferometer with retroreflector (called only interferometer from this point),
and
2. Plane mirror interferometer.

4.3.3.1 Measurement with the interferometer

Interferometer (Renishaw model XL-80) was used for the following displacement and rotational angle measurement during the development of error model and the

calibration process, which are related to the first research question as mentioned in Chapter 1:

1. the x and z motions of the linear stages of the mechanism,
2. the tip (u) and tilt (v) motions of the tripod of the mechanism,
3. the positional error of the tripod,
4. the rotational error of the tripod.

The detail experimental set-ups for displacement and rotational angle measurements using interferometer are given in the respective chapters (i.e. Chapter 6 and 7).

The principle of displacement measurement of a homodyne interferometer using standard retro-reflector and the advantages-disadvantages of using an interferometer have already been explained in section 3.5.2. Here, the principle of angular motion measurement is briefly discussed below.

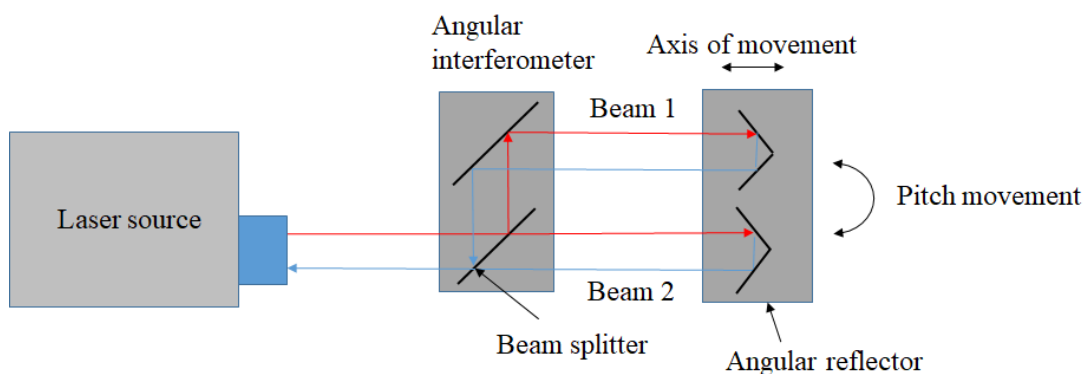


Figure 4.3 Angular motion measurement using interferometer with retro-reflector.

The rotation of angular reflector attached to the moving object whose rotation has to be measured with respect to the angular reflector (stationary) causes a change in path-difference between the two measurement beams (Figure 4.3). The change in path-difference is determined by the fringe-counting circuitry in the laser head and is converted to an angular measurement by the software. In angular measurements, the path-difference between the beams (1 and 2 in Figure 4.3) are compared. This means, the

measurement is independent of the distance between the laser head and the angular interferometer and also the distance between the angular interferometer and the angular reflector [122].

The plane mirror interferometer works differently, as discussed in section 3.5.2, from an interferometer with a retroreflector, and offers some unique benefits. The plane mirror was selected as a sensor for the in-process measurement system to measure the positional deviation of the target during the high-repetition rate operations. Plane mirror interferometer was considered as the most suitable sensor choice for this application for the following reasons:

- A. The laser head (laser source and electronics) of the interferometer can be positioned outside the chamber and beam-benders can be used to direct the laser beam through the laser chamber to the plane mirror attached to the target wheel of HAMS. Therefore, the EMP and the debris do not affect the sensitive electronics during the high-repetition rate laser operation.
- B. Plane mirror, which is much lighter than a retro-reflector, can be positioned suitably very close to the actual target position by attaching the mirrors to the target wheel. Thus, the sensor is not in the risk of damage from EMP and high-velocity debris.
- C. Interferometer is a high-accuracy and high-speed sensor option and the measurements are traceable.
- D. A unique benefit of using a plane mirror interferometer is that in this type of interferometer, the double pass of the laser beam to the plane mirror with retro reflection actually compensates a tilt of the mirror [117]. This benefit indicates that some misalignment of the plane mirror with respect to the measurement laser beam will actually not affect the position measurement of the target.

4.3.3.2 Displacement measurement uncertainty

Accuracies of the linear displacement measurements using interferometer are affected by the experimental errors that arise from the variations in air temperature, air pressure and relative humidity, since these environmental factors affect the reflective index of the ambient air [126]. As an example, while measuring a length L_{Meas} using interferometer, the sensitivity of the measured length with respect to environment (atmospheric) condition is shown in Table 4.2.

Table 4.2 Sensitivity of the measured length L_{Meas} with respect to environment (atmospheric) condition [126,127].

Environmental condition	Change or uncertainty	Change or uncertainty in the measured length L_{Meas} per meter
Air temperature, T_a	1°C	0.93 μm
Air pressure, p_a	1 hPa	-0.27 μm
Relative humidity Rh	1% Rh	0.009 μm

Based on the sensitivity data and a measurement model that is required to measure a distance using interferometer, the uncertainty of the linear displacement measurement can be estimated. In this research, for all types of linear displacement measurements using interferometer, an environmental compensator unit (Renishaw model XC-80) was used to keep track of the environmental change (temperature and humidity) to estimate the uncertainty for the measured displacements – an example is given in Appendix A. Though, the angular measurement using angular interferometer is not sensitive to environmental change, since both beams (beam 1 and 2 in Figure 4.3) used to calculate the angle are subject to same environmental change [122].

Besides using the interferometer to measure the linear displacement, the HAMS' (hybrid mechanism) internal encoders were also used to measure the linear displacements of the motors in some cases while carrying out kinematic calibration for HAMS. To get the same level of accuracy that an interferometric linear displacement measurement provides, a relation between the HAMS' internal encoder unit (called "counts") and "nanometre" was found by measuring the motions of the stages (x , y and z stages) using the interferometer. This value (1 count=159.74 nm) was used to represent all the displacement measurements related to HAMS' internal encoder.

While the above two sources of measurement uncertainty are generally considered for all the displacement measurements of this research, other sources of uncertainty have also been considered and are discussed in the relevant sections of Chapter 6 and 7.

Chapter 5 - Error modelling of the hybrid mechanism

5.1 Introduction

One of the fundamental requirements for a high-repetition rate laser system, as discussed in the literature review, is that fresh targets have to be positioned and orientated (i.e. target alignment) at the focus of the laser beam(s) with an accuracy of $\pm 4 \mu\text{m}$ at a rate of at least 0.1 Hz (with plans for 10 Hz or higher in future). To meet the accuracy and speed specifications for target positioning, HAMS has been designed and developed for mounting and motion control of targets for the Astra-Gemini high-power laser during the high-repetition rate operation.

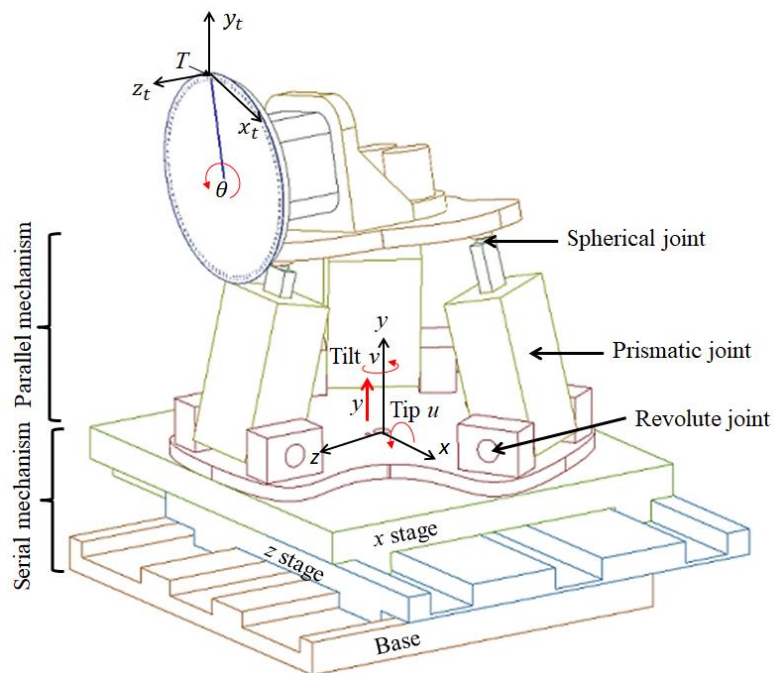


Figure 5.1 Hybrid mechanism of HAMS.

HAMS is a hybrid kinematic mechanism, which has the characteristics of both serial and parallel kinematic mechanisms (Figure 5.1). A hybrid structure is usually designed to overcome the inherent limitations of serial and parallel mechanisms: the xz stages of HAMS provide a relatively large workspace, and the tripod is designed to provide a translational motion and two rotational motions with high accuracy and

precision. The ability of HAMS to provide positioning and orientation accuracy of the target within the defined specification is dependent upon a number of factors, such as the target geometry, accumulation of errors on the motion stages and the tripod (rotational and translational motion errors, orthogonality errors, wobble/eccentricity errors, etc.), and the flatness tolerances on the wafer and interface wheel. Many of these factors are geometric errors, which can arise from the physical errors, e.g. manufacturing and assembling errors of the components and joint errors of the mechanism. The geometric errors can affect the performance of a hybrid mechanism, just like any other precision machine and, therefore, error compensation is required to minimise the positional deviations at the target during the target alignment process. Effective error compensation strategies for high-precision applications depend on identifying the sources of geometric error and, as such, developing an error model based on kinematic analysis of the mechanism is essential for this purpose.

As discussed in the literature, the development of an error model for the parallel mechanism of HAMS can be challenging for a number of reasons:

- A. Parallel mechanisms with spatial kinematic structures have complex structural architectures with many joints, links and offsets, representing many error sources. The number of error parameters for an error model is generally very high.
- B. Some error sources of parallel mechanism, for example spherical joints which are usually not used in serial mechanisms, are not well understood.
- C. The kinematic representation of the parallel mechanisms with the popular D-H method is difficult (see section 3.3.1.1).
- D. Any standard method to develop an efficient and effective model, like a MCPC model in which each error source is represented with an error parameter, is unavailable (see section 3.3.1.2).

In this chapter, error mapping of the hybrid mechanism of HAMS is performed by analyzing the key error sources of the mechanism. The identified error parameters are used to develop an error model for the hybrid mechanism. The error model not only is used to predict the positional deviations of the target because of the kinematic errors of HAMS, it is also used for carrying out kinematic calibration for the performance improvement of the hybrid mechanism as described in Chapter 6.

5.2 Motions of HAMS

In the hybrid mechanism of HAMS, two translation motions (along x and z axes, see Figure 5.1) are generated from a linear xz system, which is a two degree of freedom (DOF) serial mechanism. The tripod, the parallel part of the hybrid mechanism, provides a rotational motion about the x axis (tip u) and a translational motion along the y axis, while the rotary motor, which actuates the rotating platform mounted on the moving platform of the tripod, produces a further rotational motion about the y axis (tilt v) (Figure 5.1). The moving platform of the tripod and the rotating platform can be considered as serially connected, jointly having three degrees of freedom. Note that an additional rotary motion (about the z axis) is required to rotate the target wheel, but this motion is not related to the tripod, rotating platform or linear xz system. The description of the types of actuators used in HAMS is given in Appendix B.

Regarding the 3 DOF platforms (Figure 5.1), only the tip and tilt motions are considered for the kinematic analysis presented in this chapter, as tip and tilt motions control the orientation of the target T on the target interface wheel. The optimal location of a target is determined by the position and orientation of the coordinate system $x_t y_t z_t$ at point T (Figure 5.1) with respect to the focal spot and focal plane of the laser beam (see section 2.3.1). As such, z_t axis of $x_t y_t z_t$ should be along the laser axis and indicates the direction of the focal plane of the laser beam. Therefore, the position of coordinate

$x_t y_t z_t$ along the z axis and the direction z_t of the coordinate $x_t y_t z_t$ are considered as the most important position and direction to control during the target alignment.

Typically, the target alignment method of the CLF suggests that the target needs to be orientated to the laser beam by controlling the tip and tilt motions of HAMS, followed by the position adjustments of the target in the x , z and/or y directions by controlling the linear motions of the xz system and/or the vertical motion of the tripod, respectively (see section 4.3.2.1). However, a point to note is that the order of the angular motions (tip and tilt or tilt and tip) has effect on the final position of the target. The choice of the order to follow depends on the requirements of the application to which the mechanism is being used and the structure of the mechanism.

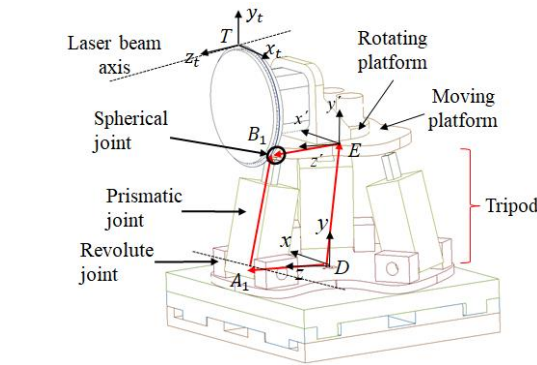
5.3 Error mapping of the parallel mechanism of HAMS

Since the linear xz system is widely used in industry and the technology is well developed [67,68], this research has focused on the error analysis of the parallel part (tripod) and the rotating platform. It is worth noting that the three modular structures of the HAMS – the xz stage, the tripod (moving platform) and the rotating platform – are serially connected, and therefore the error analysis of the three modules can be treated independently - similar to the case of a serial mechanism.

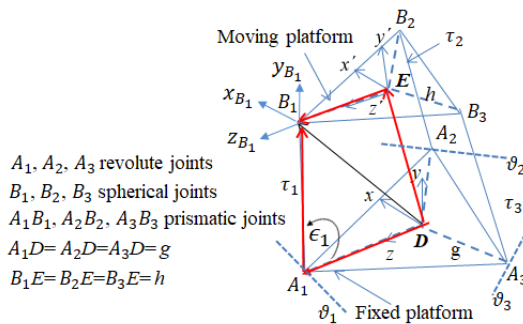
5.3.1 Analysing the error sources of tripod

Figure 5.2a shows one vector loop of the three closed loops of the tripod, where the three loops affect the position and orientation of the moving platform (E indicates the centroid of the platform). From a mechanism viewpoint, the tripod can be described as an RPS system, where R , P and S denote revolute joint, prismatic joint (linear slider) and spherical joint respectively (also see Figure 3.5). Three prismatic joints are used as the inputs to the RPS mechanism.

For convenience of analysis, the vector loop of Figure 5.2a is shown in Figure 5.2b, where two Cartesian coordinate system (x,y,z) and (x',y',z') are attached to the fixed base $A_1A_2A_3$ and moving platform $B_1B_2B_3$, respectively. In each loop, a leg, which has a variable length (say, τ_i) and is actuated by a prismatic joint, is connected to the fixed tripod platform $A_1A_2A_3$ by non-actuated revolute joints (A_1, A_2 or A_3), and to the moving platform $B_1B_2B_3$ by non-actuated spherical joints (B_1, B_2 or B_3). Three prismatic joints are used as the inputs to the RPS mechanism. Both platforms $A_1A_2A_3$ and $B_1B_2B_3$ form equilateral triangle and their centroids are at D and E , respectively. The fixed coordinate reference frame xyz for triangle $A_1A_2A_3$, is placed at D (where $DA_1 = DA_2 = DA_3 = g$), while the reference frame $x'y'z'$ for triangle $B_1B_2B_3$ is placed at E (where $EB_1 = EB_2 = EB_3 = h$).



(a)



(b)

Figure 5.2 Spatial 3-DOF RPS mechanism: (a) one of the three closed loops; (b) RPS mechanism showing relevant structural parameters and a closed loop.

The position and orientation of the moving platform $B_1B_2B_3$ with respect to the fixed platform $A_1A_2A_3$ can be described by a position vector \overrightarrow{DE} (say, \vec{P}) and by a 3×3 rotation matrix

$$\mathbf{T}_E^D = \begin{bmatrix} n_x & p_x & l_x \\ n_y & p_y & l_y \\ n_z & p_z & l_z \end{bmatrix}, \quad (5.1)$$

where \hat{n} , \hat{p} and \hat{l} are the unit vectors along n , p and l axes of the moving platform,

and

$$\vec{P} = \begin{bmatrix} P_x \\ P_y \\ P_z \end{bmatrix}. \quad (5.2)$$

As shown in Figure 5.2b, $A_1A_2A_3$ and $B_1B_2B_3$ are equilateral triangles. Therefore, the following equations can be written:

$$\overrightarrow{DA_1} = \begin{bmatrix} 0 \\ 0 \\ g \end{bmatrix}, \quad (5.3)$$

$$\overrightarrow{DA_2} = \begin{bmatrix} \frac{1}{2}g \\ 0 \\ -\frac{\sqrt{3}}{2}g \end{bmatrix}, \quad (5.4)$$

$$\overrightarrow{DA_3} = \begin{bmatrix} -\frac{1}{2}g \\ 0 \\ -\frac{\sqrt{3}}{2}g \end{bmatrix}, \quad (5.5)$$

$$\overrightarrow{EB_1} = \begin{bmatrix} 0 \\ 0 \\ h \end{bmatrix}, \quad (5.6)$$

$$\overrightarrow{EB_2} = \begin{bmatrix} \frac{1}{2}h \\ 0 \\ -\frac{\sqrt{3}}{2}h \end{bmatrix}, \quad (5.7)$$

$$\overrightarrow{EB_3} = \begin{bmatrix} -\frac{1}{2}h \\ 0 \\ -\frac{\sqrt{3}}{2}h \end{bmatrix}. \quad (5.8)$$

The position vectors for B_1, B_2 and B_3 with respect to fixed coordinate reference frame xyz , as shown in Figure 5.2b, can be written as

$$\overrightarrow{DB_i} = \vec{P} + T_E^D \overrightarrow{EB_i} \quad \text{where } i=1,2,3. \quad (5.9)$$

Substituting equations (5.1), (5.2) and (5.6) to (5.8) into equation (5.9) provides

$$\overrightarrow{DB_1} = \begin{bmatrix} P_x + hl_x \\ P_y + hl_y \\ P_z + hl_z \end{bmatrix}, \quad (5.10)$$

$$\overrightarrow{DB_2} = \begin{bmatrix} P_x + \frac{\sqrt{3}}{2}hn_x - \frac{1}{2}hl_x \\ P_y + \frac{\sqrt{3}}{2}hn_y - \frac{1}{2}hl_y \\ P_z + \frac{\sqrt{3}}{2}hn_z - \frac{1}{2}hl_z \end{bmatrix}, \quad (5.11)$$

$$\overrightarrow{DB_3} = \begin{bmatrix} P_x - \frac{\sqrt{3}}{2}hn_x - \frac{1}{2}hl_x \\ P_y - \frac{\sqrt{3}}{2}hn_y - \frac{1}{2}hl_y \\ P_z - \frac{\sqrt{3}}{2}hn_z - \frac{1}{2}hl_z \end{bmatrix}. \quad (5.12)$$

Equations (5.9) to (5.12) show that the position vectors of B_1, B_2 and B_3 , as shown in Figure 5.2b, determine the position and orientation of the moving platform $B_1B_2B_3$ with respect to the fixed platform $A_1A_2A_3$.

By considering the inclination angle of the leg ϵ_i measured from line A_iD to A_iB_i as shown in Figure 5.2b, the position vector of B_i with respect to fixed coordinate system xyz can be written as follows with the help of equations (5.3) to (5.5):

$$\overrightarrow{DB_1} = \begin{bmatrix} 0 \\ \tau_1 \sin \epsilon_1 \\ g - \tau_1 \cos \epsilon_1 \end{bmatrix}, \quad (5.13)$$

$$\overrightarrow{DB_2} = \begin{bmatrix} \frac{1}{2}(g - \tau_2 \cos \epsilon_2) \\ \tau_1 \sin \epsilon_2 \\ -\frac{\sqrt{3}}{2}h(g - \tau_2 \cos \epsilon_2) \end{bmatrix}, \quad (5.14)$$

$$\overrightarrow{DB_3} = \begin{bmatrix} -\frac{1}{2}(g - \tau_2 \cos \epsilon_2) \\ \tau_3 \sin \epsilon_3 \\ -\frac{\sqrt{3}}{2}h(g - \tau_2 \cos \epsilon_2) \end{bmatrix}. \quad (5.15)$$

Equations (5.13) to (5.15) show how the length of leg τ_i , inclination angle of the leg ϵ_i and the distance g from the centroid of base triangle $A_1A_2A_3$ to the tip of base triangle affect position vectors of B_1 , B_2 and B_3 . The stated parameters of equations (5.13) to (5.15) can be used to identify the error sources of the tripod (RPS mechanism) that affect the position and orientation of the moving platform as shown in equations (5.9) to (5.12).

Now, as shown in Figure 5.2*b*, consider only equation (5.13) for one closed loop of the RPS mechanism for error analysis. Three primary sources of error are as follows:

1. g , which is the distance from the centroid of base triangle $A_1A_2A_3$ to the tip of the base triangle,
2. ϵ_i , which is inclination angle of the leg and
3. τ_i , which is the length of leg or prismatic joint.

The value of parameter g , used in the kinematics of the mechanism's control software, can deviate from the geometrically accurate value in several ways, but important ones being:

- A. D is geometrically not at the centroid of the equilateral triangle $A_1A_2A_3$,
- B. A_i , located inside the revolute joints (ideally should be on the axis of the revolute joint), are not positioned at the tips of the triangle $A_1A_2A_3$,
- C. The rotational axis ϑ_1 of revolute joint at A_1 is not perpendicular to the vector $\overrightarrow{DA_1}$.

The above three factors affecting g are directly related to the design of the RPS mechanism. For practical reason, g is assumed to have constant effect on $\overrightarrow{DB_1}$ of

equation (5.13), and considered as constant in the error analysis for the following reasons:

- A. It was not possible to receive details design information from the HAMS' supplier,
- B. The design change of HAMS has not been the focus of this research. The main focus, as will be seen in Chapter 6, is to establish the effect of the errors at the point of interest, e.g. at target T in Figure 5.2a and 5.2b, in terms of positional deviations, and to improve the performance of HAMS.

The value of ϵ_i or inclination angle of the leg represents the angular motion of the revolute joint. The concept of constraint equations, as explained in section 3.4.2, is required to completely specify the rotational motion of the revolute joint with respect to the xyz coordinate system. Constraint equations determine how many kinematic parameters are required to describe the behaviour of revolute joint when it deviates from the ideal ϵ_1 motion. As shown in section 3.4.2, four error parameters are involved with ϵ_1 :

- A. Ideally, the orientation of the rotational axis ϑ_1 of revolute joint at A_1 should have a constant relationship with respect to xyz coordinate system. This means ϑ_1 should lie on the xz plane of fixed xyz coordinate system (i.e. ϑ_1 and xz plane parallel). In the case of non-parallelism, two rotational error parameters, say ϵ_{x_1} and ϵ_{z_1} , are required to describe the orientation of ϑ_1 with respect to xyz coordinate system.
- B. When revolute joint frame's origin, which is at A_1 of Figure 5.2b, does not lie on the rotational axis ϑ_1 of the revolute joint, two position parameters, say p_{ϑ_x} and p_{ϑ_z} , are required to express the positional deviation of A_1 .

The effect of ϵ_{x_1} and ϵ_{z_1} will be such that they represent a shift of the centre of the spherical joint B_1 , which is attached at the end of the leg A_1B_1 , from the ideal location of B_1 . This positional deviation of B_1 is due to the interaction of ϵ_{x_1} and ϵ_{z_1} with the

length of leg τ_1 (Abbe offset) during the motion of the revolute joint. As for the effect of two position parameters p_{θ_x} and p_{θ_z} , A_1 will not be positioned at the tip of the triangle $A_1A_2A_3$, affecting the ideal location of B_1 and value of g as discussed earlier.

The value of τ_i represents the translational motion of the prismatic joint to give input to the RPS mechanism. As explained in section 3.4.2, two constraint equations are required to completely specify the translation motion of the prismatic joint with respect to the xyz coordinate system; in another words, two error parameters are involved with τ_i . This is because, the axis of the prismatic joint or leg A_1B_1 should have a constant relation with respect to the xyz coordinate system. If it is not constant, two rotational error parameters, say $\epsilon_{\tau_{x_1}}$ and $\epsilon_{\tau_{z_1}}$, are required to describe the orientation of τ_1 with respect to xyz coordinate system.

The effect of $\epsilon_{\tau_{x_1}}$ and $\epsilon_{\tau_{z_1}}$ will be a shift of the centre of the spherical joint B_1 , which is attached at the end of the leg A_1B_1 , from the ideal location of B_1 . The effect of $\epsilon_{\tau_{x_1}}$ and $\epsilon_{\tau_{z_1}}$ on B_1 is similar to the effect of ϵ_{x_1} and ϵ_{z_1} . Although in both cases, the positional deviations of the centre of the spherical joint B_1 are taking place, the effect of $\epsilon_{\tau_{x_1}}$ and $\epsilon_{\tau_{z_1}}$ is expected to be much larger than that of ϵ_{x_1} and ϵ_{z_1} for the following reasons:

- A. Revolute joint has non-actuated motion. For small tip angle u of the moving platform of the tripod, revolute joint's motion is very limited.
- B. Prismatic joint is the actuated joint for the RPS mechanism. The tip angle u of the moving platform of the tripod is the direct output of the change of the length τ_i of the legs driven by the prismatic joint.

From equation (5.10) and (5.13), it follows that

$$\overrightarrow{DB_1} = \begin{bmatrix} P_x + hl_x \\ P_y + hl_y \\ P_z + hl_z \end{bmatrix} = \begin{bmatrix} \tau_1 \sin \epsilon_1 \\ 0 \\ g - \tau_1 \cos \epsilon_1 \end{bmatrix}. \quad (5.16)$$

Equation (5.16) shows that any change of the centre of the spherical joint B_1 changes the position and orientation of the centroid E of the moving platform $B_1B_2B_3$ with respect to coordinate xyz at D (Figure 5.2b). Furthermore, the discussion above suggests that the effects of the errors associated with the parameters of equation (5.13) or (5.16) (i.e. τ_1, ϵ_1, g) are reflected in the location (position and orientation) change of the coordinate system $x_{B_1}y_{B_1}z_{B_1}$ at B_1 from the ideal location of $x_{B_1}y_{B_1}z_{B_1}$ with respect to coordinate xyz at D . Therefore, it can be said that the kinematic errors of each leg of the RPS mechanism (i.e. tripod) are represented by the change of the coordinate system at the centre of the respective spherical joint.

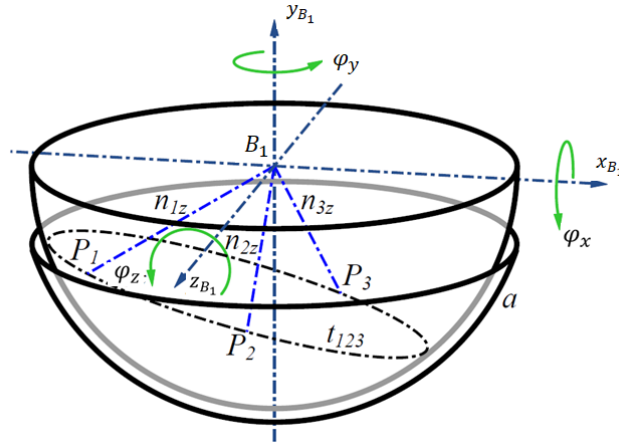


Figure 5.3 Spherical contact in the spherical joints [67].

To examine the kinematic characteristics of a spherical joint and how the change of the coordinate system at the centre of a spherical joint may take place, consider the features of a spherical joint as shown in Figure 5.3 [44]. Spherical joint has three rotational degree of freedom and does not have any specific axes of rotation as shown in Figure 5.3. Furthermore, spherical joint is based on three-point contacts, i.e. P_1 , P_2 and P_3 . The surface normal of all points in the contact area intersect at the centre of

curvature B_1 of the sphere. All points of the contact area have the same distance to B_1 . Therefore, three constraint equations are required to specify the position of coordinate $x_{B_1}y_{B_1}z_{B_1}$ at the centre B_1 of the spherical joint with respect to fixed coordinate system xyz of Figure 5.2*b*. It is important to note that the position of coordinate $x_{B_1}y_{B_1}z_{B_1}$ at the centre B_1 with respect to xyz will change if the ideal kinematic relationship of τ_i , ϵ_i and g with $x_{B_1}y_{B_1}z_{B_1}$ changes due to the errors associated with τ_1 , ϵ_1 and g . The error parameters associated with τ_1 , ϵ_1 and g can affect the position of coordinate $x_{B_1}y_{B_1}z_{B_1}$ at B_1 in two ways:

1. By the translational errors p_{ϑ_x} and p_{ϑ_z} related to inclination angle ϵ_1 and the inaccurate values of D and A_1 related to g ,
2. By the rotational error motions ϵ_{x_1} , ϵ_{z_1} , $\epsilon_{\tau_{x_1}}$ and $\epsilon_{\tau_{z_1}}$ generated from the revolute and prismatic joints (i.e. τ_1 and ϵ_1).

Error motions ϵ_{x_1} , ϵ_{z_1} , $\epsilon_{\tau_{x_1}}$ and $\epsilon_{\tau_{z_1}}$ can change both the orientation and position of coordinate $x_{B_1}y_{B_1}z_{B_1}$ at the centre B_1 of the spherical joint. Since a spherical joint does not have any specific direction of rotation, the orientation change of coordinate $x_{B_1}y_{B_1}z_{B_1}$ at B_1 with respect to fixed coordinate system xyz does not represent any error. However, the interactions of ϵ_{x_1} , ϵ_{z_1} , $\epsilon_{\tau_{x_1}}$ and $\epsilon_{\tau_{z_1}}$ with the structural parameters, e.g. leg lengths τ_1 , represent a change in the position of coordinate $x_{B_1}y_{B_1}z_{B_1}$ at the centre B_1 of the spherical joint with respect to fixed coordinate system xyz (Figure 5.2*b*). Therefore, the kinematic errors of each closed loop of the RPS mechanism (i.e. tripod) can be represented by the positional change of the centre of the respective spherical joint of that closed loop.

5.3.2 Strategy to develop error model for the parallel mechanism

In section 5.3.1, various error sources of a single closed loop have been considered to see their effects on the position and orientation of the centroid E of the moving platform $B_1B_2B_3$. It is clear from the Figure 5.2b that all three closed loops will have effect in determining the position and orientation of the centroid E of the moving platform $B_1B_2B_3$. This combined effect on E can be found by considering the constraint equations for the complete RPS mechanism, instead of the constraint equations for individual legs. The details are given below.

In the RPS mechanism, each leg is connected to the fixed base by a revolute joint (A_1, A_2 or A_3) and to the moving platform by a spherical joint (B_1, B_2 or B_3). Therefore, each leg's motion is constrained in one of the following three planes [44,86], as can be written by observing equation (5.10) to (5.12)

$$(DB_1)_x = 0, \quad (5.17)$$

where $(DB_1)_x$ and $(DB_1)_z$ are the x and z components of $\overrightarrow{DB_1}$;

$$(DB_2)_x = -\sqrt{3}(DB_2)_z, \quad (5.18)$$

where $(DB_2)_x$ and $(DB_2)_z$ are the x and z components of $\overrightarrow{DB_2}$;

$$(DB_3)_x = \sqrt{3}(DB_3)_z, \quad (5.19)$$

where $(DB_3)_x$ and $(DB_3)_z$ are the x and z components of $\overrightarrow{DB_3}$.

Substituting the x and z components of equation (5.10) to (5.12) into equations (5.17) to (5.19) provides

$$P_x + hl_x = 0, \quad (5.20)$$

$$P_x + \frac{\sqrt{3}}{2}hn_x - \frac{1}{2}hl_x = -\sqrt{3}\left(P_z + \frac{\sqrt{3}}{2}hn_z - \frac{1}{2}hl_z\right), \quad (5.21)$$

$$P_x - \frac{\sqrt{3}}{2}hn_x - \frac{1}{2}hl_x = \sqrt{3}\left(P_z - \frac{\sqrt{3}}{2}hn_z - \frac{1}{2}hl_z\right). \quad (5.22)$$

The following equation can be obtained from equations (5.20) to (5.22):

$$l_x = n_z. \quad (5.23)$$

From (5.22) and (5.23), the following equation is obtained:

$$P_z = \frac{1}{2}h(l_z - n_x). \quad (5.24)$$

Equations (5.20), (5.23) and (5.24) are the constraint equations of the RPS mechanism. Equation (5.23) is related to the orientation of the moving platform $B_1B_2B_3$ of the RPS mechanism, and equations (5.22) and (5.24) are related to the position of the centroid E of the moving platform $B_1B_2B_3$. The equations specify the conditions under which the centroid E of the moving platform can be determined with respect to the fixed coordinate system xyz of Figure 5.2*b*. However, the following kinematic factors must be taken into consideration for an RPS mechanism:

- A. RPS mechanism has only three DOF. It means, among twelve parameters of equation (5.9), which determine the position and orientational of the moving platform, only three can be chosen arbitrarily. In fact, in any case, the y motion of the moving platform must be specified (i.e. P_y of equation (5.9)) since it is not found in three constrain equations (5.20), (5.23) and (5.24). The rest two motions of the RPS mechanism will have to be chosen from the rest 11 parameters of equation (5.9).
- B. As shown in [49,124], if all positional parameters are selected for the three DOF of the RPS mechanism (i.e. P_x , P_y and P_z are the independent parameters, and the position of the centroid E of the moving platform $B_1B_2B_3$ can be determined with respect to xyz coordinate system), then eight platform orientations are possible. If, however, the tip (u) and tilt (v) motions and the P_y motion are used for the desired

DOF of the RPS mechanism, two locations of the platform are possible, as can be determined by the constraint equations (5.20), (5.23) and (5.24).

Since it has already been shown how the positional errors related to the spherical joint affect the position and orientation of the centroid E of the moving platform $B_1B_2B_3$, it is clear that for a certain orientation (i.e. tip u) of the platform, the motions P_x and P_y associated with E will contain the effects of the errors ϵ_{x_1} , ϵ_{z_1} , $\epsilon_{\tau_{x_1}}$ and $\epsilon_{\tau_{z_1}}$.

For the error analysis of the RPS mechanism of HAMS, P_x and P_z of equations (5.20) and (5.24) can be replaced with the translational error motions of the centroid of the moving platform of the tripod, where the n_x , l_x , n_z and l_z values can be determined from the moving platform's orientation. Equation (5.23) represents a rotational error motion about the direction of the moving platform (i.e. about y' axis of coordinate $x'y'z'$ as shown in Figure 5.2b). The translational and rotational error motions associated with the moving platform of HAMS are defined in section 5.6.1.

The above discussion suggests that for the development of a kinematic error model for HAMS, a strategy can be applied where the kinematic relation between the centroids of the base platform $A_1A_2A_3$ and the moving platform $B_1B_2B_3$ are considered, since the centroid of $B_1B_2B_3$ contains the effect of the errors arising from the various sources of the mechanism. This strategy for the error model is similar to the one for a serial mechanism in which joints and their associated errors are assumed to have a serial relationship (see sections 5.4 to 5.6).

5.4 Kinematic analysis of HAMS

5.4.1 Kinematic representation of HAMS for model development

Figure 5.4 schematically represents the kinematic structure of HAMS, describing the geometrical relationships among the coordinate systems placed at the points of interest for the analysis, e.g. at point T , where T indicates the target position. The machine reference frame with coordinate $x_0y_0z_0$ is placed at the centroid O of the top surface of machine base. It is assumed that the x and z stages are at A and B positions with respect to reference frame $x_0y_0z_0$, where A and B positions are at $(0, h_1, d_1)$ and $(d_2, h_2, 0)$, respectively. Here h_1, d_1, h_2, d_2 are the offset values of the origins of the coordinate systems for the x and z stages. The reference frame $x_t y_t z_t$ is placed at point T , where the direction of axis z_t indicates the orientation of the target, and (t_x, t_y, t_z) represents the coordinate position of the target T with respect to the reference coordinate $x_w y_w z_w$, placed at the centre of the target interface wheel H .

The kinematic structure of RPS mechanism, as described in section 5.4.1 for Figure 5.2b, is still valid for the RPS mechanism shown in Figure 5.4. Furthermore, point F is considered as the centroid of the rotating platform and as the centre of tilt rotation when HAMS is error-free. For simplicity, in this paper, the platforms that provide the tip and tilt motions are referred as the moving platform and the rotating platform (Figure 5.4).

For the convenience of analysis, it is assumed that the z axis of the xyz coordinate system is aligned with vector $\overrightarrow{DA_1}$, with the x axis in the same plane of the fixed triangular platform $A_1A_2A_3$, while the y axis is normal to the plane of the platform and is pointing upward. It should be noted that, for the alignment of target T , \overrightarrow{EF} should be

parallel to \overrightarrow{GH} , which means that the orientation of the target wheel is only controlled by the moving platform and by the rotating platform mounted on the moving platform.

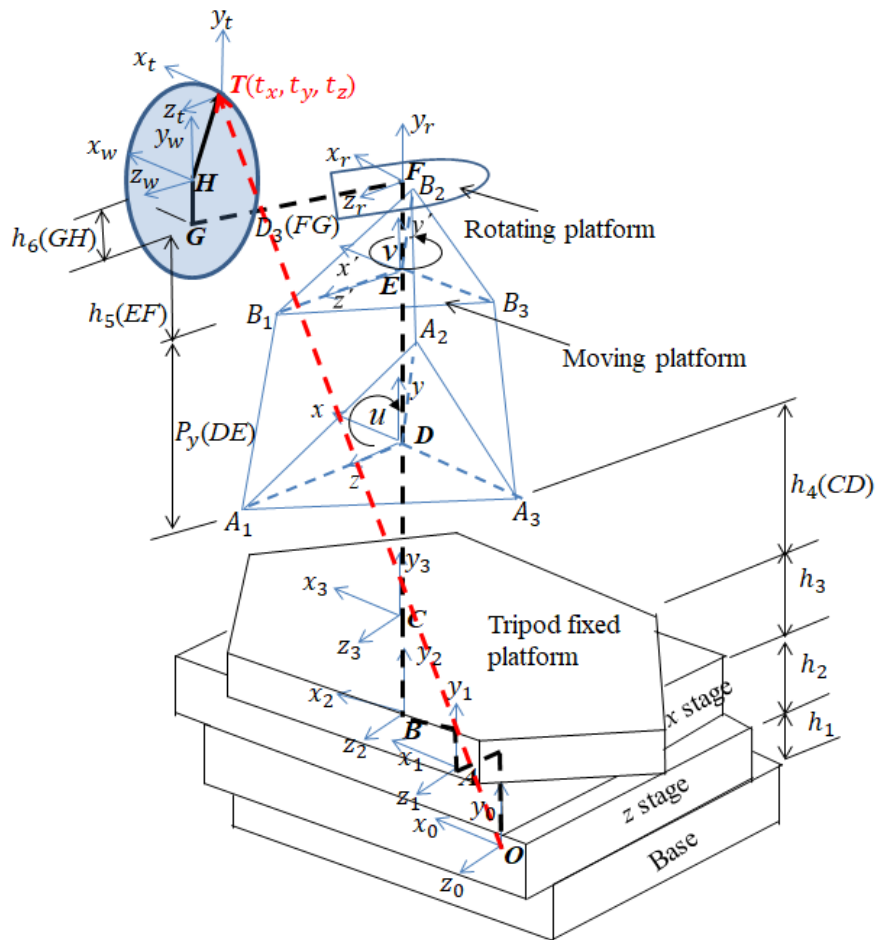


Figure 5.4 Kinematic representation of HAMS for model development.

5.4.2 Method of kinematic model

The kinematic analysis of HAMS employs the concept of the homogeneous transformation matrix (HTM), which is discussed in section 4.3.1. Based on the definition of a HTM, if the position and orientation of the end-effector frame $x_t y_t z_t$ at T , with respect to the inertial reference frame $x_0 y_0 z_0$ at O , is represented by the HTM A_T , then the elements of A_T will depend on the three position and nine orientation parameters of frame $x_t y_t z_t$ with respect to the reference frame $x_0 y_0 z_0$. The matrix A_T is formed by multiplying the A_i matrices,

$$\mathbf{A}_T = \mathbf{A}_1 \mathbf{A}_2 \mathbf{A}_3 \dots \mathbf{A}_N, \quad (5.25)$$

where \mathbf{A}_i represent the interconnected coordinates (say, N in total) between the points O and T . Equation (5.25), known as the “loop closure equation”, provides six scalar equations which give the end effector coordinates x_T^{ideal} (no error) when the mechanism’s structural parameter s (for example, offsets between the two links), and configuration parameter c (for example, joint angle) are known, as shown in the following equation [91]

$$x_T^{ideal} = f^{ideal}(s, c). \quad (5.26)$$

However, when the errors are considered, the loop closure equation becomes

$$\mathbf{A}_{T_{err}} = \mathbf{A}_1 \mathbf{E}_1 \mathbf{A}_2 \mathbf{E}_2 \mathbf{A}_3 \mathbf{E}_3 \dots \mathbf{A}_N \mathbf{E}_N, \quad (5.27)$$

where \mathbf{E}_i represents the HTMs defining the errors related to the relevant coordinates between the points O and T [139].

The end-effector’s coordinates can be calculated from equation (5.28) below

$$x_T^{real} = f^{real}(s, c, e), \quad (5.28)$$

where e denotes the vector of the errors, connecting the ideal position of T to its real position. Thus, the end effector’s position and orientation error Δx can be defined as the 6×1 matrix which represents the difference between the real position and orientation of the end-effector and the ideal one, as shown below

$$\Delta x = x_T^{real} - x_T^{ideal}. \quad (5.29)$$

Then, for a given set of errors, Δx can be calculated.

Considering that the modelling technique using loop closure equations outlines a general framework for the error analysis of a kinematic mechanism, it is worth paying attention to the following points for the case of an error analysis for a hybrid mechanism:

A. \mathbf{E}_i , as represented in equation (5.27), defines the errors for a particular frame \mathbf{A}_i .

This definition is based on the fact that physical errors change the geometric

properties of a mechanism, which may cause a particular frame \mathbf{A}_i to be displaced (translationally and/or rotationally) from its ideal location to its real location. The position and orientation of the real frame $\mathbf{A}_{i_{err}}$ with respect to the ideal frame \mathbf{A}_i can be represented by a 4×4 matrix \mathbf{E}_i . The rotation part of \mathbf{E}_i (the first three columns of the matrix as per the definition of HTM) shows the orientation change of frame \mathbf{A}_i due to rotational errors of the frame itself, while the translational part of \mathbf{E}_i (the last column of the matrix as per the definition of HTM) shows the positional deviations of the frame \mathbf{A}_i due to translational errors of the frame. In this way, the error components of \mathbf{E}_i can be used to define the errors of a particular frame \mathbf{A}_i .

B. In many cases, the arrangements of the constraints, such as joints and bearings, in a kinematic mechanism can be conveniently replaced with an equivalent kinematic system. Consider a simple example of the arrangement of the constraints applied to a cube, as given by Hale (1999) [129]. Five constraints, as shown in Figure 5.5, are applied to the cube in such an arrangement that all the constraint lines intersect at the axis located at the centre of the cube. Since there exists no constraint that can affect the moment about this axis because the lever arm length is zero, the cube is free to rotate about this axis. Thus, the arrangement of these five constraints can be uniquely defined by the body's single degree of freedom. As such, if a reference frame is placed at the centre of the cube, any physical changes in the arrangement of the five constraints will affect the position and orientation of the reference frame at the centre of the cube. Thus, for the purpose of the kinematic analysis of the cube, it is logical to consider that the study of the geometric properties of the centre of the cube will be equivalent to the study of the overall geometric properties of the cube. Therefore, an error definition matrix can be constructed for the frame of the centre of the cube, and the elements of the matrix will represent the rotational and/or

translational errors of the overall kinematic arrangement of the cube. These errors will be known as the “generalised errors”, while the equivalent points of the kinematic system (the centre of the cube of the above example) are defined as a “reaction points” in the error analysis.

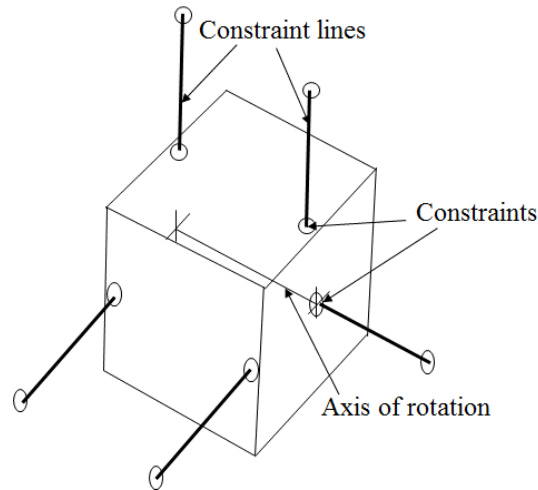


Figure 5.5 Five constraints applied to a cube result in a rotational degree of freedom at its centre [129].

C. As discussed in section 5.3.1 and 5.3.2, with careful study of the joints and their constraints in a parallel mechanism, it is possible to establish reaction point/s (e.g. E , the centroid of the moving platform $B_1B_2B_3$ as shown in Figure 5.2b and 5.4) and, hence, the use of generalised errors, e.g. $\delta_{x_{err}}$, $\delta_{z_{err}}$ and u_{err} , for the moving platform, instead of the use of the geometric errors of the individual joints associated with the moving platform. This can simplify the kinematic analysis of a complex mechanism, such as a parallel or a hybrid mechanism, and can be effective in considering the error averaging effects of a parallel mechanism.

5.5 Modelling the parallel mechanism with no error

As outlined in section 5.4.2, the first step to develop an error model to find the positional deviations at the target T , arising from the errors of the tip and tilt motions of

HAMS, is to derive the expressions (see equation (5.26)) that describe the position of the target with respect to the reference coordinate when HAMS has error-free tip and tilt motions. Assuming the axes of the coordinate frames between O and T are initially parallel to the axes of the reference coordinate frame $x_0y_0z_0$, the desired orientation of T , as determined by the direction of the axis z_t , is achieved by Roll-Pitch-Yaw angles [72,130]. Using this representation, and following CLF's standard method of laser alignment, the desired orientation of the target T is achieved by three successive rotations of the frame $x_t y_t z_t$ about its coordinate axes: rotation α about the x_T axis or pitch, followed by rotation φ about the z_T axis or roll ($\varphi = 0$ as per CLF's method), followed by a rotation β about y_T or yaw. This orientation can be achieved by the following transformation process of the frames as per equation (5.25)

$$\mathbf{T}_T^0(\mathit{ideal}) = \mathbf{T}_{\mathit{position}} \mathbf{T}_1 \mathbf{T}_2, \quad (5.30)$$

where $\mathbf{T}_T^0(\mathit{ideal})$ represents the ideal location (position and orientation) of the target with respect to the reference coordinate by using,

$$\mathbf{T}_{\mathit{position}} = \begin{bmatrix} 1 & 0 & 0 & x + d_1 + t_x \\ 0 & 1 & 0 & P_y + h_1 + h_2 + h_3 + h_4 + h_5 + h_6 + t_y \\ 0 & 0 & 1 & z + d_2 + d_3 + t_z \\ 0 & 0 & 0 & 1 \end{bmatrix} \quad (5.31)$$

where x , P_y and z are the translational motions along the x , y and z axes of the reference frame $x_0y_0z_0$; t_x , t_y and t_z represent the values of the position vector of T with respect to coordinate $x_w y_w z_w$ at H ; and $h_1, h_2, h_3, h_4, h_5, h_6, d_1, d_2$ and d_3 represent the offsets of the structure as shown in Figure 5.4. Also, by using

$$\mathbf{T}_1 = \begin{bmatrix} 1 & 0 & 0 & 0 \\ 0 & \cos \alpha & \sin \alpha & 0 \\ 0 & -\sin \alpha & \cos \alpha & 0 \\ 0 & 0 & 0 & 1 \end{bmatrix} \quad (5.32a)$$

and

$$\mathbf{T}_2 = \begin{bmatrix} \cos \beta & 0 & -\sin \beta & 0 \\ 0 & 1 & 0 & 0 \\ \sin \beta & 0 & \cos \beta & 0 \\ 0 & 0 & 0 & 1 \end{bmatrix}, \quad (5.32b)$$

$\mathbf{T}_T^0(\mathit{ideal})$ of equation (5.30) will have the following form

$$\mathbf{T}_T^0(\mathit{ideal}) = \begin{bmatrix} \cos \beta & 0 & -\sin \beta & x + d_1 + t_x \\ \sin \alpha \sin \beta & \cos \alpha & \cos \beta \sin \alpha & P_y + h_1 + h_2 + h_3 + h_4 + h_5 + h_6 + t_y \\ \cos \alpha \sin \beta & -\sin \alpha & \cos \alpha \cos \beta & z + d_2 + d_3 + t_z \\ 0 & 0 & 0 & 1 \end{bmatrix}. \quad (5.33)$$

Equation (5.30) (also equation (5.33)) represents the coordinate relationship between the frames $x_0y_0z_0$ and $x_t y_t z_t$. This is shown in Figure 5.4 by drawing a thick black line from reference point O to T (that is, vector \overrightarrow{OT}). The same position and orientation of T can also be achieved with a vector $\overrightarrow{ODEFGHT}$ that connects O and T when going through the structure of HAMS; this vector is shown as a thick red dotted line in Figure 5.4. This latter vector can be determined by structural and configuration parameters, as given in equation (5.26).

Now consider the case when the target T needs to be placed at a desired location with the position (x, P_y, z) and with the orientation defined by the rotational angles α and β . This position of target T can be achieved by two translational motions of x and z along the x_2 and z_1 directions, given by the linear xz system, and one translational motion of P_y along the vertical y axis of the xyz frame, given by the parallel RPS mechanism (Figure 5.4). The desired orientation of the α and β angles can be achieved by the tip u and tilt v motions. Tip is the rotational motion of the RPS mechanism about the x axis of the xyz frame to orientate the moving platform with respect to xyz , while tilt is the rotational motion by the motor about the y' axis of the $x'y'z'$ frame to orientate the rotating platform with respect to the $x'y'z'$ frame. The transformation matrix which

describes the orientation of the target through the use of tip u and tilt v angles is given by

$$\mathbf{T}_T^O(\mathbf{u} - \mathbf{v})_{no\ error} = \mathbf{T}_D^O \mathbf{T}_E^D \mathbf{T}(\mathbf{u}) \mathbf{T}_F^E \mathbf{T}(\mathbf{v}) \mathbf{T}_H^F \mathbf{T}_T^H, \quad (5.34)$$

$$\text{where } \mathbf{T}_D^O = \begin{bmatrix} 1 & 0 & 0 & d_1 \\ 0 & 1 & 0 & h_1 + h_2 + h_3 + h_4 \\ 0 & 0 & 1 & d_2 \\ 0 & 0 & 0 & 1 \end{bmatrix}; \quad (5.35a)$$

$$\mathbf{T}_E^D = \begin{bmatrix} 1 & 0 & 0 & 0 \\ 0 & 1 & 0 & P_y \\ 0 & 0 & 1 & 0 \\ 0 & 0 & 0 & 1 \end{bmatrix}; \quad (5.35b)$$

the HTM to represent tip motion is given by

$$\mathbf{T}(\mathbf{u}) = \begin{bmatrix} 1 & 0 & 0 & 0 \\ 0 & \cos u & \sin u & 0 \\ 0 & -\sin u & \cos u & 0 \\ 0 & 0 & 0 & 1 \end{bmatrix}; \quad (5.36)$$

the HTM to represent tilt motion is given by

$$\mathbf{T}(\mathbf{v}) = \begin{bmatrix} \cos v & 0 & -\sin v & 0 \\ 0 & 1 & 0 & 0 \\ \sin v & 0 & \cos v & 0 \\ 0 & 0 & 0 & 1 \end{bmatrix}; \quad (5.37)$$

$$\mathbf{T}_F^E = \begin{bmatrix} 1 & 0 & 0 & 0 \\ 0 & 1 & 0 & h_5 \\ 0 & 0 & 1 & 0 \\ 0 & 0 & 0 & 1 \end{bmatrix}; \quad (5.38a)$$

$$\mathbf{T}_H^F = \begin{bmatrix} 1 & 0 & 0 & 0 \\ 0 & 1 & 0 & h_6 \\ 0 & 0 & 1 & d_3 \\ 0 & 0 & 0 & 1 \end{bmatrix}; \quad (5.38b)$$

and

$$\mathbf{T}_T^H = \begin{bmatrix} 1 & 0 & 0 & t_x \\ 0 & 1 & 0 & t_y \\ 0 & 0 & 1 & t_z \\ 0 & 0 & 0 & 1 \end{bmatrix}. \quad (5.38c)$$

Substituting the values from the equations (5.35) to (5.38) into equation (5.34) yields

$$\mathbf{T}_T^O(\mathbf{u} - \mathbf{v})_{no\ error} = \begin{bmatrix} \cos v & 0 & -\sin v & A_1 \\ \sin u \sin v & \cos u \cos v \sin u & A_2 \\ \cos u \sin v & -\sin u \cos u \cos v & A_3 \\ 0 & 0 & 0 & 1 \end{bmatrix} \quad (5.39)$$

and

$$A_1 = x + d_1 - d_3 \sin v + t_x \cos v - t_z \sin v, \quad (5.40a)$$

$$A_2 = P_y + h_1 + h_2 + h_3 + h_4 + (h_5 + h_6 + t_y) \cos u + (d_3 + t_z) \cos v \sin u + t_x \sin u \sin v, \quad (5.40b)$$

and

$$A_3 = z + d_2 - (h_5 + h_6 + t_y) \sin u + (d_3 + t_z) \cos u \cos v + t_x \cos u \sin v. \quad (5.40c)$$

Comparison of the equation (5.33) with equation (5.39) shows that, for the target position of (x, P_y, z) and the orientation angles of α and β (pitch and yaw angles), both the vectors \overrightarrow{OT} and $\overrightarrow{ODEFGHT}$, as shown in Figure 5.4 can give the same orientation of the target; however, positional deviations take place at the target for the vector $\overrightarrow{ODEFGHT}$. These deviations are due to the architectural structure of HAMS and are discussed in detail in Chapter 6.

Subtracting equation (5.39) from equation (5.33) will give the positional deviations at the target T when HAMS has tip and tilt motions without any error:

$$D_{xt_{no\ error}} = t_x(\cos v - 1) - d_3 \sin v - t_z \sin v, \quad (5.41)$$

$$D_{yt_{no\ error}} = h_5(\cos u - 1) + h_6(\cos u - 1) + t_y(\cos v - 1) + (d_3 + t_z) \cos v \sin u + t_x \sin u \sin v, \quad (5.42)$$

$$D_{zt_{no\ error}} = d_3(\cos u \cos v - 1) + t_z(\cos u \cos v - 1) - (t_y + h_5 + h_6) \sin u + t_x \cos u \sin v. \quad (5.43)$$

5.6 Modelling for the mechanism with error

It is clear that when geometric errors are present in the mechanism, the transformation matrix $T_T^O(\mathbf{u} - \mathbf{v})_{no\ error}$ (equation (5.39)) will not be the same, since the spatial relationships among the frames between the points O and T will change (Figure 5.4). These geometric errors generally arise from the manufacturing and assembly errors of the components of the RPS mechanism and of the rotating platform actuated by the motor.

5.6.1 Error definitions

Assuming that parallelism and vertical errors of the HAMS are generally negligible, errors associated with the tip and tilt motions are considered in this kinematic model since they affect both the position and orientation of the target during its alignment. Tip and tilt errors are modelled as the “generalised errors” for this hybrid mechanism.

The tip error is related to the RPS mechanism. The RPS mechanism is a spatial mechanism which can provide three DOFs, that is rotational motions about the x and z axes (HAMS does not utilise rotation about the z axis and, hence, this rotation is ignored in this model) and translational motion along the y axis (all motions are with respect to the xyz frame of the RPS mechanism, as shown in Figure 5.4 and Figure 5.6a). However, the tip motion u of this mechanism induces small amount of translation motions $\delta_{x_{err}}$ and $\delta_{z_{err}}$ at point E along the x and z directions (note that E is the centroid of the moving platform, and is the origin of the coordinate frame $x'y'z'$ of the moving platform), and a rotation u_{err} about the vertical direction y (Figure 5.6a). Since these small motions take place in the constrained directions of the motion for the RPS mechanism, they may have an unwanted “decentering” effect on the moving platform, resulting in the positional

deviations at the target T .

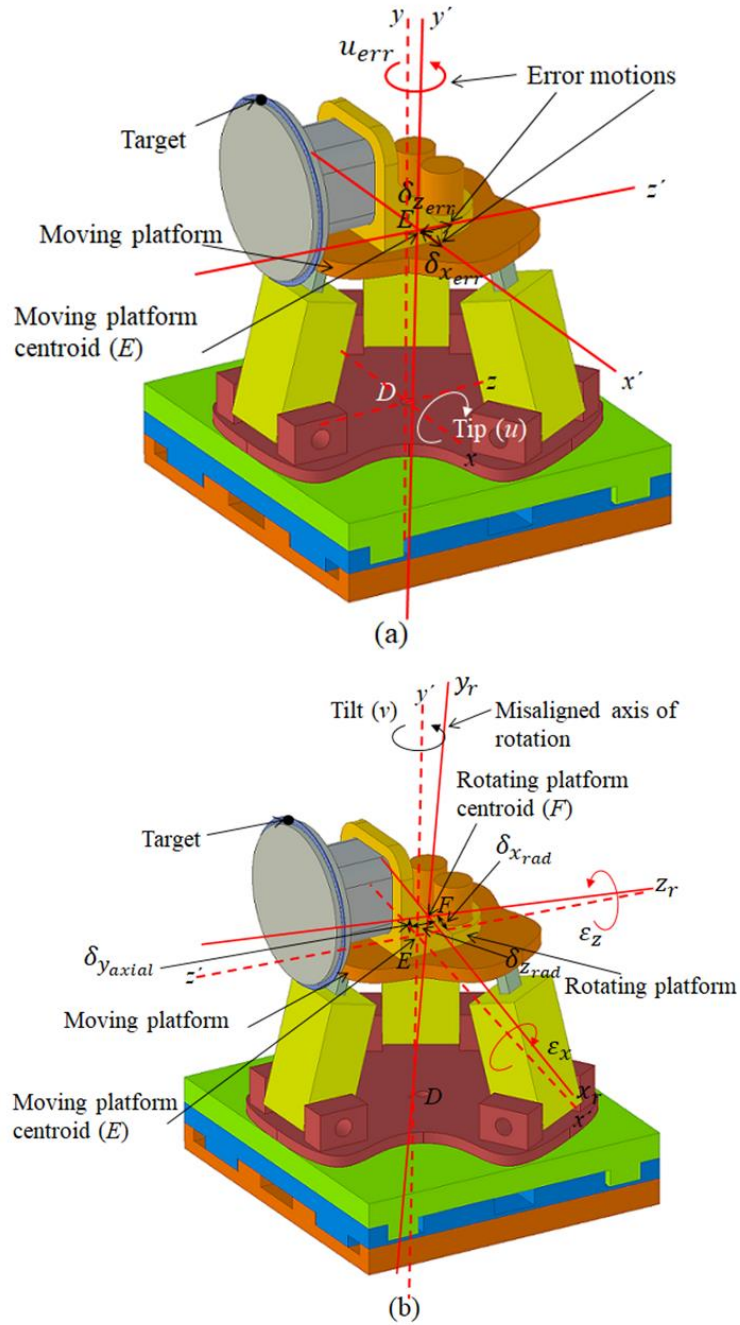


Figure 5.6 Error motions associated with: (a) tip (u) and (b) tilt (v).

A typical HTM to represent these error motions of HAMS can be written as:

$$\mathbf{T}(\mathbf{u})_{error} = (\mathbf{T}(\mathbf{u})_{err})_{pos.dev} \mathbf{T}(\mathbf{u}) \mathbf{T}(\mathbf{u}_{err}) \quad (5.44)$$

where $\mathbf{T}(\mathbf{u})$ is the HTM for tip motion, given in equation (5.35),

the HTM to represent the positional deviations at E is given by

$$(\mathbf{T}(\mathbf{u})_{err})_{pos.dev.} = \begin{bmatrix} 1 & 0 & 0 & \delta_{x_{err}} \\ 0 & 1 & 0 & 0 \\ 0 & 0 & 1 & \delta_{z_{err}} \\ 0 & 0 & 0 & 1 \end{bmatrix} \text{ and} \quad (5.45)$$

the HTM to represent the rotational error u_{err} about y' is given by

$$\mathbf{T}(\mathbf{u}_{err}) = \begin{bmatrix} \cos u_{err} & 0 & -\sin u_{err} & 0 \\ 0 & 1 & 0 & 0 \\ \sin u_{err} & 0 & \cos u_{err} & 0 \\ 0 & 0 & 0 & 1 \end{bmatrix}. \quad (5.46)$$

Substituting the values from the equations (5.45) and (5.46) and the value of $\mathbf{T}(u)$ into equation (5.44) provides:

$$\mathbf{T}(\mathbf{u})_{error} = \begin{bmatrix} \cos u_{err} & 0 & -\sin u_{err} & \delta_{x_{err}} \\ \sin u \sin u_{err} & \cos u & \cos u_{err} \sin u & 0 \\ \cos u \sin u_{err} & -\sin u & \cos u \cos u_{err} & \delta_{z_{err}} \\ 0 & 0 & 0 & 1 \end{bmatrix}. \quad (5.47)$$

$\mathbf{T}(\mathbf{u})_{error}$ is used to describe the errors associated with the tip motion while developing the positional deviation equations for the target in section 5.5.2.

It is important to note that the HTM for $(\mathbf{u})_{error}$ in equation (5.44) is written for the point E , the centroid of the moving platform as shown in Figure 5.4 and Figure 5.6a. As has been seen in section 5.4, centroid E plays an important role in writing the constraint equations of the moving platform of the RPS mechanism. Geometric errors associated with B_1 , B_2 and B_3 will affect the position and orientation of a reference frame $x'y'z'$ at point E . Therefore, E can be considered as the reaction point of the moving platform of the RPS mechanism, and the errors related to the point E , as shown in $\mathbf{T}(\mathbf{u})_{error}$, are called the generalised error parameters in this analysis.

The tilt errors are generated from the tilt motion of HAMS, which is the rotation of the rotating platform about the axis EF , as shown in Figure 5.4 to orientate the platform with respect to the moving platform's reference frame $x'y'z'$. Ideally, a rotating body should rotate about its axis of rotation without any error (EF should be aligned); however, in reality the axis of rotation of the rotating stage y_r revolves around y' with

two radial errors $\delta_{x_{rad}}$ and $\delta_{z_{rad}}$ along the x' and z' axes, one axial error $\delta_{y_{axial}}$ along the y' axis and two tilt errors ε_x and ε_z about the x' and z' axes (Figure 5.6b) [52]. Note that these six error parameters are enough to describe the positional and orientation changes of the centre of rotation F . Therefore, F can be considered as the reaction point for the rotating platform, while the six error parameters as the generalised error parameters for the tilt motion. These error motions can be described by the following HTM

$$\mathbf{T}(\mathbf{v})_{error} = (\mathbf{T}(\mathbf{v})_{err})_{pos.dev.} \mathbf{T}(\mathbf{v}) \mathbf{T}(\varepsilon_x) \mathbf{T}(\varepsilon_z) \quad (5.48)$$

where $\mathbf{T}(\mathbf{v})$ is the HTM for tilt motion as given in equation (5.37),

the HTM to represent the positional deviations at F is given by

$$(\mathbf{T}(\mathbf{v})_{err})_{pos.dev.} = \begin{bmatrix} 1 & 0 & 0 & \delta_{x_{rad}} \\ 0 & 1 & 0 & \delta_{y_{axial}} \\ 0 & 0 & 1 & \delta_{z_{rad}} \\ 0 & 0 & 0 & 1 \end{bmatrix}, \quad (5.49)$$

the HTM to represent the rotational error ε_x about x' is given by

$$\mathbf{T}(\varepsilon_x) = \begin{bmatrix} 1 & 0 & 0 & 0 \\ 0 & \cos \varepsilon_x & \sin \varepsilon_x & 0 \\ 0 & -\sin \varepsilon_x & \cos \varepsilon_x & 0 \\ 0 & 0 & 0 & 1 \end{bmatrix} \text{ and} \quad (5.50)$$

the HTM to represent rotational error ε_z about z' is given by

$$\mathbf{T}(\varepsilon_z) = \begin{bmatrix} \cos \varepsilon_z & -\sin \varepsilon_z & 0 & 0 \\ \sin \varepsilon_z & \cos \varepsilon_z & 0 & 0 \\ 0 & 0 & 1 & 0 \\ 0 & 0 & 0 & 1 \end{bmatrix}. \quad (5.51)$$

After substituting the values from the equations (5.49) to (5.51) and the value of $\mathbf{T}(\mathbf{v})$ into equation (5.48) yields (a first order approximation is applied for the expression $\mathbf{T}(\mathbf{v}) \mathbf{T}(\varepsilon_x) \mathbf{T}(\varepsilon_z)$, since the error terms are considered small compared to the tip and tilt motions):

$$\mathbf{T}(\mathbf{v})_{error} = \begin{bmatrix} \cos v A - \sin v \delta_{x_{rad}} & & & \\ \varepsilon_z & 1 & \varepsilon_x & \delta_{y_{axial}} \\ \sin v B & \cos v & & \delta_{z_{rad}} \\ 0 & 0 & 0 & 1 \end{bmatrix}, \quad (5.52)$$

where $A = (\sin v \varepsilon_x - \cos v \varepsilon_z)$ and (5.53a)

and $B = (-\sin v \varepsilon_z - \cos v \varepsilon_x)$. (5.53b)

$\mathbf{T}(\mathbf{v})_{error}$ is used to describe the errors associated with the tilt motion while developing the positional deviation equations for the target in section 5.5.3.

5.6.2 Model analysis: tip error only

The transformation matrix, which describes the position and orientation of target T when tip errors are considered (no error from the tilt), can be described as follows:

$$\mathbf{T}_T^O(\mathbf{u} - \mathbf{v})_{tip\ error} = \mathbf{T}_D^O \mathbf{T}_E^D \mathbf{T}(\mathbf{u})_{error} \mathbf{T}_F^E \mathbf{T}(\mathbf{v}) \mathbf{T}_H^F \mathbf{T}_T^H, \quad (5.54)$$

where \mathbf{T}_D^O , \mathbf{T}_E^D , \mathbf{T}_F^E , $\mathbf{T}(\mathbf{v})$, \mathbf{T}_H^F , \mathbf{T}_T^H are as before (section 5.5 and 5.6.1) and $\mathbf{T}(\mathbf{u})_{error}$ is shown in equation (5.47).

Substituting above values into equation (5.54) yields:

$$\mathbf{T}_T^O(\mathbf{u} - \mathbf{v})_{tip\ error} = \begin{bmatrix} J_1 & 0 & J_4 & B_1 \\ J_2 & \cos u & J_5 & B_2 \\ J_3 & -\sin u & J_6 & B_3 \\ 0 & 0 & 0 & 1 \end{bmatrix}, \quad (5.55)$$

where

$$J_1 = \cos v \cos u_{err} + \sin v \sin u_{err}, \quad (5.56a)$$

$$J_2 = -\cos v \sin u \sin u_{err} + \sin u \sin v \cos u_{err}, \quad (5.56b)$$

$$J_3 = -\cos u \cos v \sin u_{err} + \cos u \sin v \cos u_{err}, \quad (5.56c)$$

$$J_4 = \cos v \sin u_{err} - \sin v \cos u_{err}, \quad (5.57a)$$

$$J_5 = \cos v \sin u \cos u_{err} + \sin u \sin v \sin u_{err}, \quad (5.57b)$$

$$J_6 = \cos u \cos v \cos u_{err} + \cos u \sin v \sin u_{err}, \quad (5.57c)$$

$$\begin{aligned}
B_1 &= \delta_{x_{err}} + x + d_1 + d_3(\cos v \sin u_{err} - \sin v \cos u_{err}) \\
&+ t_x(\cos v \cos u_{err} + \sin v \sin u_{err}) + t_z(\cos v \sin u_{err} - \sin v \cos u_{err}),
\end{aligned} \tag{5.58a}$$

$$\begin{aligned}
B_2 &= P_y + h_1 + h_2 + h_3 + h_4 + (h_5 + h_6 + t_y) \cos u \\
&+ d_3 \sin u (\cos v \cos u_{err} + \sin v \sin u_{err}) - t_x \sin u (\cos v \sin u_{err} - \sin v \cos u_{err}) \\
&+ t_z \sin u (\cos v \cos u_{err} + \sin v \sin u_{err}),
\end{aligned} \tag{5.58b}$$

$$\begin{aligned}
B_3 &= \delta_{z_{err}} + d_2 + z - (h_5 + h_6 + t_y) \sin u \\
&+ d_3 \cos u (\cos v \cos u_{err} + \sin v \sin u_{err}) - t_x \cos u (\cos v \sin u_{err} - \sin v \cos u_{err}) \\
&+ t_z \cos u (\cos v \cos u_{err} + \sin v \sin u_{err}).
\end{aligned} \tag{5.58c}$$

The positional deviations at the target T as a result of the combined effects of tip motion errors and the architecture of HAMS can be found by subtracting equation (5.55) from equation (5.33):

$$\begin{aligned}
D_{xt_{tip\ error+arch.}} &= \delta_{x_{err}} - (d_3 + t_z)(\sin v \cos u_{err} - \cos v \sin u_{err}) \\
&+ t_x(\cos v \cos u_{err} + \sin v \sin u_{err} - 1),
\end{aligned} \tag{5.59}$$

$$\begin{aligned}
D_{yt_{tip\ error+arch.}} &= (h_5 + h_6 + t_y) (\cos u - 1) \\
&+ (d_3 + t_z) \sin u (\cos v \cos u_{err} + \sin v \sin u_{err}) \\
&- t_x \sin u (\cos v \sin u_{err} - \sin v \cos u_{err}),
\end{aligned} \tag{5.60}$$

$$\begin{aligned}
D_{zt_{tip\ error+arch.}} &= \delta_{z_{err}} - (h_5 + h_6 + t_y) \sin u \\
&+ (d_3 + t_z)(\cos u \cos v \cos u_{err} + \cos u \sin v \sin u_{err} - 1) \\
&- t_x \cos u (\cos v \sin u_{err} - \sin v \cos u_{err}).
\end{aligned} \tag{5.61}$$

If the generalised error parameters for the tip motion $\delta_{x_{err}}$, $\delta_{z_{err}}$ and u_{err} of the RPS mechanism and the offset values of the hybrid mechanism, such as h_5 , d_3 and t_x , are known, the positional deviations of the target in the x_0 , y_0 and z_0 directions can be calculated from the equations (5.59) to (5.61) for particular u and v angles.

5.6.3 Model analysis: tilt error only

The transformation matrix that describes the position and orientation of the target T when tilt (v) errors are considered (no error from the tip motion) can be described as follows:

$$\mathbf{T}_T^O(\mathbf{u} - \mathbf{v})_{tilt\ error} = \mathbf{T}_D^O \mathbf{T}_E^D \mathbf{T}(\mathbf{u}) \mathbf{T}_F^E \mathbf{T}(\mathbf{v})_{error} \mathbf{T}_H^F \mathbf{T}_T^H, \quad (5.62)$$

where \mathbf{T}_D^O , \mathbf{T}_E^D , \mathbf{T}_F^E , $\mathbf{T}(\mathbf{u})$, \mathbf{T}_H^F , \mathbf{T}_T^H are the same as before (section 5.5 and 5.6.1) and $\mathbf{T}(\mathbf{v})_{error}$ is shown in equation (5.52).

Substituting above values into equation (61) provides:

$$\mathbf{T}_T^O(\mathbf{u} - \mathbf{v})_{tilt\ error} = \begin{bmatrix} \cos v K_3 - \sin v C_1 \\ K_1 & K_4 & K_6 & C_2 \\ K_2 & K_5 & K_7 & C_3 \\ 0 & 0 & 0 & 1 \end{bmatrix}, \quad (5.63)$$

where

$$K_1 = \cos u \varepsilon_z + \sin u \sin v, \quad (5.64a)$$

$$K_2 = \cos u \sin v - \sin u \varepsilon_z, \quad (5.64b)$$

$$K_3 = \sin v \varepsilon_x - \cos v \varepsilon_z, \quad (5.65a)$$

$$K_4 = \cos u - \sin u (\cos v \varepsilon_x + \sin v \varepsilon_z), \quad (5.65b)$$

$$K_5 = -\sin u - \cos u (\cos v \varepsilon_x + \sin v \varepsilon_z), \quad (5.65c)$$

$$K_6 = \sin u \cos v + \cos u \varepsilon_x, \quad (5.66a)$$

$$K_7 = \cos u \cos v - \sin u \varepsilon_x, \quad (5.66b)$$

$$\begin{aligned} C_1 = & \delta_{x_{rad}} + x + d_1 - d_3 \sin v + t_x \cos v - t_z \sin v - h_6 (\cos v \varepsilon_z - \sin v \varepsilon_x) \\ & - t_y (\cos v \varepsilon_z - \sin v \varepsilon_x), \end{aligned} \quad (5.67a)$$

$$\begin{aligned} C_2 = & P_y + h_1 + h_2 + h_3 + h_4 + (h_5 + \delta_{y_{axial}}) \cos u \\ & + \delta_{z_{rad}} \sin u + \cos u + (h_6 + t_y) (\cos u - \sin u (\cos v \varepsilon_x + \sin v \varepsilon_z)) \\ & + (d_3 + t_z) (\cos v \sin u + \cos u \varepsilon_x) + t_x (\cos u \varepsilon_z + \sin u \sin v), \end{aligned} \quad (5.67b)$$

$$\begin{aligned}
C_3 &= \delta_{z_{rad}} \cos u - \delta_{y_{axial}} \sin u + d_2 + z - h_5 \sin u \\
&- (h_6 + t_y)(\sin u + \cos u (\cos v \varepsilon_x + \sin v \varepsilon_z)) \\
&+ (d_3 + t_z)(\cos u \cos v - \sin u \varepsilon_x) + t_x (\cos u \sin v - \sin u \varepsilon_z).
\end{aligned} \tag{5.67c}$$

The positional deviations at the target T as a result of the combined effects of tilt motion errors and the architecture of HAMS can be found by subtracting equation (5.63) from equation (5.33):

$$\begin{aligned}
D_{xt_{tilt\ error+arch.}} &= \delta_{x_{rad}} - (d_3 + t_z) \sin v + t_x (\cos v - 1) - h_6 (\cos v \varepsilon_z - \\
&\sin v \varepsilon_x) - t_y (\cos v \varepsilon_z - \sin v \varepsilon_x),
\end{aligned} \tag{5.68}$$

$$\begin{aligned}
D_{yt_{tilt\ error+arch.}} &= \delta_{y_{axial}} \cos u + h_5 (\cos u - 1) \\
&+ \delta_{z_{rad}} \sin u + (h_6 + t_y)(\cos u - \sin u (\cos v \varepsilon_x + \sin v \varepsilon_z) - 1) \\
&+ (d_3 + t_z)(\cos v \sin u + \cos u \varepsilon_x) + t_x (\cos u \varepsilon_z + \sin u \sin v),
\end{aligned} \tag{5.69}$$

$$\begin{aligned}
D_{zt_{tilt\ error+arch.}} &= \delta_{z_{rad}} \cos u - \delta_{y_{axial}} \sin u - h_5 \sin u \\
&- (h_6 + t_y)(\sin u + \cos u (\cos v \varepsilon_x + \sin v \varepsilon_z)) \\
&+ (d_3 + t_z) (\cos u \cos v - \sin u \varepsilon_x - 1) + t_x (\cos u \sin v - \sin u \varepsilon_z).
\end{aligned} \tag{5.70}$$

For the known generalised error parameters of the tilt motion, $\delta_{x_{rad}}$, $\delta_{y_{axial}}$, $\delta_{z_{rad}}$, $\delta_{z_{err}}$, ε_x and ε_z , of the rotating stage, and for the known offset values of the hybrid mechanism, such as h_5 , d_3 and t_x , the positional deviations at the target in the x_0 , y_0 and z_0 directions can be calculated from the equations (5.68) to (5.70) for particular u and v angles.

5.7 Analytical equations to describe the error parameters

Equations (5.59) to (5.61) and (5.68) to (5.70) show that for a set of tip, tilt and structural parameters, positional deviations at the target T due to tip and tilt errors can be determined, given that generalised error parameters, such as $\delta_{x_{err}}$, $\delta_{z_{err}}$, u_{err} , $\delta_{x_{rad}}$, $\delta_{z_{rad}}$, ε_x and ε_z , of the mechanism are known. In the following section, the relationships between the error parameters are examined analytically.

5.7.1 Tip error parameters

In the RPS mechanism, the presence of error motions $\delta_{x_{err}}$, $\delta_{z_{err}}$ and u_{err} causes positional deviations at point E and a rotation around the vertical direction at point E (Figure 5.6, left). These positional deviations at E due to the translational error motions of the RPS mechanism of HAMS can be determined by writing the constraint equations (5.20), (5.23) and (5.24) for the HAMS' RPS mechanism for a certain tip motion. The constraint equations that represent the positional deviations at E of the HAMS' RPS mechanism take the following form with the help of equation (5.47), which shows the orientation of the moving platform in the presence of $\delta_{x_{err}}$, $\delta_{z_{err}}$ and u_{err} :

$$\delta_{x_{err}} = h \sin u_{err} \quad \text{and} \quad (5.71)$$

$$\delta_{z_{err}} = \frac{h \cos u_{err} (\cos u - 1)}{2}. \quad (5.72)$$

The error parameters $\delta_{x_{err}}$, $\delta_{z_{err}}$ and u_{err} can be measured experimentally and will be used in Chapter 6 for the calibration of the tripod of HAMS. However, an alternative strategy to determine the rotational error motion of the RPS mechanism can be outlined as follows: the positional deviations of the centroid of the moving platform E in the x and z directions, when measured, represent $\delta_{x_{err}}$ and $\delta_{z_{err}}$ of the equations (5.71) and (5.72). Then, for the particular values of u and v angles, and for the known radius of the moving platform h (see Figure 5.2b), the rotational error motion u_{err} can be determined from the stated equations. However, the accuracy of determining u_{err} will depend on the ability of measuring the positional deviations at or very close to the centroid E . This may be difficult to achieve in some cases, for example, due to not being able to place the reflector of an interferometer at point E . In such cases, offsets in the x and z directions, arising from the placement of the measurement equipment, may need to be taken into considerations, and u_{err} should be determined using equations (5.59)

and (5.61), along with the equations (5.71) and (5.72) (offset d_3 of equations (5.59) and (5.61) will be replaced with the offset that arise from the placement of the measurement equipment).

5.7.2 Tilt error parameters

Ideally, in the absence of the errors that may arise from the tilt motion, the centroids of the moving stage and the rotating stage, that is E and F respectively, should be collinear (Figure 5.4 and Figure 5.6b). However, when the rotating stage has a misaligned axis of rotation, then the centroid F will be positionally deviated from E in the x' , y' and z' directions by δ_{xrad} , δ_{yaxial} and δ_{zrad} . Considering the new location of F is F' ,

$$\overrightarrow{EF} = \begin{bmatrix} 0 \\ h_5 \\ 0 \end{bmatrix}, \quad (5.73)$$

where h_5 is the distance between E and F along the y' direction as shown in Figure 5.4. The orientation of F with respect to E will take the form of a 3×3 rotation matrix T_F^E as shown below,

$$T_F^E = \begin{bmatrix} n'_x & p'_x & l'_x \\ n'_y & p'_y & l'_y \\ n'_z & p'_z & l'_z \end{bmatrix}. \quad (5.74)$$

Then, $\overrightarrow{EF'}$ can be written as

$$\overrightarrow{EF'} = \begin{bmatrix} \delta_{xrad} + h_5 p'_x \\ \delta_{yaxial} + h_5 p'_y \\ \delta_{zrad} + h_5 p'_z \end{bmatrix}. \quad (5.75)$$

Since \overrightarrow{EF} and $\overrightarrow{EF'}$ should be collinear, the following constraint equations can be written for the rotating platform, noting that matrix T_F^E actually represents the orientation

components of the matrix $T(v)_{error}$ of equation (5.52):

$\delta_{x_{rad}} + h_5 p'_x = 0$, which gives:

$$\delta_{x_{rad}} = -h_5 (\sin v \varepsilon_x - \cos v \varepsilon_z) \text{ and} \quad (5.76)$$

$\delta_{x_{rad}} + h_5 p'_z = 0$, which gives:

$$\delta_{z_{rad}} = h_5 (\sin v \varepsilon_z + \cos v \varepsilon_x). \quad (5.77)$$

Similar to the case of tip error parameter, $\delta_{x_{rad}}$, $\delta_{z_{rad}}$, ε_x and ε_z can be determined experimentally. An alternative strategy to find the tilt error parameters ε_x and ε_z can be described as follows: the displacements at or near the centre of rotation of the rotating platform F (that is, the reaction point of the rotating platform) in the x' and z' directions are measured to use in the equations (5.76) and (5.77), giving the tilt error parameters ε_x and ε_z for particular values of u , v and h_5 . However, offsets arising from the placement of the measurement equipment may need to be dealt with the similar way as described in section 5.6.1 using equations (5.68) and (5.70) along with the above two equations.

5.8 Conclusion

Developing an error model for a kinematic mechanism is an important step for the performance improvement of the mechanism. Error model helps mapping the error of the mechanism by identifying error sources. Furthermore, the model and the error parameters are required for the calibration and compensation of the mechanism (covered in Chapter 6). An error model for a complex spatial kinematic structure with closed loops, such as RPS mechanism of HAMS, can become complicated to develop, mainly due to the presence of many error sources, and, hence, the requirement for many error parameters to define the mechanism kinematically. From the error analysis of the RPS (tripod) mechanism of HAMS, it is found that at least 36 (12×3) individual error

parameters may be required to completely define the moving platform of the tripod with respect to the fixed platform of the tripod. This is because, each leg can be associated with 12 error sources (three related to the geometric position of the reference coordinate system, four related to revolute joint, two related to prismatic joint and three related to spherical joint). However, it has been shown that with careful analysis of the constraint equations associated with the legs and the complete RPS mechanism, the error parameters can be reduced to only three parameters, which can kinematically represent the effects of the errors stemmed from the various sources of the mechanism.

In this chapter, an error model is developed to find the equations that estimate the positional deviations of the target by considering the mechanism's two rotational motions (tip and tilt) and their associated error motions. An alternative method of developing an effective, but simple error model is applied based on the minimum number of error parameters that can be found in the error analysis of the RPS mechanism. In this method, key points of the mechanism, named as the reaction points, are established and the error motions, associated with the rotational motions (tip or tilt) of HAMS, are considered with reference to the reaction points. The error motions are called "generalised error parameters" in this research, since these errors are enough to describe the deviations of the geometric properties of the kinematic system of HAMS.

It is shown that the use of reaction points and generalised error parameters simplify the development of the error model for the complex hybrid mechanism of HAMS, since each mechanism can be considered as serially connected modules. Similar to the case of a serial mechanism, the positional and rotational errors of each mechanism are successively added up through the use of HTM to find the positional deviations at the target. The generalised error parameters can be determined analytically or

experimentally. The experimentally measured generalised error parameters are used for the calibration of the HAMS, as described in Chapter 6.

Chapter 6 - Calibration and compensation

6.1 Introduction

As discussed in the literature review, the accuracy of the final position of the target of a mechanism is influenced by the kinematic errors of the mechanism (usually the main sources) arising from the geometric sources, such as manufacturing and assembly errors of the joints. These errors should be addressed with an appropriate error compensation method rather than changing the structure or the design of the mechanism, which is often expensive. It has also been discussed that kinematic calibration and compensation (hereafter, just called calibration) can be an effective method for the compensation for these kinematic errors.

Kinematic calibration of a mechanism (serial, parallel or hybrid) can be defined as a procedure to estimate the numerical values of the errors, which represent the differences between the actual and nominal values of the kinematic parameters to better describe the kinematics of the mechanism, and these values can be used to improve the mechanism's accuracy by acting on the mechanism's controller [21]. Generally, the calibration process has four steps: development of a model to relate the 3D Cartesian position of the end-effector (or target) to the kinematic parameters of the mechanism; acquisition of the actual end-effector positions and orientations using a measuring instrument; identification of the kinematic error parameters based on the model and measurement; and error compensation by adjusting the parameters of the controller [86].

Although it has been shown that kinematic calibration can be a practical and economical way for enhancing the accuracy of parallel mechanisms, the calibration process is more complex than for a serial mechanism. This complexity, as discussed in literature in section 3.4, is due to the significant difficulty in describing the kinematic mechanism using a minimum set of error parameters, which can be easily determined in

a time- and cost-effective manner without compromising the accuracy of the calibration results. Although some general strategies for calibration based on minimum set of error data exist for serial mechanisms, for parallel mechanisms only calibration methods for individual mechanisms have been reported. Finding general strategies for the cost-effective calibration is an important area of the current research in parallel mechanisms [20-24,27-31,86-87].

In this chapter, a practical and cost-effective solution to the kinematic calibration of a hybrid mechanism is outlined to demonstrate the improvement of the accuracy of HAMS based on minimum set of error data, simplifying the steps of the calibration process.

6.2 Strategy for the calibration

The four-step calibration process for the performance improvement of HAMS was developed to meet the following objectives:

1. the calibration procedure to follow should be time and cost-effective,
2. the procedure should be simple for the user of mechanism to carry out,
3. the procedure is focused on application, e.g. target alignment of the laser operation.

When the above objectives are translated into the practical considerations for the development of a calibration process for HAMS, the following observations can be made:

- A. The tools/techniques for the calibration should be accurate and reliable, but they should be simple for the HAMS users to perform calibration on a regular interval to ensure the accuracy of HAMS' motions for the laser operations. Calibrations by the vendors are usually expensive and time-consuming due to the requirement of: 1. details error model with many error parameters, 3. lengthy experimental procedure,

3. complex error parameter identification method and 4. details compensation procedure involving changes to structural parameter and/or kinematics in control software. It is impractical for the general users of a mechanism with a complex kinematic structure to carry out such complicated calibration procedure. An easy-apply, software-based calibration and compensation process is required for the performance improvement of HAMS.
- B. Some positioning and orientation specifications are important for the standard target alignment process of the laser operation (see section 2.3 and 4.3.2.1). HAMS motions, e.g. tip (u) and tilt (v), are required to meet the stated specifications during the alignment process. Knowing the pose requirements for a standard target alignment process can reduce the amount of measurements required in the calibration process.
- C. The control software of HAMS, like many other mechanisms supplied by the commercial suppliers, has its own specific parameters to write the inverse and forward kinematics for the mechanism. In many cases, the descriptions of the kinematic parameters are not given with enough details to let the users make changes to the kinematics in the control software. In fact, this information is restricted and not shared by the suppliers with the customers for commercial confidentiality. Also, there is a risk of making errors in the kinematics if the users do not have sufficient knowledge and expertise in the mechanism and its control software. This is one of the main issues (see section 3.4.5) that make the implementation of the calibration (i.e. compensation) difficult. However, some features of the control software, e.g. actuator and encoder parameters, user-defined motion programme, are customisable. These available features should be carefully investigated before developing a calibration process to facilitate the implementation of the results of the calibration.

Based on the above considerations, the following strategies were followed while developing the kinematic calibration procedure for HAMS:

A. The capabilities of HAMS and the software of the HAMS' control system, called Turbo PMAC, were evaluated at first. HAMS is a hybrid mechanism where x and z linear stages can be controlled independently by Turbo PMAC. This unique feature of HAMS can be used to generate compensations for the positional deviations of the target arising from the kinematic errors of the mechanism. A motion programme, using the controller-specific parameters for the motion control of xz stages, can be written so that a compensation in the x or z direction is automatically generated for a particular input, say tip (u) or tilt (v). This is possible if the relation between the input (u or v) and the positional deviations is known from the error model of the mechanism.

The ability of the positional compensations for target using linear stages can be a major advantage of using hybrid mechanisms in some applications. Considering that many of the issues of the development of a kinematic calibration for a parallel or hybrid mechanism are related to the error identification and implementation steps, the independently-controlled xz stages of the hybrid mechanism can make the implementation of the calibration easier.

B. The error model plays the key role to take the advantage of the hybrid mechanism's unique feature mentioned above. Not only does the error model help to identify the error sources and evaluate the performance of the mechanism, the error model also serves the following purposes for the calibration process:

a) As described in section 3.3.1.2, the model used for the calibration should have the characteristics of a MCPC model. Using such model, the mechanism is described with minimum number of error parameters. The use of "reactions

points” and the “generalised error parameters”, as described in Chapter 5, can help finding a MCPC model for the calibration of HAMS.

- b) If these generalised error parameters can be related to the motions of HAMS, e.g. tip and tilt, and the errors’ effects on the target’s position (i.e. positional deviation) are known, then a relationship between the HAMS’ motions and the positional deviation can be found. In such case, the “error identification” step of the calibration actually becomes an integral part of the model development process.
- C. The relationship of the generalised errors and the positional deviations with the tip and tilt motions of HAMS should be easily verifiable using simple measurements, for example, measuring linear and angular displacements using laser interferometer.
- D. Partial pose measurements (see section 3.3.2), representing the tip (u) and tilt (v) motions of a standard target alignment process of the CLF’s laser operation, are used for the calibration.
- E. A modular approach is adopted for the kinematic calibration of HAMS. This means, for calibration purpose, serially connected modules of HAMS - moving platform of tripod, the rotating platform and the xz linear stages - are considered as individual mechanisms. For small angles, the tripod’s tip motion and the rotating platform’s tilt motion can be considered independently to determine the effects of the individual mechanism’s errors on the positional accuracy of the target. However, since the focus of this research is on the parallel mechanism, the calibration process in this chapter is described for the tripod of HAMS with some reference to the positional accuracy improvement of xz linear stages and the rotating platform.
- F. A flow-diagram of the calibration process for HAMS is shown in Figure 6.1.

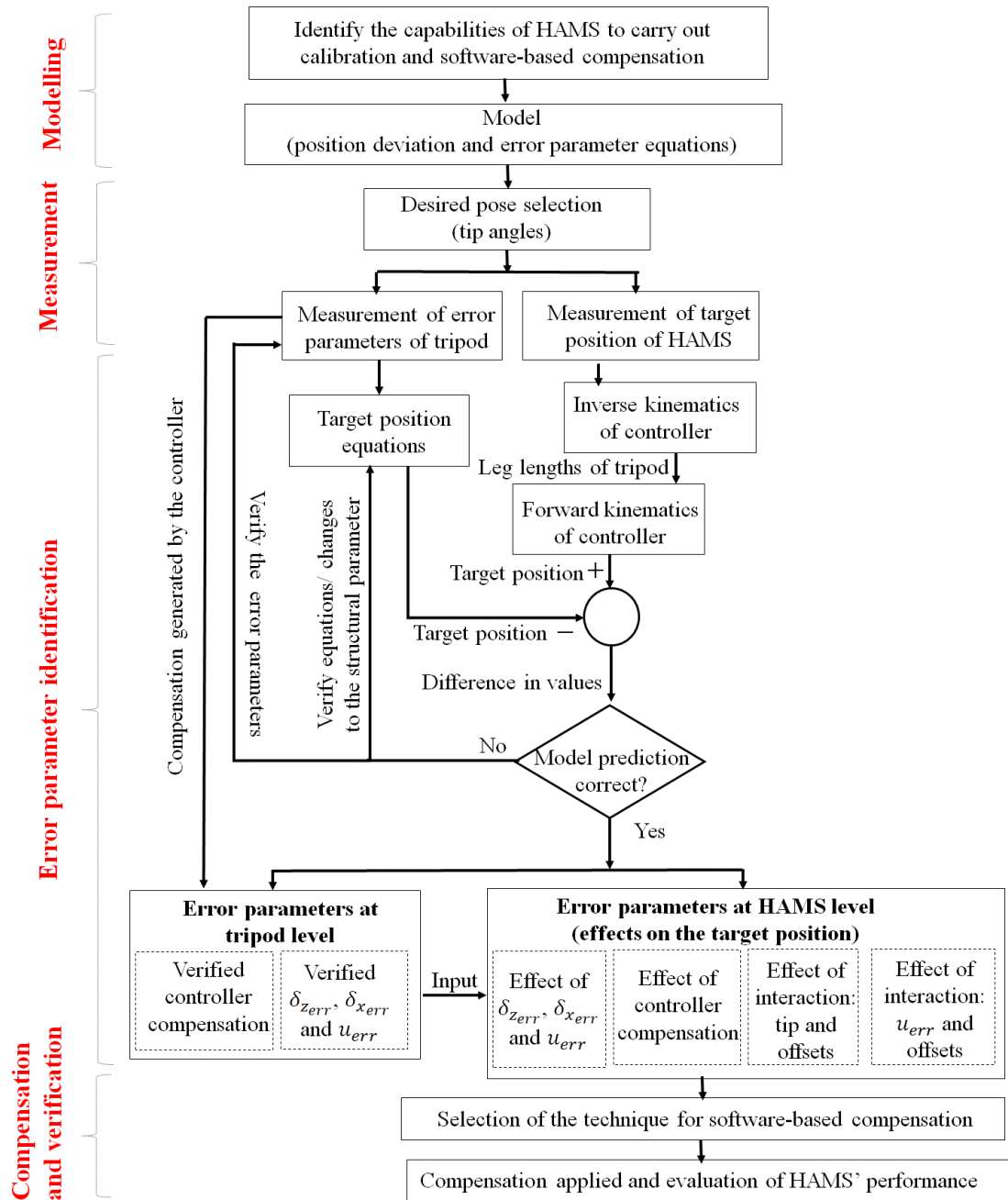


Figure 6.1 The calibration process flow-diagram for HAMS.

6.3 Kinematic modelling for calibration

Of the two approaches used to build a MCPC model, as explained in section 3.3.1.2, differential error model approach is used, so that the errors of the HAMS can be described by a separate set of parameters, which are not attributed to any specific structural parameters of the HAMS mechanism. The details of the development of an

error model, using generalised error parameters, have been discussed in chapter 5. The analytical equations of the model used in the calibration are given in this section.

Considering no tilt (v) motion from the rotating platform, equations (5.59) to (5.61) become the following equations that show the positional deviations of target for the tip (u) motion of the tripod and the errors associated with u :

$$D_{xt_{tip\ error+arch.}} = \delta_{x_{err}} + (d_3 + t_z) \sin u_{err} + t_x (\cos u_{err} - 1) \quad (6.1)$$

$$D_{yt_{tip\ error+arch.}} = (h_5 + h_6 + t_y) (\cos u - 1) + (d_3 + t_z) \sin u \cos u_{err} - t_x \sin u \sin u_{err}, \quad (6.2)$$

$$D_{zt_{tip\ error+arch.}} = \delta_{z_{err}} - (h_5 + h_6 + t_y) \sin u + (d_3 + t_z) (\cos u \cos u_{err} - 1) - t_x \cos u \sin u_{err}. \quad (6.3)$$

Also, considering no tip (u) motion from the tripod, equations (5.68) to (5.70) become the followings that show the positional deviations of target for the tilt (v) motion of the rotating platform and the errors associated with v :

$$D_{xt_{tilt\ error+arch.}} = \delta_{x_{rad}} - (d_3 + t_z) \sin v + t_x (\cos v - 1) - h_6 (\cos v \varepsilon_z - \sin v \varepsilon_x) - t_y (\cos v \varepsilon_z - \sin v \varepsilon_x), \quad (6.4)$$

$$D_{yt_{tilt\ error+arch.}} = \delta_{y_{axial}} + h_5 (\cos u - 1) + (h_6 + t_y) - 1 + (d_3 + t_z) \varepsilon_x + t_x \varepsilon_z, \quad (6.5)$$

$$D_{zt_{tilt\ error+arch.}} = \delta_{z_{rad}} - (h_6 + t_y) (\cos v \varepsilon_x + \sin v \varepsilon_z) + (d_3 + t_z) (\cos v - 1) + t_x \sin v. \quad (6.6)$$

Equations (6.1) to (6.3) and (6.4) to (6.6) show that, theoretically, four sources are responsible for the positional deviations of the target:

1. Tip (u) and tilt (v) motions,

2. Structural parameters between the centroid of the moving and rotating platforms and the target,
3. Positional deviations at the centroid of the platforms that include the error motions $\delta_{z_{err}}$ and $\delta_{x_{err}}$ for tip (u) and $\delta_{x_{rad}}$ and $\delta_{z_{rad}}$ for tilt (v),
4. The rotational error motion u_{err} related to tip (u) and the rotational error motions ε_x and ε_z related to tilt (v).

Furthermore, from model's equations, once the theoretical relation of the target's position with the HAMS' motion (tip or tilt), error parameters and structural parameters is known, the measurements are required for the following purposes:

- A. To determine the positional deviations of the target during tip or tilt rotation of HAMS,
- B. To determine the error parameters of HAMS,
- C. To verify the error model of HAMS so that the model can be used to predict the real position of the target (as opposed to the nominal position of HAMS' controller) and use for the compensations for the target's position deviations.

6.4 Measurements

6.4.1 Types of measurements

Three types of measurements were carried out for the tip (u) motion of the tripod:

1. Linear displacements of the target in the x and z directions while the tip motions were given to the HAMS controller (x , y and z positions were unchanged with respect to the $x_0y_0z_0$ reference coordinate of HAMS; also tilt (v) remained unchanged (see Figure 5.4)),
2. Linear and rotational displacements at the centroid of the moving platform of the tripod (point E of Figure 5.4 and 5.6a) for the change of tip motions,

3. With the change of tip motions, the change of the length of the tripod's legs that were read from the encoder readings of the motors actuating the legs. The recorded leg-lengths were used as the inputs to the controller to generate the tip (u) motions for HAMS. With the tip motions, the resulting linear displacements of the target in the x and z directions were measured.

The first type of measurement was carried out to find the positional deviations of the target due to the tip motions. HAMS' controller uses its software's inverse kinematics solution to calculate the leg-lengths for the tip motions required. The second type of measurement was carried out to measure the error motions $\delta_{z_{err}}$, $\delta_{x_{err}}$ and u_{err} of the tripod. The third type of measurement was carried out to use the forward kinematic solution of the control software to generate the tip motions for HAMS and record the resulting positional deviations of the target.

With regard to the tilt motions (v) of HAMS, two types of measurements were carried out:

1. Linear displacements of the target in the x and z directions while the tilt motions were given to the HAMS controller (x , y and z positions were unchanged with respect to the $x_0y_0z_0$ reference coordinate of HAMS; also tip (u) remained unchanged (see Figure 5.4)),
2. Linear and rotational displacements at the centroid of the rotating platform of HAMS (point F of Figure 5.4 and 5.6b) for the change of tilt motions.

The first type of measurement was carried out to find the positional deviations of the target for the tilt motions. The second type measurements were carried out to measure the $\delta_{x_{rad}}$, $\delta_{z_{rad}}$, ε_x and ε_z error motions of the rotating platform.

6.4.2 Methods of the measurements

The positional deviations in the z and x directions as a result of the error motions of tip and tilt were measured using an interferometer (Renishaw model XL-80) with retroreflector. The working principles of linear and angular displacements using interferometer are already given in sections 3.5.2 and 4.3.2. The measurements of the positional deviations were achieved by determining the linear displacements of the moving part (moving stage, rotating stage and target wheel) during the rotational motions of HAMS (u and v). In the interferometer set up (Figure 6.2), the retroreflector was mounted on the moving part using appropriate fixtures while using the beam-splitter as the fixed optic.

The rotational motions considered in this study to measure the linear displacement were in the range of $\pm 1.4^\circ$, which represents a typical tip and tilt motion range for the target alignment of the CLF. All the measurements were repeated at least five times for each tip or tilt rotation of an experiment.

The error measurements were carried out following two steps:

1. Rotations and linear displacements were measured for the moving stage and the rotating stage by placing the reflectors as close to the centroid of the moving stage or the rotating stage as practicable (Figure 6.2*a-b*).
2. Linear displacements were measured at the target point of the target interface wheel by placing the reflector as close to the target as feasible (Figure 6.2*c*).

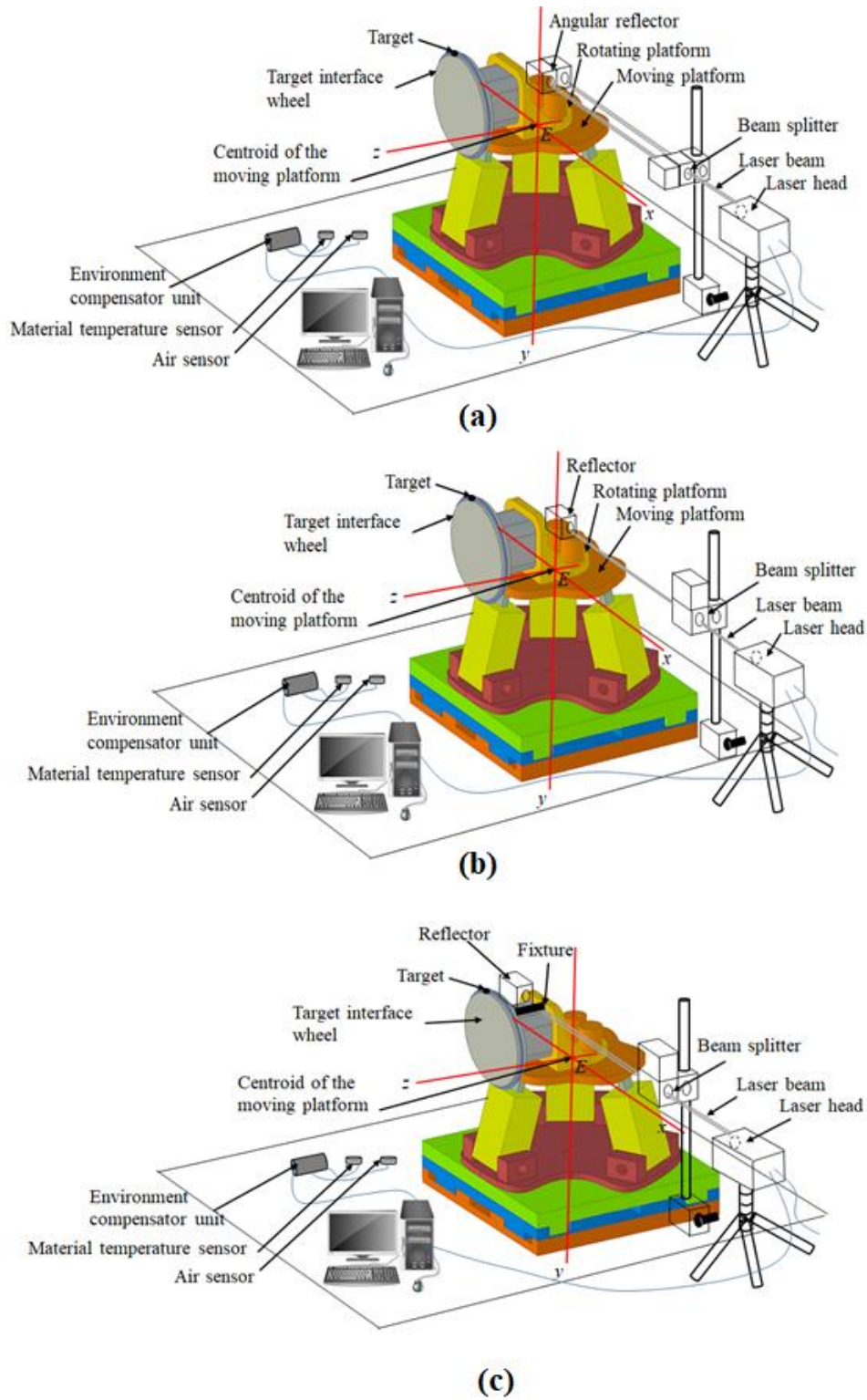


Figure 6.2 Schematic representation of the interferometer setup. The setup shown in the figure is to measure (a) the tip angular error u_{err} close to the centroid of the moving platform E (b) tip displacement error $\delta_{x_{err}}$ in the x direction close to E , and (c) positional deviation $D_{xtip\ error+arch.}$ close to the target in the x direction due to tip motion.

6.5 Error parameter identification

As described in section 6.3 and shown in Figure 6.3, the positional deviation of the target T due to the tip motion of the tripod will be the sum of: (1) the errors arise from the tripod and (2) the displacements that arise as the effects of the interactions of the angular motions associated with u and the structural offsets (EH and ET as shown in Figure 6.3) between E and T (E is the centroid of the moving platform of the tripod).

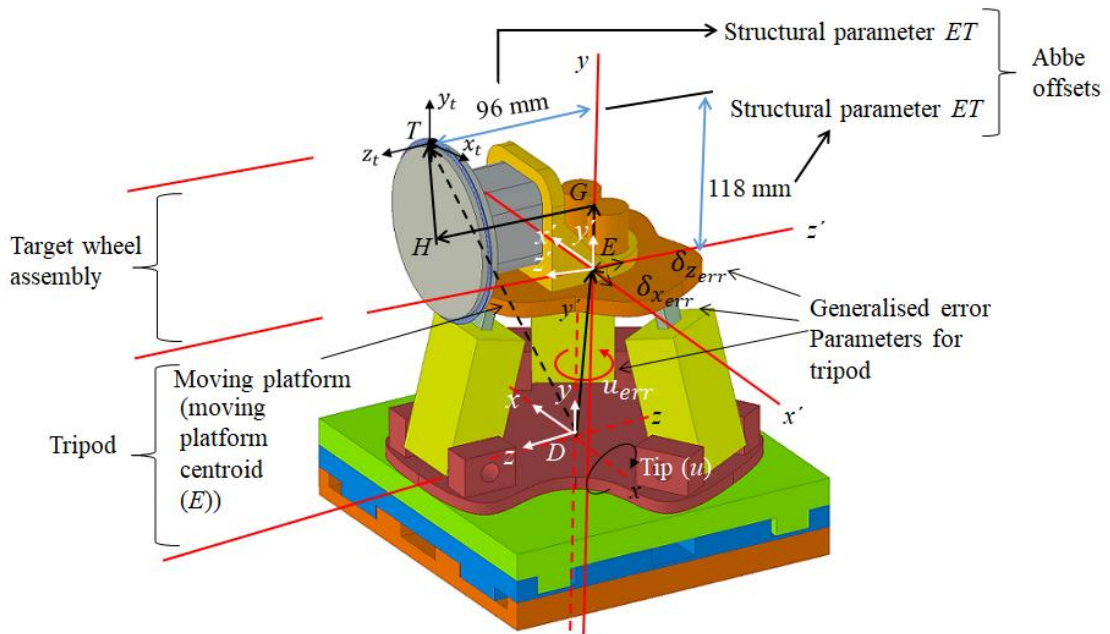


Figure 6.3 HAMS showing Abbe offsets and generalised error parameters for tip motion.

6.5.1 Identifying the error parameters of the tripod (RPS mechanism)

The translational errors, $\delta_{z_{err}}$ and $\delta_{x_{err}}$ in the z and x directions, and the rotational error, u_{err} about the y axis of the xyz coordinate system, measured at the centroid E of the moving platform are shown in Figure 6.4 and 6.5, respectively. With respect to the $\delta_{z_{err}}$ and $\delta_{x_{err}}$ motions measured, a compensatory motion by the HAMS controller was observed while the tip motions were being executed (profile K of Figure 6.6.). This compensatory motion was performed by the z stage in the z direction, and, as such, could be read from the encoder of the z stage's motor. However, comparison of this

compensatory motion with the measured error motions $\delta_{z_{err}}$ (profile *L* of Figure 6.6) and $\delta_{x_{err}}$ (profile *M* of Figure 6.6) shows that:

- A. As compared to $\delta_{z_{err}}$ motion, the controller's automatic compensation is much higher in value,
- B. Controller does not compensate for $\delta_{x_{err}}$ in the x direction.

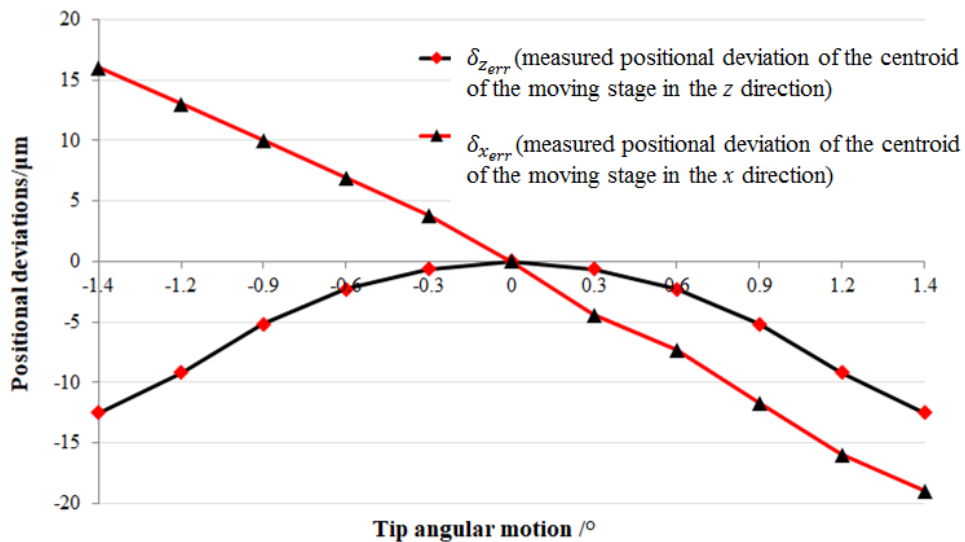


Figure 6.4 Translational error motions $\delta_{z_{err}}$ and $\delta_{x_{err}}$ of the tripod in the z and x directions.

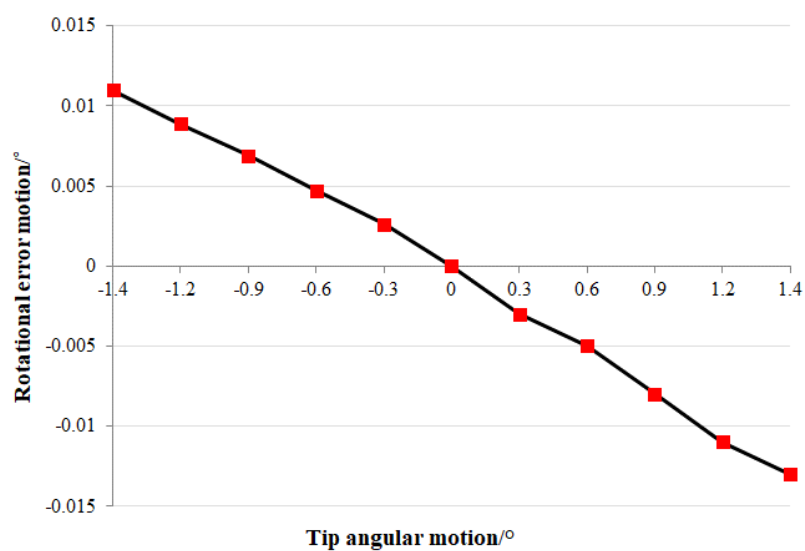


Figure 6.5 Rotational error motion u_{err} of the tripod (RPS mechanism) of HAMS.

HAMS controller's such response to the error motions $\delta_{z_{err}}$ and $\delta_{x_{err}}$ has the following effects on the performance of HAMS:

- A. As can be seen from equation (6.3), $\delta_{z_{err}}$ forms part of the positional deviation at the target T . Overcompensation for $\delta_{z_{err}}$ means that any positional deviation measurement at target T will actually give wrong information about the target's actual position. This will be made clearer in the section 6.5.2.

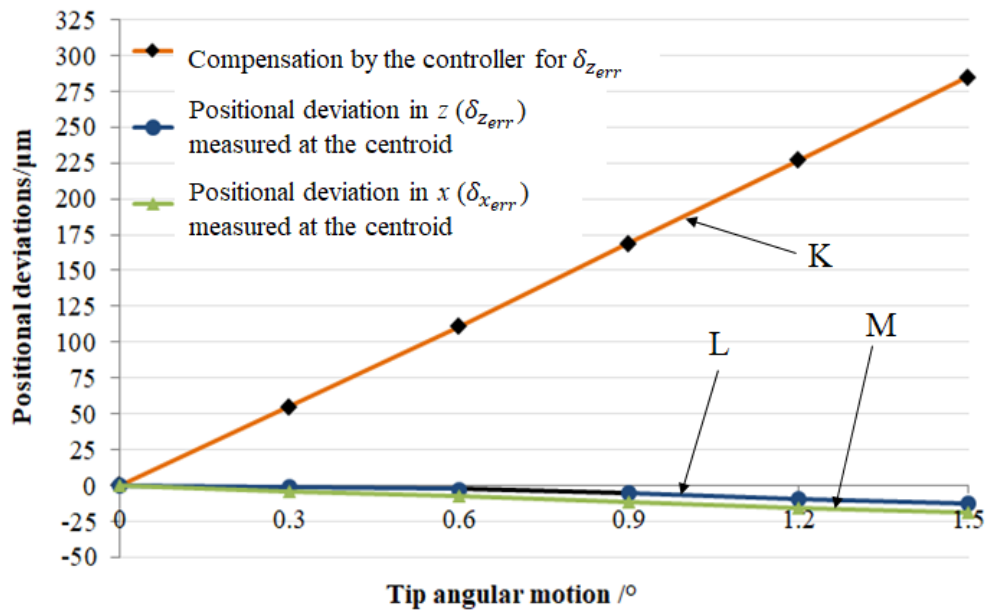


Figure 6.6 Error parameters of the RPS mechanism (tripod) and the controller's compensation in the z direction.

- B. It is possible that the controller's automatic compensation is designed to eliminate the error motion of the RPS mechanism (tripod) in the z direction (i.e. $\delta_{z_{err}}$). It is also possible that the generated overcompensation is actually designed to minimize the effect/s of the errors of the structural parameter/s used in the inverse kinematics of the control software. However, it is impossible for the user of an RPS mechanism or a hybrid mechanism to know this overcompensation information unless a calibration process is carried out.

C. While the controller is overcompensating for the positional deviation in the z direction, there is no compensation in the x direction. Although the positional accuracy in the z direction is the most sensitive to the target alignment process, the x and y direction accuracies are also important; otherwise, the laser will miss the targets.

Furthermore, of the three error parameters $\delta_{z_{err}}$, $\delta_{x_{err}}$ and u_{err} , the rotational error parameter u_{err} has relatively smaller effects on $\delta_{z_{err}}$ and $\delta_{x_{err}}$, as can be seen from equations (5.71) and (5.72). However, u_{err} has much larger effect for creating positional deviation at the target T in the x direction, as will be discussed in the next section.

6.5.2 Identifying the error parameters affecting the target position T

As mentioned in section (6.3), four sources of error are responsible for the positional deviations of target T . The identification of the errors based on their effects on the ideal or desired positions of target is outlined below.

6.5.2.1 Positional deviations of the target T in the z direction

6.5.2.1.1 Effect of $\delta_{z_{err}}$ parameter

To understand the effect of the controller's overcompensation for $\delta_{z_{err}}$ on the positional deviation of target, forward and inverse kinematic experiments (see section 6.4.1) were carried out, so that the positional deviations of the target can be compared for both experiments. For inverse kinematics experiment, the positional deviations of the target T were measured after giving a range of tip (u) motions to HAMS' controller as input (i.e. controller uses its inverse kinematics to calculate the lengths of the legs for the desired tip motions), and the lengths of the three legs of the tripod were recorded from the encoders of the motors actuating the legs (see profile A of Figure 6.7). Note

that the results of the inverse kinematics experiments will include the controller generated compensations.

For forward kinematics experiments, the recorded lengths of the legs from the inverse kinematics experiments were used as input to the HAMS' controller, and the positional deviations of the target were measured (see profile *B* of Figure 6.7). Forward kinematics experiments will not include any controller generated compensations. Comparison of profile *B* with *A* shows that the differences of the values are almost identical with the values of profile *K* of Figure 6.6.

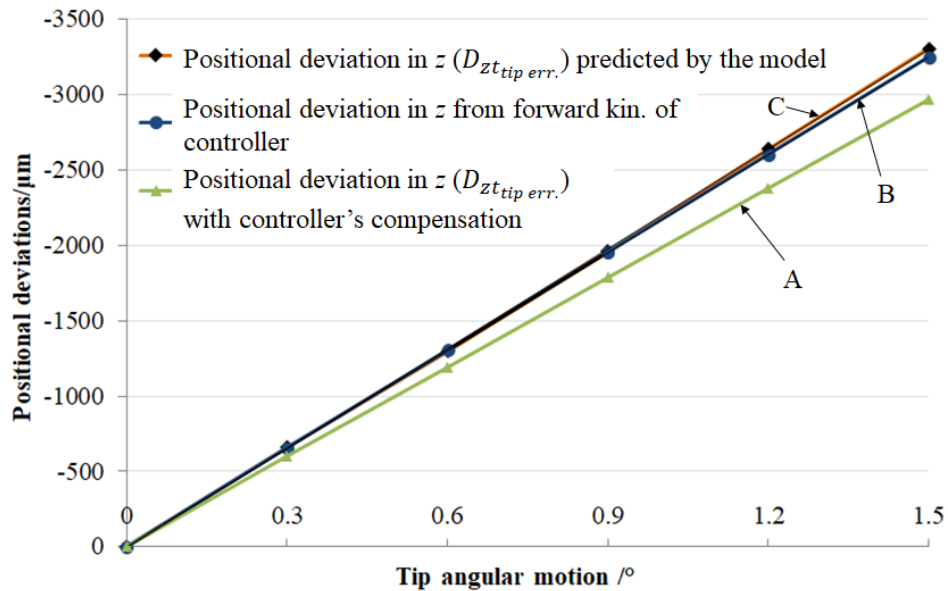


Figure 6.7 Comparison of the target's positional deviations in the z direction determined by the forward and inverse kinematics experiments and predicted by the error model.

Furthermore, using the experimentally determined $\delta_{z_{err}}$ and u_{err} values (Figure 6.4 and 6.5), the theoretically calculated positional deviation of the target T , as determined by the model's equation (6.3), can be found (see profile *C* of Figure 6.7). Comparison of profiles *A*, *B* and *C* of Figure 6.7 shows that the model's predicted values are almost identical with the positional deviation values (profile *B* of Figure 6.7) of the forward kinematics experiments.

Observation of the results of both experiments suggests that:

- A. The controller's compensation for $\delta_{z_{err}}$ associated with the tip motion of the tripod is incorrect,
- B. The use of a simplified kinematic model with generalised error parameters, described in Chapter 5, is valid for the calibration of the parallel mechanism of HAMS – a hybrid mechanism.

6.5.2.1.2 Effect of tip motion (u)

Profiles *A*, *B* and *C* of Figure 6.7, irrespective of the differences in $\delta_{z_{err}}$ values, all show significant positional deviations at T with the tip (u) motions of HAMS. In fact, tip motion itself plays a major role in contributing to the positional deviations. This can be understood: 1. by checking the $[(h_5 + h_6 + t_y) \sin u]$ term of equation (6.3), where the structural offsets can be found in Figures 5.4 and 6.3, and 2. from Figure 6.8, which shows the theoretical values of the positional deviations of target in the x , y and z directions as calculated from equation (6.1) to (6.3) without considering any other motions (tilt v or error motions, e.g. $\delta_{z_{err}}$).

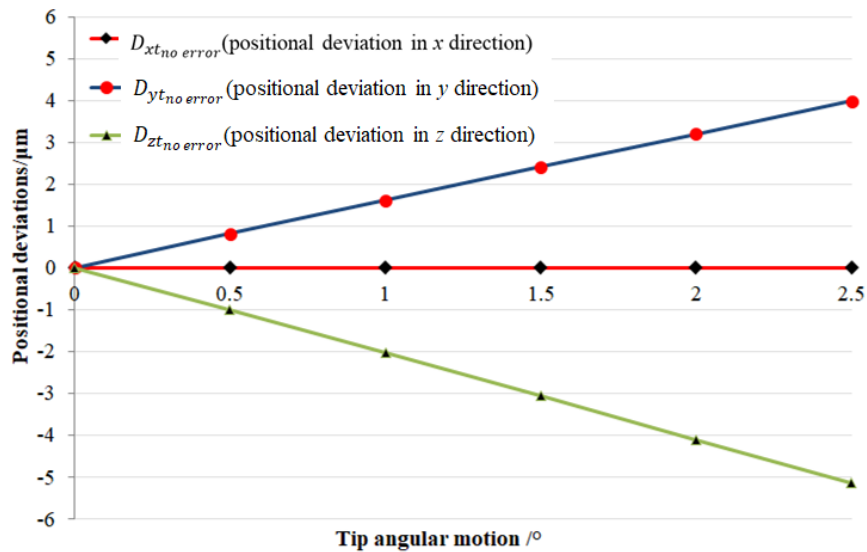


Figure 6.8 Theoretically calculated (equations (6.1) to (6.3)) positional deviations at varying tip angular motions (no tilt motion v or errors considered).

6.5.2.1.3 Effect of rotational error motion u_{err}

The rest of the positional deviation values of profiles A , B and C of Figure 6.7 are attributed to the effects of the interaction between the rotational error motion u_{err} of the tripod and the structural offsets between the centroid E of the moving platform and the target T . These effects, small in values, can be found in the equation (6.3) as $[(d_3 + t_z)(\cos u \cos u_{err} - 1)]$ and $[t_x \cos u \sin u_{err}]$.

6.5.2.2 Positional deviations of the target T in the x direction

As compared to the z direction, the positional deviation of the target T in the x direction is relatively smaller. However, the positional accuracy in the x direction is also important to ensure that the laser beam is hitting the target within specifications. Equation (6.1) in section 6.3 shows different sources of error that affect the positional deviation of target T in the x direction.

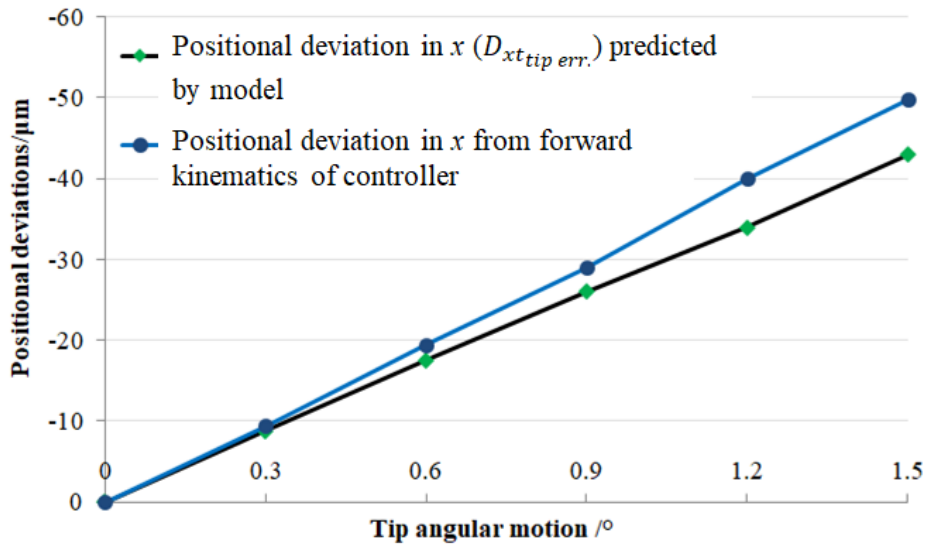


Figure 6.9 Comparison of the target's positional deviations in the x direction determined by the forward kinematics experiments (the inverse kinematics experiment results show the same values) and predicted by the error model.

Figure 6.9 shows the positional deviations measured in the x direction from the forward kinematics experiments. Unlike Figure 6.7 which shows different values in the

z direction for the forward and inverse kinematics experiments, the target's positional deviations in the x direction are same for both experiments. This is because, for the tip rotation of HAMS, there is no controller generated automatic compensation for the translational error motion $\delta_{x_{err}}$ associated with the centroid of the tripod. Therefore, $\delta_{x_{err}}$ forms part of the the positional deviation of the target in the x direction (Figure 6.6). However, rotational error motion u_{err} plays a major role in contributing to the positional deviation of the target T in the x direction due to the interaction of the u_{err} with the structural offsets (check the term $[(d_3 + t_z) \sin u_{err}]$ of equation (6.1) and Figure 6.9).

6.6 Implementation of the calibration results: compensation

The xz stages of the hybrid mechanism of HAMS, as mentioned in section 6.2, can be used to compensate for the positional deviations of the target in the x and z directions. This is possible for the known relationship between the tip (u) motions of HAMS and the resulting positional deviations at the target T . Based on the outcomes of the error identification step (Figure 6.4 to 6.9), linear relationships can be observed between the following error motions and the tip (u) motion of HAMS (for small tip angles):

1. error motions $\delta_{x_{err}}$, $\delta_{z_{err}}$ and u_{err} (Figure 6.4 to 6.6) associated with the centroid E of the moving platform of the tripod (see Figure 6.3),
2. error motions $D_{xt_{tip\ error+arch.}}$ and $D_{zt_{tip\ error+arch.}}$ (Figure 6.7 to 6.9) at the target T of HAMS (see Figure 6.3).

Of the two relationships, the first one, in fact, is valid for the tripod (RPS mechanism) of HAMS. This means, any RPS mechanism with xz stages can take advantage of this linear relationship for calibration and compensation purposes. The

second relationship, however, is valid for the specific kinematic structure of HAMS. This is because, although HAMS' base kinematic structure is built on the xz stages and RPS mechanism, additional structures, e.g. rotating platform and the target wheel accessories, are added to the base structure for the purpose of the laser operation of CLF, resulting in offsets in the x and z directions between the centroid E of the moving platform and the target T (Figure 6.3). Therefore, the second relationship can be used for the position compensation of target T .

Most of the research activities related to implementing calibration results (i.e. compensation) are, in fact, empirical in nature, where data and information from various sources, e.g. technical documents, investigation of the hardware and software elements of HAMS, were collected to find an appropriate technique for compensation. The principle of the chosen compensation technique for the positional deviation of target is discussed below. The outcomes of the compensation, in terms of HAMS' positional accuracy improvement, have been discussed in section 6.7.

- A. Calibration results should be implemented by making changes to the kinematic parameters of the inverse kinematics of the control software. However, to do this, the person, responsible for the implementation of the calibration, should have a good understanding of the various features, e.g. parameters, motion programmes, kinematics algorithm, of the control software. For example, Appendix C shows the inverse kinematics used in the HAMS' controller (i.e. Delta-Tau's Turbo PMAC control system). The parameters used in the algorithm are Delta-Tau's control software-specific and many of the parameter's definition cannot be found in the technical manuals.
- B. To overcome the implementation problem, an alternative technique for applying the compensation is to use a user-defined motion programme that can be written

following the prescribed manner of the control software. An example is shown in Appendix D. In this technique, when a command input is given to HAMS for a tip (u) motion, a simultaneous and linear compensatory motion, e.g. $z=2000*u$ for line A of Figure 6.7 where z is the linear motion in z direction, is executed (i.e. $P1009=2000*P1002$ in Appendix C). It is also possible to use a GUI-based software to interface with Delta-Tau's Turbo PMAC control software, where the software will execute the tip and compensatory motions simultaneously without the requirement of a motion programme. However, this GUI-based software development was not the focus of the research, but the focus was to demonstrate the effectiveness of a simple, economical method of calibration and compensation for HAMS.

6.7 Results and discussions

After carrying out calibration and compensation, the laser interferometer was used to measure the positional deviations of the target for various tip rotations. The results were compared with the positional deviations of the target before calibration (see Figure 6.7 and 6.9) to verify the improvement achieved through this calibration process. The key points of the calibration and compensation experiments are discussed below.

6.7.1 Performance improvement of HAMS

Figure 6.10 and 6.11 show that the positional accuracies of the target T in the z and x directions improved significantly after the calibration and compensation process. Calibration and compensation had the most improvement effect (approximately 97%) in the z direction – the sensitive direction for the target positioning and orientation at the laser focus. As for the target positional accuracy improvement in the x direction, 85% improvement was achieved.

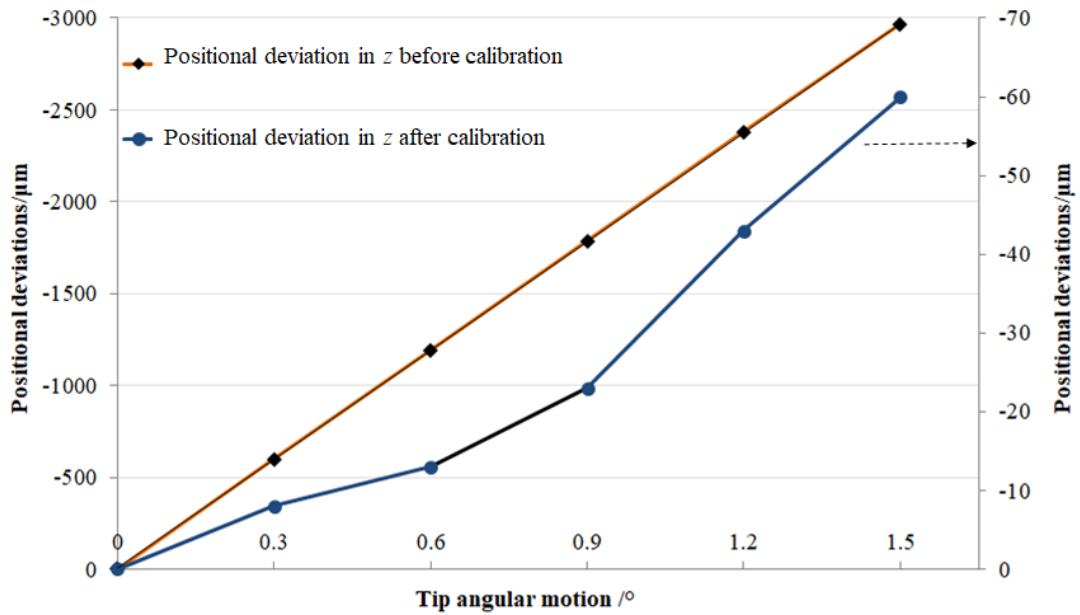


Figure 6.10 Target position accuracy improvement in the z direction through the calibration and compensation process.

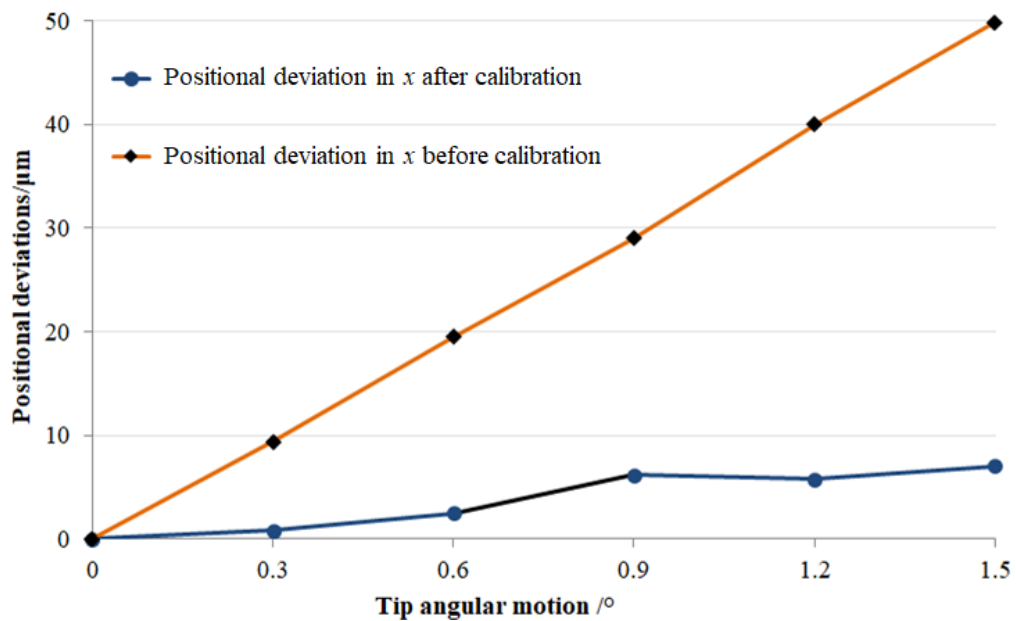


Figure 6.11 Target position accuracy improvement in the x direction through the calibration and compensation process.

The degree of improvement achieved through the calibration and compensation process highlights the importance of carrying out the calibration process in a regular interval during the service period of a complex mechanism like HAMS, which is

employed as a high-accuracy target positioning and alignment system for laser operations. It is important to understand the effects of the errors of HAMS on the ideal positions (error free condition) of the target – not only to improve the performance of HAMS, but also to carry out all the alignment activities efficiently and effectively for the laser operations. In actual applications of HAMS during the laser operations, the calibration data, in terms of accuracy, repeatability and resolution of the motion stages of HAMS, provided by the supplier of HAMS may offer little benefit to the users. This is because, in most cases, these data represent the performance of the individual mechanism of HAMS, i.e. xz stages, the tripod and the rotational motor of the rotating platform. However, the purpose-built structure, e.g. the wheel accessories as shown in Figure 6.3, added to the base structure of HAMS (i.e. tripod and xz stages) is not taken into consideration in the calibration data of the HAMS supplier. It has been discussed in section 6.5.1.2.1 (also shown in Figure 6.8) that the structural offsets between the centroid of rotating platform of tripod and the target T represent the Abbe offsets and have significant contribution to the positional deviation of the target. Furthermore, these structural offsets may change over time for various reasons, for example 1. change in the load condition in some part of wheel accessories 2. structural deformation due to the factors, e.g. temperature variation and fatigue of structural material 3. change in perpendicularity between the structures in the wheel assembly. It is important to keep track of the effects of the changes to these parameters on the target's position through the calibration process, so that necessary compensations can be applied with the control software.

6.7.2 Evaluation of the compensation technique applied

The significant performance improvement through the calibration process suggests that:

1. The use of reactions points and generalised error parameters in the error model can effectively represent the high number of error parameters associated with the various error sources of the parallel mechanism of HAMS, as described in Chapter 5.
2. The simplified error model is a valid error mapping tool for the hybrid mechanism and can be used in the calibration process.
3. The measurement scheme described in this calibration process is time and cost-effective.
4. The number of error parameters to identify are only a few (i.e. three parameters for the RPS mechanism of HAMS) and can be determined experimentally with simple procedure.
5. The error compensation can be carried out with some understanding of the key parameters of the control software and the motion programme.

Despite the improvement achieved, Figure 6.10 shows that target's positional accuracy in the z direction is not within the position specifications (i.e. $\pm 4 \mu\text{m}$ in the z direction) unless the tip (u) motions are very small (e.g. 150 mdeg). The target's positional accuracy in the x direction, on the other hand, can be considered satisfactory (position specification for target in the x direction is $\pm 10 \mu\text{m}$).

To improve the target's positional accuracy in the z direction further, several compensation techniques were trialled based on the information collected from various sources, e.g. Turbo PMAC software manual, web portal and the understanding gained from researching with the HAMS controller. An interesting solution to solve the positional deviation problem of target was found, the principle of which is outlined in the following section.

6.7.3 Improvement of the compensation technique

The coordinate system $x'y'z'$ at the centroid E of the moving platform is used for the tip rotation not only for the tripod, but also for the complete hybrid mechanism of HAMS (Figure 6.3). However, as discussed before, the offsets between E and the target T , i.e. Abbe offsets, are the cause of the positional deviations at T during the tip (u) motion of HAMS. If, target point T , instead of the centroid E of the moving platform, can be made the centre of tip rotation, then theoretically there will not be any positional deviation at T , and all the rotations can be referred with respect to the coordinate system $x_t y_t z_t$ at T . This can be achieved if the coordinate system $x'y'z'$ at the centre of tip rotation E is translated to T point in the y and z directions as shown in Figure 6.3.

Translation of the coordinate system $x'y'z'$ from E to the target point T for the tip rotations can be carried out in the following way: modify some Turbo PMAC-specific parameters (called p variables) that represent the translations in the x , y and z directions, followed by running a command in the terminal window of the control software (the main channel of communication between the user and Turbo PMAC control system). The stated technique was used to test the improvement of the target's positional accuracy, although translation of the coordinate system can also be carried out by writing a user-defined motion programme or by a GUI-based software.

Translating the coordinate system means that any subsequent translational motions in the x , y and z directions remain unaffected and can be considered in the same way as before the change of the coordinate system. However, any subsequent rotational motions (tip or tilt) required must be carried out with respect to the new coordinate system at the target point T .

It can be seen from Figure 6.12 that, of the two compensation techniques used for the performance improvement of HAMS, translation of the coordinate system to the

target point was more effective than using a motion programme to generate the compensatory z motion. However, this was not the case for the target positional accuracy in the x direction - translation of the coordinate system to the target point effectively did not change the performance of HAMS (Figure 6.13). This has been discussed in section 6.5.1.2.2 that the HAMS' controller does not generate any compensatory motions to minimise the effects of the error motion u_{err} or $\delta_{x_{err}}$, stemmed from the RPS mechanism of the tripod. Therefore, positional deviation at the target T due to $[(d_3 + t_z) \sin u_{err}]$ (see equation (6.1)) remains uncompensated, and the compensation technique using the motion programme of control software (section 6.6.) is required to improve the target positional accuracy in the x direction.

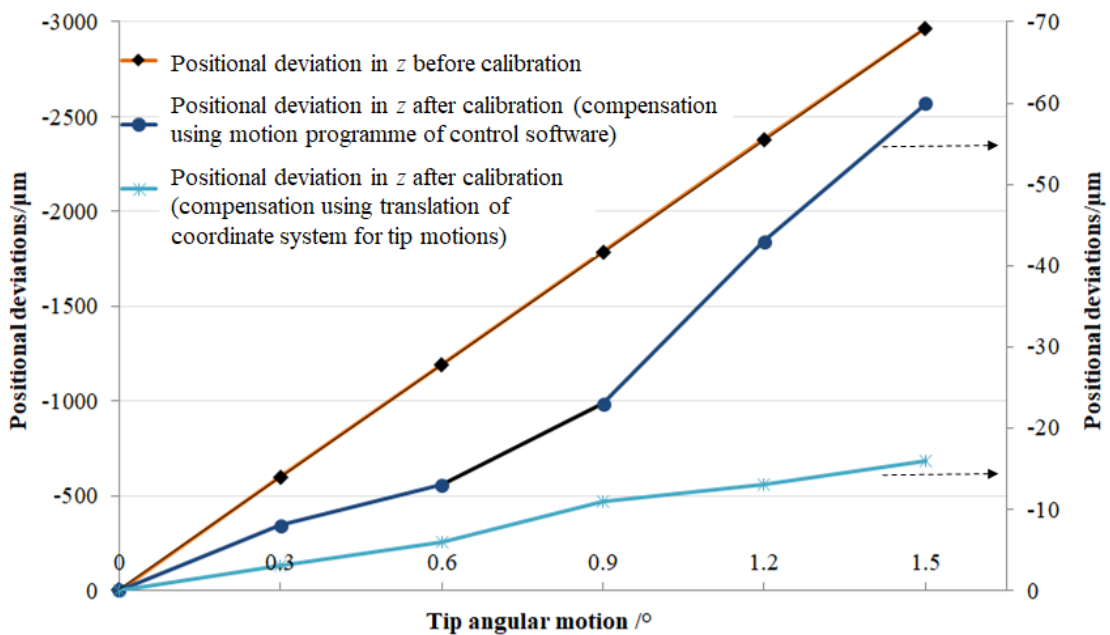


Figure 6.12 Comparison of the two compensation techniques to improve the target positional accuracy in the z direction.

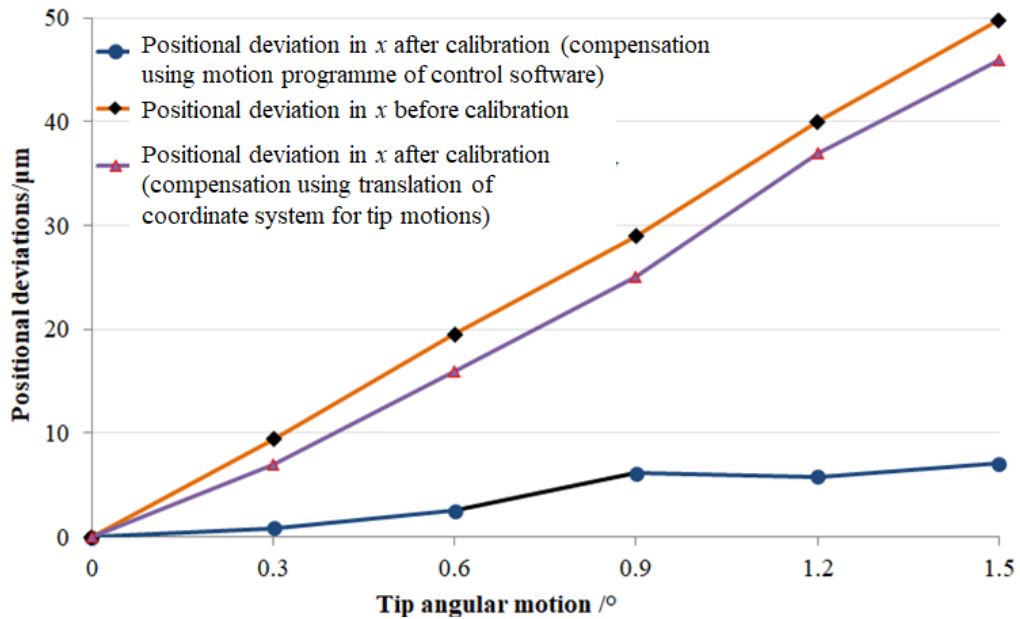


Figure 6.13 Comparison of the two compensation techniques to improve the target positional accuracy in the x direction.

Although the compensation technique by translating the coordinate system from the centroid of the tripod to the target point is an improved compensation technique than the one that uses motion programme, the coordinate translation technique has some limitations – one of which has already been discussed that target’s positional deviation in the x direction is not compensated (Figure 6.13). The main limitation of the coordinate translation technique is that the offsets between the centroid of the moving platform and the target in the y and z directions are assumed to be constants in this technique. If the incorrect values of the offsets are entered as the Turbo PMAC parameters (p variables) or even the actual offset values change over time, target positional deviations will take place at T during the tip (u) rotation of the HAMS. This explains why the coordinate translation technique still shows some positional inaccuracies in the z direction (Figure 6.12) even though the tip rotations of HAMS were referenced to the coordinate system $x_t y_t z_t$ at T .

6.7.4 Calibration uncertainty

The target positional accuracy in the x and z directions achieved through the calibration and compensation (Figure 6.10 to 6.13) can be affected by a number of measurement uncertainties arising from different sources, as discussed below.

6.7.4.1 Experimental errors

Accuracy of the linear displacement measurements using interferometer is affected by the experimental errors that arise from the environmental factors affecting the reflective index of the ambient air – this uncertainty has already been discussed in the research method (section 4.3.3.2). The overall measurement uncertainty arising from the repeatability of the measured distances and from the atmospheric effects on the interferometric measurements was estimated to not to exceed 180 nm (at a coverage factor $k=2$, giving a confidence level of approximately 95%). The values of measurement uncertainty, compared to the positional deviations measured on the micrometre scale, are not shown in the calibration results (Figure 6.4, 6.6, 6.7, 6.9, 6.10-6.13) as they are of the order of nanometre.

However, there will be other error sources related to experimental set-up (section 6.4.2) that will contribute towards the measurement uncertainties. For example, determination of the error parameters of the tripod requires the measurements of rotational error motions u_{err} and linear displacements $\delta_{x_{err}}$ and $\delta_{z_{err}}$ to be measured at the centroid of the moving platform of the tripod (section 6.4.2). For this measurement, the retro-reflector of the interferometer should be ideally placed at the centroid of the moving stage. In reality, the reflector was placed slightly above the centroid due to inaccessibility to the centroid area. However, with careful design of the setup of the experiment, it was possible to avoid some sources of experimental uncertainties and improve the measurement accuracy. For example, considering small tip motions,

rotational error u_{err} measurement (also displacement error $\delta_{x_{err}}$) should be carried out in the x direction (Figure 6.2a-b), instead of the measurement in the z direction. This is because the reflector's displacement (angular or linear) in the x direction is negligibly affected by the tip rotation about x axis and by the reflector's placement slightly above the centroid area.

Another source of calibration uncertainty can be tip motion (u) itself. In all calibration results (Figure 6.4 to 6.13), linear or angular displacements were determined as a function of tip motions, which were read from the HAMS' position encoders. The accuracy of the encoder reading for the tip motion can affect the calibration results. When measured with the angular interferometer, the error of the encoder reading for the tip motion was found to be negligible (approximately $\pm 0.0002^\circ$ per degree measured or $\pm 0.02\%$ error). Furthermore, the error for the displacement encoder of HAMS was also negligible (approximately $\pm 0.006\mu\text{m}$ per micrometre measured or $\pm 0.6\%$ error).

6.7.4.2 Errors in compensation

Some sources of uncertainty related to the generation of the compensations for the positional deviations of target have already been discussed in sections 6.7.2 and 6.7.3. It has been described how the use of incorrect values of the structural parameters of HAMS - especially the offsets between the centroid of the moving platform and the target - in the control software can affect the results of the compensation for both techniques (i.e. compensations using motion programme and translating the coordinate system) as shown in Figure 6.12 and 6.13.

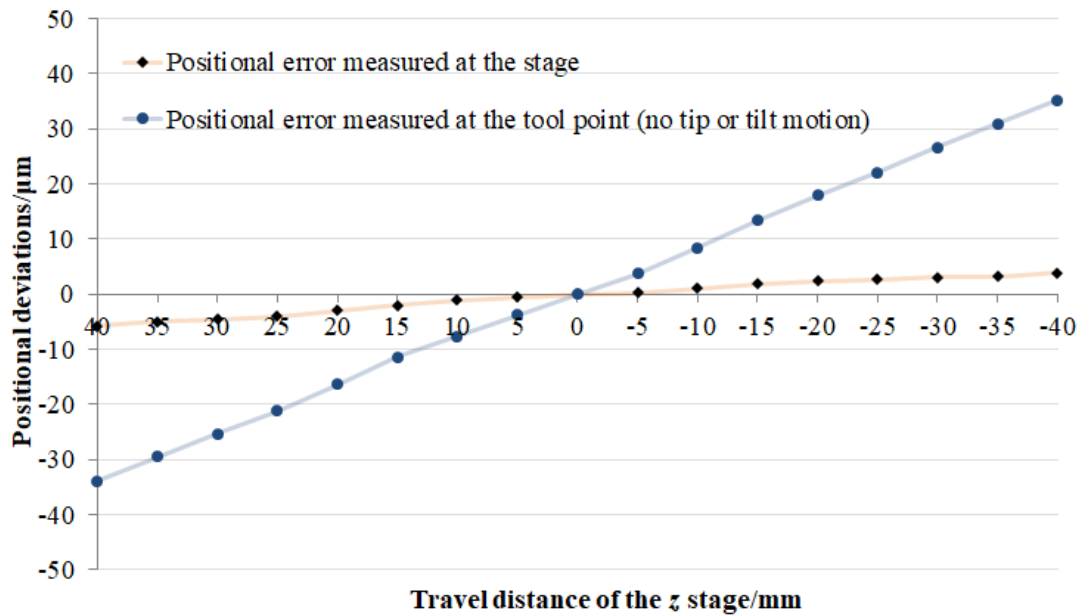


Figure 6.14 Comparison of the accuracy of the motions of z stage when measured at the stage and at the tool point (z stage travel range is ± 40 mm).

Another source of uncertainty during the compensation process can be related to the accuracy of the motions generated by the xz stages for the compensation. Figure 6.14 shows the accuracy of the motion of the z stage for its travel distance of ± 40 mm. It is important to note the difference between the accuracies of the motions when measured at two different places – at the motion stage and at the target point. Considering the maximum displacement required for the compensation is ± 3 mm, the accuracy of the motion of the z stage (± 340 nm) when measured at the stage appears to be acceptable for the target positioning and alignment operation. This accuracy data, in fact, matches with the calibration data provided by the supplier of HAMS. However, in practice, the accuracy of the motion of the z stage when measured at the target point is more important for the high-accuracy target positioning. As can be seen from Figure 6.14, the positional error for ± 3 mm displacement is now quite large (± 2.2 μm), which can directly affect the accuracy of the compensation for the positional deviation of the target. This partly explains why positional error remains after the calibration and compensation for the

target positional deviation in the z direction (Figure 6.12).

The difference between the accuracy measured at the stage and the target point is due to the amplification of the rotational error motion of the xz stage by the structural offsets between the xz stage and the target point. It is possible to compensate for the positional error of the xz stages in addition to any compensations required for the positional deviations associated with the tip or tilt motion of HAMS. However, this is an area of future research.

6.7.5 Positional deviations of the target T for tilt (ν) motion

The effect of the errors, associated with the tilt (ν) motion of the rotating platform of HAMS, on the positional deviation of the target T can be treated as the case of finding the effects of the errors associated with the motion of the rotatory motor that actuates the platform, where the functional point (target T) is at some z and y offsets from the effective point (i.e. centroid of the rotating platform F as shown in Figure 5.4 and 5.6, right). The translational error parameters $\delta_{x_{rad}}$ and $\delta_{z_{rad}}$ and the rotational error parameters ε_x and ε_z have been used to describe the errors associated with the tilt (ν) motion of the rotating platform (see section 5.6.1 and 5.7.2) to find the positional deviations equations for the target (equations (5.58) to (5.70) and equations (6.4) to (6.6)).

For the tilt motion, the experimental results and the model predictions (equations (6.4) to (6.6)) for the positional deviations of the target T agree well with each other, as shown in Figure 6.15. It can be seen from the model equations and Figure 6.15 that tilt motion and its associated error motions ε_x , ε_z , $\delta_{x_{rad}}$ and $\delta_{z_{rad}}$, which originate at the centroid of the rotating platform due to the misaligned axis of rotation of motor, cause considerable positional deviations at the target T in the x and z directions. The deviation in the x direction is much higher compared to the deviation in the z direction. This

deviation in the x direction is mainly due to the magnification of: 1. the tilt motion by the 96 mm Abbe offset (see Figure 6.3) - note the $[(d_3 + t_z) \sin v]$ term in equation (6.4)) and 2. the error motion ε_z by the 118 mm Abbe offset - note the term $[h_6 (\cos v \varepsilon_z - \sin v \varepsilon_x)]$ in equation (6.4). On the other hand, the positional deviation in the z direction is mainly contributed by the magnification of the error motion ε_x by the 118 mm Abbe offset (see Figure 6.3) - note the $[(h_6 + t_y) (\cos v \varepsilon_x + \sin v \varepsilon_z)]$ term in equation (6.6).

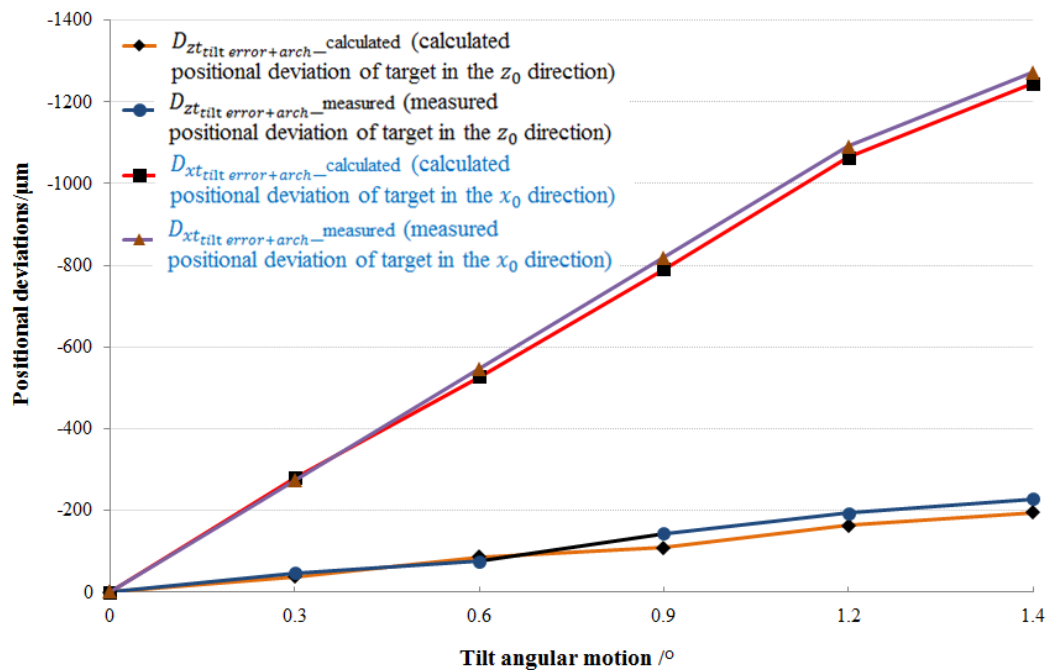


Figure 6.15 Comparison of the calculated and measured positional deviations of target (tool point) due to tilt rotational errors (in z and x directions).

The positional deviation of the target T due to error motions associated with the tilt (v) motion can be compensated by the two techniques (i.e. compensations using motion programme of control software and translation of the coordinate system) described for the tip (u) motion of the moving platform (section 6.6). However, this compensation process is an area of future research.

6.8 Conclusion

Calibration of a parallel or hybrid mechanism is a difficult problem in terms of developing a suitable kinematic model, identifying error parameters, adopting cost-effective measurement plans and implementing compensations into the mechanism's controller. This problem is approached in this study in a practical way with the help of a simplified model with minimum error parameters, by carrying out simple measurements and by compensating the errors using effective software-based compensation technique, resulting in a significant improvement in the target positioning accuracy. With 1. known sources of error of HAMS's stages, 2. HAMS improved capability for high-accuracy target positioning and 3. practical position compensation techniques, the requirements for the development of a real-time position control system for the targets of the high-repetition operation are fulfilled.

Chapter 7 - Development of a real-time target alignment system

7.1 Introduction

The target alignment at high-repetition rate depends on the ability of the motion stages of HAMS to generate the translational and rotational motions to locate the target with the required accuracy and repeatability. The performance of HAMS, in terms of its ability to achieve high-accuracy target positioning, has been described in Chapter 5 and 6. However, high-accuracy target alignment in high-repetition rate operation means that a real-time position compensation method is required to maintain the target's reference position and plane throughout the operation. This can be achieved by the HAMS controller with the use of a closed loop control when the target positions (and ideally orientations) are known throughout the operation. This measurement requirement can be fulfilled by using in-process metrology (see section 3.5.1 and 3.5.2) but comes with a number of challenges. For laser operation, the major challenges are: 1. adverse operating conditions (EMP of the laser) for the sensor, 2. space constraints inside the laser chamber and 3. the measurement speed required to follow the high-repetition rate. Furthermore, the necessity for the targets to be placed at the laser focus and perpendicular to the laser beam (see Figure 2.4 and 2.5) means that information about both the target's position and orientation are needed by the controller to make the necessary compensations for the target alignment. Irrespective of the applications (laser or non-laser), in-process measurement of the target's orientation can be difficult, as comprehensive information about the target's location is required throughout the operation.

This chapter details the development of a closed loop control system using an Abbe-complaint, in-process position measurement system for real-time alignment of the targets for high-repetition rate laser operations. The design principles of the in-process

target position measurements are discussed, followed by the derivation of a model showing the relationship between the positional deviations of the target, which form the feedback information to the sensor, and the error sources related to the high-repetition rate system. The hardware set-up, control scheme of the closed loop system and the experimental procedure are described. Implementation issues with the closed loop control are discussed in light of the experimental results and the model, which led to strategies for improving the performance of the closed loop control for the real-time target alignment.

7.2 The need for closed loop control for precision target alignment

In high-repetition rate laser operation, as outlined in section 4.3.2.1, target alignment (positioning and orientation) follows a two-step process: initial alignment and dynamic alignment. Once the target's reference position is set in the initial alignment step, any further alignment of the target can be carried out during the high-speed wheel rotation when targets need to be repositioned automatically at the laser focus. The positional deviations of the target can be compensated in real-time when a position measurement system with sufficient accuracy sends the target position feedback information to the controller of the HAMS motion stages, thus completing a closed loop control system.

Improvement of the target positioning accuracy achieved by kinematic calibration of HAMS (Chapter 6) does not guarantee that the target's reference position will be maintained throughout the high-repetition rate operation, especially when some repeatability errors are either not compensated or difficult to compensate using a kinematic calibration. Furthermore, there may exist random errors due to the disturbances from the environmental sources (vibration, temperature variations etc). In

these circumstances, a closed loop control system, as opposed to an open-loop control (no feedback system), can offer a robust and high-accuracy target positioning system.

7.3 Design of the control system for high-repetition rate laser operations

Considering the performance of a positioning system in terms of the positional accuracy of the target, the following three locations of the system's elements with respect to the system's coordinate system are critical for closed loop control [131]:

1. The actuator's location;
2. The sensor's location; and
3. The target's location.

For closed loop control of a precision positioning system, the location of the sensor in the system is an important consideration, because the locations of the actuators and sensors influence the “observability” and “controllability” of an active control positioning system [98,132]. In the case that the positioning system's sensor and actuator are non-collocated, which is often the case, the functionality of the positioning system can be impaired. In such cases, the controller is unable to improve the system's dynamic behaviour due to closed loop instability or a time-delay in the feedback loop [131,132]. Furthermore, non-collocation of the sensor and the target may result in Abbe errors in the position measurement of the target, which in turn mean that the controller's compensation for the target position, based on the sensor's measurement, can be ineffective, leading to inaccuracy in target re-positioning during high-repetition rate operation.

The design of the position measurement system for the target is examined in the following sections in light of the Abbe principle. The development of an analytical model is then outlined to show the relationship between the target position feedback (i.e.

the z positional deviations of the target with respect to its reference position) and the factors affecting the feedback.

7.3.1 Target position measurement for the high-repetition rate operation: applying the Abbe principle

The generalised Abbe principle, reformulated by Bryan [133], states that “the path of the effective point (EP) of a displacement measuring system should be collinear with the path of the functional point (FP) whose displacement is to be measured. If collinearity is not possible, either the slideways that transfer the displacement must be free of angular motion or angular motion data must be used to calculate the consequences of the offset” [11]. In this respect, one technique for achieving an Abbe compliant measurement system for a two or three degree of freedom (DOF) system is to keep the FP stationary with respect to the reading head of the sensor (EP), when the FP is always coincident with the path of the EPs of the sensor during the measurement. This configuration is attainable only if the sensor measures the movement of the target surface surrounding the workpiece or the motion stages, at the same time allowing the target surface to move in a direction perpendicular to the sensor’s measurement direction [10,11]. A measurement configuration based on the above principle was proposed by Bosmans et al. to develop an ultra-precision, Abbe-compliant position measurement system with linear encoders [11].

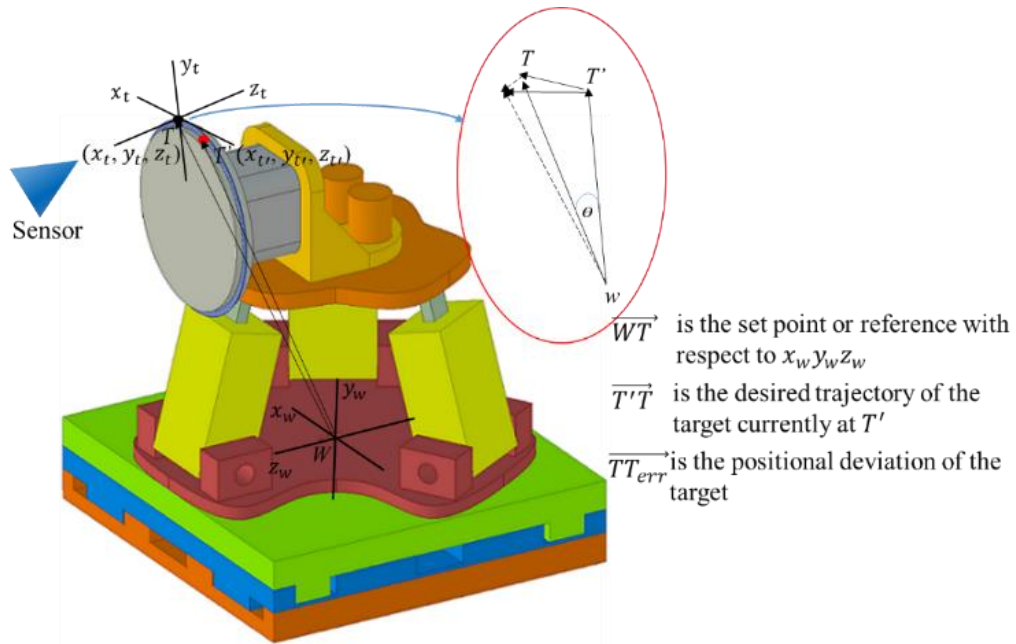


Figure 7.1 Concept of the closed loop control for z position compensation.

The measurement configuration stated above can be applied to develop an Abbe compliant measurement system to measure the positional deviation of a target T (FP in this case) located at the target wheel rotating at a certain speed. For example, in Figure 7.1 consider \overrightarrow{WT} as a vector representing the reference position and orientation of the target T with the coordinate position (x_t, y_t, z_t) . When the target at position T' moves to T , the coordinate position of T' has to be within x, y and z specifications of (x_t, y_t, z_t) . However, if error motions arise due to some disturbances (e.g. the kinematic errors of the wheel), T' will reach T_{err} , generating a positional error $\overrightarrow{TT_{err}}$ at point T . Provided this error motion along the z axis can be detected by the interferometer and then fed back to the controller for compensation, the target will be repositioned at T before the laser hits the target. In this way, all the targets around the target wheel will be within the z specification of the laser focus (only the z positional deviation is considered in this paper, since z is considered as the sensitive direction for the target alignment). If plane mirrors can be placed around the circumferential edge of the wheel (this mirror setting will be referred as “target position setting” henceforth) and an interferometer is

used to measure the relative movement between the sensor and target point T , then the FP and EP become coincident. However, it is very difficult to place the plane mirrors around the circumferential edge of the wheel along with the target sectors. Therefore, plane mirrors are placed at the front face of the wheel around the circumference, functioning as a target surface (this mirror setting will be referred as “mirror position setting” henceforth) as described before. In this arrangement, although the EP of the mirror position setting (M on the plane mirror as shown in Figure 7.2) is at some offsets to the FP of the target position setting (T as shown in Figure 7.2), the interferometer measures the movement of the target surface while allowing the target surface to move in a direction perpendicular to the interferometer’s measurement direction (along x direction as shown in Figure 7.2) during the wheel rotation.

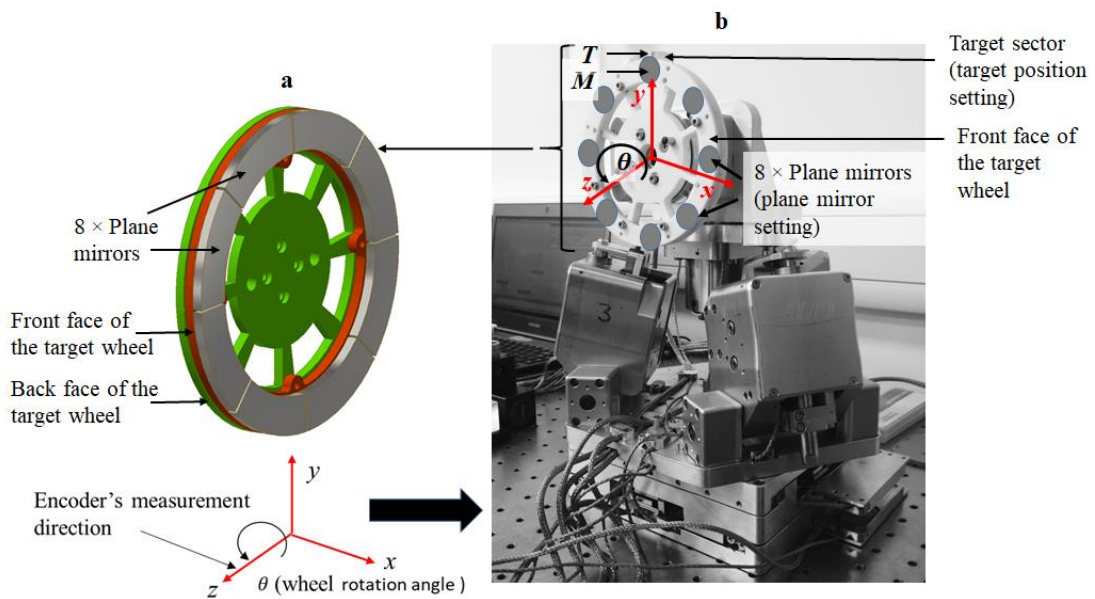


Figure 7.2 Plane mirror position (a) ideal mirror setting (b) actual mirror setting.

7.3.2 In-process measurement system for real-time target alignment

A plane mirror interferometer (Renishaw model XL-80) was used as the feedback system for the closed loop control system to generate the compensations (Figure 7.2). In a plane-mirror interferometer, the mirror is placed on the moving object

whose displacement has to be measured. In this measurement system, as shown in Figure 7.2, suitably sized plane mirrors are attached to the front face of the target wheel around the circumference.

7.4 Positional deviation of target during wheel rotation: model

An equation needs to be found that describes the positional deviation of the target in the z direction when the target moves from point T' to point T during wheel rotation, as shown in Figure 7.3. T is represented by a coordinate system $x_T y_T z_T$ whose position is (x_t, y_t, z_t) with respect to the machine's reference coordinate $x_w y_w z_w$. In the error-free condition, (x_t, y_t, z_t) will be the reference position of the target, while T' is represented by a coordinate system $x_{T'} y_{T'} z_{T'}$ whose position is $(x_{t'}, y_{t'}, z_{t'})$ with respect to the machine's reference coordinate $x_w y_w z_w$. T' is positioned at an angular distance θ from T , and the equation to be derived will provide the positional deviation of the target for a complete wheel rotation.

The positional deviation of the target is generated from the interferometer's measurement of the change of z_t of the reference point (x_t, y_t, z_t) , when all the T' points around the circumference of the wheel pass through the point T in a complete rotation of the wheel. The positional deviation response shows the effect of the error motions related to the wheel rotation, arising from different error sources, such as geometric and dynamic disturbances. Assuming that the displacement measurement by the interferometer takes place in a controlled environment and, therefore, has negligible random errors from environmental disturbances, the positional deviation of the target in the z direction can be described in terms of the "face runout" of the wheel as a result of the geometric disturbances. Face runout can be defined as the total displacement measured parallel to the z reference axis at a specified radial location of the wheel by an

instrument sensing against a moving surface or moved with respect to a fixed surface [52]. Assuming that a reference coordinate $x_0'y_0'z_0'$ (Figure 7.3a) is placed at point O' of the interferometer's quarter-wave plate, from which the measurement beam emerges from the interferometer, the relative motion between the reference coordinates of the interferometer (i.e. $x_0'y_0'z_0'$) and the wheel (i.e. $x_Ty_Tz_T$) measured by the interferometer will determine the face motion of the wheel.

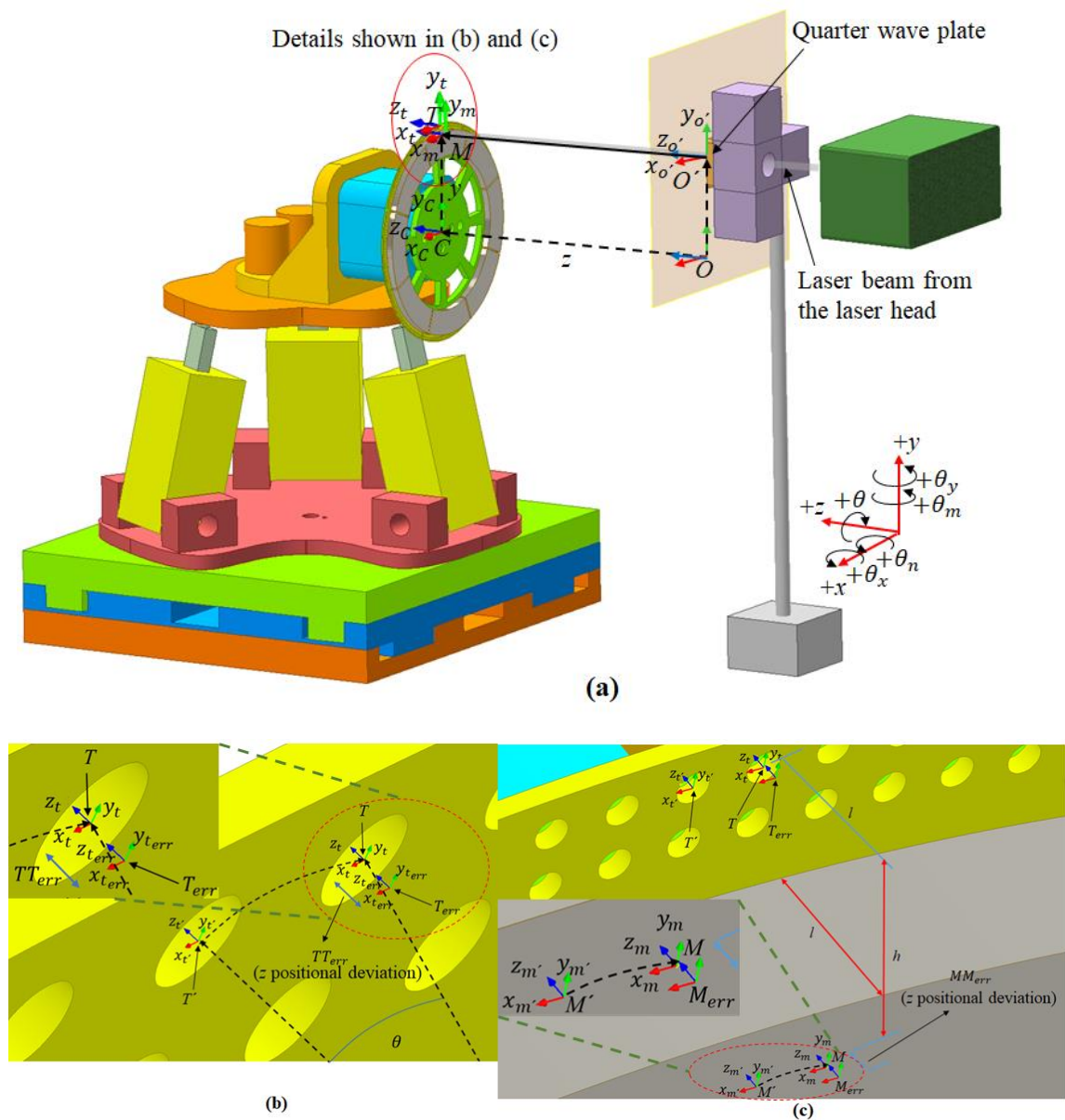


Figure 7.3 Coordinate systems for the error model (a) with the effective and functional points shown in (b) and (c).

The coordinate systems are placed at points of interest within the system (the motion stages of HAMS and the interferometer) as shown in Figure 7.3, namely $x_C y_C z_C$ at the centre of the wheel C and $x_0 y_0 z_0$ at point O (O is perpendicularly below O' on the same plane). Note that in Figure 7.3 point M of the mirror, which has the coordinate $x_M y_M z_M$ placed at (x_m, y_m, z_m) , corresponds to target point T . This means that offsets exist between the FP (i.e. T) and EP (i.e. M) in the y and z directions, called l and h respectively. Ideally, T and M should be aligned (i.e. no offset in the x direction) to minimise Abbe error. However, an offset s in the x direction is also considered in the model for the sake of generality.

Consider that T is directly above the centre of the wheel C . If a plane mirror can be placed at T so that the interferometer can measure the z displacement of T (ideally, the interferometer plane should be parallel to the wheel's plane), the interferometer will read the value $O'T$, which is equal to $(z + l)$, where z is the perpendicular distance between O of the interferometer plane and the centre of the wheel C (see Figure 7.3a), and l is the perpendicular distance in the z direction between point M and target T (see Figure 7.3c).

The positional deviation of the target in terms of the wheel's face runout can be derived using a homogeneous transformation matrix (HTM) [see section 4.3.1]. In the current analysis, it is possible to define an HTM for each successive position and orientation change of the mirror, with respect to the fixed $x_{O'} y_{O'} z_{O'}$ coordinate of the interferometer, to determine the final position of the target. This is because the reflected beam from the plane mirror (at the target position or mirror position setting) entering the interferometer is directly affected by the position and orientation change of the plane mirror with respect to $x_{O'} y_{O'} z_{O'}$.

In the case that the wheel does not have any face motion (i.e. error-free condition) and T' corresponds to T as shown in Figure 7.3a and 7.3b, the position and orientation of T' with respect to the coordinate $x_o'y_o'z_o'$ ($x_o'y_o'z_o'$ and $x_o y_o z_o$ have the same orientation) can be represented by the following HTM (z distance measured by the interferometer should remain unchanged, since T and T' are the same point of the mirror):

$$\mathbf{T}_{T \text{ no error}}^O = \mathbf{T}_{Target}^O \mathbf{T}(\theta), \quad (7.1)$$

where \mathbf{T}_{Target}^O is the HTM to describe the position of the target with respect to $x_o'y_o'z_o'$ when there is no wheel rotation, and is given by

$$\mathbf{T}_{Target}^O = \begin{bmatrix} 1 & 0 & 0 & s \\ 0 & 1 & 0 & y + h \\ 0 & 0 & 1 & z + l \\ 0 & 0 & 0 & 1 \end{bmatrix}, \quad (7.2)$$

where y is the radius of the wheel or the distance between C and M , as shown in Figure 7.3. $\mathbf{T}(\theta)$ is the HTM to describe the rotation of wheel about z_c of $x_c y_c z_c$, and is given by

$$\mathbf{T}(\theta) = \begin{bmatrix} \cos \theta & \sin \theta & 0 & 0 \\ -\sin \theta & \cos \theta & 0 & 0 \\ 0 & 0 & 1 & 0 \\ 0 & 0 & 0 & 1 \end{bmatrix}. \quad (7.3)$$

By combining equations (7.2) and (7.3), $\mathbf{T}_{T \text{ no error}}^O$ in equation (7.1) will have the following form

$$\mathbf{T}_{T \text{ no error}}^O = \begin{bmatrix} \cos \theta & \sin \theta & 0 & (h + y) \sin \theta + s \cos \theta \\ -\sin \theta & \cos \theta & 0 & (h + y) \cos \theta - s \sin \theta \\ 0 & 0 & 1 & z + l \\ 0 & 0 & 0 & 1 \end{bmatrix}. \quad (7.4)$$

The face motion of the wheel, expressed in terms of the positional deviation of the target T , results in two rotational error motions that are generated due to imperfect wheel rotation about the z_c axis of $x_c y_c z_c$. One error motion (θ_x) is the tip error that represents a rotation about x_c of $x_c y_c z_c$, and the other is the tilt error (θ_y) that represents a rotation

about y_C of $x_C y_C z_C$. Since the face motion distorts the ideal wheel rotation path, when the wheel rotates, a point T' on the wheel reaches to point T_{err} instead of point T (see Figure 7.3b), resulting in the change in the z distance measured by the interferometer. The position and orientation of T_{err} with respect to the coordinate $x_o' y_o' z_o'$ ($x_o' y_o' z_o'$, $x_o y_o z_o$, $x_C y_C z_C$, $x_R y_R z_R$ and $x_T y_T z_T$ have the same orientation at the outset of the wheel rotation) can be represented by the following HTM

$$\mathbf{T}_{T_{err}}^O = \mathbf{T}_C^O \mathbf{T}(\theta_n) \mathbf{T}(\theta_m) \mathbf{T}(\theta_y) \mathbf{T}(\theta_x) \mathbf{T}(\theta) \mathbf{T}_T^C, \quad (7.5)$$

where \mathbf{T}_C^O is the distance between C and O with respect to $x_o y_o z_o$, and is given by

$$\mathbf{T}_C^O = \begin{bmatrix} 1 & 0 & 0 & 0 \\ 0 & 1 & 0 & 0 \\ 0 & 0 & 1 & z \\ 0 & 0 & 0 & 1 \end{bmatrix}. \quad (7.6)$$

$\mathbf{T}(\theta_n)$ is the misalignment of the mirror described by the rotation θ_n about the x_C axis of coordinate $x_C y_C z_C$, and is given by

$$\mathbf{T}(\theta_n) = \begin{bmatrix} 1 & 0 & 0 & 0 \\ 0 & \cos \theta_n & -\sin \theta_n & 0 \\ 0 & \sin \theta_n & \cos \theta_n & 0 \\ 0 & 0 & 0 & 1 \end{bmatrix}. \quad (7.7)$$

$\mathbf{T}(\theta_m)$ is the misalignment of the mirror described by the rotation θ_m about the y_C axis of coordinate $x_C y_C z_C$, and is given by

$$\mathbf{T}(\theta_m) = \begin{bmatrix} \cos \theta_m & 0 & \sin \theta_m & 0 \\ 0 & 1 & 0 & 0 \\ -\sin \theta_m & 0 & \cos \theta_m & 0 \\ 0 & 0 & 0 & 1 \end{bmatrix}. \quad (7.8)$$

$\mathbf{T}(\theta_y)$ is the tilt error motion of the wheel with respect to $x_o' y_o' z_o'$ or $x_C y_C z_C$, and is given by

$$\mathbf{T}(\theta_y) = \begin{bmatrix} \cos \theta_y & 0 & \sin \theta_y & 0 \\ 0 & 1 & 0 & 0 \\ -\sin \theta_y & 0 & \cos \theta_y & 0 \\ 0 & 0 & 0 & 1 \end{bmatrix}. \quad (7.9)$$

$T(\theta_x)$ is the tip error motion of the wheel with respect to $x_{o'}y_{o'}z_{o'}$ or $x_Cy_Cz_C$, and is

$$\text{given by } T(\theta_x) = \begin{bmatrix} 1 & 0 & 0 & 0 \\ 0 \cos \theta_x & -\sin \theta_x & 0 & 0 \\ 0 \sin \theta_x & \cos \theta_x & 0 & 0 \\ 0 & 0 & 0 & 1 \end{bmatrix}. \quad (7.10)$$

T_T^C is the offset between C and T with respect to $x_Cy_Cz_C$, and is given by

$$T_T^C = \begin{bmatrix} 1 & 0 & 0 & S \\ 0 & 1 & 0 & y + h \\ 0 & 0 & 1 & l \\ 0 & 0 & 0 & 1 \end{bmatrix}. \quad (7.11)$$

Note that the sequence of HTMs in equation (7.5) is selected based on the following considerations:

1. The z distance OC is assumed to be not affected by the error motions related to θ .
2. Misalignment of mirror affects all the subsequent changes to the position and orientation of the target, therefore, $T(\theta_m)$ and $T(\theta_n)$ are placed before $T(\theta_y)$, $T(\theta_x)$, $T(\theta)$ and T_T^C .
3. Wheel rotational motion θ is affected by the error motions θ_x and θ_y ; hence $T(\theta_x)$ and $T(\theta_y)$ are placed before $T(\theta)$. The target is affected by all the changes, so T_T^C is placed as the right-most term in equation (7.5).

Substituting the values from equation (7.3) and equations (7.6) to (7.11) into equation (7.5) yields

$$T_{T_{err}}^O = \begin{bmatrix} K_1 & L_1 & M_1 & N_1 \\ K_2 & L_2 & M_2 & N_2 \\ K_3 & L_3 & M_3 & N_3 \\ 0 & 0 & 0 & 1 \end{bmatrix} \quad (7.12)$$

where $K_1, K_2, K_3, L_1, L_2, L_3, M_1, M_2, M_3, N_1, N_2$ and N_3 (i.e. equations (7.13) to (7.24)) are shown in Appendix E.

Subtracting equation (7.1) from equation (7.12) provides the HTM T_{error} , which represents the position and orientation deviation of the target when it moves from T' to T . Therefore,

$$T_{error} = \begin{bmatrix} A_1 & B_1 & C_1 & D_1 \\ A_2 & B_2 & C_2 & D_2 \\ A_3 & B_3 & C_3 & D_3 \\ 0 & 0 & 0 & 1 \end{bmatrix} \quad (7.25)$$

where $A_1, A_2, A_3, B_1, B_2, B_3, C_1, C_2, C_3, D_1$ and D_2 (i.e. equations (7.26) to (7.36)) are shown in Appendix F,

and

$$D_3 = (h + y)(\sin \theta \cos \theta_n \sin(\theta_y + \theta_m) + \cos \theta (\cos \theta_x \sin \theta_n + \sin \theta_x \cos \theta_n \cos(\theta_y - \theta_m))) - s(\cos \theta \cos \theta_n \sin(\theta_y + \theta_m) - \sin \theta (\cos \theta_x \sin \theta_n + \sin \theta_x \cos \theta_n \cos(\theta_y - \theta_m))) - l(\sin \theta_n \sin \theta_x - \cos \theta_x \cos \theta_n \cos(\theta_y - \theta_m)) - l. \quad (7.37)$$

Equation (7.37) represents the positional deviation of the target TT_{err} in the z direction as measured by the interferometer. To derive a simpler form of equation (7.37), assume that the misalignments of the mirror are negligible, which means θ_m and θ_n are zero (the effects of misalignment and their avoidance are discussed in section 7.6.2). Also, assume that s in equation (7.37) is zero, which means M and target point T are aligned, as shown in Figure 7.3. Therefore, equation (7.37) becomes

$$z_{error} = TT_{err} = (h + y)(\sin \theta \sin \theta_y + \cos \theta \sin \theta_x \cos \theta_y) + l \cos \theta_x \cos \theta_y - l. \quad (7.38)$$

Taking $(h + y) \sin \theta_y = E_r \cos \alpha$ and $(h + y) \sin \theta_x \cos \theta_y = E_r \sin \alpha$, equation (7.38) can be re-written as the periodic function equation

$$z_{error} = E_r \sin(\theta + \alpha) + l \cos \theta_x \cos \theta_y - l \quad (7.39)$$

where

$$E_r = (h + y) \sqrt{((\sin \theta_y)^2 + (\sin \theta_x \cos \theta_y)^2)}, \quad (7.40)$$

and

$$\alpha = \tan^{-1} \frac{\sin \theta_x}{\tan \theta_y}. \quad (7.41)$$

The sine function in equation (7.39) relates the rotational distance travelled by the wheel (i.e. θ) to the corresponding positional deviation of the target in terms of wheel's error motions θ_x and θ_y . Note that $(h + y)$ in equation (7.40) becomes $\frac{(h+y)}{\cos \theta}$ at angle θ and is subject to change by θ_x and θ_y . So, equation (7.40) becomes

$$E_r = \frac{(h+y) \sqrt{((\sin \theta_y)^2 + (\sin \theta_x \cos \theta_y)^2)}}{\cos \theta}. \quad (7.42)$$

From the model described, the following observations are important for the analysis of the experimental data in section 7.7.

1. As mentioned before, since it is practically very difficult to place the mirror exactly at the target position T (i.e. target position setting) to read the displacement and, therefore, the mirrors are placed at the front face of the wheel around the circumference (i.e. mirror position setting), the resultant position deviation at point M as read by the interferometer will be determined by

$$z_{error \text{ at } M} = E_r \sin(\theta + \alpha) \quad (7.43)$$

where

$$E_r = \frac{y \sqrt{((\sin \theta_y)^2 + (\sin \theta_x \cos \theta_y)^2)}}{\cos \theta}. \quad (7.44)$$

2. The difference between equations (7.39) and (7.43), as shown in equation (7.45), represents the error in the target position feedback because of the use of the mirror position setting (EP) in the control system, i.e.

$$z_{feedback\ error} = \left(\frac{h \sqrt{(\sin \theta_y)^2 + (\sin \theta_x \cos \theta_y)^2}}{\cos \theta} \sin(\theta + \alpha) \right) + (l \cos \theta_x \cos \theta_y - l). \quad (7.45)$$

7.5 Design of the closed loop control system

The hardware set-up for the closed loop system is shown in Figure 7.4, and the control scheme is presented in Figure 7.5. The HAMS motion stages use Delta Tau's multi-axis motion control system (Turbo PMAC) to control the seven servo motors (three for the tripod, two for the two linear stages, one for the rotating platform and one for the wheel rotation) of the motion stages with the use of the quadrature signals generated from the seven encoders of the respective motors. The eighth encoder channel of the controller accepts the quadrature signal from the interferometer to provide the real-time position information about the target. Although the position encoders of the motion stages and the interferometer are both incremental encoders, the resolution of the encoders of the motion stages is not as high as the resolution of the interferometer. Therefore, the quadrature signal generated by the interferometer is converted to the equivalent encoder counts through the use of an encoder conversion table (a characteristic feature of the Turbo PMAC controller); the counts can then be used by the controller's servo motors for the position compensations.

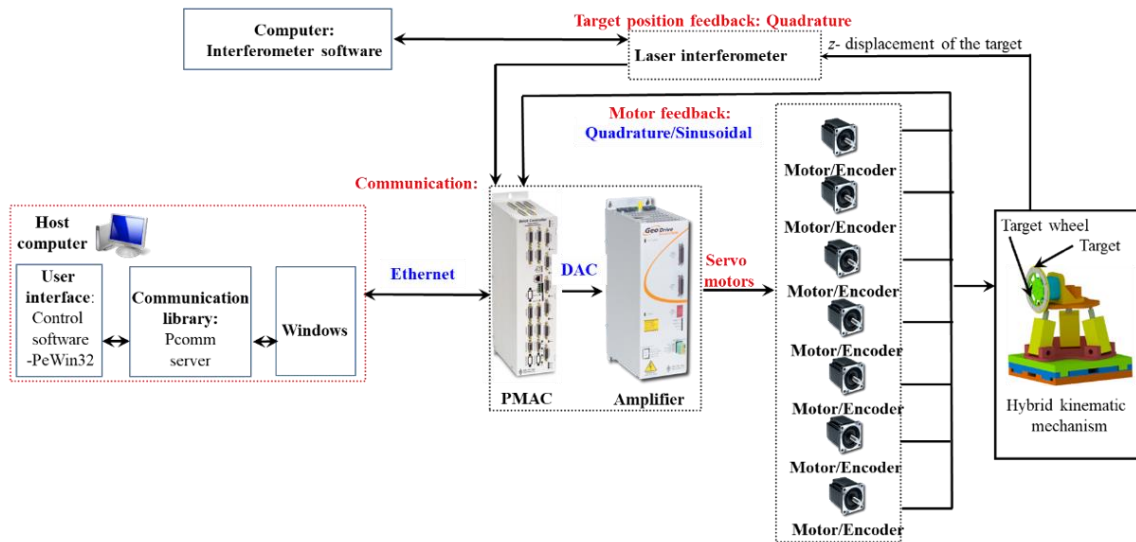


Figure 7.4 Hardware set-up for the closed loop control of the target.

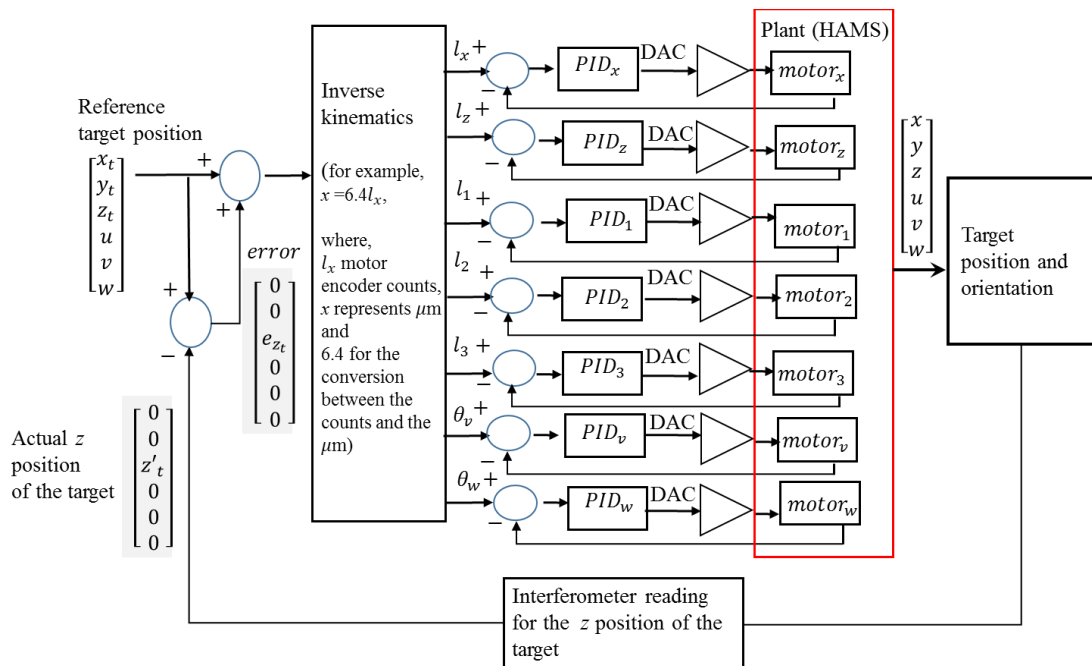


Figure 7.5 Control diagram of the closed loop control for HAMS motion stages.

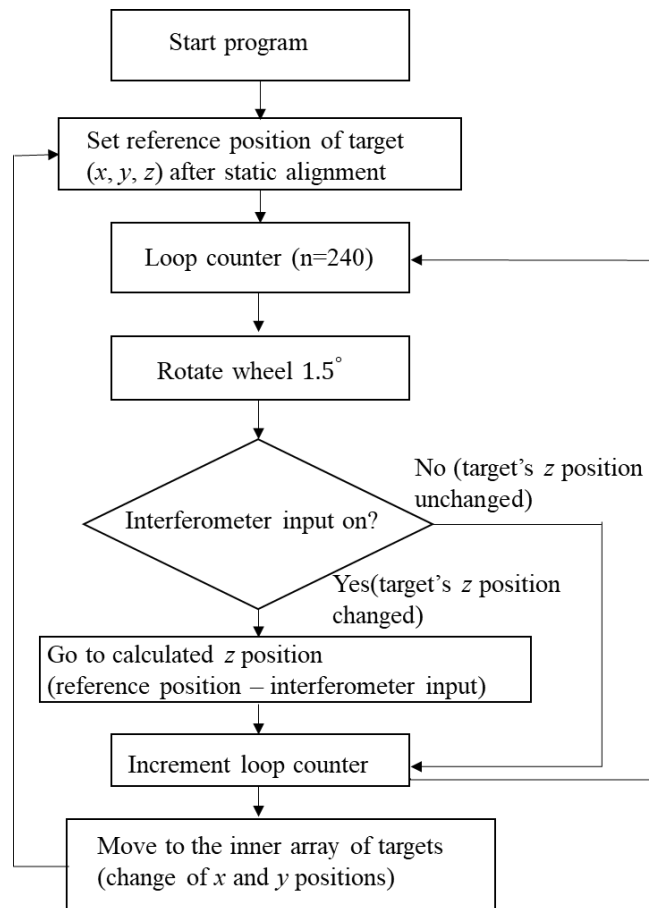


Figure 7.6 Simplified flow-diagram of the motion program for the high-repetition rate operations.

HAMS turbo PMAC controller provides a position loop servo filter based on PID, feedforward and a notch filter (servo filter not shown in the Figure 7.4) [134,135]. Usually, this servo filter is enough to control the motion system, where the filter can be tuned by setting the appropriate variables for each motor [134]. For example, some variables, called *I*-variables, provide the adjustment of the proportional, differential and integral gain of the motors, while other *I*-variables provide the settings for the velocity and acceleration feedforward gain of the motor. The configuration, control and troubleshooting of the HAMS motion stages are carried out using a Delta-Tau's control software (PeWin32pro2), which can also be used to write and execute user-defined motion programs for the motors. As such, a motion program was written in the

controller's language, using the controller's various functional parameters, to run the target wheel at a specified speed, read the position information from the interferometer and then compensate the position deviations by actuating the motion stage/s. The simplified flowchart of the motion program is shown in Figure 7.6.

7.6 Experimental validation of the closed loop design for the high-repetition rate laser operation

7.6.1 Experimental procedure

Experiments were carried out to verify the design of the closed loop control, as described in section 7.5, for real-time target alignment for high-repetition rate laser operations. The experiments can be divided into two groups: open-loop and closed loop, while the main objectives are as follows.

1. For the open-loop experiments: evaluate, with respect to the required positional accuracy of target ($\pm 4 \mu\text{m}$ in the z direction), the high-repetition rate system's behaviour in open-loop control by measuring the z positional deviations (magnitudes and directions) for a complete wheel rotation.
2. For closed loop experiments:
 - a) find a functional closed loop design capable of generating the position compensations with the target position feedback; and
 - b) find an optimised closed loop design capable of producing the necessary compensations to position the targets within the z position specification of the reference position.

7.6.1.1 Open-loop experiments

The set-up of the experiment is shown in Figure 7.3a, and the procedure of the target position measurement using the plane mirror interferometer is described in sections 7.3.1

and 7.3.2. For the mirror position setting, eight square plane mirrors (Thor Lab's 1"×1" broadband dielectric mirror, 400 nm to 750 nm) were attached to the wheel at the angular positions 0°, 45°, 90°, 135°, 180°, 225°, 270° and 315°, covering a total angular distance of 189° of 360° of the wheel's circumference (see Figure 7.2 and 7.3). For the target position setting, eight mirrors were placed around the circumferential edge of the wheel, maintaining the alignment with the corresponding eight mirror positions of the mirror position setting.

Position measurements were taken with the interferometer at the target position and mirror position settings for a complete wheel rotation to measure the z positional deviation at FP and EP, respectively, (T and M as shown in Figure 7.2 and 7.3) without any influence of closed loop control (no position compensations). Note that the position measurements were taken at 0.5 Hz, representing 0.5 Hz repetition rate laser operation, which means there was a 2 s time-gap for each repetition, during which period a target moves from a position to the next position of the wheel (i.e. 1.5°).

7.6.1.2 Closed loop experiments

The same interferometer set-up as described in section 7.6.1.1 was used to find a functional closed loop design. The tasks of the closed loop set-up, such as the connection between the interferometer and the HAMS controller, the controller's software settings, etc. were carried out as described in section 7.5 and Figure 7.4, 7.5 and 7.6. With a functional closed loop control system, a series of experiments were carried out to find the optimal condition/s at which $\pm 4 \mu\text{m}$ position accuracy could be achieved. A critical task of the optimisation process was to improve the motion program (see Figure 7.6), so that the controller-generated position compensations were correct - both in magnitude and direction - based on the z positional deviations at the EP (mirror position setting). As will be shown in section 7.7, the investigation of the issues of the closed loop control

system led to suitable compensation techniques (angular compensation) for the target's alignment for the high-repetition rate operations. All closed loop experiments were carried out at 0.5 Hz repetition rate.

7.6.2 Measurement uncertainties

Since the closed loop control uses the interferometer to measure the z positional deviation of the target (feedback), and then uses the motion of the z position stage for the compensation, the experimental results related to z position measurements are subject to some sources of measurement uncertainties, for example:

- A. Errors from the conversion of the interferometer's quadrature signal to equivalent counts of the controller;
- B. Accuracy of the motion of the z position stage; and
- C. Misalignment of the plane mirrors that may cause parallel and/or orthogonality errors.

The interferometer's quadrature signal for position is converted to equivalent counts for the position measurement of the servo loop of the controller. Comparison of a number of z displacements measured by the interferometer and the controller's encoder (in terms of counts) shows that 1 μm for the interferometer is equivalent to 991 nm for the controller's encoder. Considering that the HAMS with closed loop control will not show a positional deviation of more than $\pm 5 \mu\text{m}$ during the wheel rotation, the maximum error related to the equivalent counts of the controller's encoder will be 45 nm.

The uncertainty from the positional accuracy of the z stage has already been discussed in section 6.7.4.2. Considering that the controller's compensation will not exceed $\pm 5 \mu\text{m}$ in a closed loop control, the uncertainty related to the accuracy of the travelled distance in the z direction is negligible (approximately 4 nm).

In the proposed control system design with a plane mirror interferometer, the alignment of the mirror with respect to the coordinate system of the wheel (xyz in Figure 7.2) is important, since the position of the target is determined by direct reference to the mirror [136]. Parallel error arises when the mirror is not aligned parallel to the x axis of the wheel's coordinate xyz as shown in Figure 7.2. Orthogonality error is produced when a mirror is not aligned perpendicular with the y axis of the wheel's coordinate xyz as shown in Figure 7.2. In the experiments, while aligning the mirror, the parallel and orthogonality misalignments were minimised by carrying out the procedure described in Appendix G. However, although the parallel and orthogonality errors should be avoided as much as possible, it is worth mentioning the unique benefit of using a plane mirror interferometer for position measurements. In the plane mirror interferometer, the double pass of the laser beam to the plane mirror with retro reflection actually compensates a tilt of the mirror [121].

7.7 Results and discussion

7.7.1 Characterisation of the high-repetition rate process in the open-loop control system

For the high-repetition rate operation in open-loop control, the study of the z positional deviations at EP and FP essentially indicates a “wheel characterisation” process, since the errors of the wheel are mapped through this process.

Figure 7.7 shows the profiles of the position feedback (z positional deviations) for eight locations of the wheel, as discussed in section 7.6.1. The feedback, as shown in Figure 7.7, has two components: the magnitude and the direction of the z positional deviation. Based on the position feedback from EP and FP (i.e. mirror and target position

settings), two types of behaviour of the system can be observed during a complete wheel rotation.

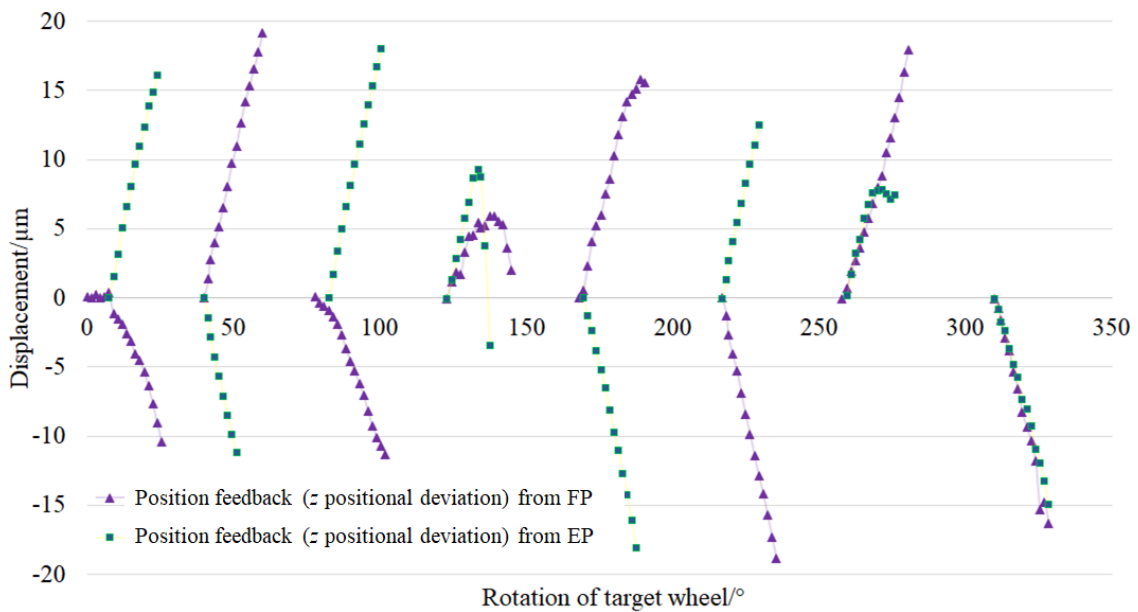


Figure 7.7 Profiles of the position feedback (z positional deviations) for eight locations of the target wheel.

- A. At some locations of the wheel (0° , 45° , 90° , 180° and 225° as shown in Figure 7.7), the position feedback from EP does not comply with the feedback from FP (the term “non-compliance” is used henceforth to indicate this). In all such cases, the directions and magnitudes of the z position deviations are non-compliant to each other.
- B. At some locations of the wheel (135° , 270° and 325°) as shown in Figure 7.7, the position feedback from both EP and FP comply with each other (the term “compliance” is used henceforth). At location 325° , both the magnitude and direction of the z positional deviation are almost the same for EP and FP. However, at locations 135° and 270° , the positional deviations at EP and FP initially appear to comply with each other but deviate (in magnitude and/or direction) at the later stage with further rotation of the wheel.

7.7.2 Performance evaluation of the closed loop design

Following the examination of the system's open-loop characteristics, the closed loop behaviour was studied by evaluating the control system's performances in terms of its ability to re-position the target within $\pm 4 \mu\text{m}$ of the reference position. Analysis of the experimental results showed that the controller's position compensations were able to reposition the target within $\pm 1 \mu\text{m}$ of the reference position by using the position feedback (z positional deviation) from EP or FP (indicated by the compensation values of the O and P profiles in Figures 7.8 and 7.9). However, although the accuracy level ($\pm 1 \mu\text{m}$) indicates that the closed loop system is functioning well, the results of the closed loop experiments highlight the problems related to the position feedback from EP and FP (see section 7.7.1). The key observations, as shown in Figure 7.8 and 7.9, are the following.

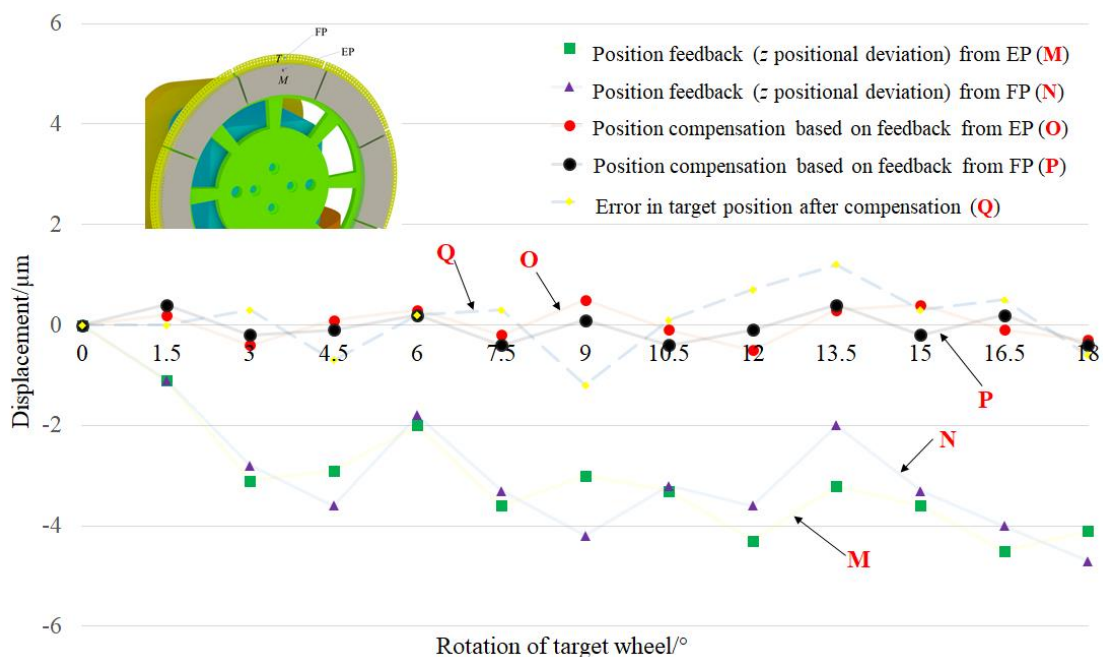


Figure 7.8 Closed loop control system in which mirror position setting represents the target position (i.e. complaint case where position feedback from EP and FP are same- also see Figure 7.3).

A. Figure 7.8 and 7.9 show typical behaviours of the closed loop system for the complaint and non-complaint cases, respectively. These two characteristic behaviours indicate that, while at some locations the position feedback from EP (the mirror position setting) can be representative (check M and N profiles of Figure 7.8) of the actual positional deviation of the target or FP (with $\pm 1 \mu\text{m}$ error as indicated by profile Q in Figure 7.8), the position feedback from EP cannot represent (see M and N profiles of Figure 7.9) the target position or FP at other locations (i.e. non-complaint cases).

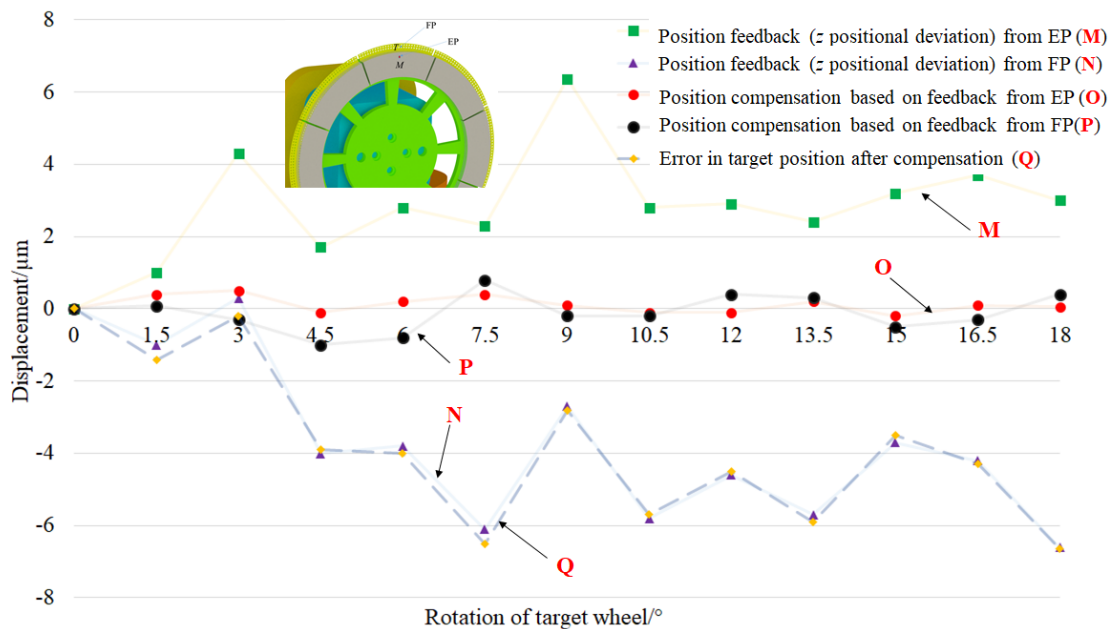


Figure 7.9 Closed loop control system in which mirror position setting does not represent the target position (non-complaint case where position feedback from EP and FP are not same – also see Figure 7.3).

B. For the non-complaint cases, the compensation by the controller based on the feedback from EP does not produce any benefit, and the positional deviation of the target (FP) remains uncompensated, as indicated by profile Q of Figure 7.9. Note that profile P of Figure 7.9 represents the controller's compensation based on the position feedback from EP.

C. The zigzag upward or downward trend (Figure 7.8 and 7.9) of the positional deviation curves indicates that the plane of the wheel with respect to the interferometer's measurement beam is changing with each wheel rotation angle (1.5°), representing the change of reference plane of the target (i.e. reference orientation of the target). The change of the plane of the target wheel results in the accumulation of the z positional deviations of the target at each wheel rotation angle, even though the controller's compensations can reposition the target to the reference position after every 1.5° rotation. Since the target plane needs to be perpendicular to the laser beam in high-power laser operation, the change of the reference orientation of the target during the wheel rotation indicates a serious problem for real-time target alignment for high-repetition rate operation.

From the above discussion, it is clear that the uncertainty in determining the position and orientation of the targets based on the position feedback from EP makes the closed loop control ineffective in achieving required accuracy ($\pm 4 \mu\text{m}$) for the real-time target alignment for the high-repetition rate laser operations.

7.7.3 Investigating the closed loop design issues using the model

The relation between the positional deviations of the target during the wheel rotation and the sources of the contributing errors can be analysed using the model derived in section 7.4. The model equations (7.39) to (7.42) predict the positional deviations of the target for a complete wheel rotation by taking account of the interactions of the following contributing elements: the wheel rotation angle (θ), rotational error motions of the wheel (tip θ_x and tilt θ_y) and the structural parameters of the wheel system (wheel diameter y and the offsets, l and h , between the target and the mirror).

The experimental data for the z positional deviations (in open-loop) at EP and FP, as shown in Figure 7.7, was fitted with the periodic function of the model as shown in equations (7.39) and (7.43) by letting the θ_x and θ_y angles vary between 0° to 90° (Figure 7.10). The θ_x and θ_y angles, resulting from the model fitting, are shown in Figures 7.11 and 7.12 for EP and FP. The resultant angular error of the wheel α related to θ_x and θ_y , as can be calculated from the equation (7.41), is shown in Figure 7.15 and 7.16. The key observations are the following.

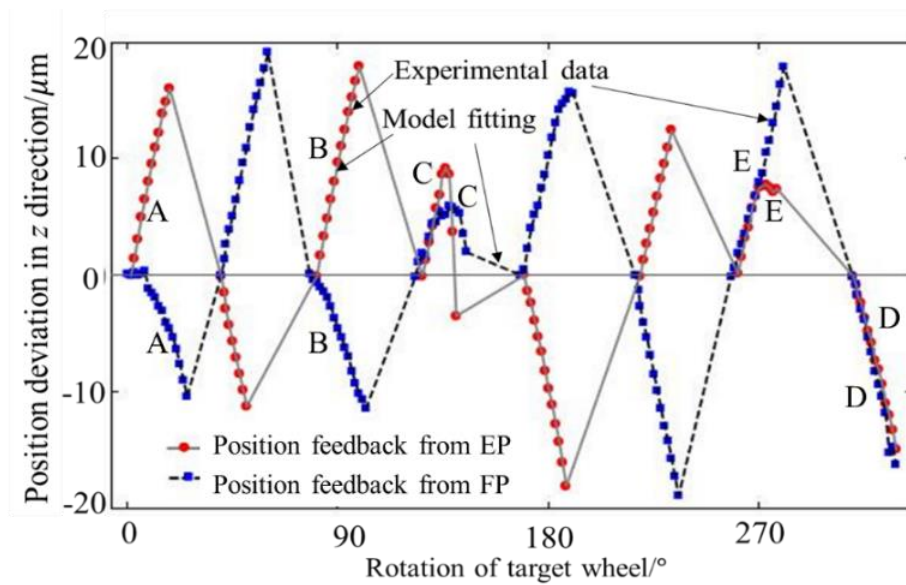


Figure 7.10 Experimental data (in open-loop) and model fitting for both mirror (EP) and target position (FP) settings.

- A. Comparative study of Figures 7.10, 7.11 and 7.12 shows the role of θ_x and θ_y on the magnitude and phase differences of the position feedbacks from EP and FP at different locations of the wheel. Noting that the experimental z positional deviation data are used to calculate θ_x and θ_y of Figure 7.11 and 7.12, the differences in the magnitudes of θ_x and θ_y are due to the vertical offset (h) and the horizontal offset (l) between the EP and FP – see equation (7.45).

B. Comparison of Figures 7.10, 7.11 and 7.12 also suggests that the θ_x values accumulated with the wheel rotation have greater values than the θ_y values, and the magnitudes of the z position deviation are mainly contributed by θ_x .

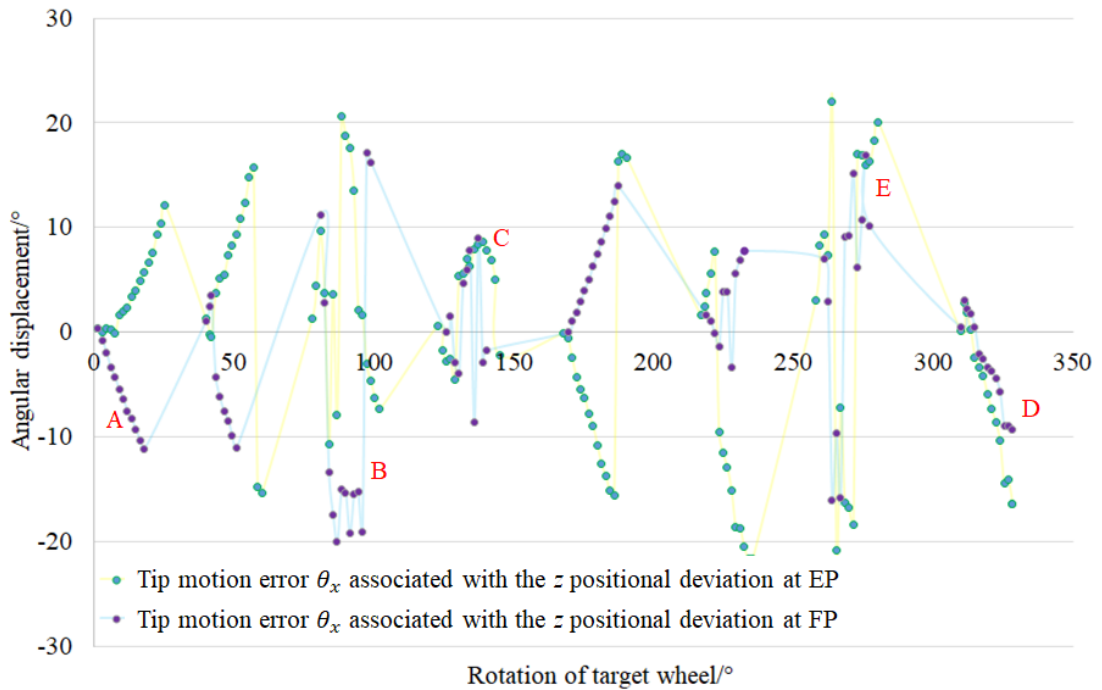


Figure 7.11 Tip motion error (θ_x) of the wheel calculated from the model fitting.

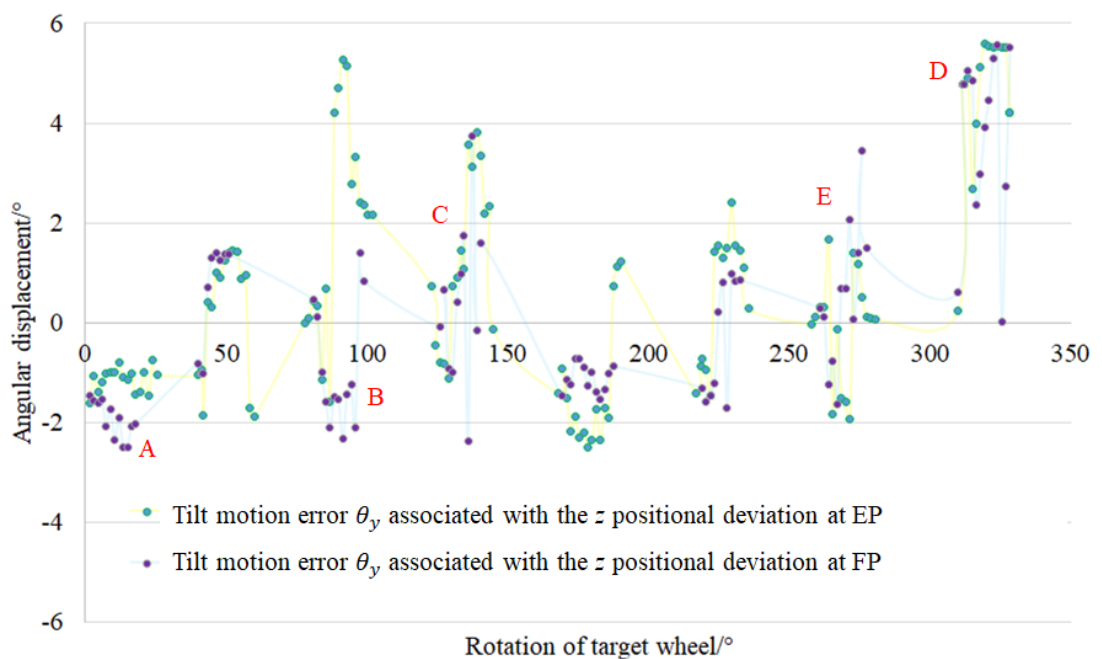


Figure 7.12 Tilt motion error (θ_y) of the wheel calculated from the model fitting.

C. Based on the magnitude and phase difference of the position feedbacks from EP and FP, the behaviour of the open-loop high-repetition rate system (i.e. wheel rotation) can be fundamentally divided in five categories as shown in Table 7.1 (identified by *A*, *B*, *C*, *D* and *E* profiles in Figure 7.10, 7.11 and 7.12). As will be seen later that understanding the behaviours of profile *A* and *D* as ideal non-complaint and complaint cases, respectively, is necessary to explain the behaviours of profile *B*, *C* and *E*.

Table 7.1 Different categories of behaviour of the open-loop high-repetition rate system (i.e. wheel rotation).

Profile	Magnitudes of the feedback from EP and FP	Phases of the feedback from EP and FP	Note
A	Non-complaint	Non-complaint	180° phase difference between EP and FP
B	Non-complaint	Non-complaint	180° phase difference between EP and FP. Note the random and opposite behaviour of θ_x and θ_y for both EP and FP
C	Approximately complaint	Approximately complaint	Approximately no phase difference between EP and FP. Some random behaviour of θ_x and θ_y for both EP and FP
D	Complaint	Complaint	No phase difference between EP and FP
E	Combination of complaint and non-complaint	Combination of complaint and non-complaint	Compliance of the profiles becomes non-compliance with further wheel rotation

D. To understand the nature of the magnitudes and phases of profile A and D for EP (mirror setting), let's consider the following two cases of equation (7.43), which is written for EP:

I. $z_{error\ at\ EP} = E_r \sin(\theta + \alpha) = 0$ when no or minimum positional deviations read at EP
or $\theta = -\alpha$ (7.46)

II. $\sin(\theta + \alpha) = 1$ when maximum position deviation read at EP
or $\theta + \alpha = \frac{\pi}{2}$ (7.47)

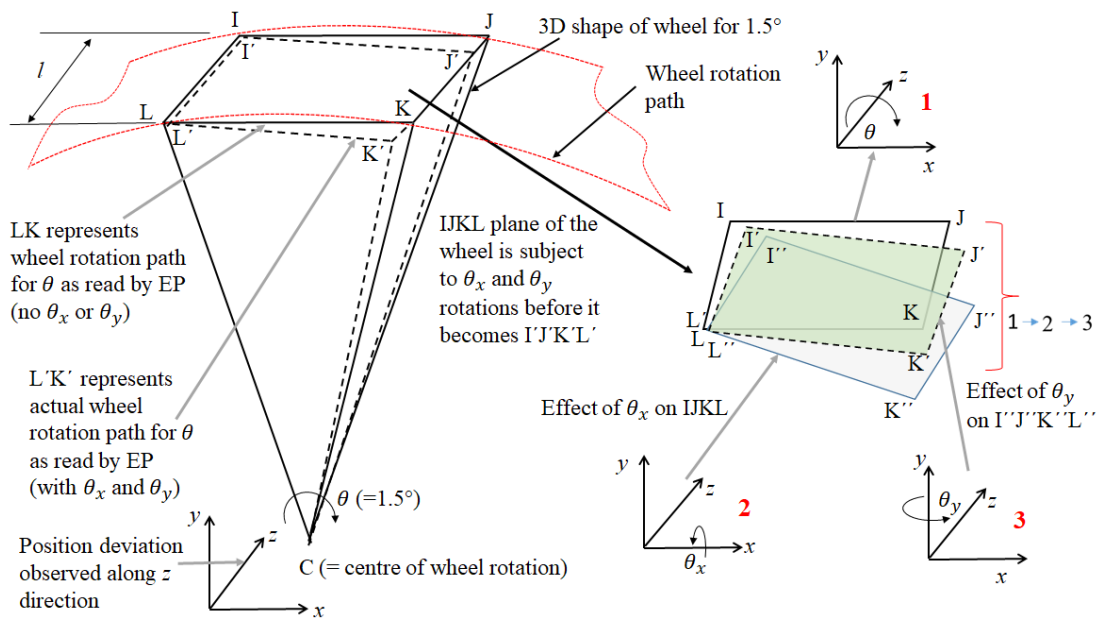


Figure 7.13 Examination of the wheel rotation path for 1.5° when no or minimum positional deviation read by EP.

Now, consider the wheel rotation for only 1.5° , the 3D shape of the wheel for 1.5° , the path of 1.5° as read by the EP and the associated error motions θ_x and θ_y for 1.5° – as shown in Figure 7.13 and 7.14. As can be seen in Figure 7.13 for case I, the wheel rotation path LK read by EP becomes $L'K''$ due to θ_x and finally $L'K'$ due to θ_y . Therefore, $L'K'$ represents the effect of resultant angular error α

($\alpha = \tan^{-1} \frac{\sin \theta_x}{\tan \theta_y}$ as shown in equation (7.41)). $L'K'$ approaches to LK (i.e. equation (7.46)) when θ_x and θ_y are approximately equal in magnitudes, but opposite in directions to cause least positional deviations as read by EP. This behaviour can be observed for small error motions of θ_x and θ_y . Note that the profile D for EP of Figure 7.11 and 7.12 exhibits the characteristics of case I.

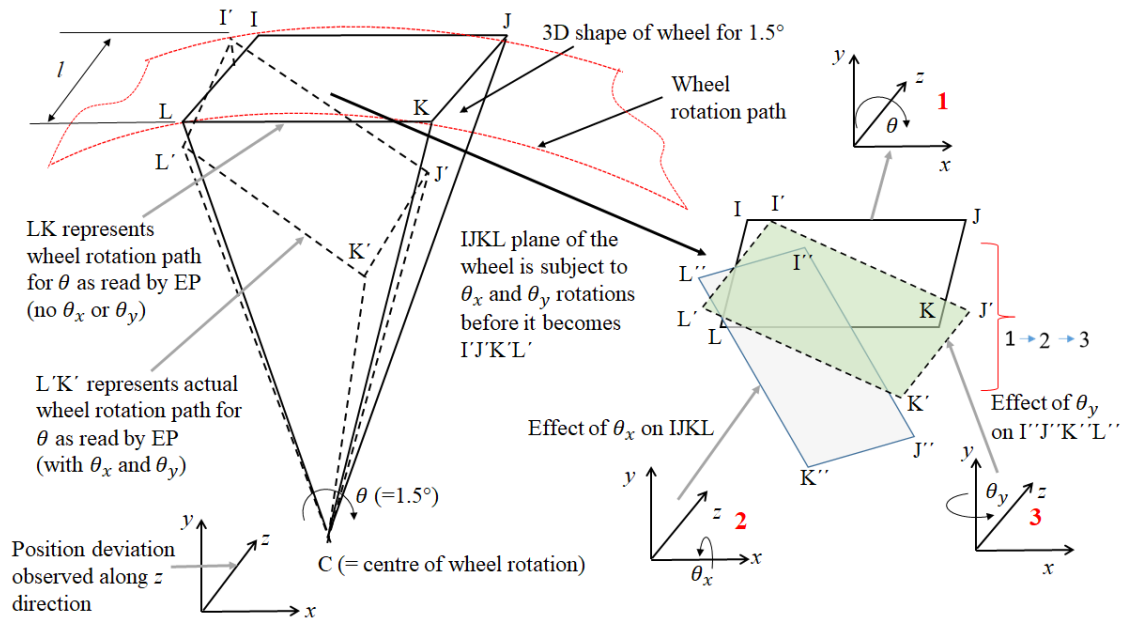


Figure 7.14 Examination of the wheel rotation path for 1.5° when maximum positional deviation read by EP (note LK and $L'K'$ are not shown in perpendicular to each other for the clarity of the figure).

On the other hand, as shown in Figure 7.14 for case II, $L'K'$ will be at maximum angular distance from LK (i.e. equation (7.47)) when the effect of θ_y is minimum (i.e. θ_x is comparatively much larger than θ_y). The characteristics of case II can be found in the profile A for EP in Figure 7.11 and 7.12. Also, note the significant shape difference of the IJKL plane of Figure 7.14 as compared with the plane of Figure 7.13.

E. After examining the behaviour of EP for minimum and maximum positional deviations scenarios, let's examine the condition at which the positional deviation

information from EP and FP should be same (i.e. complaint case). In such case, z_{error} of equation (7.39) is equal to $z_{error at M}$ of equation (7.43). Therefore, from equation (7.39) and (7.43), the following can be written:

$$\sin(\theta + \alpha) = \frac{l(\cos \theta_x \cos \theta_y - 1)}{h \sqrt{((\sin \theta_y)^2 + (\sin \theta_x \cos \theta_y)^2)}} \quad (7.48)$$

$$\text{or } \theta + \alpha = \sin^{-1} \left(\frac{l(\cos \theta_x \cos \theta_y - 1)}{h \sqrt{((\sin \theta_y)^2 + (\sin \theta_x \cos \theta_y)^2)}} \right) \quad (7.49)$$

When, $\cos \theta_x = \frac{1}{\cos \theta_y}$, equation (7.49) becomes equation (7.46) for EP.

However, $\cos \theta_x = \frac{1}{\cos \theta_y}$ is possible if θ_x and θ_y are small in values and approximately equal. In such case, the position deviation information from EP and FP should be complaint (check the profiles D for EP and FP in Figure 7.10, 7.11 and 7.12).

$$\text{Now, when, } \left(\cos \theta_x \cos \theta_y - 1 = \frac{h \sqrt{((\sin \theta_y)^2 + (\sin \theta_x \cos \theta_y)^2)}}{l} \right) \text{ equation}$$

(7.49) becomes equation (7.47) for EP. However, $(\cos \theta_x \cos \theta_y - 1)$ is negative, and equation (7.49) represents 180° phase change with respect to the condition shown in equation (7.47) for EP. In such case, the positional deviation information from EP and FP will show non-compliance in phase due to the term $l(\cos \theta_x \cos \theta_y - 1)$ of equation (7.45) or (7.49), and the magnitude of the positional deviation information from FP will be determined by the equation (7.45). The profiles of A for EP and FP in Figure 7.10, 7.11 and 7.12 show the characteristics of such non-compliance behaviour, indicating comparatively much larger θ_x with respect to θ_y .

Table 7.2 Slopes of the θ_x , θ_y and α profiles as shown in Figure 7.11, 7.12 and 7.15.

Profile type	EP (mirror setting)			FP (target setting)			Note
	θ_x (°)	θ_y (°)	α (°)	θ_x (°)	θ_y (°)	α (°)	
A	1.14	-0.02	0.08	-0.89	0.02	0.09	$ \alpha_{FP} > \alpha_{EP} $
B	-2.21	-0.18	-0.02	8.72	0.72	-0.08	$ \alpha_{FP} > \alpha_{EP} $
E	5.26	0.16	0.13	3.72	0.60	-0.01	$ \alpha_{FP} < \alpha_{EP} $
C	-0.80	-0.15	0.23	-1.65	0.32	0.46	$ \alpha_{FP} > \alpha_{EP} $
D	-1.81	-0.32	0.06	-1.24	-0.09	-0.04	$ \alpha_{FP} < \alpha_{EP} $

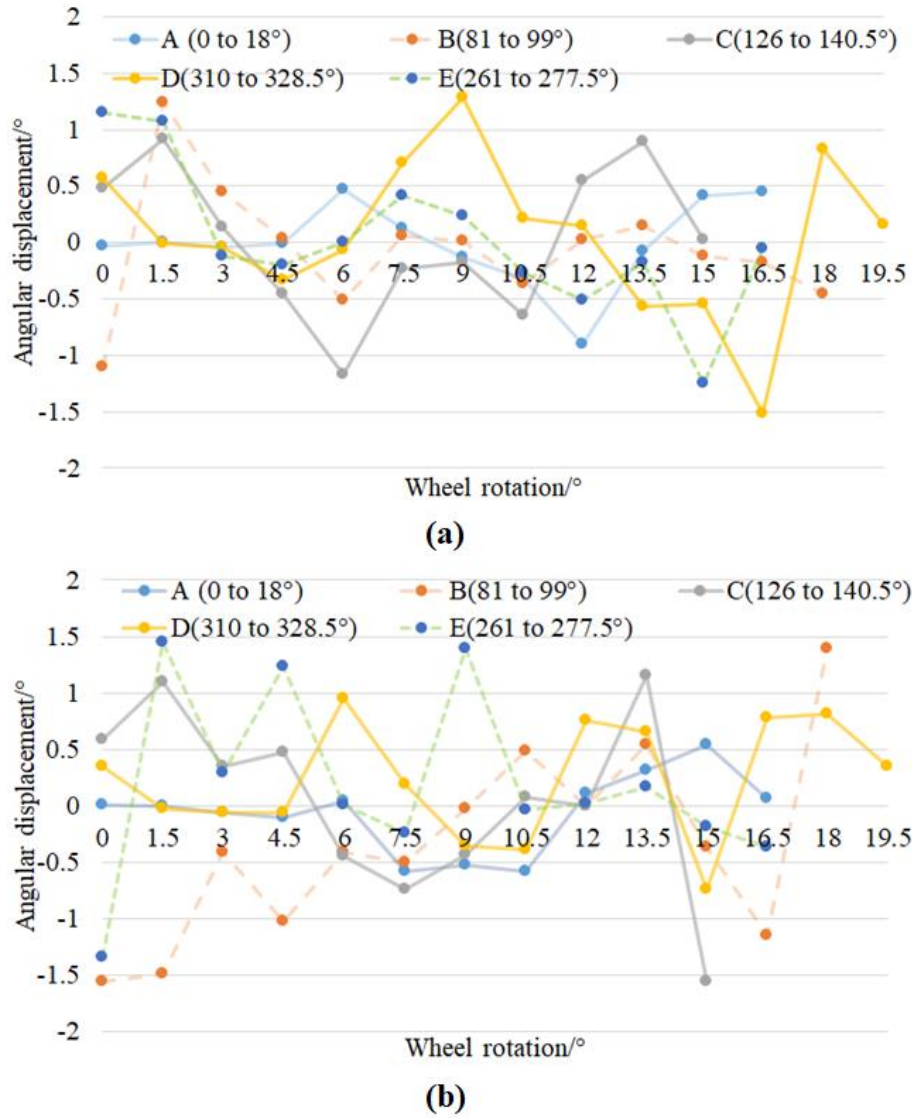


Figure 7.15 Resultant angular error α for some selective locations of the wheel as calculated from the θ_x and θ_y associated with EP (a) and FP (b).

F. Based on the observations of the above points (A to E), the behaviours of all the five categories of complaint and non-complaint feedback information from EP and FP

(Table 7.1) can be explained. For this purpose, the slopes of the θ_x and θ_y profiles for the five categories (Figure 7.11 and 7.12) are taken to calculate the profiles of the resultant angular error α for both EP and FP. The results are shown in Table 7.2 and Figure 7.15. Note the changes in the magnitude and the directions of the slopes for the FP profiles with respect to the EP profiles in Table 7.2, and also the shape difference between any two α profiles for EP and FP in Figure 7.15. In the absence of a horizontal offset l between EP and FP, the shapes of the α profiles are not expected to change; only the α magnitudes will increase or decrease.

G. The examination of the slopes of the θ_x , θ_y and α profiles of five different categories (A to E) presented in Table 7.2 suggests that the compliance between the position feedback from EP and FP depends on two conditions:

1. The ratio between two error motions θ_x and θ_y (i.e. $\frac{\theta_x}{\theta_y}$); and
2. The change of the resultant angular error α associated with FP with respect to α of EP.

Considering these two conditions, profile A and profile D show ideal non-complaint and ideal complaint cases, respectively (see Figure 7.7 and 7.10). This is based on the observation that if $\frac{\theta_x}{\theta_y}$ has a large value, and the resultant angular error α for FP has a higher value than that for EP, the non-compliant behaviour is expected. As such, for profile A in Table 7.2, θ_x related to EP (i.e. 1.14°) is comparatively much larger than θ_y of the same EP (i.e. -0.02°), which makes $\frac{\theta_x}{\theta_y}$ equal to 57. The interaction of θ_x and θ_y with the offset l generates a resultant angular error α (i.e. 0.09°) for the FP, which is higher than that for the EP (i.e. 0.08°). On the other hand, for profile D, θ_x and θ_y have relatively comparable values (-1.81° and -0.32°

respectively) for EP, which makes $\frac{\theta_x}{\theta_y}$ equal to 6. In this case, the resultant angular error α (i.e. 0.04°) for the FP is lower than that for the EP (i.e. 0.06°). The behaviours of *B*, *C* and *E* are the combinations of the behaviours of profile *A* and *D*. For example, although it is seen that $|\alpha_{FP}| > |\alpha_{EP}|$ for profile *C*, the result is a complaint case with some anomaly, since $\frac{\theta_x}{\theta_y}$ has lower value (i.e. 5). In contrast, for profile *E*, although it can be seen that $|\alpha_{FP}| < |\alpha_{EP}|$, $\frac{\theta_x}{\theta_y}$ is higher (i.e. 33). Therefore, in this case, the z positional deviation at EP shows some compliance with the z positional deviation at FP, but eventually the two behaviours become non-complaint (Figure 7.7 and 7.10). For profile *B*, with $|\alpha_{FP}| > |\alpha_{EP}|$, the result is a non-complaint case with significant anomaly, since $\frac{\theta_x}{\theta_y}$ is higher (i.e. 12), but not as high as in the case for *A*. A closer look at the slopes of the α profiles of Figure 7.15 also supports the above observations.

H. In the design of the in-process position measurement system (section 7.3.1), the EP and FP were positioned aligned to avoid the Abbe errors. However, the reference plane of the wheel changes throughout its rotation due to resultant angular error α ($\alpha = \tan^{-1} \frac{\sin \theta_x}{\tan \theta_y}$). The interaction of the error motions (θ_x and θ_y) with the

structural offsets between EP and FP (horizontal offset l and vertical offset h) gives rise to a (1) cosine error in the form of $(l \cos \theta_x \cos \theta_y - l)$ and (2) a sine error in

the form of $\left(\frac{h \sqrt{(\sin \theta_y)^2 + (\sin \theta_x \cos \theta_y)^2}}{\cos \theta} \sin(\theta + \alpha) \right)$ as shown in equation

(7.45). Depending upon the relative values of θ_x and θ_y , these sine and cosine errors cause the target position information from EP either comply or non-comply with the actual target position. In other words, measuring the target position with respect to

EP may provide incorrect and non-representative feedback information about the actual target position, representing uncertainty in determining target position for generating compensations by the closed loop control.

- I. Equations (7.39) and (7.43) suggest that if the resultant angular error α value can be measured directly at both EP and FP, α will be same for both EP and FP. As can be seen in Figure 7.15 and 7.16, the profiles of the resultant angular error α for both EP and FP show similar behaviour. However, as indicated before, the differences in the α values for EP and FP are due to the fact that the experimental z positional deviations were used to calculate θ_x and θ_y values, from which α values were determined. Since the z positional deviation at FP contains the sine and cosine errors (see equation (7.45)), the calculated θ_x and θ_y (and hence the α) for FP will be different from those for the EP.

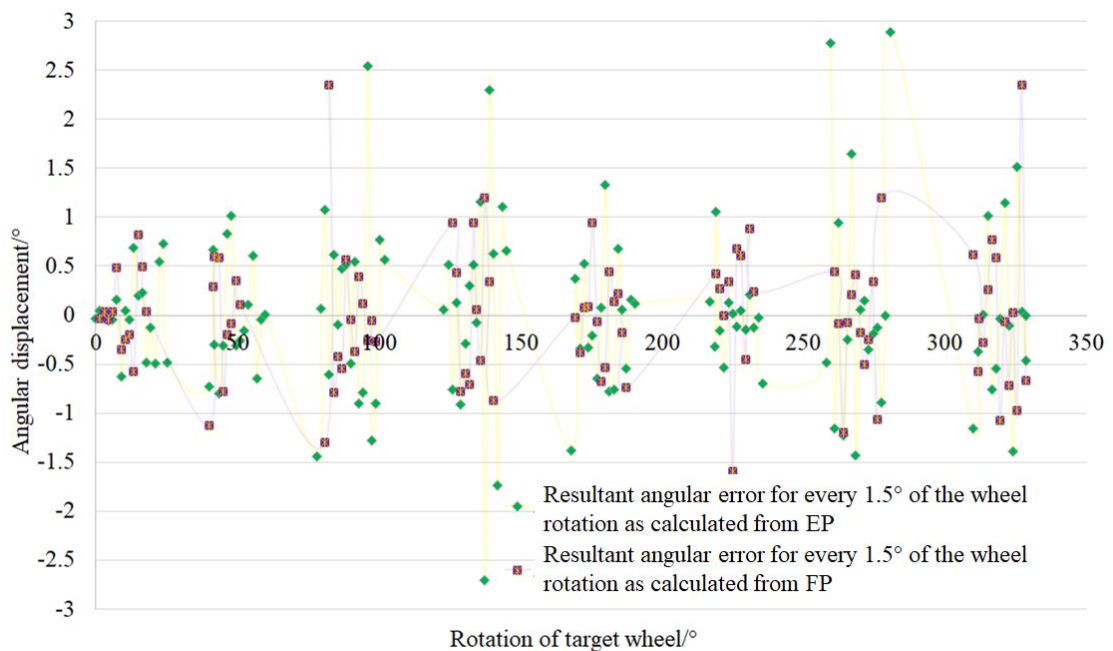


Figure 7.16 Comparison of the resultant angular errors α of the wheel between two settings as calculated from the information in Figure 7.11 and 7.12.

7.8 Improvement of the closed loop control design

The above discussion suggests that, if the angular errors of the wheel (α) with respect to the reference position and orientation of the target are known for each repetition (described in section 7.6.1.1), the angular motions (tip u and/or tilt v about x and y axes, respectively) of the tripod of HAMS can be used to generate the angular compensations for α . For this, direct measurement of the angles at or near the target is required, which is possible with a measurement instrument, such as dual displacement measurement interferometer for both distance and angle [121]. Alternatively, the z positional deviation at EP measured by the plane mirror interferometer can be used in the motion program (see Figure 7.6) to determine the new angular positions of the target, instead of the “calculated z position” of the motion program as shown in Figure 7.6.

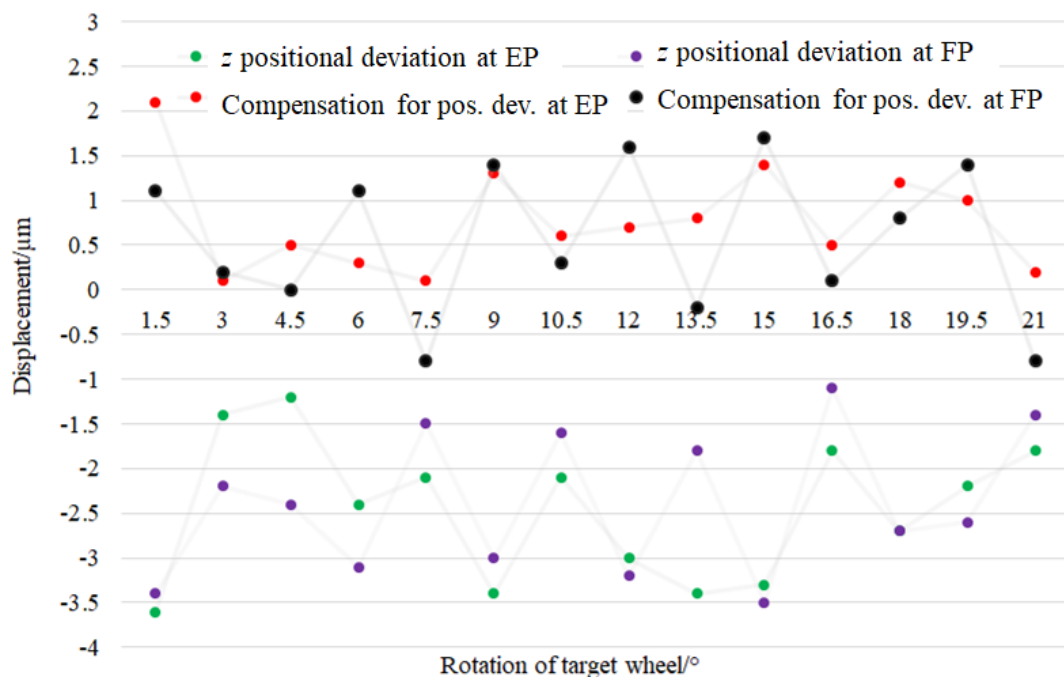


Figure 7.17 Performance of the improved scheme of the closed loop control using angular compensation.

Various angular compensation methods were examined by carrying out the experiments described in section 7.6.1.2 to improve the performance of the closed loop

control. For angular compensation, a simple way to determine the resultant angular error of the wheel (α) was to find an equivalent θ_x angle with the following: position deviation information at EP (mirror position setting) and the distance between the EP to the centre of the wheel (see Figure 7.2 and 7.3a). The principle behind this strategy is due to the dominant contribution of θ_x in α (see Figures 7.11,7.12,7.15 and 7.16). Figure 7.17 shows the outcome of applying one such angular compensation scheme, in which the tripod's tip angular motion (u) was used to generate the angular compensation for the equivalent θ_x values. Since the θ_x , which accumulates over time with the wheel rotation, is now compensated, the positional deviation profile of the new scheme (Figure 7.17) does not show any upward or downward trend as compared with the positional deviation profiles related to the position compensation scheme (Figure 7.8 or 7.9). However, the use of equivalent θ_x leaves some errors in the z positional deviation profiles. The zigzag pattern of the position deviation profile in Figure 7.17 shows the effects of the uncompensated θ_y values. Also, a point to note is that the accuracy of the target position after angular compensation has not improved appreciably as compared with the target positional accuracy achieved by the position compensation scheme (see Figure 7.8 or 7.9). This is because, as is described in Chapter 6 for the calibration of HAMS , the tip or tilt motion of the tripod may cause significant positional deviation of the target if the compensation for these positional deviations are not included in the controller as part of a kinematic calibration process (section 6.5.1.2.1).

To overcome the limitation of the above angular compensation scheme and improve the target positional accuracy, another angular compensation scheme is proposed. This scheme is based on the working principle of the compensation technique by translating the coordinate system from the centroid of tripod to the target point, as developed during the compensation process for HAMS (see section 6.7.3). In this

scheme, instead of using the radius of the wheel y , the distance between the centroid of the tripod and the EP (mirror position setting) is used to calculate an equivalent θ_x , such that the reference coordinate position of EP always remain the same for all the tip motions (u) of the tripod required to generate the θ_x values for the angular compensations. This scheme, in fact, improves the positional accuracy of the target (Figure 7.18), although it needs further development and an area for future research.

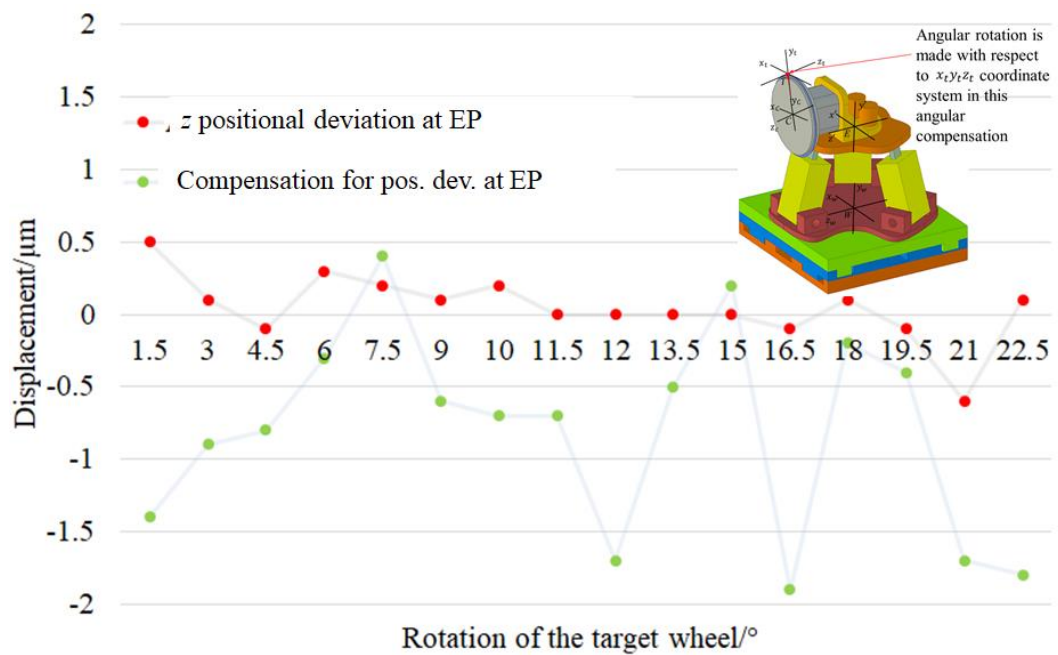


Figure 7.18 Performance of the improved closed loop control using different approach to angular compensation.

The angular compensation technique for the closed loop control can provide the following benefits over the positional compensation technique, when considered for real-time target alignment for the high-repetition rate laser operations.

- A. In angular compensation, true target alignment (both position and orientation of the target), avoiding Abbe errors, is possible since reference position and orientation of the target are maintained throughout the high-repetition rate operation.

- B. The feedback processing time of the controller for each repetition cycle will be faster for the angular compensation schemes than for the position compensation scheme. This is because the accumulation of the positional deviations of the target with the wheel rotation is small for the angular compensation technique.

7.9 Conclusion

For the target positioning system for high-power high-repetition rate laser operation, real-time target position control is required for the accurate repositioning of the target (especially, in the z direction along the laser axis) at the reference target position. A closed loop control, commonly used for actuator control, can fulfil this requirement. However, getting accurate and reliable feedback of the target position for the controller poses a significant challenge. One of the main reasons for this is due to the inclusion of Abbe errors to the target position measurement, since the functional point (target) and the effective point (where the target position is actually measured) are often not same. This chapter presents a closed loop control method for a high-repetition rate target positioning system (a target interface wheel controlled by the motion stages of a hybrid mechanism) based on a target position measurement system designed to avoid Abbe errors. A plane mirror interferometer is used as the sensor, and the target position feedback is used by the controller of the motions stages to generate the compensations for the positional deviation of the target in the z direction. The plane mirror (effective point) is placed at a location on the wheel as close to the target (functional point) as practical, with the smallest possible offsets between the two points. The experimental results of the closed loop control method show that, while the control system is capable of repositioning the targets within $\pm 1 \mu\text{m}$ of the reference target position during the wheel rotation, this is not the case for all the locations of the targets whose positions are to be determined by the corresponding effective points of the plane

mirror. The non-linear position data at different locations of the wheel causes magnitude and phase differences (direction) between the position feedback (i.e. z positional deviation) from the target and the effective point at various locations of the target, resulting in inaccurate position compensations generated by the controller.

To understand the cause of the errors in the position feedback of the control system, a model was developed to find the relationship between the target position feedback (i.e. z positional deviation) and the errors affecting the feedback accuracy. Fitting the experimental data of the z positional deviations (in open-loop control) into the model's equations suggests that two conditions are important to determine the magnitude and phase differences between the feedback from the target and the effective point: (1) the relative magnitudes of the wheel's rotational error motions, which determine the resultant angular error of the wheel, associated with the effective point and (2) the change of the resultant angular error of the target with respect to that of the effective point. To overcome the closed loop feedback problem, a solution is proposed where the controller generates the angular compensations based on the resultant angular errors calculated from the z positional deviation at the effective point (mirror). With this approach, a positional accuracy of $\pm 1 \mu\text{m}$ is achieved, while it is possible to maintain the target's reference plane throughout the wheel rotation and, hence, avoid the Abbe error for the target position measurement.

Chapter 8 - Conclusions and future work

8.1 Overview

In the research presented in this thesis, the capability development of the target alignment (position and orientation) process for high-repetition rate laser operations has been outlined by demonstrating a system of controlling the position and orientation of targets in real-time. The research objectives, as reflected in the research questions stated in Chapter 1, were

- To understand the requirements for fulfilling the positional and orientation accuracies of the targets for the real-time target alignment system.
- To evaluate the capabilities of the motion control system (i.e. HAMS) of the real-time target alignment system to understand the effects of the errors on the positional and orientation deviations of the targets.
- To develop a practical method of improving the performance of the hybrid mechanism of HAMS.
- To identify a method to determine the positional and orientation deviations of the targets due to the errors arising from high-repetition rate operations.
- To develop a method to effectively compensate for the positional and orientation deviations of the targets during high-repetition rate operations.

Through an extensive literature survey and a range of empirical research methods, such as first-hand experience of high-power laser operations at the central laser facility and analysis of technical documents (e.g. manuals, design data), the requirements for the positional and orientation accuracies of the targets for high-repetition rate laser operations were captured. It was identified that fundamentally, three elements – an in-process sensor, a control system and a mechanism with its actuators – were required for an effective and real-time position and orientation control system for targets for high-

repetition rate laser operations. To evaluate the performance of the hybrid mechanism of HAMS, a kinematic analysis of the mechanism was carried out, followed by the development of an error model of HAMS. To improve the positional and orientation accuracies of the hybrid mechanism of HAMS, a practical and cost-effective procedure of the kinematic calibration was developed by using a minimum set of error data as determined by the error model and measuring the linear and angular error motions of HAMS with the help of a retro-reflector interferometer.

To estimate the positional deviations of targets that may arise during a high-repetition rate process, an analytical model was developed, followed by the characterisation of the high-repetition rate process through the displacement measurements using a plane mirror interferometer. Then, real-time target alignment system was designed, tested and implemented based on a closed loop control system in which interferometer was used as the in-process measurement system for targets' positions.

8.2 Conclusions

8.2.1 Requirements for the target alignment for high-repetition rate laser operation

The research described in this thesis shows that although the primary function of HAMS is to provide the necessary motions (translational and rotational) to the targets for an alignment process -irrespective of high-repetition rate or current semi-automated laser operation, HAMS' motions must compensate for the errors that cause positional and orientation deviation of the targets with respect to the reference position set for the high-repetition rate operation. This is because, as shown in Figure 8.1, errors generate at different processes of the high-repetition rate operation and flow through the

processes to the process of initial target alignment where the target sectors are mounted on the target interface wheel for the laser operation. Some static errors, e.g. misalignment of target sectors with the target wheel due to fixturing problem and misalignment of the target wheel with respect to laser beam axis, can be rectified during the initial alignment process, which is actually required for both high-repetition or current semi-automated laser operation. However, during a high-repetition rate operation (i.e. when target wheel rotates to deliver the fresh targets to the laser focus in an automated way), many of these static errors become kinematic errors with the motions of HAMS (e.g. tip, tilt and rotation of target wheel), causing positional and orientation deviations at the target. The mechanism of the positional and orientation deviations of target stemmed from the kinematic errors of HAMS and target wheel have been discussed in the thesis (Chapter 5, 6 and 7).

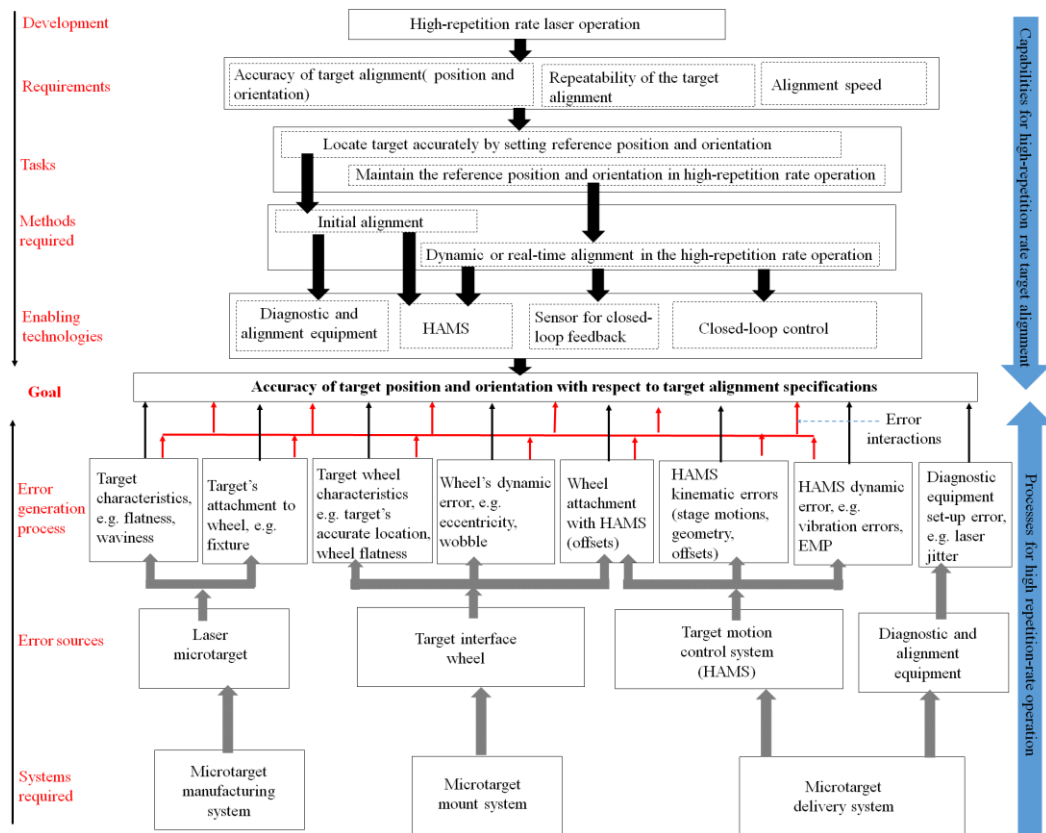


Figure 8.1 Conceptual flow-diagram of the target alignment process and other processes for the high-repetition rate laser operations.

The outcomes of the research, as shown in Figure 8.1, suggest that to qualify for high-repetition rate operation, a target alignment process must have the characteristics of a dynamic or real-time target alignment process to reduce the effects of the kinematic errors, which have not been compensated during calibration or initial alignment process, and any other non-repeatable errors arising from sources, e.g. vibrations, temperature change. Thus, in a high-repetition rate operation, while the initial alignment process will find the reference position and orientation of the target, the real-time alignment, requiring three components (a closed loop control system, a sensor for the feedback to the closed loop control and HAMS for the motion control), will maintain the reference position and alignment throughout the high-repetition rate operation.

It has been shown in the thesis that HAMS, like any other precision mechanism, has its own sources of error, predominantly kinematic errors arising from geometric errors (e.g. joint errors, link errors, assembly errors). Since HAMS is used as a high-accuracy motion control system for the alignment process (in fact, for both initial and real-time alignment processes), HAMS performance, in terms of positional accuracy, needs to be known and improved, if required. For this reason, in this research, the performance improvement of HAMS was performed at first through the development of an error model (Chapter 5) and a kinematic calibration and compensation procedure (Chapter 6). The HAMS with an improved performance and the knowledge and understanding achieved through the performance improvement process were used for the development of a real-time target alignment control for the high-repetition rate laser operation, as outlined in Chapter 7.

8.2.2 Error model for HAMS

Since the performance of HAMS in terms of positional accuracy is affected by the kinematic errors (errors arising from dynamic influences, e.g. vibration, are not

considered in this study), which are the main sources of error, an error model serves the following purposes for this research:

1. Identify the error sources of HAMS and show the mechanism of the generation of the positional error in HAMS,
2. Find the positional deviation equations for target to include the effects of the kinematic errors of HAM.

Strategies applied to this research for developing an error model for HAMS are such that the error model plays a key role for the performance improvement of HAMS through the calibration and compensation procedure (Chapter 6).

An error model for a complex spatial kinematic structure with closed loops, e.g. the RPS mechanism of HAMS, can become complicated to develop, mainly due to the presence of many error sources, and, hence, the requirement for many error parameters to define the mechanism kinematically. From the error analysis of the RPS (tripod) mechanism of HAMS, it is found that at least 36 (12×3) individual error parameters may be required to completely define the moving platform of the tripod with respect to the fixed platform of the tripod. However, it has been shown that with careful analysis of the constraint equations associated with the legs and the complete RPS mechanism, the error parameters can be reduced to only three parameters, which can kinematically represent the effects of the errors stemmed from the various sources of the mechanism (Chapter 5).

Based on the results of the error analysis of HAMS, an effective, but simple, error model was developed for HAMS following the two strategies below:

1. Key kinematic points of HAMS, named as the “reaction points”, are established and the error motions (named as “generalised error parameters”) associated with

the rotational motions (tip or tilt) of HAMS are considered with reference to the reaction points.

2. With the introduction of generalised error parameters and reaction points, individual mechanisms of HAMS are considered as serially connected - like the case of a serial mechanism.

8.2.3 Performance improvement of HAMS

Developing a calibration method for a parallel or hybrid mechanism is a complex problem mainly due to 1. the number of error parameters required for an error model to define the mechanism kinematically, 2. requirements of many sets of experiment to represent the poses of a spatial mechanism with closed loops, 3. requirements of a computationally demanding method to identify the large number of error parameters, and 4. difficulty to find an effective method to implement the calibration results in the mechanism's control software.

A simple and time- and cost-effective four-step calibration method was developed in this research, so that HAMS users can apply the calibration in a regular interval to evaluate the performance of HAMS and apply software-based compensations for the positional deviations of target. The strategies applied to the calibration method were aimed to take the advantages of: 1. the unique feature of a hybrid mechanism (i.e. positional deviations arising from the tip or tilt motion of HAMS can be compensated by the independently controlled xz stages), 2. the use of an error model with only three error parameters, 3. experimental determination of the error parameters, 4. partial-pose measurements of HAMS to determine the positional deviations of target, and 4. the use of error model to predict the positional deviations of target and generate software-based compensations for the positional deviations of target.

Unlike a calibration method used for a serial or a parallel mechanism, both a forward and an inverse kinematics experiments were used in the calibration process of HAMS, and the comparison of the two experiments suggest that:

1. The model's prediction of the positional deviation of the target is valid,
2. Controller's automatic generation of compensation for position deviations are incorrect or inadequate,
3. For small angles, tip or tilt rotation of HAMS has a linear relationship with the associated error motions of the tripod or the rotating platform of HAMS.

Based on the findings, the stated linear relationship was used in the motion control software to actuate the linear xz stages to generate compensatory motion for the positional deviations of the target during the tip rotation of HAMS.

The performance evaluation of HAMS after the calibration and compensation process shows that the positional accuracies of HAMS have improved significantly for the tip rotations of the tripod of HAMS – 97% accuracy improvement in the z direction and 85% improvement in the x direction. Not only that, the calibration process clearly demonstrates the effect of the following key error sources on the positional deviations of the target during the tip and tilt rotations of the target:

1. The tip or tilt motion,
2. The structural offsets – the Abbe offsets – between the functional point (i.e. the centroids of the moving platform of tripod and the rotating platform, where the centroids act as the centre of rotations of HAMS for the tip and tilt motions) and the effective point (i.e. target),
3. Translational motions at the centroids of the moving and rotating platforms,
4. The rotational error motions at the centroids of the moving and rotating platforms.

Of the four types of error source, the interactions between the tip or tilt motion with the Abbe offsets of HAMS contribute the most to the positional deviations at target. The second largest contributing source can be the rotational error motion at the centroid, since they also can interact with the Abbe offsets during the tip or tilt motion and cause positional deviation at the target.

The results of the calibration process also show the importance of carrying out kinematic calibration and compensation process for HAMS on a regular basis. One such important factor is that the structural offsets of HAMS can change due to operating condition, for example, change of load condition of HAMS, change of temperature, and a calibration process is required to keep track of the change and take necessary actions.

8.2.4 Real-time target alignment

A real-time position control solution was developed for the targets to maintain the reference position and orientation throughout the high-repetition rate laser operations (Chapter 7). The design of the control system was based on an Abbe-compliant, in-process position measurement system of targets, employing a plane mirror interferometer and HAMS as the motion control system. An error model was developed to characterise the position feedback information of the target in a high-repetition rate process to determine the effects of the non-collocation of the interferometer's measurement point (effective point) and target (functional point) on the control system's performance - a challenge for the real-time position control of targets. The behaviour of the control system was investigated with the error model and experimental data.

The experimental results of the closed loop control method show that, while the control system is capable of repositioning the targets within $\pm 1 \mu\text{m}$ of the reference target position during the wheel rotation, this is not the case for all the locations of the targets whose positions are to be determined by the corresponding effective points of the

plane mirror. The non-linear position data at different locations of the wheel causes magnitude and phase differences (direction) between the position feedback (i.e. z positional deviation) from the target and the effective point at various locations of the target, resulting in inaccurate position compensations generated by the controller. The closed loop experiment also shows that target's reference plane (orientation) will not be maintained with the position compensations generated by the controller.

Fitting the experimental data of the z positional deviations (in open-loop control) into the model's equations suggests that two conditions are important to determine the magnitude and phase differences between the feedback from the target and the effective point: (1) the relative magnitudes of the wheel's rotational error motions, which determine the resultant angular error of the wheel, associated with the effective point and (2) the change of the resultant angular error of the target with respect to that of the effective point. To overcome the closed loop feedback problem, a solution is proposed where the controller generates the angular compensations based on the resultant angular errors calculated from the z positional deviation at the effective point (mirror). With this approach, a positional accuracy of $\pm 1 \mu\text{m}$ can be achieved, while it is possible to maintain the target's reference plane throughout the wheel rotation and, hence, avoid the Abbe error for the target position measurement.

8.3 Future work

The scope of the work presented in this thesis identifies a number of areas for future work, which can be broadly categorised as two types: research areas involving the high-repetition rate laser operation and research areas involving the enabling technologies used in the real-time target alignment system. While the first type of research areas are related to the requirements for the further development of the high-repetition rate laser operation, the second type of research areas are more specific to the

methods, tools, techniques and technologies related to the development of a real-time target alignment system.

8.3.1 High-repetition rate laser operation

The research presented in this thesis demonstrates a model of the real-time target alignment system by outlining the requirements, tasks, methods and technologies for the target alignment for high-repetition rate laser operations, as shown in Figure 8.1. Although technologies like HAMS, interferometer (position feedback sensor) and a closed loop control using HAMS' controller (Delta-Tau's Turbo PMAC) have been used in this research, the infrastructure shown in Figure 8.1 is believed to be generic for developing a target alignment solution for the high-repetition rate laser operation of a high-power laser facility. The research also demonstrates the importance of a real-time target alignment process by highlighting the fact that the errors generated in the upstream process of a high-repetition rate process (e.g. target manufacture, target mount, target delivery) and the non-repeatable errors arising from sources, e.g. vibration, temperature variation, all affect the final process (i.e. target alignment) of the high-repetition rate operation.

The experimental works to demonstrate the model of the real-time target alignment presented in this research were carried out in a controlled metrology laboratory environment at the University of Nottingham. However, in a real-world high-repetition rate laser operation, several influencing factors can affect the performance of the elements of the real-time alignment control system (i.e. the sensor, the HAMS and the closed loop control), eventually affecting the accuracy of the target. The effect of such dynamic factors, e.g. vibration from any other motors of the laser chamber, change in temperature of the laser chamber, shock from EMP during laser-target interaction, have not been considered for the error model or the experiments carried out in laboratory

condition. Therefore, the model of the real-time target alignment needs to be verified using high-power laser at the CLF.

The experiments of the real-time target alignment were carried out at low speed (0.5 Hz). Some promising results were achieved running the system at higher speed (1 Hz). However, further research is required to confirm if the required $\pm 4 \mu\text{m}$ accuracy in the z direction can be consistently maintained. Furthermore, the research mostly focused on the accuracy improvement in the z direction along the laser axis, which is considered as the most sensitive direction. However, accuracy of the target position in the x and y directions are also important to make sure the laser beam does not miss the target during laser-target interaction (tolerance in the x and z directions is $\pm 10 \mu\text{m}$).

As has been shown in Chapter 6 while describing the calibration results that the built-in structure added to the base RPS mechanism of HAMS is a considerable source of error. The offsets between the target and the centroids of the moving and rotating platform generate a significant amount of positional deviations at the target if compensations are not applied. This design of HAMS with a large Abbe offsets in the y and z directions is not actually a good design for a precision machine. Design change of HAMS was not the focus of this research; however, the research clearly shows that a careful re-design of HAMS will remove a large source of error to reduce the positional deviation of the target.

8.3.2 Error model and the calibration process for parallel and hybrid mechanisms

The ideas of “generalised error parameters” and “reaction points” stemmed from the error analysis have been used in the error model of HAMS to simplify the development of an error model for a complex spatial kinematic mechanism with closed loops (i.e. RPS mechanism of HAMS). In the error analysis of the RPS mechanism,

instead of the individual error sources, the followings have been considered to find the reaction points, which are kinematically equivalent and representative to the error sources of the mechanism: 1. the constraint equations of the elements (e.g. joint, link) and the complete mechanism and 2. the possible effects (in terms of translational or rotational motions) of the interaction of the errors with the elements of the mechanism (see section 5.3.1). Since the calibration results validate the prediction of the model with its kinematically simplified form, it is reasonable to believe that this method of simplifying the error model may work for other mechanisms that have parallel kinematic structure, for example 4-DOF four RPUR chains, 5-DOF three PRRRR chains (see section 3.1.2.1). As such, the applicability of the ideas of generalised error parameters and the reaction points for the error analysis of other parallel and hybrid mechanisms can be an interesting area for potential future research.

The kinematic calibration, as described in Chapter 6 as a performance improvement technique for the parallel mechanism of HAMS, was developed based on partial-pose measurements, representing limited range of tip motions of the tripod. For a more robust calibration procedure, measurement scheme covering a wider range of tip motions is required. Calibration is also required for the tilt motion of the rotating platform of HAMS. Furthermore, the strategies used in this research to develop a practical and cost-effective kinematic calibration and compensation method for the hybrid mechanism of HAMS can be extended to other parallel and hybrid mechanisms to verify the applicability of the strategies.

8.3.3 Real-time alignment control for target

Although the development of an effective closed loop control solution discussed in this thesis is for real-time target alignment for high-repetition rate laser operation, some findings appear to be generally valid for wider precision applications, especially

for design considerations of a high-accuracy positioning or measurement system. For example,

1. To predict the position measurement uncertainty of the end-effector of a positioning system, e.g. a motion stage, which may have been designed to avoid the Abbe errors but is subject to a periodic motion, e.g. sinusoidal straightness error of guideways, and its associated rotational error motions (θ_x and θ_y). A high-accuracy positioning system requiring real-time position compensation for the end-effector may become ineffective due to the stated uncertainty of the position measurement of the end-effector.
2. To predict the positional deviation of the end-effector of a high-repetition rate positioning system if the error motions and the structural parameters (see the model equations (7.39), (7.43), (7.45) and so on) are known.
3. Based on the positional deviation equations of the model, to construct a position compensation table which can be included in the controller of the positioning system to carry out pre-calibrated error compensation for the end-effector.
4. To develop a real-time position control of the end-effector based on angular compensation technique to avoid Abbe error and maintain the reference position and orientation of the end-effector of a positioning system.

The future work in the area of developing a closed loop system for real-time target alignment involves further improvement of the angular compensation techniques to increase the target position accuracy. The behaviour of the closed loop system can also be examined at higher repetition rate operations (>0.5 Hz). Case-studies will need to be carried out to evaluate the applicability of the following research findings for such precision applications that require high positional accuracy of target or end-effector: 1. Abbe complaint design principles for the real-time end-effector control system, 2. the

error model to characterise a system that is subject to a periodic motion and its associated error motions and 3. the proposed two conditions that determine the uncertainty in target position measurement due to non-collocation of the effective point and the functional point.

References

- [1] McKenna P, Quinn MN. Energetic electron generation and transport in intense laser-solid interactions. In: Mckenna P, Neely D, Bingham R, Jaroszynski DA, (ed.). Laser-plasma interactions and applications. Springer: 2013.
- [2] Danson C, Hillier D, Hopps N. Petawatt class lasers worldwide. In: Lin Z, Danson C, (ed.). High-power laser science and engineering. Chinese laser press Cambridge University Press: 2015.
- [3] Spindloe C, Tolley MK, Hiscock P, Beardsley M, Spencer JJ. An update of target fabrication techniques for the mass production of advanced fast ignition cone targets. *Fusion Sc. Technol.* 2011;59(1):221-226
- [4] Booth N, Clarke R, Heathcote R, Neely D, Pattathil R, Rusby D, Spindloe C, Symes D, Tolley MK, Tomlinson S. High-rep rate target development for ultra-intense interaction science at the central laser facility. *Proc SPIE* 2014;9211:1-8.
- [5] Tolley M, Spindloe C. Microtargetry for high-power lasers in laser-plasma interactions. In: Mckenna P, Neely D, Bingham R, Jaroszynski DA, (ed.). Laser-plasma interactions and applications. Springer: 2013.
- [6] Symes DR, Booth N, Baraclough M, Indorf G, Oliver P, Scott GG, Neely D, Spindloe C, Heathcote RI, Clarke RJP, Foster S, Gregory CD, Rajeev PP. Progress on positioning of solid targets for Gemini. *Central Laser Facility Annual Report* 2014;15.
- [7] Gao Y, Bin J, Haffa D, Kreuzer C, Hatmann J, Speicher M, Lin, OM Tobias, Hilz P, RF Thomas, Lindner FH, Ostermayr TM, Hilz P, Rosch TF, Lehrack S, Englbrecht F, Seuferling S, Gilljohann M, Ding H, Ma W, Parodi K, Schreiber J. An automated 0.5 Hz nano-foil target positioning system for intense laser plasma experiments. *High-Power Laser Sc. And Eng.* 2017;5(12)
- [8] Karim S, Piano S, Leach RK, Tolley M. Error modelling and validation of a high-precision five degree of freedom hybrid mechanism for high-power high-repetition rate laser system. *Prec. Eng.*, 2018;54:182-197.
- [9] Karim S, Piano S, Leach RK, Branson D, Tolley M. Calibration and adjustment of high-precision five degree of-freedom hybrid mechanism. *Proc. ASPE.* 2018.
- [10] Ruijl T. Ultra precision coordinate measuring machine-design, calibration and error compensation. PhD thesis Delft University, 2001.
- [11] Bosmans N, Qian J, Reynaerts D. Design and experimental validation of an ultra-precision Abbe-compliant linear encoder-based position measurement system. *Prec. Eng.* 2017.
- [12] Schmitt, R, Mallmann, G, Winands, K, Pothen, M. Inline process metrology system for the control of laser surface structuring processes. *Physics Procedia* 2012, 39, 814–822.
- [13] Schmitt, R, Mallmann, G, Winands, K, Pothen, M. Automated process

initialization of laser surface structuring processes by inline process metrology. *Physics Procedia* 2013;41:887–895.

- [14] Ramesh R, Mannan M, Poo AN. Error compensation in machine tools — a review. *Int. J. Mach. Tool. Manufac.* 2000;40:1257-1284.
- [15] Schwenke, H, Knapp, W, Haitjema, H, Weckenmann, A, Schmitt, R, Delbressine, F. Geometric error measurement and compensation of machines—An update. *Ann. CIRP* 2008;57:660–675.
- [16] Sartori S, Zhang GX. Geometric Error Measurement and Compensation of Machines. *Annals of the CIRP* 1995;44(2):599–609.
- [17] Yang, S, Zhang, G. A review of interferometry for geometric measurement. *Meas. Sci. Tech.* 2018;29; 102001
- [18] Colledani, M, Tolio, T, Fischer, A, Lung, B, Lanza, G, Schmitt, R, Vancza, J. Design and management of manufacturing systems for production quality. *CIRP Annals. Man. Tech.* 2014;63:773–796.
- [19] Syam WP, Rybalcenko K, Gaio A, Crabtree J, Leach RK. Methodology for the development of in-line surface measuring instruments with a case study for additive surface finishing. *Opt. Lasers Eng.*, 2019;121:271-288.
- [20] Legnani G, Tosi D, Adamini R, Fassi I. Calibration of parallel kinematic machines: theory and applications. In: Low KH, (ed.). *Industrial robotics: programming, simulation and applications. Advanced Robotic Systems International: 2007.*
- [21] Fassi I, Legnani G, Tosi D, Omodei A. Calibration of serial manipulators: theory and applications. In: Low KH, (ed.). *Industrial robotics: programming, simulation and applications. Advanced Robotic Systems International: 2007.*
- [22] Ren, XD, Feng, ZR, Su, CP. A new calibration method for parallel kinematics machine tools using orientation constraint. *Intl. J. of Mach. Tool and Manu.* 2009;49(9):708-721.
- [23] Huang, P, Wang, J, Wang L, Yao, R. Kinematical calibration of a hybrid machine tool with Regularization method. *Intl. J. of Mach. Tools and Manu.* 2011;51(3):210-220.
- [24] Wu, Y, Fu, Z, Xu, JN, Yan, WX, Liu, WH, Zhao, YZ. Kinematic calibration of 5-DOF hybrid parallel robot. In: Liu H, Kubota N, Zhu X, Dillmann R, Zhou D, (ed.). *Intelligent Robotics and Applications. ICIRA: 2015.*
- [25] Nategh, MJ, Agheli, MM. A total solution to kinematic calibration of hexapod machine tools with a minimum number of measurement configurations and superior accuracies. *Intl. J. of Mach. Tools and Manu.* 2009;49:1155-1164.
- [26] Zhaung, H, Wang, K, Roth, ZS. Optimal selection of measurement configurations for robot calibration using simulated annealing. *ICRA1994;* 393–398.
- [27] Song, Y, Zhang J, Lian, B, Sun, T. Kinematic calibration of a 5-DOF parallel kinematic machine. *Prec. Eng.* 2016;45:242-261.

- [28] Verner, M, Xi, F, Mechefske, C. Optimal Calibration of Parallel Kinematic Machines. *ASME. J. Mech. Des.* 2005;127(1):62–69.
- [29] Ziegert, JC, Jokiel, B, Huang CC. Calibration and Self-Calibration of Hexapod Machine Tools. In: Boër, CR, Molinari-Tosatti, L, Smith KS, (ed.). *Parallel Kinematic Machines. Advanced Manufacturing.* Springer: 1999.
- [30] Wang, J, Masory, O. On the Accuracy of a Stewart Platform— Part I the Effect of Manufacturing Tolerances. *Proc. IEEE Int. Conf. Robot.* 1993;1:114-120
- [31] Wang, H, Fan, K. Identification of strut and assembly errors of a 3-PRS serial-parallel machine tool. *Intl. J. of Mach. Tools and Manu.* 2004;44:1171-1178.
- [32] Science and Technology Facilities Council. Central Laser Facility. Project specification and proposal wafer target positioner. Central Laser Facility 2013 (restricted).
- [33] Spindloe C, Arthur G, Hall F, Tomlinson S, Potter R, Kar S, Green J, Higgingsbotham A, Booth N, Tolley MK. High volume fabrication of laser targets using MEMS techniques. *J. Phys. Conf. Ser.* 2016;713:012002.
- [34] Andreev AA. *Generation and Application of Ultra-high Laser Fields.* NOVA Science Publishers Inc.: 2001.
- [35] Science and Technology Facilities Council. Central Laser Facility: Making light work. Available from: https://www.clf.stfc.ac.uk/Pages/Lasers_Brochure_2016.PDF [Accessed 20th November 2016]
- [36] Pfalzner S. *An Introduction to Inertial Confinement Fusion.* Taylor and Francis: 2006.
- [37] The European High-Power laser Energy Research facility. HiPER:Laser energy for the future. Available from: <http://www.hiper-laser.org/20fusion.html> [Accessed 20th August 2016]
- [38] The European High-Power laser Energy Research facility. HiPER Preparatory Phase Final Report. Available from: http://www.hiper-laser.org/Resources/HiPER_Preparatory_Phase_Completion_Report.pdf [Accessed 20th August 2016]
- [39] Massachusetts Institute of Technology. On the right path to fusion energy. Available from: <http://news.mit.edu/2018/nas-report-right-path-fusion-energy-1221> [Accessed 20th February 2020]
- [40] Science and Technology Facilities Council. Central Laser Facility Annual Report 2009-2010. www.clf.stfc.ac.uk/clf/resources/PDF/ar09-10_lsd_full_target_fab.pdf. [Accessed 13th July 2015]
- [41] Science and Technology Facilities Council. Central Laser Facility Annual Report 2013-2014. www.clf.stfc.ac.uk/CLF/resources/PDF/Monday_all.pdf [Accessed 13th July 2015]
- [42] Booth N, Clarke R, Heathcote R, Neely D, Pattathil R, Rusby D, Spindloe C, Symes D, Tolley MK, Tomlinson S. High-rep rate target development for ultra-

- intense interaction science at the central laser facility. Proc SPIE 2014;9211:1-8.
- [43] Spindloe C, Tolley MK, Divall E, Schaumann G, Nazarov W. High Repetition Rate Microtarget Delivery to the Astra Gemini Laser. CLF Central Laser Facility Annual Report 2009.
- [44] Carroll D C, McKenna P, Foster P, Symes D, Pattathil R, Neely D, Kar S, Borghesi. An imaging system for accurate target positioning for fast focusing geometries. Central Laser Facility Annual Report 2011-12.
- [45] Anderson T, Booth N, Foster P, Symes D. The design and characterization of an improved target positioning system. Central Laser Facility Annual Report 2013-14.
- [46] Miller J. Metrology. In: Leach RK, Smith ST, (ed.). Basics of precision engineering. CRC Press: 2018.
- [47] Schwenke H, Knapp W, Haitjema H, Weckenmann A, Schmitt R, Delbressine F. Geometric error measurement and compensation of machines—an update. Ann. CIRP 2008;57(2):660-675.
- [48] Dornfeld DA, Lee DE. Precision manufacturing. Springer-Verlag: 2008.
- [49] Youssef HA, El-Hofy H. Machining technology: Machine tools and operations. Taylor and Francis: 2008.
- [50] Wada R. Ultra-precision Machine and Elements. Proc. 1st IMEC 2008, JMTBA:36-60.
- [51] Donaldson RR. Error Budgets. Tech. of Mach. Tools 1980;5:1–14.
- [52] Slocum AH. Precision machine design. Prentice-Hall: 1992.
- [53] Smith ST, Chetwynd DG. Foundations of ultra-precision mechanism design. Gordon & Breach Science Publishers: 1992
- [54] Torralba M, Yagiie-Fabra JA, Albajez JA, Aguilar JJ. Design optimisation for the measurement accuracy improvement of a large range nanopositioning stage. Sensors 2016;16:84.
- [55] Weekers WG. Compensation for Dynamic Errors of Coordinate Measuring Machines, PhD Thesis Eindhoven University of Technology, 2016.
- [56] Schellekens P, Rosielle N, Vermeulen H, Vermeulen M, Wetzels S, Pril W. Design for Precision, Current Status and Trends. Annals of the CIRP 1993;1;47: 557–586
- [57] Sartori S, Zhang GX. Geometric error measurement and compensation of machines. Ann. CIRP 1995;44:599–609.
- [58] Wang C. Current Issues in Error Modeling -3D volumetric Positioning errors. In: Mekid S (ed.). Introduction to Precision Machine Design and Error Assessment. CRC Press: 2008.

- [59] Bryan, JB. The Abbe principle revisited: An updated interpretation. *Precis. Eng.* 1979;1:129–132.
- [60] Evans, C. 1989. *Precision engineering: An evolutionary view*. Bedford, UK: Cranfield Press: 1989.
- [61] Leach, RK. Abbe error/offset. In: Laperrière, L, Reinhart, G (ed.). *CIRP Encyclopedia of Production Engineering*. Berlin: Springer: 2015.
- [62] Buice E. Alignment and assembly principles. In: Leach RK, Smith ST, (ed.). *Basics of precision engineering*. CRC Press: 2018.
- [63] Niku, SB. *Introduction to robotics: Analysis, control, applications*. John Wiley and Sons: 2010.
- [64] Vinogradov, O. *Fundamentals of kinematics and dynamics of machines and mechanisms*. CRC Press: 2000.
- [65] Zhang, D. *Parallel robotic machine tools*. Springer Science and Business Media: 2009.
- [66] Liu, XJ, Wang, J. *Parallel kinematics*. Springer-Verlag: 2014.
- [67] Karim S. Kinematic design. In: Leach RK, Smith ST, (ed.). *Basics of precision engineering*. CRC Press: 2018.
- [68] Eckhardt, HD. *Kinematic design of machines and mechanisms*. New York: McGraw-Hill: 1998.
- [69] Allen, JM, Axinte, DA, Pringle, T. Theoretical analysis of a special purpose miniature machine tool with parallel kinematic architecture: Free leg hexapod. *Proc. IMechE Part B: J. Eng.* 2011;226:412–430.
- [70] Warnecke, HJ, Neugebauer, R, Wieland, F. Development of Hexapod based machine tool. *Ann. CIRP* 1998;47:337–440.
- [71] Gao, F, Li, W, Zhao, X, Jin, Z, Zhao, H. New kinematic structure for 2-, 3-, 4- and 5-DOF parallel manipulator designs. *Mech. Mach. Theory* 2002;37:1395–1411.
- [72] Tsai, LW. *Robot analysis: The mechanics of serial and parallel manipulators*. John Wiley & Sons: 1999.
- [73] Liu, XJ, Wang, J. *Parallel kinematics*. Springer-Verlag: 2014.
- [74] Mekid, S. Introduction to parallel kinematic machines. In: Mekid, S, (ed). *Introduction to precision machine design and error assessment*. CRC Press: 2008.
- [75] Weck, M, Staimer, D. Parallel kinematic machine tools-current state and future potentials. *Ann. CIRP* 2002;51:671–683.
- [76] Rugbani, A, Schreve, K. Modelling and analysis of the geometrical errors of a parallel manipulator micro-CMM. *Int. Precision Assembly Semin.* 2012; 371:105–117.
- [77] Soons, JA. Measuring the geometric errors of a hexapod. *Proc. of the 4th*

LAMDAMAP Conf. 1999, New Castle Upon-Tyne, United Kingdom.

- [78] El-Khasawneh, BS. The kinematics and calibration of a 5 degree of freedom hybrid serial parallel kinematic manipulator. 8th Int. Symp. on Mech. and its Appl. 2012, 1–7.
- [79] Harib, KH, Moustafa, KAF, Sharifullah, AMM, Zenieh, S. Parallel, serial and hybrid machine tools and robotics structure: Comparative study on optimum kinematic designs. In: Kucuk, S, (ed.). Serial and parallel robot manipulators-kinematics, dynamics, control and optimization. InTech: 2012.
- [80] Hu PH, Yu CW, Fan KC, Dang XM, Li RJ. Error averaging effect in parallel mechanism coordinate measuring machine. Appl. Sci. 2016;6:383-395.
- [81] Chen SL, Chang TH, Hsei MH. Analytical modelling of the effects of manufacturing errors on the accuracy for a TRR-XY hybrid parallel link machine tool. Proc. Mech. Eng. 2001;215:1203-1216.
- [82] Milutinovic, M, Slavkovic, N, Milutinovic, D. Kinematic modelling of hybrid parallel serial five axis machine tool. FME Tran. 2013;41:1–10.
- [83] Harib, KH, Sharifullah, AMM, Moustafa, KAF. Optimal design for improved hybrid kinematic machine tools. Ann. CIRP 2013;12:109–114.
- [84] Bosmans N, Reynaerts D. Force loops. In: Leach RK, Smith ST, (ed.). Basics of precision engineering. CRC Press: 2018.
- [85] Abtahi, M, Pendar H, Alasty, A, Vossoughi, G. Experimental kinematic calibration of parallel manipulators using a relative position error measurement system. Robotics and Computer-integrated Man. 2010;26(6):799-804.
- [86] Wu JF, Zhang R, Wang RH, Yao YX. A systematic optimisation approach for the calibration of parallel kinematics machine tools by a laser tracker. Int. J. Mach. Tools & Man. 2014;86:1-11.
- [87] Wu JF, Zhang R, Wang RH, Yao YX. A systematic optimisation approach for the calibration of parallel kinematics machine tools by a laser tracker. Int. J. Mach. Tools & Man. 2014; 86:1-11.
- [88] Abderrahim, M, Khamis, A, Garrido, S, Moreno, L. Accuracy and Calibration Issues of Industrial Manipulators. In: Low KH, (ed.). Industrial Robotics: Programming, Simulation and Applications. Intech Open: 2006.
- [89] Everett, LJ, Driels, M, Mooring, BW. Kinematic modelling for robot calibration. IEEE Int. Conf. on Robotics and Autom. 1987.
- [90] Mooring, BW, Roth, JS, Driels MR. Fundamentals of manipulator calibration. John Wiley and sons: 1991.
- [91] Mavroidis, C, Dubowsky, S, Drouet, P, Hintersteiner, J, Flanz, J. A systematic error analysis of robotic manipulators: application to a high performance medical robot, Proc. of Int. Conf. on Robotics and Autom. 1997, Albuquerque, NM, USA.
- [92] Rauf, A, Pervez, A, Ryu, J. Experimental results on kinematic calibration of parallel manipulators using a partial pose measurement device. IEEE

transactions on robotics 2006;22(2):379-384.

- [93] Yu, L, Yan, Y, Ren, S, Zhao, J. Vision-based method of kinematic calibration and image tracking of position and posture for 3-RPS parallel robot. IEEE Intl. Conf. on Mecha. and Autom. (ICMA) 2017, Takamatsu.
- [94] Soons, JA. On the Geometric and Thermal Errors of a Hexapod Machine Tool. In: Boër, CR, Molinari-Tosatti, L, Smith KS, (ed.). Parallel Kinematic Machines. Advanced Manufacturing. Springer: 1999.
- [95] Gao W, Haitjema, H, Fang, FZ, Leach, RK, Cheung, CF, Savio, E, Linares, JM. On-machine and in-process surface metrology for precision manufacturing. CIRP Annals. Man. Tech. 2019, 68(2), 843–866.
- [96] McKeown PA, Wills-Moren WJ, Read RF (1987) In-situ metrology and machine based interferometry for shape determination. Proceedings of SPIE:802
- [97] Hansen HN, Carneiro K, Haitijema H, Chiffre LD. Dimensional micro and nano metrology. CIRP Annals. 2006;55:721–743.
- [98] Schmidt RM, Schitter G, Rankers A, Eijk JV. The design of high performance mechatronics. Delft University Press: 2014.
- [99] Ludwick S. Control system for precision motion. In: Leach RK, Smith ST, (ed.). Basics of precision engineering. CRC Press: 2018.
- [100] Haitjema, H. Measurement uncertainty. In: Leach RK, Smith ST, (ed.). Basics of precision engineering. CRC Press: 2018.
- [101] Dorf, RC, Bishop, RH. Modern control systems. Pearson: 2011
- [102] Franklin GF, Powell JD, Emami-Naeini A. Feedback control of dynamic systems. Pearson: 2015.
- [103] Wu SC, Tomizuka M. Repeatable runout compensation for hard disk drives using adaptive feedforward cancellation. Proc. American Control conf., Minnesota, 14-16 Jun 2006.
- [104] Soloman, S. Sensor and control system in manufacturing. McGraw-Hill: 2010.
- [105] Weckenmann, A, Bernstein, J. Optical multi-sensor-measurements in the shop by compensating environmental influences. Procedia CIRP 2013;10:61–69.
- [106] Muhamedsalih, H, Jiang, X, Gao, F. Vibration compensation of wavelength scanning interferometer for in-process surface inspection. The 10th Proc. of Comp. and Engg. Annal. Researchers' Conf. 2010. 148–153.
- [107] Barker, A, Syam, WP, Leach, RK. Measurement noise of a coherence scanning interferometer in an industrial environment. Proceeding ASPE 2016:594-9.
- [108] Schwenke, H, Knapp, W, Haitjema, H, Weckenmann, A, Schmitt, R, Delbressine, F. Geometric error measurement and compensation of machines—An update. CIRP Annals - Manufacturing Technology 2008;57:660–675.
- [109] Mayr, J, Jędrzejewski, J, Uhlmann, E, Alkan Donmez, M, Knapp, W, Härtig, F, Wendt, K, Moriwaki, T, Shore, P, Schmitt, R, Christian, C, Würz, T, Wegener,

- K. Thermal issues in machine tools. *CIRP Annals – Manu. Tech.* 2012;61:771–791.
- [110] Leach, RK, Smith ST. *Basics of Precision Engineering*; CRC Press: 2018.
- [111] Bos, E, Moers, T, Riel, MV. Design and verification of an ultra-precision 3D coordinate measuring machine with parallel drives. *Measurement Science and Technology* 2015;26:085904.
- [112] Liu, MY, Cheung, CF, Whitehouse, D, Cheng, CH. An autonomous multisensor in situ metrology system for enabling high dynamic range measurement of 3D surfaces on precision machine tools. *Measurement Science and Technology* 2016;27:115015.
- [113] Darukumalli, S, Santoso, T, Syam, WP, Helmi, F, Leach, R. On-machine optical surface topography measurement sensor based on focus variation. *Proc. of the 19th euspen Intl. Conf.* 2019.
- [114] Wilhelm, RG, Hocken, R, Schwenke, H. Task specific uncertainty in coordinate measurement. *CIRP Annals Manu. Techn.* 2001;50:553–563.
- [115] Vrba, I, Palencar, R, Hadzistevic, M, Strbac, B, Spasi-Jokic, V, Hodolic, J. Different approaches in uncertainty evaluation for measurement of complex surfaces using coordinate measuring machine. *Meas. Sci. Review* 2015;15:111–118.
- [116] National Physical Laboratory. SI units. Available from: <https://www.npl.co.uk/si-units/metre> [Accessed: 15th February 2020].
- [117] Nomura, T, Yoshikawa, K, Tashiro, H, Takeuchi, I, Ozawa, N, Okazaki, Y, Suzuki, M, Kobayashi, F, Usuki, M. On-machine shape measurement of workpiece surface with Fizeau interferometer. *Prec. Engg.* 1992;14(3):155-159.
- [118] Schwenke, H, Neuschaefer-Rube, U, Pfeifer, T, Kunzmann, H. Optical Methods for Dimensional Metrology in Production Engineering. *CIRP Annals* 2002;51(2):685-699.
- [119] Suh, YS. Laser Sensors for Displacement, Distance and Position. *MDPI Sensors* 2019;19:1924.
- [120] Bai, J, Li, X, Wang, X, Zhou, Q, Ni, K. Chromatic Confocal Displacement Sensor with Optimized Dispersion Probe and Modified Centroid Peak Extraction Algorithm. *MDPI Sensors* 2019;19:3592.
- [121] Leach, R. *Fundamental principles of engineering nanometrology*. Elsevier: 2014.
- [122] Badami VG, deGroot PJ. Displacement measuring interferometry, in: Harding K (ed.) *Handbook of optical dimensional metrology*. CRC Press: 2013.
- [123] Flint, Tony. *Plane mirror interferometer: Marketing specifications*. Renishaw PLC transducer Ltd. 1998 (commercial restricted).
- [124] Mingers, J. Combining IS research methods: towards a pluralist methodology. *Information systems research* 2007;2(3):240-259.

- [125] Ahmed, S. Empirical research in engineering practice. *J. of design research* 2007;6(3):359-380.
- [126] Haitjema H. Achieving traceability and sub-nanometer uncertainty using interferometric techniques. *Meas. Sci. Technol.* 2008;19(8):1-6.
- [127] Bonsch G, Potulski E. Measurement of the refractive index of air and comparison with modified Edlen's formulae. *Metrologica* 1998;35:133-139.
- [128] Song, SM, Zhang, MD. A Study of Reactional Force Compensation Based on Three-Degree-of-Freedom Parallel Platforms 1995;12(12):783-794.
- [129] Hale LC. Principles and techniques for designing precision machines. PhD thesis. Massachusetts Institute of Technology, 1999.
- [130] Seugling R. System modelling. In: Leach RK, Smith ST, (ed.). *Basics of precision engineering*. CRC Press: 2018.
- [131] Bruant I, Gallimard L, Nikoukar S. Optimal piezoelectric actuator and sensor location for active vibration control, using genetic algorithm. *J. of sound and vibration*, 2010;329(10):1615-1635.
- [132] Yang SM, Lee YJ. Optimisation of noncollocated sensor/actuator location and feedback gain in control systems. *Smart Mater. Struct.* 2, 1993:96-102.
- [133] Bryan J. The Abbe principle revisited: an updated interpretation. *Prec. Eng.*, 1979;1(3):129-132.
- [134] Delta Tau Data System, Inc. 2008. Turbo PMAC user manual: programmable multi-axis controller. Chatsworth: CA.
- [135] Zhang Y, Yao S. Research of a high-precision motion control system based on turbo PMAC. *Proc. 3rd Intl. Conf. on Comp. Sc. and Info. Tech.* 2010; 39-42.
- [136] Renishaw, PLC. 2015. Application note: plane mirrors for laser application. Gloucestershire: UK.
- [137] de Groot, P., Di Sciacca, J. Surface-height measurement noise in interference microscopy. *International Society for Optics and Photonics - Interferometry XIX* 2018
- [138] Muhamedsalih, H., Jiang, X., Gao, F. Vibration compensation of wavelength scanning interferometer for in-process surface inspection. *The 10th Proc. of Compu. and Engg. Annal Researchers' Conf.* 2010, 148–153.
- [139] Carretero JA, Phdhorodeski RP, Nahon MA, Gosselin CM. Kinematic analysis and optimisation of a new three degree of freedom spatial parallel manipulator. *J. Mech. Design* 2000;122:17-24.

Appendix A

An example of uncertainty budget for distance measurement by a laser interferometer

Quantity	Estimation (measured)		Uncertainty		Sensitivity	Contribution to standard uncertainty in $P_{20}/\mu\text{m}$
X_i	x_i		u_i		$c_i = \frac{\partial P_{20}}{\partial X_i}$	$= c_i u_i$
$L_{nominal}$	40	mm	0	μm	1	0.000
L_{20}	40.000287	mm	0.085	μm	1	0.085
T_s	20.5	$^{\circ}\text{C}$	0.2	$^{\circ}\text{C}$	0.00046	0.092
α_s	0.0000115	K^{-1}	0.0000007	K^{-1}	20.0001435	0.014
T_a	21	$^{\circ}\text{C}$	1	$^{\circ}\text{C}$	0.0000372	0.037
P_a	1020	hPa	2	hPa	0.0000216	0.043
H	50	%Rh	10	%Rh	0.0000036	0.036
P_{20}		μm	$u(L_{1,x}) = \sqrt{\sum (u_i \cdot c_i)^2}$			0.143

Appendix B

Properties of the actuators used in the motion stages of HAMS

Axis name	Actuator type	Make	Travel	Resolution	Repeatability	Accuracy
<i>x</i> (horizontal)	Linear servo motors	Alio industries	100 mm	5 nm	±100 nm	±2μm/25 mm
<i>y</i> (vertical)	Linear servo motors in the prismatic joints	Alio industries	24 mm	5 nm	±100 nm	±2μm/25 mm
<i>z</i> (horizontal)	Linear servo motors	Alio industries	100 mm	5 nm	±100 nm	±2μm/25 mm
<i>u</i>	Linear servo motors in the prismatic joints	Alio industries	±4.4°	0.02 arc-sec	±0.05 arc-sec	±20 arc-sec
<i>v</i>	Mechanical bearing rotary stage with servo motors	Alio industries	±4.4°	0.02 arc-sec	±0.05 arc-sec	±20 arc-sec
<i>w</i>	Mechanical bearing rotary stage with servo motors	Alio industries	360°	0.04 arc-sec	±0.05 arc-sec	±20 arc-sec

Appendix C

Inverse kinematics of HAMS extracted from the HAMS control software

&1 Open INVERSE Clear

IF(M5182=0)

Q207=(Q201+Q204)

Q208=(Q202+Q205)

Q209=(Q203+Q206)

Q1051=(Q1031+Q1021)

Q1052=(Q1032+Q1022)

Q1053=(Q1031-Q1021)

Q1054=(Q1032-Q1022)

Q1055=(COS(Q2))

Q1056=(COS(Q3))

Q1057=(SIN(Q2))

Q1058=(SIN(Q3))

Q1059=(((-1*Q1057*Q1058*Q1054)+((-1/(SQRT(3))))*Q1056*Q1052)+(-1*Q1055*Q1053)+(2/(SQRT(3))))*Q1056*Q1012)/(((2/(SQRT(3))))*Q1056*Q1011)+((1/(SQRT(3))))*Q1056*Q1051)+(Q1057*Q1058*Q1053)+(-1*Q1055*Q1054))

Q1091=(ATAN(Q1059))

Q1061((((COS(Q2))*COS(Q1091)))+(((SIN(Q2))*SIN(Q3))*SIN(Q1091))))

Q1062(((1*(COS(Q2))*SIN(Q1091)))+(((SIN(Q2))*SIN(Q3))*COS(Q1091))))

Q1063=((SIN(Q2))*COS(Q3))

Q1071=((COS(Q3))*SIN(Q1091))

Q1072=((COS(Q3))*COS(Q1091))

Q1073=(-1*(SIN(Q3)))

Q1081(((1*(SIN(Q2))*COS(Q1091)))+(((COS(Q2))*SIN(Q3))*SIN(Q1091))))

Q1082((((SIN(Q2))*SIN(Q1091)))+(((COS(Q2))*SIN(Q3))*COS(Q1091))))

Q1083=((COS(Q2))*COS(Q3))

Q1098((-1*Q1071*Q1011)+(-1*Q1072*Q1012)+(-1*Q1073*Q1013))

Q1097(((1/(SQRT(3))))*((Q1098)+(Q1071*Q1021)+(Q1072*Q1022)+(Q1073*Q1023))-((Q1061*Q1021)+(Q1062*Q1022)+(Q1063*Q1023)))

Q1096(((1/(SQRT(3))))*((Q1098)+(Q1071*Q1031)+(Q1072*Q1032)+(Q1073*Q1033))-((Q1061*Q1031)+(Q1062*Q1032)+(Q1063*Q1033)))

Q1311((((COS(Q2))*COS(Q1)))+(((SIN(Q2))*SIN(Q3))*SIN(Q1))))

Q1312(((1*(COS(Q2))*SIN(Q1)))+(((SIN(Q2))*SIN(Q3))*COS(Q1))))

Q1313=((SIN(Q2))*COS(Q3))

Q1321=((COS(Q3))*SIN(Q1))

Q1322=((COS(Q3))*COS(Q1))

Q1323=(-1*(SIN(Q3)))

Q1331(((1*(SIN(Q2))*COS(Q1)))+(((COS(Q2))*SIN(Q3))*SIN(Q1))))

$Q1332=(((\sin(Q2))*\sin(Q1))+((\cos(Q2))*\sin(Q3))*\cos(Q1))))$
 $Q1333=((\cos(Q2))*\cos(Q3))$
 $Q1401=((Q207)-((Q207*Q1311)+(Q208*Q1312)+(Q209*Q1313)))$
 $Q1402=((Q208)-((Q207*Q1321)+(Q208*Q1322)+(Q209*Q1323)))$
 $Q1403=((Q209)-((Q207*Q1331)+(Q208*Q1332)+(Q209*Q1333)))$
 $Q1511=((Q1097)+(Q1061*Q1011)+(Q1062*Q1012)+(Q1063*Q1013)-(Q1111))$
 $Q1512=((Q1098)+(Q1071*Q1011)+(Q1072*Q1012)+(Q1073*Q1013)-(Q1112))$
 $Q1513=((Q9)+(Q392)+(Q1081*Q1011)+(Q1082*Q1012)+(Q1083*Q1013)-(Q1113)+(Q1403))$
 $Q1521=((Q1097)+(Q1061*Q1021)+(Q1062*Q1022)+(Q1063*Q1023)-(Q1121))$
 $Q1522=((Q1098)+(Q1071*Q1021)+(Q1072*Q1022)+(Q1073*Q1023)-(Q1122))$
 $Q1523=((Q9)+(Q392)+(Q1081*Q1021)+(Q1082*Q1022)+(Q1083*Q1023)-(Q1123)+(Q1403))$
 $Q1531=((Q1097)+(Q1061*Q1031)+(Q1062*Q1032)+(Q1063*Q1033)-(Q1131))$
 $Q1532=((Q1098)+(Q1071*Q1031)+(Q1072*Q1032)+(Q1073*Q1033)-(Q1132))$
 $Q1533=((Q9)+(Q392)+(Q1081*Q1031)+(Q1082*Q1032)+(Q1083*Q1033)-(Q1133)+(Q1403))$
 $Q1601=(\text{SQRT}((Q1511*Q1511)+(Q1512*Q1512)+(Q1513*Q1513)))$
 $Q1602=(\text{SQRT}((Q1521*Q1521)+(Q1522*Q1522)+(Q1523*Q1523)))$
 $Q1603=(\text{SQRT}((Q1531*Q1531)+(Q1532*Q1532)+(Q1533*Q1533)))$
 $\text{IF}(Q6012<0.1\text{AND}Q6022<0.1\text{AND}Q6032<0.1\text{AND}Q6092<0.1)$
 $P1=((Q1601-Q394)*Q211)$
 $P2=((Q1602-Q394)*Q212)$
 $P3=((Q1603-Q394)*Q213)$
 $P4=((Q7+Q1401-Q1097)*Q214)$
 $P5=((Q8+Q1402-Q1098)*Q215)$
 $P6=((Q1-Q1091)*Q216)$
 $P7=(Q4*2912.71111)$
ELSE
 $M5182=1$
 $Q41=Q1$
 $Q42=Q2$
 $Q43=Q3$
 $Q47=Q7$
 $Q48=Q8$
 $Q49=Q9$
 $Q51=Q6011$
 $Q52=Q6021$
 $Q53=Q6031$
 $Q59=Q6091$
 $Q1=0$
 $Q2=0$
 $Q3=0$
 $Q7=0$

Q8=0
Q9=0
ENDI
ELSE
M5182=1
ENDI
CLOSE

Appendix D

Example of a motion programme for generating compensation for the positional deviation of target in the z direction for a given tip rotation of HAMS

```
CLOSE
END GATHER
DELETE GATHER
OPEN PROG 118 CLEAR
P990=0
F(Q222)
TS(Q223)
TA(Q224)
FRAX
INC
LINEAR
B(P1002)Z(P1009) X(P1107); simultaneous motion of tip (u) and compensatory
motion in z and x
Q222=5
Q223=500
Q224=1000;
P1002=0.3; P1002 is for tip (u) input
P1009=2000*P1002; linear relation between tip and the compensatory motion
P1107=30*P1002; linear relation between tip and the compensatory motion
CLOSE;
```

Appendix E

$K_1, K_2, K_3, L_1, L_2, L_3, M_1, M_2, M_3, N_1, N_2$ and N_3 , as shown below, represent the elements of the matrix in equation (7.12) of section 7.4:

$$K_1 = \cos \theta \cos(\theta_y - \theta_m) + \sin \theta \sin \theta_x \cos(\theta_y + \theta_m), \quad (7.13)$$

$$K_2 = \cos \theta \sin \theta_y \sin(\theta_y + \theta_m) + \sin \theta (\cos \theta_n \cos \theta_x - \sin \theta_x \sin \theta_n \cos(\theta_y - \theta_m)), \quad (7.14)$$

$$K_3 = \sin \theta (\cos \theta_x \sin \theta_n + \sin \theta_x \cos \theta_n \cos(\theta_y - \theta_m)) - \cos \theta \cos \theta_n \sin(\theta_y - \theta_m), \quad (7.15)$$

$$L_1 = \cos \theta \sin \theta_x \sin(\theta_y + \theta_m) - \sin \theta \cos(\theta_y - \theta_m), \quad (7.16)$$

$$L_2 = \cos \theta (\cos \theta_n \cos \theta_x - \sin \theta_x \sin \theta_n \cos(\theta_y - \theta_m)) - \sin \theta \sin \theta_n \sin(\theta_y + \theta_m), \quad (7.17)$$

$$L_3 = \sin \theta \cos \theta_n \sin(\theta_y + \theta_m) + \cos \theta (\cos \theta_x \sin \theta_n + \sin \theta_x \cos \theta_n \cos(\theta_y - \theta_m)), \quad (7.18)$$

$$M_1 = \cos \theta_x \sin(\theta_y + \theta_m), \quad (7.19)$$

$$M_2 = -\cos \theta_n \sin \theta_x - \cos \theta_x \sin \theta_n \cos(\theta_y - \theta_m), \quad (7.20)$$

$$M_3 = \cos \theta_x \cos \theta_n \cos(\theta_y - \theta_m) - \sin \theta_n \sin \theta_x, \quad (7.21)$$

$$N_1 = s(\cos \theta \sin(\theta_y - \theta_m) + \sin \theta \sin \theta_x \sin(\theta_y + \theta_m)) - s \cos \theta - \cos \theta \sin \theta_x \sin(\theta_y + \theta_m) - (h + y) \sin \theta + l \cos \theta_x \sin(\theta_y + \theta_m), \quad (7.22)$$

$$N_2 = -(h + y)(\sin \theta \sin \theta_n \sin(\theta_y + \theta_m) - \cos \theta (\cos \theta_y \cos \theta_x - \sin \theta_x \sin \theta_y \cos(\theta_y - \theta_m))) + s(\cos \theta \sin \theta_y \sin(\theta_y + \theta_m) + \sin \theta (\cos \theta_n \cos \theta_x - \sin \theta_x \sin \theta_n \cos(\theta_y - \theta_m))) - l(\cos \theta_y \sin \theta_x + \cos \theta_x \sin \theta_y \cos(\theta_y - \theta_m)), \quad (7.23)$$

$$N_3 = (h + y)(\sin \theta \cos \theta_n \sin(\theta_y + \theta_m) + \cos \theta (\cos \theta_x \sin \theta_n + \sin \theta_x \cos \theta_n \cos(\theta_y - \theta_m))) - s(\cos \theta \cos \theta_n \sin(\theta_y + \theta_m) - \sin \theta (\cos \theta_x \sin \theta_n + \sin \theta_x \cos \theta_n \cos(\theta_y - \theta_m))) - l(\sin \theta_n \sin \theta_x - \cos \theta_x \cos \theta_n \cos(\theta_y - \theta_m)) - l + z. \quad (7.24)$$

Appendix F

$A_1, A_2, A_3, B_1, B_2, B_3, C_1, C_2, C_3, D_1$ and D_2 , as shown below, represent the elements of the matrix in equation (7.25) of section 7.4:

$$A_1 = \cos \theta \cos(\theta_y - \theta_m) + \sin \theta \sin \theta_x \cos(\theta_y + \theta_m) - \cos \theta, \quad (7.26)$$

$$A_2 = \sin \theta + \cos \theta \sin \theta_y \sin(\theta_y + \theta_m) + \sin \theta (\cos \theta_n \cos \theta_x - \sin \theta_x \sin \theta_n \cos(\theta_y - \theta_m)), \quad (7.27)$$

$$A_3 = \sin \theta (\cos \theta_x \sin \theta_n + \sin \theta_x \cos \theta_n \cos(\theta_y - \theta_m)) - \cos \theta \cos \theta_n \sin(\theta_y - \theta_m), \quad (7.28)$$

$$B_1 = \cos \theta \sin \theta_x \sin(\theta_y + \theta_m) - \sin \theta \cos(\theta_y - \theta_m) - \sin \theta, \quad (7.29)$$

$$B_2 = \cos \theta (\cos \theta_n \cos \theta_x - \sin \theta_x \sin \theta_n \cos(\theta_y - \theta_m)) - \sin \theta \sin \theta_n \sin(\theta_y + \theta_m) - \cos \theta, \quad (7.30)$$

$$B_3 = \sin \theta \cos \theta_n \sin(\theta_y + \theta_m) + \cos \theta (\cos \theta_x \sin \theta_n + \sin \theta_x \cos \theta_n \cos(\theta_y - \theta_m)), \quad (7.31)$$

$$C_1 = \cos \theta_x \sin(\theta_y + \theta_m), \quad (7.32)$$

$$C_2 = -\cos \theta_n \sin \theta_x - \cos \theta_x \sin \theta_n \cos(\theta_y - \theta_m), \quad (7.33)$$

$$C_3 = \cos \theta_x \cos \theta_n \cos(\theta_y - \theta_m) - \sin \theta_n \sin \theta_x - 1, \quad (7.34)$$

$$D_1 = s(\cos \theta \sin(\theta_y - \theta_m) + \sin \theta \sin \theta_x \sin(\theta_y + \theta_m) - s \cos \theta - (h + y)(\sin \theta \cos(\theta_y - \theta_m) - \cos \theta \sin \theta_x \sin(\theta_y + \theta_m))) - (h + y) \sin \theta + l \cos \theta_x \sin(\theta_y + \theta_m), \quad (7.35)$$

$$D_2 = s \sin \theta - (h + y) \cos \theta - (h + y)(\sin \theta \sin \theta_n \sin(\theta_y + \theta_m) - \cos \theta (\cos \theta_y \cos \theta_x - \sin \theta_x \sin \theta_y \cos(\theta_y - \theta_m))) + s(\cos \theta \sin \theta_y \sin(\theta_y + \theta_m) + \sin \theta (\cos \theta_n \cos \theta_x - \sin \theta_x \sin \theta_n \cos(\theta_y - \theta_m))) - l(\cos \theta_y \sin \theta_x + \cos \theta_x \sin \theta_y \cos(\theta_y - \theta_m)). \quad (7.36)$$

Appendix G

Procedure to avoid the plane mirror's misalignment during the experimental set-up

The following steps were followed during the experimental set-up to avoid plane mirror misalignment.

- Lock any z or y motions of the stages, and then move the x stage along the x -axis of the wheel for the full-length of the mirror in its parallel direction (see Figure 7.2). Carry out these for all eight mirrors to ensure they are parallel with the x -axis of the wheel when it rotates.
- Lock any z or x motions of the stages, and then move tripod along the y -axis for the full-length of the mirror in its vertical direction (see Figure 7.2). Carry out these for all eight mirrors to ensure they are parallel with y -axis of the wheel when it rotates.

